Nanopartikel-Biotestung mittels *in-vitro*-Kulturen von Säugerzellen

Von der Naturwissenschaftlichen Fakultät

der Gottfried Wilhelm Leibniz Universität Hannover

zur Erlangung des Grades

DOKTORIN DER NATURWISSENSCHAFTEN

(Dr. rer. nat.)

genehmigte Dissertation

von

M. Sc. Franziska Sambale

geboren am 26. Mai 1987 in Hannover

2015

Referent: Prof. Dr. Thomas Scheper

Korreferent: Prof. Dr. Detlef W. Bahnemann

Korreferent: Prof. Dr. Arno Kwade

Tag der Promotion:13.10.2015

„Wir müssen unbedingt Raum für Zweifel lassen, sonst gibt es keinen Fortschritt, kein Dazulernen.

Man kann nichts Neues herausfinden, wenn man nicht vorher eine Frage stellt.

Und um zu fragen, bedarf es des Zweifelns.“

[Richard P. Feynman, 1918-1988]

Danksagung

Ich danke Herrn Prof. Dr. Thomas Scheper für die Möglichkeit am Institut für Technische Chemie der Leibniz Universität Hannover meine Dissertation anfertigen zu können sowie für die Bereitstellung des interessanten, hochaktuellen Themas.
Besonders möchte ich mich bei Herrn Prof. Dr. Thomas Scheper und Herrn Prof. Dr. Detlef W. Bahnemann für die wissenschaftliche Betreuung dieser Arbeit, für die Förderung während meiner Promotion und für die Möglichkeit zur Teilnahme an zahlreichen Konferenzen bedanken. Außerdem bedanke ich mich für die gute Arbeitsatmosphäre, den gewährten Freiraum bei der Bearbeitung des Themas sowie das entgegengebrachte Vertrauen. Herrn Prof. Dr. Detlef W. Bahnemann und Herrn Prof. Dr. Arno Kwade danke ich zudem für die Übernahme des Korreferats.

Meinem Arbeitsgruppenleiter Dr. Frank Stahl möchte ich für die hilfreichen Anregungen, das Vertrauen, das ausgezeichnete Arbeitsklima und die netten Gespräche bedanken.
Bei Prof. Dr. Cornelia Kasper bedanke ich mich für die anregenden Diskussionen und den Wissensaustausch auf dem Gebiet der Zellkulturtechniken.

Weiterhin danke ich allen Partnern und Doktoranden des Nanokomp-Projektes für den sehr guten wissenschaftlichen Austausch und die anregenden interdisziplinären Diskussionen. Vor allem Jutta Hesselbach danke ich für die produktive Zusammenarbeit.

Bei Martin Pähler und Martina Weiß möchte ich mich für die unverzichtbare Hilfsbereitschaft in allen Belangen des Institutsalltages bedanken.

Für das sorgfältige und kritische Korrekturlesen meiner Arbeit sowie meiner Publikationen bedanke ich mich bei Prof. Dr. Thomas Scheper, Prof. Dr. W. Detlef Bahnemann, Dr. Frank Stahl, Dr. Iliyana Pepelanova, Dr. Antonina Lavrentieva, Jörg Stövesand, Kenneth Rider, Paul Maschhoff, meiner Schwester Saskia und meiner Mutter Ingrid.

Außerdem möchte ich mich bei meinem engagierten und wissbegierigen kleinen Forschungsteam bedanken, das an meinem wissenschaftlichen Projekt involviert war. Im Besondern danke ich meiner Masterstudentin Stefanie Thoms, meinen Bachelorstudenten Josefin Sippel, Birte Schnaars und Marline Kirsch, meiner wissenschaftlichen Hilfskraft Marline Kirsch und bei meinem Bundesfreiwilligendienstler Timon Harries.

Des Weiteren möchte ich mich bei allen meinen TCI-Freunden und -Kollegen für die einzigartige TCI-Gemeinschaft und die unvergessliche Zeit bedanken. Das gemeinschaftliche Mittagessen in der Mensa, die lustigen Kaffeepausen, die spannenden Fußball-WM/EM-Abende auf der Terrasse, die erlebnisreichen Betriebsausflüge sowie die ausgelassenen Sommerfeste, Weihnachtsfeiern und Oktoberfeste werde ich in guter Erinnerung behalten und zukünftig sehr vermissen.

Mein Dank gilt auch die *Cell culture and friends* Rebecca, Tonya, Fred, Kathrin und Jule für das Teilen von Ideen, Begeisterungen, Erfolgen, Frustrationen und die gemeinsamen Dienstreisen.
Ich danke Michi, Emi, Miri und Martin für die schöne Atmosphäre im *Headquarter*-Büro. Vielen Dank, dass wir unsere wissenschaftlichen und privaten Erfahrungen sowie den wichtigen TCI-Tratsch miteinander geteilt und gemeinsam vielen lustige Büronachmittage verbracht haben.

Bei Tonya möchte ich mich für den wertvollen Erfahrungs- und Wissensaustausch, die vielen kleinen Geschenke und für die wunderschönen Backabende in deiner Landhausküche danken. Das Keksebacken mit dem selbstgemachtem Glühwein, der leckeren Suppe und den Weihnachtsliedern hat uns allen die Adventszeit versüßt. Christan Ude möchte ich für seine kreativen Ideen, seine stetige Hilfsbereitschaft und den Erfahrungsaustausch danken.

Meinem Hockeyteam von Hannover 78 danke ich für den sensationellen Ausgleich zum wissenschaftlichen Alltag und die einmalige Gemeinschaft. Ich bin sehr froh ein so tolles Team gefunden zu haben.

Von ganzem Herzen möchte ich meinen Eltern Ingrid und Burkhard, meinen Geschwistern Saskia, Jacqueline und Marc-Pascal, meiner Oma Blanka und meinen Freunden für den Rückhalt und die moralische Unterstützung auf jeglicher Art und Weise während meines Studiums und des gesamten Zeitraums meiner Arbeit danken.
Meinem Freund Philip möchte ich für seine bedingungslose Unterstützung, seine Geduld und sein Verständnis, sein offenes Ohr für die abstrakten Labor-Herausforderungen und seinen Beistand bei nächtlichen oder wochenendlichen Laborschichten danken. Vielen Dank für deinen ausgeprägten Humor, der mich immer wieder zum Lachen bringt.

Kurzfassung

Die Nanotechnologie ist mittlerweile vollständig in unser alltägliches Leben integriert. Nanopartikel verbessern Produkteigenschaften, so dass sich ihr Anwendungsspektrum in nahezu allen Bereichen erweitert. Dennoch sind etwaige Risiken der Nanoprodukte für Mensch und Umwelt nicht umfassend geklärt. Gründe hierfür sind unter anderem die hohe Anzahl an Nanoprodukten, die unzureichenden Detektionsmethoden sowie die komplexen Interaktionen der Nanopartikel mit ihrer Umgebung und den Organismen. Um in Zukunft den Erfolg dieser Technologie weiter garantieren zu können, ist daher eine umfangreiche Risikobewertung der Nanoprodukte und deren Vorläufer durchzuführen. Hierbei muss die Stabilität der Nanoprodukte während ihres Anwendungszyklus geklärt werden.

In dieser Arbeit wurde ein zellbasiertes, hierarchisches *Screening*-System entwickelt, mit dem die prozessbegleitende toxikologische Analyse in einem hohen Durchsatz ermöglicht wird. Dieses wurde in ein *Pre*-, *Fine*- und *Complex-Screening* gegliedert und beinhaltet verschiedene Zellsysteme und Toxizitätstests. Hierbei kamen Viabiliätstests, Zellmorphologie-, Genexpressions- oder Zelladhäsions-Analysen zum Einsatz. Als Zellsysteme wurden neben den klassischen zweidimensionalen (2D) Kulturen verschiedene dreidimensionale (3D) Kulturen sowie dynamische Kultivierungsbedingungen angewendet. Die Sensitivität der Methoden sowie die Komplexität der Zellsysteme wurden im Verlauf des *Screenings* erhöht. Die Nanopartikel wurden als Suspension sowie alternativ auch als Beschichtung oder Komposit analysiert.

Zinkoxid (ZnO)-, Titandioxid (TiO_2)- und Silber (Ag)-Nanopartikel haben exemplarisch das entwickelte *Screening*-System durchlaufen und deren toxikologische Wirkung auf NIH-3T3-Zellen (Fibroblasten) und A549-Zellen (Lungenepithelzellen) wurde überprüft. Die ZnO-Nanopartikel wirkten in 2D, in 3D-Modellen sowie unter dynamischen Bedingungen toxisch auf die Zellen. Dabei verminderten die ZnO-Nanopartikel direkt nach Zugabe die Zelladhäsion. Der Durchmesser der 3D-Zellagregate (Sphäroide) wurde durch die ZnO-Nanopartikel beeinflusst. Des Weiteren waren im Vergleich zu der statischen Kultivierung die Zellen unter dynamischen Bedingungen sensitiver. Bei den TiO_2-Nanopartikeln wurden erst im *Complex-Screening* Effekte auf die Zellen beobachtet. Anstelle eines einzelnen 3D-Sphäroids wurden viele kleine Sphäroide gebildet, deren Anzahl mit der TiO_2-Konzentration zunahm. Unter dynamischen Bedingungen orientieren sich zudem die NIH-3T3-Zellen bei TiO_2-Exposition nicht in die Flussrichtung. Die Ag-Nanopartikel waren im Vergleich zu Silber-Ionen wesentlich toxischer und induzierten Apoptose. Zusätzlich wurden Aluminiumoxid-Nanopartikel und -Komposite für die Entwicklung von hydrophoben Oberflächen prozessbegleitend mit dem *Screening*-System analysiert.

Das entwickelte *Screening*-System ist hocheffizient, kostenminimierend und bietet die Möglichkeit eine Vielzahl von verschiedenen Nanoprodukten auf deren toxikologische Wirkung auf Zellsysteme zu überprüfen. Durch Etablierung von komplexen Zellsystemen, die die physiologischen Bedingungen im menschlichen Organismus simulieren, könnten langfristig Tierexperimente reduziert werden.

Stichwörter: Nanotoxikologie, Nanopartikel, 3D-Zellwachstum, dynamische Kultivierung

Abstract

The application range of nanoparticles covers multiple technological areas, where nanotechnology has provided innovative products and solutions. Nevertheless, the risk of nanoproducts for humans being and the environment has not been fully examined. The main reasons for this are the high number of nanoproducts, insufficient detection methods for nanoparticles, and the complex interaction of nanoparticles with organisms and their environment. In order to guarantee the success and safety of this technology in the future, a comprehensive risk assessment of nanoproducts and their precursors is required. In particular, the stability of nanoproducts during their complete life cycle needs thorough investigation.

In this work, a cell-based and hierarchical screening system was developed to realize the analysis of a variety of nanoparticles and nanomaterials under defined and reproducible conditions. The screening can be performed during nanoproduct development. It is divided into pre-, fine-, and complex-screening and includes various cell systems and various toxicity tests to determine the effect of the nanoproduct on metabolic activity. For this purpose, viability assays, cell morphology, gene expression or cell adhesion analysis were performed. In addition to common two-dimensional (2D) cell cultures, different three-dimensional (3D) cell culture models and dynamic culture conditions were applied. The sensitivity of the methods as well as the complexity of the cellular systems was increased in the progress of the screening. Apart from nanoparticle suspensions, nanoparticle coatings or nanocomposites can also be investigated with the established screening system.

Zinc oxide (ZnO), titanium dioxide (TiO_2), and silver (Ag) nanoparticles have been exemplary screened and their impact on NIH-3T3 cells (fibroblasts) and A549 cells (lung cell line) was examined. ZnO nanoparticle exposure caused several cytotoxic effects in the cells growing either in 2D, 3D, or under dynamic model conditions. Cell adhesion was reduced immediately after ZnO nanoparticle addition and the diameter of the 3D cell aggregates (spheroids) was affected. In addition, the cells under dynamic conditions were more sensitive to the nanoparticles in comparison to cells growing under static culture conditions. For TiO_2 nanoparticles significant effects on the cells were only observed during complex screening. Instead of the formation of a single spheroid, multiple smaller spheroids were formed after TiO_2 nanoparticle addition, the number of which correlated with the TiO_2 concentration. Furthermore, the NIH-3T3 cells were not orientated in the direction of flow when TiO_2 nanoparticles were present in the dynamic culture. The Ag nanoparticles were more toxic in comparison to silver ions and induced apoptosis. In addition, the screening system was implemented on every development stage of a nanoproduct composed of aluminum oxide nanoparticles composites and intended for the manufacture of innovative hydrophobic surfaces.

The designed screening system is highly efficient, reduces costs, and enables the analysis of a variety of different nanoproducts. The establishment of complex cell systems that mimic the physiological conditions in the human organism could reduce the amount of animal studies in the future.

Keywords: Nanotoxicology, nanoparticles, 3D cell growth, dynamic cultivation

Vorbemerkung

Die vorliegende Arbeit wurde im Zeitraum von November 2012 bis Juni 2015 am Institut für Technische Chemie der Gottfried Wilhelm Leibniz Universität Hannover unter der Leitung von Herrn Prof. Dr. Thomas Scheper angefertigt. Teile dieser Arbeit wurden in international anerkannten Zeitschriften veröffentlicht oder auf internationalen Fachkonferenzen in Form von Vorträgen oder Posterpräsentationen vorgestellt. Teile der Arbeit wurden im Rahmen des Forschungsvorhabens „Nanokomp“ (Europäischer Fond für regionale Entwicklung (EFRE), Projektnummer: 60421066) durchgeführt.

In der nachfolgenden Publikationsliste ist der geleistete Anteil der wissenschaftlichen Arbeit der Autoren in Prozent angegeben. In der vorliegenden Dissertation wird auf die jeweiligen Veröffentlichungen mit den römischen Zahlen der Publikationsliste verwiesen.

Veröffentlichungen und Kongressbeiträge

Veröffentlichungen

I **Franziska Sambale** (50 %) and Jutta Hesselbach (50 %), Benedikt Finke, Carsten Schilde, Frank Stahl, Detlef Bahnemann, Thomas Scheper, Arno Kwade, Surface and mechanical properties of nanoparticulate resin coatings and their toxicological characterization, eingereicht beim *Journal of Nanoparticle Research* am 19.08.2015

II **Franziska Sambale** (100 %), Frank Stahl, Detlef Bahnemann, Thomas Scheper, *In vitro* toxicological nanoparticle studies under flow exposure, *Journal of Nanoparticle Research* (2015)17:298:p. 1-12, DOI 10.1007/s11051-015-3106-2

III **Franziska Sambale** (90 %), Frank Stahl, Ferdinand Rüdinger (10 %), Dror Seliktar, Cornelia Kasper, Detlef Bahnemann, Thomas Scheper, Iterative cellular screening system for nanoparticle safety testing, *Journal of Nanomaterials*, Volume 2015 (2015), Article ID 691069, DOI: 10.1155/2015/691069

IV Mehriban Ulusoy (70 %), Antonina Lavrentieva, **Franziska Sambale** (30 %), Mark Green, Frank Stahl, Thomas Scheper, Evaluation of CdTe/CdS/ZnS Quantum dots toxicity on three-dimensional monocellular spheroids, *Toxicology Research,* 2015, Advance Article, DOI: 10.1039/C5TX00236B

V Daniel Pöhnert, Mahmoud Abbas, Lavinia Maegel, **Franziska Sambale** (10 %), Antonina Lavrentieva, Hans-H. Kreipe, Jürgen Klempnauer, Markus Winny, Evaluation of the biological tolerability of the starch-based medical device 4DryField® PH in vitro and in vivo a rat model, *Journal of Biomaterials Applications* 0(0) 1–9, 2015, DOI: 10.1177/0885328215592257

VI **Franziska Sambale** (50 %), Stefanie Wagner (50 %), Frank Stahl, Renat R. Khaydarov, Thomas Scheper, Detlef Bahnemann, Investigations of the toxic effect of silver nanoparticles on mammalian cell lines, *Journal of Nanomaterials*, Volume 2015 (2015), Article ID 136765, DOI: 10.1155/2015/136765

VII **Franziska Sambale** (100 %), Antonina Lavrentieva, Frank Stahl, Cornelia Blume, Meike Stiesch, Cornelia Kasper, Thomas Scheper, Three Dimensional Spheroid Cell Culture for Nanoparticle Safety Testing, *Journal of Biotechnology* 205 (2015) 120–129, DOI: 10.1016/j.jbiotec.2015.01.001

VIII **Franziska Sambale** (100 %), Frank Stahl, Cornelia Kasper, Detlef Bahnemann, Thomas Scheper, Screening-System für Nano-Komposite und Nanomateralien, Issue 8 (2014), nanotechnologie aktuell, Nano- und Materialinnovation Niedersachen e.V. (NMN)

IX Tim H. Lücking (60 %), **Franziska Sambale** (40 %), Birte Schnaars, David Bulnes-Abundis, Sascha Beutel, Thomas Scheper, 3D-printed individual labware in biosciences by rapid prototyping: In vitro biocompatibility and applications for eukaryotic cell cultures, *Engineering in Life Sciences*, 2015. 15(1): p. 57-64, DOI: 10.1002/elsc.201400094

X Tim H. Lücking (70 %), **Franziska Sambale** (30 %), Sascha Beutel, Thomas Scheper, 3D-printed individual labware in biosciences by rapid prototyping: A proof of principle, *Engineering in Life Sciences*, 2015. 15(1): p. 51-56, DOI: 10.1002/elsc.201400093

Vorträge

I 245th ACS National Meeting & Exposition 2013, New Orleans, USA, **Franziska Sambale**, Detlef Bahnemann, Frank Stahl, Thomas Scheper, Novel cellular screening system for nanoparticle safety testing

Poster

I J. Schaeske, A. Winkel , S. Grade, K. Doll, H. Hartwig, A. Lavrentieva, C. Blume, **F. Sambale**, H. Fullriede, G. Zahn S., Schlie-Wolter, E. Fadeeva, D. Bahnemann, B. N. Chichkov, P. Behrens, T. Scheper, M. Stiesch, Cytocompatibility of Innovative Implant Materials, Biofabrication Symposium, Hannover, Germany, 2015

II **Franziska Sambale**, Heiko Richter, Antonina Lavrentieva, Ferdinand Ruedinger, Thomas Scheper, Online monitoring of 3D cell cultures with the help of time lapse microscopy, Focus on Microscopy 2015, Gottingen, Germany, 2015

III **Franziska Sambale**, Jutta Hesselbach, Frank Stahl, Detlef Bahnemann, Arno Kwade, Thomas Scheper, Toxicological Characterization of Nanocomposites, Second Conference of Lower Saxony and Israel, Hannover, Germany, 2015

IV **Franziska Sambale**, Frank Stahl, Cornelia Kasper, Detlef Bahnemann, Thomas Scheper, Cell-based screening-system during nanoparticle development, NMN-Workshop „NANOKOMP– from the development to the production, Braunschweig, Germany 2014

V **Franziska Sambale**, Frank Stahl, Detlef Bahnemann, Thomas Scheper, 3D Cell Culture for nanoparticle safety testing, 3D Cell Culture 2014, Freiburg, Germany, 2014

VI **Franziska Sambale**, Frank Stahl, Detlef Bahnemann, Thomas Scheper, Investigation of the cytotoxic effects of zinc oxide nanoparticles using 3D cell culture models, Advances in Cellular Assays & Cell Culture, Barcelona, Spain, 2014

VII Kathrin von der Haar, Antonina Lavrentieva, **Franziska Sambale**, Frank Stahl, Thomas Scheper, Cornelia Blume, Cell Signature for the tracking of transplanted autologous Cells, Biofabrication for NIFE Cluster-Meeting (Retreat), Hannover, Germany, 2014

VIII Ferdinand Rüdinger, Antonina Lavrentieva, **Franziska Sambale**, Iliyana Pepelanova, Frank Stahl, Thomas Scheper, Cornelia Blume, Development of dynamic three-dimensional cell culture models for *in vitro* biocompatibility testing, Biofabrication for NIFE Cluster-Meeting (Retreat), Hannover, Germany, 2014

IX N. Barth, W. Exner, C. Mette, **F. Sambale**, B. Finke, J. Hesselbach, A. Kockmann, J. Melcher, A-C. Möller, W. Surjoseputro, D. Bahnemann, M. Binnewies, K. Dilger, G. Garnweitner, T. Scheper, M. Sinapius, G. Ziegmann, A. Kwade, NanoKomp – Nanostructured composite materials – from development to the application and production, Nano- und Materialinnovation Niedersachsen e.V. (NMN) Symposium 2013, Hannover, Germany, 2013

X **Franziska Sambale**, Frank Stahl, Detlef Bahnemann, Thomas Scheper, Exposure analysis of nanoparticles on mammalian cell lines, NanoDay, 2013, Hannover, Germany, 2013

XI **Franziska Sambale**, Frank Stahl, Detlef Bahnemann, Thomas Scheper, Real-time impedance analysis of the toxic effect of nanoparticles on mammalian cell lines, First Conference of Lower Saxony and Israel, Hannover, Germany, 2013

XII **Franziska Sambale**, Frank Stahl, Detlef Bahnemann, Thomas Scheper, Real-time impedance analysis of the toxic effect of nanoparticles on mammalian cell lines, 2nd Conference on Impedance-Based Cellular Assays 2013, Budapest, Hungary, 2013

XIII Zhaopeng Li, **Franziska Sambale**, Bernd Tscheschke, Frank Stahl, Ursula Rinas, Thomas Scheper, Production of cytokines for tissue engineering and stem cell culture applications, Rebirth Cluster of Excellence 2013, Hannover, Germany, 2013

XIV **Franziska Sambale**, Frank Stahl, Thomas Scheper, Detlef Bahnemann, Cytotoxic effects of nanoparticles on mammalian cells, Dechema Spring Meeting of Biotechnology 2013, Frankfurt, Germany, 2013

Abkürzungsverzeichnis

2D	zweidimensional, *two-dimensional*
3D	dreidimensional, *three-dimensional*
A549	humane Lungenepithelzelllinie, *carcinomic human alveolar basal epithelial cell line*
AC	Wechselstrom, *alternating current*
AFM	Rasterkraftmikroskop, *atomic force microscopy*
Ag	Silber, *silver*
$AgNO_3$	Silbernitrat, *silver nitrate*
Al_2O_3	Aluminiumoxid, *aluminium oxide*
ANOVA	Varianzanalyse, *ANalysis Of Variance*
APH	saure Phosphatase, *acid phosphatase*
ATP	Adenosintriphosphat, *adenosine triphosphate*
Au	Gold, *gold*
B	Bor, *boric*
BET	Brunauer Emmett Teller
BrdU	Bromdesoxyuridin, *Bromodeoxyuridine*
BUND	Bund für Umwelt und Naturschutz Deutschland e. V
C3A	Komplementfaktoren 3a*, complement component 3a*
C6	Ratten-Hirntumor-Zellen, *rat glioma cells*
Caco-2	humane Darmkrebszellinie, *heterogeneous human epithelial colorectal adenocarcinoma cells*
$CaCO_3$	Calciumcarbonat, *calcium carbonate*
CAD	rechnerunterstütztes Konstruieren*, computer-aided design*
$CaPO_4$	Calciumphosphat, *calcium phosphate*
$CdCl_2.2^{1/2}\ H_2O$	Cadmiumchlorid (hemi-pentahydrat), *cadmium chloride hemi(pentahydrate*
CdS	Cadmiumsulfid, *cadmium sulfide*
CdTe	Cadmiumtellurid, *cadmium telluride*
CeO_2	Cerdioxid, *cerium oxide*
CHARMM	*Chemistry at HARvard Macromolecular Mechanics*
CHO	Zelllinie aus Ovarien des chinesischen Hamsters, *Chinese Hamster Ovary cells*
CHOMACS CD	Kultivierungsmedium für CHO-Zellen, *cultivation medium for CHO cells*
CLP	Einstufung, Kennzeichnung und Verpackung, *Classification, Labeling and Packaging*
CNT	Kohlenstoffnanoröhren, *carbon nanotubes*
CO_2	Kohlenstoffdioxid, *carbon dioxide*
COOH	Carbonsäure, *carboxyl acid*
CPSC	*Consumer Product Safety Commission*
CSS	Kern-Schale-Schale, *core shell shell*
CT	Computertomographie, c*omputed tomography*
CTB	CellTiter-Blue®
Cu	Kupfer, *copper*
CuO	Kupferoxid, *copper oxide*
CV	Bestimmtheitsmaß, *coefficient of variance*
DCF	2',7'-Dichlorodihydrofluorescein-diacetate, *2',7'-Dichlorodihydrofluorescein diacetate*
DLS	*dynamic light scattering*
DMEM	*Dulbecco's Modified Eagle Medium*
DNA	Desoxyribonukleinsäure, d*eoxyribonucleic acid*
DPD	*Dissipative Particle Dynamic*s

DPPC	Dipalmitoyl-Phosphatidyl-Cholin, *dipalmitoylphosphatidylcholine*
DPPG	Diamitoyl-Phosphatidyl-Glycerol, *diamitoylphosphatidylglycerol*
DSMZ	Deutsche Sammlung von Mikroorganismen und Zellkulturen GmbH, *German Collection of Microorganisms and cell cultures*
ECHA	*European Chemicals Agency*
ECIS	*Electric-Cell-Substrate-Impedance-Sensing*
ECM	Extrazellularmatrix, *extracellular matrix*
EDTA	Ethylendiamintetraessigsäure, *ethylenediaminetetraacetic acid*
EDX	Energiedispersive Röntgenspektroskopie, *energy dispersive X-ray spectroscopy*
EFRE	Europäischer Fond für regionale Entwicklung
EFSA	Europäische Behörde für Lebensmittelsicherheit
EG	Europäische Gemeinschaft, *European Community*
EGF	Epidermaler Wachstumsfaktor, *epidermal growth factor*
EGFR	Rezeptor für epidermale Wachstumsfaktoren, *epidermal growth factor receptor*
EL	Belastungsgrenze, *exposure limits*
EPA	*Environmental Protection Agency*
ER	Endoplasmatisches Retikulum, *endoplasmic reticulum*
ESI	elektronische Zusatzinformationen, *electronic supplementary information*
ESI-Q-TOF-MS	*electrospray ionization time of flight mass spectrometry*
EU	Europäische Union, *European Union*
EWG	Europäische Wirtschaftsgemeinschaft, *European Economic Community*
FCS	Fetales Kälberserum, *fetal calf serum*
FDA	*Food and Drug Administration*
FDM	Schmelzschichtung, *fused deposition modeling*
Fe	Eisen, *iron*
FITC	Fluoresceinisothiocyanat, *fluorescein isothiocyanate*
FR	Folatrezeptor, *folate receptor*
GAPDH	Glycerinaldehyd-3-phosphat-Dehydrogenase, *glyceraldehyde 3-phosphate dehydrogenase*
GROMOS	*GROningen MOlecular Simulation computer program package*
GTP	Guanosintriphosphat, *guanosine-5'-triphosphat*
HaCaT	Keratinozyten- Zelllinie, *keratinocyte cell line*
hAD	human adipös, *human adipose*
HCI-H292	humane Lungenkrebsepithelzelllinie, *mucoepidermoid pulmonary carcinoma epithelial cell line*
HCl	Salzsäure, *hydrochloric acid*
HeLa cells	humane Eierstockkrebszelllinie, *human adenocarcinoma epithelial cell line*
HEPES	2-(4-(2-Hydroxyethyl)-1-piperazinyl)-ethansulfonsäure, *4-(2-hydroxyethyl)-1-piperazineethanesulfonic acid*
HepG2	humane hepatozelluläre Karzinomzellinie, *hepatocellular carcinoma cells*
HK-3	Hexokinase 3, *hexo kinase 3*
HPA	Helixpomatia Agglutinin, *helix pomatia agglutinin*
HPRT	Hypoxanthin-Guanin-Phosphoribosyltransferase, *hypoxanthine-guanine phosphoribosyltransferase*
HS	Humanserum, *human serum*
Hsp70	Hitzeschockprotein 70, *heat shock protein 70*
HUVEC	humane Nabelvenen-Endothelzellen, *Human Umbilical Vein Endothelial Cells*
IC_{50}	inhibitorische Konzentration, *inhibitory concentration*
iCAM-1	intrazelluläres Adhäsionsmolekül, *Intercellular Adhesion Molecule 1*
Il-8	Interleukin-8, *interleukin-8*

ISO	Internationale Organisation für Normung, *International Organization for Standardization*
JRC	*European Commision Joint Research Centre*
KCl	Kaliumchlorid, *potassium chloride*
KH_2PO_4	Kaliumdihydrogenphosphat, *potassium dihydrogen phosphate*
k_LA	volumenbezogener Stoffübergangskoeffizient, *volumetric mass transfer coefficient*
La_2O_3	Lanthanoxid, *lanthanum oxide*
LDH	Lactatdehydrogenase, *lactate dehydrogenase*
LDL	Lipoprotein niedriger Dichte, *low density lipoprotein*
LDLR	Rezeptor für Lipoproteine niedriger Dichte, *low density lipoprotein receptor*
MAPK	Mitogenaktivierte Proteinkinase, *mitogen-activated protein kinase*
MEM-α	Minumum Essential Medium Alpha
Mg	Magnesium, *magnesium*
MMP	Matrix-Metalloproteasen, *matrix metallopepitdases*
MPA	3-Mercaptopropionsäure, *3-mercaptopropionic acid*
mRNA	messe*nger ribonucleic acid*
MRT	Magnetresonanztomographie, *magnetic resonance imaging*
MSC	Mesenchymale Stammzelle, *mesenchymal stem cells*
MTT	3-(4,5-Dimethylthiazol-2-yl)-2,5-Diphenyltetrazoliumbromid, *3-(4,5-dimethylthiazol-2-yl)-2,5-diphenyltetrazolium bromide*
MWCO	Molekulargewichts-Grenze, *molecular weight cutoff value*
PES	Polyethersulfon, *polysulfone*
Na_2HPO_4	Dinatriumhydrogenphosphat, *disodium hydrogen phosphate*
Na_2TeO_3	Natriumtellurit, *sodium tellurite*
NAA	Neutronenaktivierungsanalyse, *neutron activation analysis*
$NaBH_4$	Natriumborhydrid, *sodium borohydride*
NaCl	Natriumchlorid, *sodium chloride*
NAD	Nicotinamidadenindinukleotid, *nicotinamide adenine dinucleotide*
NaOH	Natriumhydroxid, s*odium hydroxide*
NICNAS	*National Industrial Chemicals Notification and Assessment Scheme*
NIH-3T3	Mäusefibroblastenzelllinie, *murine fibroblast cell line*
NiO	Nickeloxid, *nickel(II) oxide*
NIOSH	*National Institute for Occupational Safety and Health*
NLS	Kernlokalisierungssignal, *nuclear localization signal*
NNI	*National Naotechnology Initiative*
NOAC	höchste Testkonzentration ohne beobachtete Wirkung, *No Observed Adverse Effect Concentration*
NP	Nanopartikel, *nanoparticles*
NPC	Kernpore, *nuclear pore complex*
OD	Optische Dichte, *optical density*
OECD	*Organisation for Economic Co-operation and Development*
OEL	Arbeitsgrenzwerte, *occupational exposure limit*
OSHA	*Occupational Safety and Health Administration*
P/S	Penicillin/Streptomycin, *penicillin/streptomycin*
PA	Polyamid*, polyamide*
PAK	Proteinkinase, *protein kinase*
PAS	Perjodidsäure, P*eriodic acid schiff*
PBS	Phosphatgepufferte Salzlösung, *phosphate buffered saline*
PC-12	Rattennebennieren-Zelllinie, *rat adrenal gland cells*
PCR	Polymerase-Kettenreaktion, *polymerase chain reaction*

PDMS	Polydimethylsiloxane, *polydimethylsiloxane*
PEG	Polyethylenglycol, *polyethylene glycol*
PI	Propidiumiodid, *propidium iodide*
PLGA	Polylactic-co-Glycolid, *poly(lactic-co-glycolic acid)*
PS-COOH	Carboxyl-modifiziertes Polystyren, *carboxyl-modified polystyrene*
PVAL	Polyvinylalkohol, *poly(vinyl alcohol)*
QD, Qdot	Quantenpunkt, *Quantum Dots*
qPCR	quantitative Echtzeit-PCR, *quantitative real-time PCR*
REACH	Registrierung, Bewertung, Zulassung,Beschränkung, *Registration, Evaluation, Authorisation, Chemicals*
REL	Empfohlene Grenzwerte, *recommended exposure limit*
RNA	Ribonukleinsäure, *ribonucleic acid*
ROS	Reaktive Sauerstoffspezies, *reactive oxygen species*
RP	schnelle Prototypentwicklung, *rapid prototyping*
RPMI	Roswell Park Memorial Institute (Zellkulturmedium)
Ru	Ruthenium, *ruthenium*
S/N	Signal-Rausch-Verhältnis, *signal-to-noise*
SCENIHR	*Scientific Commitee on Emerging and Newly Identified Health Risks*
SD	Standardabweichung, *Standard deviation*
SDS	Natriumdodecylsulfat, *sodium dodecyl sulfate*
SEM	Rasterelektronenmikroskop, *scanning electron microscope*
SiO_2	Siliziumdioxid, *silicon dioxide*
SLS	Selektives Lasersintern, *selective laser sintering*
SMMC-7721	humane Leberkrebszellline, *human hepatoma cells*
SRHA	Huminsäure, Suwannee River humic acids
SSC	Seitwärtsstreulicht, *Side Scatter*
SU	Einweg, *single-use*
SWCNT	Einwandige Kohlenstoffröhren*, Single-Wall Carbon Nanotubes*
TEM	Transmissionselektronenmikroskopie, *transmission electron microscopy*
TfR	Transferrin, *transferrin*
TfR	Transferrin Rezepetor, *transferrin receptor*
Thp-1	humane Monozyten-Zelllinie, *human monocytic cell line*
TiN	Titannitrid, *titanium nitride*
TiO_2	Titandioxid, *titanium dioxide*
TLC	Lethalkonzentration, *Total Lethal Concentration*
TPP	trans-proteomische Leitung, *trans proteomic pipeline*
TSCA	*Toxic Substances Control Act*
USP	United States Pharmacopeia
UV	ultraviolett, *ultraviolet*
VHP	verdampftes Wasserstoffperoxid, *Vaporized hydrogen peroxide*
VO	Verordnung
w eq	mit Äquilibrierung, *with equilibration*
w/o eq	ohne Äquilibrierung, *without equilibration*
WPMN	*Working Party on Manufactured Nanomaterials*
WPN	*Working Party on Nanotechnology*
WST-1	4-(3-(4-Iodophenyl)-2-(4-Nitrophenyl)-2H-5-Tetrazolio)-1,3-Benzenedisulfonat, *4-[3-(4-iodophenyl)-2-(4-nitrophenyl)-2H-5-tetrazolio]-1,3-benzene disulfonate (water soluble tetrazolium)*
Z-DEVD-R110	Bis-(N-CBZL-Aspartyl-L-Glutamyl-L-Valyl-L-Aspartsäureamide, *glutamyl-L-valyl-L-aspartic acid amide*
$ZnCl_2$	Zinkchlorid, *zinc chloride*

ZnO	Zinkoxid, *zinc oxide*
ZnS	Zinksulfid, *zinc sulfide*
ZrO_2	Zirkoniumdioxid, *zirconium dioxide*

Tabellenverzeichnis

Abbildungsverzeichnis

Inhaltsverzeichnis

1 Einleitung und Zielsetzung

1.1 Einleitung

Die Nanopartikel haben viele Industrie- und Konsumprodukte revolutioniert und sind mittlerweile vollständig in unser alltägliches Leben integriert. Die Anwendungsmöglichkeiten der Nanopartikel sind nahezu unbegrenzt. Bereits 1959 demonstrierte Richard Feynmann mit seinem Vortrag "*There's Plenty of Room at the Bottom*", welches enorme technologische Potential in der Anwendung von nanopartikulären Strukturen und Materialien geschaffen werden könnte. Aber worin besteht das Geheimnis der Nanopartikel? Als Nanopartikel werden Materialien bezeichnet, die weniger als ein Zehntel Mikrometer groß sind. Oder anschaulicher ausgedrückt, ein Stecknadelkopf ist ca. 10.000fach größer als ein Nanopartikel. Es ist also offensichtlich, dass man sie mit bloßen Augen nicht sehen kann. Ihr Geheimnis ist also ihre Größe, so dass sie nur mit hochauflösenden Mikroskopen sichtbar gemacht werden können.

Doch warum faszinieren die Nanopartikel die Wissenschaftler? Die winzigen Materialien haben im Gegensatz zu den „großen" Partikeln, vor allem bedingt durch ihr Oberflächen-Volumen-Verhältnis, andere Eigenschaften. Den Produkten werden z.B. verbesserte mechanische, elektrische, optische, chemische und antibakterielle Eigenschaften verliehen. Wissenschaftler ersehnen sich Lösungen für derzeit noch ungeklärte Probleme in der Krebstherapie oder für die Entwicklung von Ressourcen-schonenden und effizienten Energietechniken. Bisher werden Nanopartikel in der Medizintechnik als Träger von Wirkstoffen, in der Kosmetik als UV-Filter in Sonnencremes oder in der Textilindustrie als antimikrobielle und geruchshemmende Zusätze eingesetzt. Es scheint, dass mit den Nanopartikeln plötzlich alles denkbar und lösbar ist.

Doch vor lauter Euphorie wurde die Risikobewertung der Nanoprodukte vernachlässigt. Der rasche Fortschritt der Nanotechnologie hat somit vorab eine umfassende Sicherheitsanalyse eingebüßt. Die Nanopartikel könnten sich z.B. aus den Produkten herauslösen und somit mit dem Menschen in Kontakt kommen oder über Emissionen in die Umwelt gelangen. Zu wenig ist bekannt über die möglichen gesundheitlichen Gefahren, einschließlich der konkreten Umweltbelastung. Es fehlen Detektionsmethoden, Grenzwerte und umfangreiche Daten über die Kurz- und Langzeitwirkung auf den Menschen sowie auf die komplexen Ökosysteme. Nur damit können spezielle Gesetze abgeleitet werden. Die folgenden Fragstellungen sind hier richtungsweisend: Können sich Nanopartikel im Lebewesen anreichern? Welche Folgeschäden sind zu erwarten? Welche Konzentrationen am Arbeitsplatz oder beim Konsumenten sind kritisch?

Für den langfristigen Erfolg der Nanotechnologie müssen diese Fragen dringend hinreichend geklärt werden. Gerade in der heutigen Zeit, in der uns die Folgen von unzureichenden Sicherheitskontrollen, bedingt durch den reinen Idealismus, wieder einholen, sollte aus der Vergangenheit gelernt werden. Es sind Strategien zu entwickeln mit denen die vielfältigen Nanoprodukte und -materialien standardisiert

toxikologisch untersucht werden können. Vor allem die spezifischen Eigenschaften der Nanopartikel wie Größe, Oberfläche, Stabilität, Agglomeration und die chemische Modifikation sollten genau berücksichtigt werden. Die innovativen Versuchsmodelle sollten möglichst realistisch die Bedingungen im menschlichen Organismus simulieren. Auf diese Weise könnte zukünftig der Einsatz von Tierexperimenten reduziert werden. Insgesamt sind schnelle, effiziente und detaillierte Testmethoden für eine fundierte Risikoeinschätzung die Erfolgsgaranten, die das vorzeitige Ausbremsen neuer Nanopartikel-Innovationen verhindern.

Zudem muss ein Dialog zwischen Wissenschaftlern und Bevölkerung geschaffen werden, so dass diffuse Ängste und Befürchtungen der Konsumenten sensibel wahrgenommen und eliminiert werden. Bei der Gentechnologie z.B. wurde diese Kommunikation versäumt, so dass die Vorteile der Technologie in den Hintergrund gerieten und Bedenken medienwirksam geschürt werden konnten. Daher ist es immens wichtig bei der Nanotechnologie, die Journalisten und die Bevölkerung mehr am Kenntnisstand der Wissenschaftler teilhaben zu lassen und sie zu integrieren.
Insgesamt ist für eine zukunftsorientierte Forschung eine Balance zu schaffen zwischen der wissenschaftlichen Neugier und einem zielgerichteten Risikomanagement.

1.2 Zielsetzung

Ziel der vorliegenden Arbeit ist es, die derzeitige Risikobewertung der Nanoprodukte zu optimieren, so dass eine umfangreiche, detaillierte und vor allem standardisierte Untersuchung der Nanomaterialien ermöglicht wird. Es soll eine Strategie konzipiert werden, mit der die Wirkung von einer Vielzahl von Nanoprodukten und deren Vorläufern analysiert werden kann. Die *in-vitro*-Testung soll so optimiert werden, dass der Einsatz von Tierexperimenten für die Risikoanalyse der Nanomaterialien minimiert werden kann. Hierfür soll ein hierarchisches *Screening*-System aufgebaut werden, bei dem der Umfang und die Sensitivität der eingesetzten Methoden sowie die Komplexität der Zellsysteme zunehmen. Dabei sollen Methoden zur Bestimmung der Stoffwechselaktivitäten in den Zellen optimiert, standardisiert und auf ihre Sensitivität überprüft werden. Es sollen verschiedene Zellsysteme in das *Screening*-System integriert werden, die die physiologischen Bedingungen im menschlichen Organismus besser simulieren können. Hierfür sollen dreidimensionales Zellwachstum und dynamische Kultivierungsbedingungen zum Einsatz kommen. Zinkoxid- und Titandioxid-Nanopartikel dienen als Benchmark-Partikel, die das entwickelte *Screening*-System exemplarisch durchlaufen sollen.

Die vorliegende Arbeit ist in fünf Kapitel gegliedert, deren Ergebnisse in international anerkannten Fachzeitschriften veröffentlicht bzw. zur Veröffentlichung eingereicht sind. Jeder Veröffentlichung ist eine deutsche Zusammenfassung vorangestellt, die die wesentlichen Erkenntnisse darstellt. Zunächst wird das entwickelte *Screening*-System für Nanopartikel beschrieben. Dieses ist hierarchisch aufgebaut und in *Pre*-, *Fine*- und *Complex-Screening* gegliedert. In jeder Hierarchieebene werden unterschiedliche Methoden und Zellsysteme eingesetzt. In dem Kapitel wird zudem demonstriert, dass

das gesamte entwickelte *Screening-System* auch für die Testung von weiteren Materialien anwendbar ist. So kann es auch für die Biokompatibilitäts-Testung von Materialien für das 3D-Druckverfahren oder für Medizinprodukte verwendet werden kann.

In den folgenden Kapiteln werden mögliche Erweiterungen des *Screening-Systems* vorgestellt. Es wird detailliert auf einige Zellsysteme und Methoden eingegangen, die in das *Screening*-System integriert werden sollten. Beim *Screening* ist zu berücksichtigen, dass sich bei Metall-Nanopartikeln Ionen ablösen können. Daher wurden Silber-Nanopartikel sowie Silber-Ionen mit verschiedenen Methoden des *Pre-* und *Fine-Screenings* separat untersucht. Um das *Complex-Screening* weiter aufzubauen und zukünftig den Einsatz von Tierexperimente bei der Materialtestung minimieren zu können, wurden verschiedene Kultivierungsbedingungen erprobt. Es folgen zwei Kapitel über komplexe Zellsysteme, die im letzten Schritt des *Screening*s eingesetzt werden sollen. Hierbei werden Unterschiede der Zellantwort von zweidimensionalen und dreidimensionalen Sphäroid-Zellkulturen untersucht. Des Weiteren ist der Einfluss von dynamischen Kultivierungsbedingungen auf die Nanopartikelexposition aufgeführt. Abschließend wird im letzten Kapitel die prozessbegleitende Anwendung des *Screening*-Systems für die Entwicklung von nanopartikulären und hydrophoben Sanitärkeramiken gezeigt. Auf diese Weise kann durch die parallele Toxizitätstestung die Produktion von Nanokompositen gesteuert werden.

2 Theoretische Grundlagen

2.1 Perspektiven und Anwendungen von Nanopartikeln

Die Nanotechnologie ist eine der am schnellsten wachsenden Industrien weltweit [1]. Für Wissenschaftler, Politiker und Verbraucher ist sie daher gleichermaßen von großem Interesse. Im Vergleich zu den Bulkchemikalien sind Nanopartikel mit einer Größe von 1-100 nm deutlich kleiner, so dass ihre Oberfläche im Verhältnis zum Volumen größer ist [2]. Daher ergeben sich erweiterte magnetische, elektrische, optische, mechanische und strukturelle Eigenschaften [2]. Aufgrund ihrer besonderen Disposition finden sie Anwendung in über 1.800 Konsumgütern (Stand 2014) [3]. Sie kommen zum Einsatz in der Industrie, bei Farben und Lacken, im Energie- und Umweltsektor und in der Landwirtschaft [4]. Zudem werden sie in der Medizin und in der Kosmetik [5] sowie in der Lebensmittel- [4] und Textilindustrie [6] eingesetzt (Tab. 2-1). Die breite Anwendung zeigt auf, dass die Nanotechnologieprodukte vollständig im alltäglichen Leben integriert sind. Eine detaillierte Übersicht über die häufigsten Anwendungsbereiche der verschiedenen Nanopartikel ist in Tab. 2-1 zusammengestellt. Die weltweite Produktion von Cerdioxid (CeO_2), Eisenoxid-, Aluminiumoxid (Al_2O_3)- und Zinkoxid (ZnO)-Nanopartikeln und Kohlenstoffnanoröhren (*Carbon nanotubes*, CNT) wurde auf 100-1.000 t/Jahr und für Titandioxid (TiO_2)-Nanopartikel sogar auf 10.000 t/Jahr geschätzt [7].

In der Industrie- und Automobilbranche verbessern Nanomaterialien die mechanischen Eigenschaften wie Elastizität, Bruch- und Kratzfestigkeit und Härte von Baustoffen und Bauteilen [8]. Außerdem können selbstreinigende Fensterscheiben und Oberflächen erzeugt werden. In der Automobil-Branche kommen Nanopartikel z.B. bei der Herstellung der Reifen sowie bei Beschichtungen und in der Elektronik zum Einsatz [8]. Bei Farben und Lacken soll das Anwachsen von Mikroorganismen, Algen und Flechten auf Häuserfassaden oder anderen behandelten Oberflächen minimiert werden. Diese antimikrobielle Eigenschaft wird durch Nanopartikel wie Silber (Ag), Kupfer (Cu), Siliziumdioxid (SiO_2) und TiO_2 erreicht [9]. In Europa werden für die Farbherstellung 35 % der Ag-Nanopartikel-Produktion und 25 % der TiO_2-Nanopartikel-Produktion verwendet [10]. Die Ag-Nanopartikel interagieren mit der Zellwand der Bakterien, binden an Proteine und induzieren den Zelltod [9]. Das photokatalytisch aktive TiO_2 generiert unter UV-Beleuchtung Hydroxyl-Radikale, die das Wachstum der Mikroorganismen hemmen. Des Weiteren werden die mechanischen Eigenschaften der Farben und Lacke durch den Einsatz von Nanopartikeln optimiert [9]. Vor allem SiO_2 verbessert die Kratzbeständigkeit, den Schutz vor Verätzung und verleiht Lacken ihren Glanz [9]. Nanopartikel werden als Katalysatoren, für Beschichtungen in Solarzellen, für die Brennstofferzeugung sowie als Kraftstoff- oder Klebstoffzusatz eingesetzt [11]. In der Elektronik werden sie zudem bei Schaltungen und Batterien verwendet [12]. Bei der Luft- und Wasserfiltration werden die Nanopartikel aufgrund ihrer antimikrobiellen Wirkung integriert [12, 13].

Tab. 2-1 Übersicht über die wichtigsten Anwendungsbereiche von Nanopartikeln.
Abkürzungen: Kohlenstoffnanoröhre (carbon nanotubes, CNT), Polyvinylalkohol (PVAL), Polylactid-co-Glycolid (PLGA,) Quantum Dots (QD)

Bereich	Anwendung und Wirkung	Partikel
Industrie und Automobil	Autoreifen (Stabilität, Dehnbarkeit, Rollwiderstand)	CNT, SiO_2 [8]
	Nanokomposite (Härte, Bruchfestigkeit, Elastizität, Dehnbarkeit)	CNT, SiO_2, TiO_2 [8], ZnO [8, 14], ZrO_2, [8]
	Schmutzabweisend	TiO_2 [8]
Farben und Lacke	Antimikrobiell	Ag [9, 15], CuO, SiO_2, TiO_2 [9, 16]
	Optimierte Reinigung (hydrophob)	SiO_2 [17, 18], TiO_2 [8, 9]
	Kratz- und Säurebeständigkeit, Stabilität	CNT [8], SiO_2, TiO_2 [8, 9], ZnO, ZrO_2 [8]
Energie	Katalysatoren, Brennstoffzelle	Ag [16], Au [19], $BaCO_3$ [20], Cu/Ag [21], CuO [16], Pt [21-23], Pt/Au [16, 21], Pt/Ru [24], Silicon, TiO_2 [16]
	Solarenergie	SiO_2 [17], ZnO [25-27], ZnO/TiO_2 [28, 29]
	Kraftstoffzusatz	Al [30, 31], B [31], CeO_2 [32, 33], CNT [33], Fe [31], La_2O_3 [34]
	Mikroelektronik	Ag, CuO [12], TiO_2[35], ZnO [35, 36]
Umwelt	Luftfilter	Ag, CuO [12]
	Wasserfilter	Al_2O_3, CNT, CuO, Fe-Oxid, TiO_2, ZrO_2 [37]
Medizin	Wirkstofftransport	Al [38], Albumin [39], Au [40-44], $CaPO_4$ [38], CeO_2, CNT [40-44], Fe-Oxid [45], Liposom [38, 44, 46, 47], PLGA [48], Polymer [38, 44], QD, Silica, Ti [38], ZnO [49, 50]
	Therapie	Ag [51], Au [41, 42, 52-55], QD [56-58], ZnO [50, 59]
	Antimikrobiell	Ag [2, 60]
	Implantate	TiO_2 [61]
	Detektion/Markierung	Ag [62], Au [42, 52, 53, 55, 63, 64], Fe-Oxid [38, 65-67], QD [38, 41, 56, 68, 69], ZnO [70-72]
Kosmetika	UV-Schutz	TiO_2 [16, 73-75], TiO_2/ZnO [76], ZnO [74, 77, 78] CuO [12]
	Schutz vor Metallionen	$CaCO_3$, $CaPO_4$ [79], Fulleren [80]
	Antimikrobiell	Ag, Au [74, 81], Cu-SiO_2, ZnO [74]
	Antifalten	Al_2O_3 [74], Dendrimer, Fullerene [80]
Lebensmittel	Zusätze (Konservierung, Farbstoff, Struktur)	Ag, Liposom, SiO_2, TiO_2 [82, 83],
	Verpackungen (inert, antibakteriell)	Ag [82, 84], CNT, SiO_2, [84], TiN [82], TiO_2 [83], ZnO [82, 84]
Textilien	Antimikrobiell	Ag [60, 85, 86]
	Wasser-/Schmutzabweisend	SiO_2, [18], TiO_2 [87]
	Wärmeisolierung	CNT [87], PVAL [88]
	Strapazierfähigkeit, Schutz	Al_2O_3, CNT, SiO_2, ZnO [87], ZnO [89]

In der Medizin werden Nanopartikel für den gezielten Wirkstofftransport sowie für therapeutische Zwecke verwendet [46]. Ziel der therapeutischen Strategien ist der gerichtete Wirkstofftransport zu

einem spezifischen Organ, Gewebe, einer Zelle oder einem Zellorganell [44]. Nanopartikel sollen mit bestimmten Liganden funktionalisiert werden, so dass diese von bestimmten Zellen aufgenommen werden und/oder ein definiertes Zielorganell erreichen [44]. Auch der Transport der Nanopartikel innerhalb der Zelle soll kontrolliert werden, da z.B. nicht alle Nanopartikel in dem sauren Milieu der Endosomen stabil vorliegen [44].

Viele Studien belegen, dass mit markierten Nanopartikeln ein besserer therapeutischer Effekt erzielt werden kann als mit nicht markierten. Daher sollen Nanopartikel an bestimmte Rezeptoren binden wie die Folat-, die Transferin-, die epidermalen Wachstumsfaktor- sowie die G-Protein-gekoppelten Rezeptoren [90]. Diese Rezeptoren werden von kranken Zellen verstärkt exprimiert [90]. Des Weiteren können Nanopartikel die Sensitivität von bildgebenden Verfahren wie der Röntgen Computertomographie oder der Magnetresonanztomographie (MRT) erhöhen und bestimmte Regionen im Organismus markieren [46]. Für die Markierung von zellulären Strukturen sind vor allem Quantum Dots (QD) geeignet, die eine hohe Fluoreszenzintensivität aufweisen [38]. Als QD werden Nanopartikel bezeichnet die aus einem Halbleitermaterial, wie beispielswiese Cadmium, bestehen und quantenmechanische Eigenschaften haben [41]. Die Elektronen der QD können nur diskrete Energiezustände annehmen [38]. Durch die Bindung von rekombinanten epidermalen Wachstumsfaktoren an superparamagnetische Metalloxid-Nanopartikel konnte die Bildgebung mittels MRT deutlich verbessert werden [65]. Forschungsergebnisse zeigen dabei auch ein hohes Potential für Nanopartikel bei der fotothermischen oder fotoakustischen Therapie. Zusätzlich finden Nanopartikel bei Implantaten zur Erhöhung der Proliferation und Differenzierung Anwendung [61]. Bei Medizinprodukten wie Wundsprays oder medizinischen Verbandsmaterial kommen zudem Ag-Nanopartikel aufgrund ihrer antibakteriellen Wirkung zum Einsatz [2]. Auch in Textilien wird diese Eigenschaft der Ag-Nanopartikel genutzt [60]. Außerdem werden Textilien durch Nanopartikel schmutzabweisender, wärmeisolierender und strapazierfähiger [3]. In Kosmetika und Pflegeprodukten liefern Nanopartikel UV-Schutz, reduzieren Falten und wirken z.B. in Zahnpasta antibakteriell [12, 73]. Auch in Lebensmittelzusätzen oder auch bei Lebensmittelverpackungen kommen Nanopartikel zum Einsatz [3, 60].

2.2 Regularien für Nanomaterialien

Neben dem enormen gesellschaftlichen Nutzen der Nanotechnologie muss auch die Sicherheit für Mensch und Umwelt gewährleistet sein. Eine zentrale Rolle bei der Risikoeinschätzung von Nanomaterialien ist deren Klassifizierung. Um Regularien und rechtliche Bestimmungen für den Umgang dieser Materialien auf nationaler und internationaler Ebene festlegen zu können, bedarf es einer genauen Definition. Im Oktober 2011 veröffentlichte daher die Europäische Kommission ein Empfehlungsschreiben [91], unterstützt durch die Berichte der *European Commisison Joint Research Centre* (JRC) und der wissenschaftlichen Ausarbeitung des *Scientific Commitee on Emerging and Newly Identified Health Risks* (SCENIHR) [92]. Darin werden Materialien als nanopartikulär

bezeichnet, sobald mehr als 50 % der Partikel eine Größe zwischen 1-100 nm aufweisen [91]. Dies gilt für Partikel im ungebundenen Zustand sowie für Agglomerate und Aggregate [91]. Ergänzend kann die Oberflächengröße von 60 m^2/cm^3 nanopartikuläre Strukturen von Materialien anzeigen, die größer als 100 nm sind [91, 92]. Die Deklaration von Nanomaterialien aufgrund ihrer Größe, deren Größenverteilung sowie der Oberflächengröße wird jedoch stark kritisiert [92]. Obwohl in vielen Richtlinien dieser Größenbereich angegeben wird, gibt es keine definierte Größe ab der sich die physiochemischen Eigenschaften ändern [92]. Die Größengrenze von 100 nm ist willkürlich gewählt und ist eher politisch als wissenschaftlich begründet [92].

Diverse Beispiele verdeutlichen, dass die Definitionskriterien zukünftig angepasst werden müssen. Die TiO_2-Nanopartikel zum Beispiel, die in Lebensmitteln als E171 gezeichnet werden, weisen eine durchschnittliche Größe von 110 nm auf und werden daher nicht als Nanomaterial definiert [92, 93]. Dabei sind 36 % der Partikel kleiner als 100 nm und könnten Auswirkungen auf den Menschen haben [92, 93]. Neben dem Definitionsbereich sollten zudem die Messmethoden für die chemische Zusammensetzung, Größe, Oberflächengröße und den Agglomerationsstatus geregelt und vereinheitlicht werden [92]. Da die Partikelgrößenverteilung von der Messmethode abhängt und sich die BET-Oberflächen nur von Pulvern bestimmen lassen, werden weitere Messmethoden entwickelt [92]. Um die Bedingungen am Arbeitsplatz von Industriearbeitern vollständig charakterisieren zu können, sind präzise Messgeräte und Messmethoden erforderlich [94]. Derzeitige werden unterschieden in direkte Messmethoden, bei denen die aktuelle Konzentration ermittelt wird und in zeitabhängige Methoden, bei denen über einen bestimmten Zeitraum Material gesammelt wird [94]. Außerdem beziehen sich die Richtlinien nur auf die ursprünglichen Partikel. Dabei können sich Partikel und Materialien während ihres Lebenszyklus verändern, indem sie agglomerieren, an andere Materialien binden oder sich z.B. ihre chemische Oberfläche verändert [92]. Die Formulierung im Nanoprodukt kann demnach andere Eigenschaften aufweisen. Für eine Risikoeinschätzung ist der existierende Definitionsbereich und die Messmethode nicht ausreichend, vielmehr muss das Risiko im Gesamtkontext begutachtet werden.

Die Definition der Nanomaterialien entscheidet über die politische Regelung, denn nur darüber können Verordnungen und Gesetze in Zukunft geltend gemacht werden. Hierüber können schließlich die Risiken eingeschätzt werden. Materialen, die als nanopartikulär eingestuft werden, sollten dementsprechend anderen Richtlinien unterliegen. Derzeit bestehen auf nationaler und internationaler Ebene wenig rechtliche Bestimmungen, die speziell für den Umgang und die Herstellung der Nanomaterialien ausgerichtet sind. Nachfolgend sind die wichtigsten europäischen Verordnungen und Richtlinien für die Verwendung von Nanomaterialien aufgeführt. Da Nanopartikel sehr vielseitig eingesetzt werden, sind auch viele Rechtsbereiche betroffen [95]. Regularien sind vor allem für Lebensmittel, Lebensmittelkontaktmaterialien, Kosmetika, Arzneimittel und Medizinprodukte

notwendig [95]. Des Weiteren sind Bestimmungen für Biozide, Pflanzenschutzmittel, Tiernahrung, Arbeitsschutz und Umweltschutz erforderlich [95].

Für Chemikalien regelt die REACH-Verordnung (VO (EG) Nr. 1907/2006) die Herstellung, das Inverkehrbringen und die Anwendung [95]. Nanomaterialien werden von der REACH-Verordnung eingeschlossen, wobei die Bewertung in der Verantwortung der Hersteller liegt [95]. Für die Nanomaterialien gelten daher größtenteils die gleichen Richtlinien wie für die Bulkchemikalien, wobei sich die Eigenschaften, vor allem bedingt durch die sehr geringe Größe, stark unterscheiden. Auch die CLP-Verordnung (*Classification, Labeling and Packaging*, VO (EG) 1272/2008) enthält keine expliziten Regelungen für die Kennzeichnung von Nanomaterialien [95].

Lebensmittelzusätze werden durch die Verordnung EG Nr. 258/97 geregelt, in der jedoch Nanomaterialien kaum erfasst werden [95]. Erneuerungen sind hier ebenso vorgesehen wie die Einführung der Kennzeichnungspflicht [95]. Nach der Verordnung (EG) Nr. 178/2002 dürfen Lebensmittel mit nanopartikulären Zusätzen in Verkehr gebracht werden [95]. Zukünftig soll die Sicherheit von einigen Lebensmittelzusatzstoffen neu bewertet werden (VO (EG) 1333/2008) [95]. Lebensmittelzusätze wie auch TiO_2 sollen daher 2020 neu evaluiert werden [92]. Für Lebensmittelkontaktmaterialien muss ausgeschlossen werden, dass sich Stoffe ablösen können (VO (EG) 1935/2004, 10/2011, 450/2009, Richtlinien 2007/42/EG) [95].
Die Verwendung von Nanomaterialien in Kosmetika ist in der Verordnung EG 1223/2009 enthalten, wobei viele Regelungen erst 2013 in Kraft getreten sind [95]. Es wird vorgeschrieben die Identität der Nanomaterialien, die Menge, die Sicherheitsdaten sowie die Expositionsbedingungen anzugeben [95]. Aufgrund der chemischen Zusammensetzung und des Einsatzes von Nanopartikeln in Sonnencremes wird gefordert, dass diese nach der europäischen CLP-Verordnung gekennzeichnet werden [1].
Die Richtlinien für Arzneimittel (2001/83/EG) und Medizinprodukte (90/385/EWG, 93/42/EWG, 98/79/EG) werden als sehr umfassend eingeschätzt [95]. In der Medizin ist die Unterscheidung zwischen Arzneimitteln und Medizinprodukten, die Nanopartikel enthalten, jedoch erschwert [95]. Zukünftig sollten die Regularien weiter auf Nanomaterialien und deren besonderen Eigenschaften spezialisiert werden [95].
Vorgaben für die Zulassung von Pflanzenschutzmitteln sind in der Pflanzenschutz-Verordnung (EG 1107/2009) geregelt, die jedoch keine Sonderregeln für Nanomaterialien enthält [95]. Auch in der Biozid-Richtlinie 98/8/EG werden Nanomaterialien nur indirekt erfasst [95]. Nach der neuen Verordnung (EU 528/2012) sind Nanomaterialien zukünftig kennzeichnungspflichtig und Erfahrungsberichte im Umgang mit den Biozid-Produkten werden gefordert [95].
Für den Arbeitsschutz besteht die Richtlinie 89/391/EWG, die laut Kommission Nanomaterialien miteinschließt [95]. Zusätzlich wird in Einzelrichtlinien der Schutz der Arbeiter geregelt (89/655/EG, 98/24/EG, 99/92/EG, 2004/37/EG) [95]. Die möglichen Aufnahmewege der Nanopartikel sollten für den Arbeitsschutz untersucht werden, um das potenzielle Risiko abschätzen zu können [96].

Für den Umweltschutz bestehen diverse Richtlinien (91/686/EWG, 96/82/EG, 2000/60/EG, 2006/12/EG, 2006/118/EG, 2008/1/EG, 2008/98/EG, 2010/75/EU), die jedoch nicht explizit auf die Nanomaterialien eingehen [95]. Zukünftig sind Änderungen der Richtlinien erforderlich, gerade in Bezug auf das EU-Abfallverzeichnis für Nanomaterialien [95].

Neben den europäischen Regelungen und Initiativen für den Umgang mit Nanomaterialien gibt es auch internationale Strategien. Die *Organisation for Economic Co-operation and Development* (OECD) gründete die OECD *Working Party on Nanotechnology* (WPN) sowie die OECD *Working Party on Manufactured Nanomaterials* (WPMN) [95]. Die WPN beschäftigt sich mit politischen Themen, während die WPMN den Fokus auf die Risikoeinschätzung der Nanomaterialien legt [95]. In der OECD-Datenbank (*Datenbank on Research into Safety of Manufactured Nanomaterials)* werden die Forschungsprojekte weltweit zur Risikoeinschätzung von Nanomaterialien gesammelt [95]. In den USA z.B. haben sich in den letzten Jahren diverse Regierungsorganisationen gebildet [95]. Die *National Nanotechnology Initiative* (NNI) beschäftigt sich seit 2001 mit den Auswirkungen der Nanotechnnologie auf Umwelt, Gesundheit und Sicherheit [95]. Ziel der NNI ist es, die Forschung und Entwicklung von Nanopartikeln zu optimieren und die Forschungsgruppen besser miteinander zu vernetzen [96]. Zudem werden die Risiken der Nanomaterialien von den bestehenden Organisationen wie der *Food and Drug Administration* (FDA), der *Environmental Protechtion Agency* (EPA), der *Occupational Safety and Health Administration* (OSHA) und der *Consumer Product Safety Commission* (CPSC) untersucht [95]. Laut der OSHA liegt z.B. die maximale Luftbelastungsgrenze von Nanopartikeln für den Menschen bei 5 mg/m³ [43].

Durch den *Toxic Substances Control Act* (TSCA) wird die Registrierung von Chemikalien in den USA reguliert [95]. Die EPA überprüft derzeit, ob zukünftig Nanomaterialien als neue Stoffe meldepflichtig werden sollen [95]. Strategien für die Risikoeinschätzung von Nanopartikeln am Arbeitsplatz werden von der Organisation *National Institute for Occupational Safety and Health* (NIOSH) entwickelt [96]. Um für die Nanopartikel Arbeitswertgrenzwerte OEL (*Occupational exposure limit*) zu definieren, werden die Eigenschaften der Partikel (Löslichkeit, Toxizität) und die Belastungsgrenze (*exposure limits* (EL)) berücksichtigt [94]. Die NISOH hat 2010 für TiO_2-Nanopartikel und für CNTs empfohlenene Grenzwerte (*recommended exposure Limit* (REL)) definiert, basierend auf toxikologischen Untersuchungen [94]. Für TiO_2-Nanopartikel liegt der REL-Wert bei 2,4 mg/m³, für ultrafeine TiO_2-Nanopartikel (50% kleiner als 4 µm) bei 0,3 mg/m³ und für CNT bei 7 µg/m³ [94]. Die REL-Werte beziehen sich dabei auf die lebenslange Arbeitsbelastung mit einer 40-Stundenwoche für 50 Wochen pro Jahr über einen Zeitraum von 45 Jahren [94].

Da die derzeitigen Gesetze und Verordnungen nicht umfassend sind, gibt es von vielen Verbänden Bestrebungen die Regulierungen zu verbessern [95], sei es durch Datenbanken, Zertifizierungen oder ISO-Normen (*International Organization for Standardization*), die häufig in Forschungsprojekten erarbeitet wurden. Aufgrund der Komplexität der Nanomaterialien können nie alle Aspekte

berücksichtigt werden. Zur Standardisierung und Normierung bestehen derzeit diverse ISO-Normen zur Synthese, Charakterisierung, Klassifizierung sowie zur Entwicklung von Datenblättern [95]. Außerdem stehen ISO-Normen für Gesundheits- und Sicherheitsmethoden, Endotoxin-Tests sowie für das berufliche Risikomanagement zur Verfügung [95].

Zukünftig sollen mittels detaillierter toxikologischer Untersuchungen Anpassungen der EU-Regulierungen vorgenommen und viele Lebensmittelzusätze neu evaluiert werden [92]. International einheitliche Standards und Regularien für die Bewertung der Risiken der Nanomaterialien sind gefordert [95]. Dazu müssen geeignete Messmethoden zur Bestimmung der Nanopartikelkonzentration entwickelt werden, um Emissionsgrenzen und Qualitätsnormen festzulegen [95]. In weiteren Arbeiten sollte daher untersucht werden, inwiefern die Nanopartikel-Größe ein entscheidender Faktor ist [92]. Es wird empfohlen die Größenbegrenzung von 100 nm auf 300 nm auszuweiten [95]. In der REACH-Verordnung soll der Standarddatensatz um nanopartikuläre Eigenschaften ergänzt und die Grenzwerte für Nanomaterial-Mengen gesenkt werden [95]. Für aussagekräftigere OEL-Werte könnte die Dosis im Verhältnis zum Körpergewicht gesetzt werden [94]. Des Weiteren müssen die Verbraucher durch Inhaltsstofflisten hinreichend informiert werden [91]. In Deutschland besteht bereits seit 2013 für Kosmetika und seit 2014 für Lebensmittel eine Kennzeichnungsflicht für Nanomaterialien. Zur besseren Aufklärung des Verbrauchers hat zudem 2010 der BUND (Bund für Umwelt und Naturschutz Deutschland e. V) eine Nanoproduktdatenbank (nanowatch.de) erstellt, die Informationen über Nanoprodukte liefert. Die Verbraucherschutzverbände fordern zusätzlich, dass Nanomaterialien neu zugelassen werden müssen und Vorsorgestrategien erforderlich sind [95]. Es wird außerdem diskutiert, ob Nanomaterialien ein eigenständiges Zulassungsverfahren, bzw. bei einer mangelnden Datenbasis nur eine vorläufige Zulassung erhalten [95].

2.3 Risiken und Gefahren von Nanomaterialien

Die Anzahl der Veröffentlichungen über Nanopartikel hat in den letzten Jahren exponentiell zugenommen, wobei der Anteil der Studien über die Risiken für Mensch und Umwelt geringer ist (Fig. 2-1). Obwohl die Verwendung von Nanopartikeln in den letzten Jahren enorm gestiegen ist, sind die Auswirkungen auf die Umwelt noch nicht hinreichend untersucht [97].

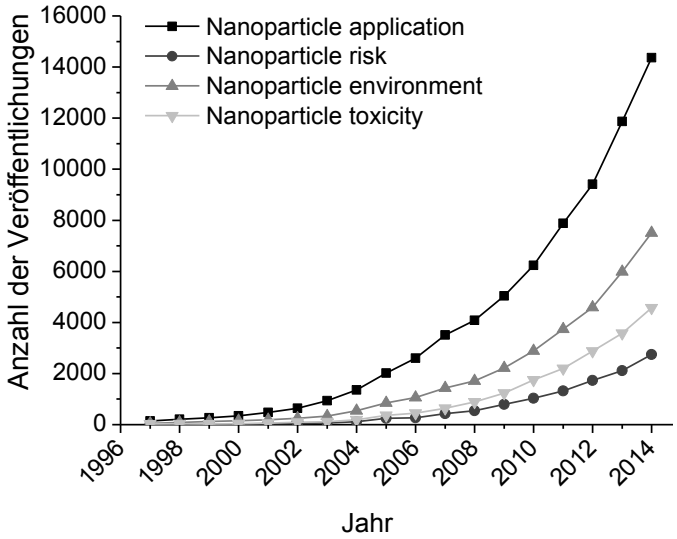

Fig. 2-1 Absolute Verteilung der Veröffentlichungen zum Thema Nanopartikel in den letzten zwanzig Jahren (1997-2014). Es wurden dabei die folgenden Suchbegriffe verwendet: „*nanoparticle application*“, „*nanoparticle risk*“, „*nanoparticle environment*“ und „*nanoparticle toxicity*“. Die Daten wurden mit der Suchmaschine *ScienceDirect* erhoben

2.3.1 Umweltbelastungen

Da Nanopartikel vielfältige Anwendungen in der Industrie sowie im Haushalt aufweisen, können sie auf verschiedenste Art und Weise in die Umwelt gelangen. Besonders Konsumgüter wie Lebensmittelverpackungen, Sprays, Elektrogeräte, Textilien und Beschichtungen bergen mögliche Gefahren [98]. In welchem Maße sich Nanopartikel von den Produkten ablösen, hängt dabei von der Einarbeitung in das Material, äußeren physikalischen und chemischen Einflussfaktoren, dem Gebrauch und dem Abrieb ab [98]. Des Weiteren können sich die Produkteigenschaften während des Anwendungszyklus ändern [98].

In Elektrogeräten sind vielfach Nanopartikel enthalten, die beim Recyceln oder bei der Müllentsorgung freigesetzt werden [98]. Kosmetika enthalten häufig TiO_2- und ZnO-Nanopartikel, die bei der Herstellung und Erzeugung sowie bei der Anwendung in das Abwasser gelangen können [99]. Für den UV-Schutz in Sonnencremes werden TiO_2-Nanopartikel aufgrund ihrer photokatalytischen Aktivität eingesetzt [1, 100]. Da sich die Nanopartikel aus den Sonnencremes herauslösen und sich in Gewässern anreichern können, ist die Umweltbelastung von TiO_2-Nanopartikeln in vielen Touristengebieten enorm gestiegen [1]. Im Mittelmeerraum betrug die Anzahl an Touristen im Jahr 2013 mehr als 202 Millionen [1]. Gelangen die TiO_2-Nanopartikel in die Umwelt könnten sie unter UV-Bestrahlung reaktive Sauerstoffspezies (ROS) generieren [100]. Um die Bildung von ROS zu unterbinden, werden daher die TiO_2-Nanopartikel an der Oberfläche mit Aluminiumhydroxid modifiziert [100]. Dabei ist noch ungeklärt, wie lange diese Schutzhülle während des Lebenszyklus bestehen bleibt [100]. Die Produktion von Wasserstoffperoxid im Meerwasser aufgrund von herauslösenden TiO_2-Nanopartikeln wurde bereits gezeigt und könnte einen toxischen Effekt auf den marinen Phytoplankton ausüben [1]. Die Überlebensrate und das Wachstum von Daphnien wurde bei 4,5-7,5 mg/l TiO_2-Nanopartikeln signifikant reduziert [101]. Untersuchungen an Pflanzen zeigten

keine biologischen Effekte aber hohe Konzentrationen von Titan und Aluminium in den Pflanzenwurzeln [100].

Nanopartikel können sich zudem beim Waschen aus Textilien lösen und über das Abwasser die Umwelt belasten [98]. Das Herauslösen der Nanopartikel aus Textilen stellt dabei einen Anteil von rund 25 % der gesamten Umweltbelastung dar, von denen 5 % in die Luft und 90-95 % in das Wasser gelangen [98]. Häufig werden Ag-Nanopartikel aufgrund der antimikrobiellen Wirkung in den Textilien eingesetzt. Dabei hat das verwendete Matrixmaterial einen Einfluss auf die Freisetzung der Partikel [98]. Baumwolle weist eine poröse und raue Oberfläche auf und die Luftfeuchtigkeit beim Tragen führt zur Destabilisierung der Wasserstoffbindungen [98]. Polyester ist im Gegensatz dazu eher hydrophob und abriebbeständig, jedoch anfällig für heiße alkalische Lösungen beim Waschen [98]. Während die Textilien aus Baumwolle mehr Nanopartikel beim Tragen in die Luft freisetzen, werden bei den Materialien aus Polyester vermehrt Nanopartikel beim Waschen herausgelöst [98]. Generell lösen sich aus Polyester die Nanopartikel leichter heraus als aus Baumwolle [98]. Die Freisetzung von Ag-Nanopartikeln in Gewässer bürgt dabei ein potentielles Risiko für Mikroorganismen, Daphnien, Fische oder Algen [60]. Untersuchungen an Muscheln haben gezeigt, dass Ag-Nanopartikel DNA-Schädigungen hervorrufen [12]. Die Aggregation der Nanopartikel spielt dabei bei der Risikobetrachtung eine entscheidende Rolle [60]. Äußere Faktoren wie Scherkräfte, Licht, Hitze oder auch die chemische Zusammensetzung der Lösungen können die Stabilität der Aggregate beeinflussen [60]. Die Größe und Struktur der Aggregate im Flusswasser ist dabei dynamisch und hängt von den äußeren Faktoren ab [60]. In der Gegenwart von hohen Calcium-Konzentrationen fördern z.B. natürliche organische Substanzen die Aggregation von Ag-Nanopartikeln [60].

Auch Hausfassaden, die mit Nanopartikel-enthaltenden Farben bestrichen wurden, könnten zur Anreicherung von TiO_2-Nanopartikeln und ZnO-Nanopartikeln im Regen- und Grundwasser führen [9, 100]. Untersuchungen haben gezeigt, dass sich bei natürlichen Wetterbedingungen 8-16 µg Ti/l (einmaliges Abwaschen) im Abwasser befanden [97, 102]. Zudem wird eine jährliche Ablagerung im Boden von 2.000 µg/kg TiO_2-Nanopartikeln, 0,4 µg/kg Fullerenen, 1,2 ng/kg Ag-Nanopartikeln und 0,01 µg/kg ZnO-Nanopartikeln anhand der Produktionsraten prognostiziert [99]. Grundsätzlich fehlen allerdings noch ausreichende empirische Datenmenge über die Konzentration der Nanopartikel in der Umwelt, da es an geeigneten Messmethoden mangelt [97, 103]. Des Weiteren weichen Nanopartikel in ihrem Verhalten und ihrer Wirkung deutlich von anderen Kontaminationen ab [97]. In den vergangenen Jahren wurden daher Modelle zur Simulation der Umweltbelastung entwickelt, basierend auf der Produktions- und der Emissionsrate der Nanoprodukte [97, 103]. Sie unterscheiden sich jedoch erheblich in den getroffenen Annahmen sowie der Nanopartikel-Form und -Größe [103]. Die Verteilung und Anreicherung von Nanopartikeln in der Nahrungskette sowie die Wirkung auf kleine Ökosysteme wird ebenfalls betrachtet [97]. Dies erfolgt unter kontrollierten Bedingungen im

Labor oder in Freilandversuchen, so dass äußere Faktoren wie z.B. die Wetterbedingungen integriert werden können [97].

Die Übertragung von verschiedenen Nanopartikeln in der Nahrungskette wurde bereits an diversen Organismen untersucht [97]. Ob es zu einer Anreicherung in der Nahrungskette kommt, ist derzeit nicht eindeutig geklärt, da die wenigen zur Verfügung stehenden Studien nicht miteinander vergleichbar sind [97]. Tabakpflanzen, in Kontakt gebracht mit Au-Nanopartikeln, wurden an Tabakschwärmer verfüttert [104]. Dabei konnte eine deutliche Anreicherung der Nanopartikel in den Tabakschwärmern beobachtet werden [104]. Ebenso wurde die Übertragung von Au-Nanopartikeln über Regenwürmer zu Fröschen festgestellt [105]. Quantum Dots werden von Wimperntierchen, aber nicht von *Escherichia Coli* Bakterien aufgenommen [106]. Da Bakterien den Wimperntierchen als Nahrung dienen, wurde hier keine Anreicherung in der Nahrungskette festgesellt [106]. Zusätzlich wurden Algen mit Nanopartikeln in Kontakt gebracht und dann von Muscheln, Schnecken, Daphnien, Ruderfußkrebsen konsumiert [97]. Bei der Untersuchung der dreistufigen Nahrungskette von TiO_2-Nanopartikeln über Grünalgen zu Daphnien und zu Zebrafischen konnten in den Zebrafischen keine Nanopartikel nachgewiesen werden [107].

Außerdem wird die Wirkung von Nanopartikeln auf ein komplexes System, bestehend aus vielen verschiedenen Organsimen, betrachtet. Die Unterscheidung zwischen direkter und indirekter Toxizität ist dabei erschwert [97]. Während manche Organsimen direkt auf die Nanopartikel reagieren und bestimmte Abwehrmechanismen aktivieren, reagieren andere Spezies indirekt auf diese Mechanismen [97]. Zum Beispiel wurde die Wirkung von TiO_2-Nanopartikel auf ein Ökosystem aus Algen und Schnecken [108] sowie von Au-Nanopartikeln auf ein Sumpfgebiet untersucht [109]. Mit den kleinen Ökosystemen wird analysiert, ob sich Änderungen in der Biomasse, der Komposition oder der Diversität beobachten lassen [97]. Diese Effekte wurden bereits mit Ag-Nanopartikeln, Metalloxid-Nanopartikeln, Quantum Dots und organischen Nanopartikeln beobachtet [97]. Änderungen der Komplexität der Mikroorganismen können dabei weitgehende Folgen haben, so können wichtige Funktionen wie die Denitrifikation betroffen sein [97].
Um realistischere Bedingungen zu generieren, werden zudem auch Freilandexperimente durchgeführt, so dass ein größerer Maßstab gewählt werden kann [97]. Diese sind jedoch schwierig kontrollier- und reproduzierbar und dauern länger [97]. In Langzeitstudien mit Ag-Nanopartikeln wurde die Verteilung sowie die Toxizität in einem miniaturisierten Ökosystem, bestehend aus verschiedenen Pflanzen, Algen und Bakterienkolonien, untersucht [110]. Zusätzlich wurde das Herauslösen von Nanopartikeln aus Konsumgütern und deren Wirkung auf das Ökosystem analysiert [97]. In den ersten 60 Tagen lösen sich 82-99 % des gesamten Silbers aus Socken und Teddybären heraus [111].

Trotz der vielen Modellexperimente und Vorhersagen ist eine umfassende Risikobewertung der Nanopartikel auf die Umwelt derzeit noch nicht gegeben. Der Vergleich der einzelnen Studien ist durch unterschiedliche Komplexitäten, Verwendungen von Nanopartikeln und Organismen

erschwert [97]. Des Weiteren werden vorrangig die Auswirkungen auf Wasserorganismen betrachtet [97]. Da Nanopartikel häufig im Wasser agglomerieren und zu Boden sinken, sollte auch das Ökosystem im Boden analysiert werden [97]. Zukünftige Studien müssen daher weitere Umweltszenarien darstellen und die Freisetzung von Nanopartikeln im täglichen Umgang mit Nanoprodukten abschätzen. Innovationen bei der Herstellung der Textilien könnten durch abschließende mechanische und chemische Prozesse die Stabilität erhöhen [98]. Die Stabilität von hydrophoben Nanokompositen für den Einsatz im Sanitärbereich wurde im Rahmen der Dissertation überprüft und in Kapitel 7 diskutiert.

2.3.2 Risiken für den Menschen

Neben den möglichen Risiken der Nanomaterialien auf die Umwelt müssen auch potenzielle Gefahren für den Menschen geklärt werden. Aufgrund der neuen Eigenschaften der Nanopartikel werden bisher nicht dokumentierte Gesundheitsrisiken erwartet [94]. Das Gefährdungspotential der Materialien hängt von der Produktionsmenge, der Anwendung sowie der Stabilität ab [11]. Während des Lebenszyklus der Nanomaterialien kommen verschiedene Bevölkerungsgruppen wie Industriearbeiter, Wissenschaftler, Konsumenten und Wertstoffarbeiter in Kontakt mit den Materialien, wobei sich die Gefährdungspotentiale unterscheiden. Für die Industriearbeiter besteht ein erhöhtes Kontaktrisiko beim Dispergieren der Nanopartikel zur Herstellung der Nanomaterialien. Beim Umgang mit großen Mengen an pulvrigen Nanopartikeln können sich Aerosole bilden, die die Gesundheit der Arbeiter belasten [94]. Basierend auf dem Produktionsprozess kann die Emission der Nanopartikel am Arbeitsplatz kalkuliert werden. Im Durchschnitt hat ein Arbeiter eine tägliche Belastung mit Nanopartikeln von 3,9 µg/ml [112]. Die derzeitigen Grenzwerte für Nanopartikel am Arbeitsplatz sind jedoch vorrangig mittels Toxizitätstestungen definiert worden [94].

Konsumenten kommen nicht mit den Rohstoffen, sondern mit den Endprodukten in Kontakt. Trotz einer potentiell hohen Gefahr eines Ausgangsstoffes, kann daher das Risiko des Produktes minimal und somit die Wahrscheinlichkeit der Exposition des Konsumenten gering sein [96]. Bei Konsumprodukten ist von besonderem Interesse, ob und in welchen Maße sich toxische Substanzen ablösen können [96]. Vor allem bei Produkten wie Sonnencremes (ZnO, TiO_2), Mundpflege (Hydroxyapatit), Pharmazeutika (Ag), Kraftstoffen (CeO_2), Beschichtungen, Klebstoffen (Polymere) und Reinigungsmitteln (Al_2O_3, TiO_2, Polyurethane, andere) besteht eine hohe Wahrscheinlichkeit, dass Verbraucher in Berührung mit Nanomaterialien kommen [11].

Die Nanopartikel können dermal, okular, respiratorisch oder gastrointestinal vom menschlichen Organismus aufgenommen werden [3]. Für Industriearbeiter ist das Inhalationsrisiko bei den Arbeiten mit synthetisierten Nanopartikeln besonders hoch [43]. Täglich gelangen rund 20-30 m³ Luft in die Lunge, die eine relativ große Oberfläche von ca. 75-150 m² aufweist [43]. Während der Atmung kann die Lunge mit Millionen von Nanopartikeln in Kontakt kommen [113]. Die Nanopartikel-Aufnahme über die Haut ist dagegen eher gering [114] und hängt von Größe, Oberflächenchemie und Form der

Partikel sowie der Beschaffenheit der Haut ab [3]. Durch die orale Aufnahme gelangen Nanopartikel in den Gastrointestinaltrakt und können über den Darm in die Blutbahn gelangen und somit weitere Organe erreichen [3]. Die Makrophagen, die als erster Abwehrmechanismus des Atmungssystems dienen, können das Eindringen der Nanopartikel nur mäßig verhindern [3, 43]. Dadurch können Nanopartikel durch die Epithelschicht der Lunge diffundieren, in den Blut- und Herzkreislauf [115] sowie in das Lymphsystem gelangen [116] und somit im gesamten Organismus verteilt werden. Da Proteine und Ionen häufig an Nanopartikel adsorbieren, wird eine erhöhte Interaktion mit dem Blutserum, Schleimhäuten oder anderen Körperflüssigkeiten prognostiziert [2]. Aufgrund ihrer kleinen Größe könnten Nanopartikel auch die Blut-Hirn-Schranke oder die Plazenta-Schranke überwinden, die funktionelle Barrieren darstellen [11].

Nanopartikel-Aufnahme in die Zelle

Generell wird die Wirkung der Nanopartikel durch die Interaktion mit der Zellmembran sowie deren Aufnahme in die Zelle entscheidend bestimmt [3]. Dabei bedeutet allerdings eine Aufnahme in die Zellen nicht unbedingt, dass ein toxikologischer Effekt ausgelöst wird [3]. Die Zellmembran dient als zelluläre Barriere für Moleküle und ermöglicht den gezielten Stoffaustausch [3]. Je nach Zelltyp und den charakteristischen Eigenschaften der Nanopartikel wie Größe, Form und Oberflächenchemie können die Partikel über Phagozytose, Makropinozytose, Pinozytose, Clathrin-unabhängige Endozytose, Clathrin-vermittelte Endozytose und Caveolae-Endozytose aufgenommen werden [3, 44]. In Fig. 2-2 sind die möglichen Aufnahmewege der Nanopartikel in die Zelle schematisch dargestellt.

Verschiedene Zelltypen wie z.B. Epithelzellen, Fibroblasten oder Immunzellen können mittels Phagozytose Partikel aufnehmen, dabei werden über 500 nm große Vesikel gebildet [44]. Die Phagozytose kann ausgelöst werden durch die Bindung von Liganden oder löslichen Faktoren wie Antikörpern oder Acetylcholin an die Oberflächenrezeptoren [44]. Die Makropinozytose wird dagegen nicht von einem Rezeptor vermittelt und ist eine Aktin-abhängige Endozytose [44]. Bei der Pinozytose wird zwischen der Clathrin-vermittelten Endozytose (Vesikelgröße 100-120 nm) und der Clathrin-unabhängigen Endozytose (Vesikelgröße ~90 nm) unterschieden [44]. Die Clathrin-vermittelte Endozytose kann zudem noch in die Caveolae-vermittelte Endozytose (Vesikelgröße 60-80 nm) und in den Caveolae-unabhängigen Transport unterteilt werden [117]. Am häufigsten werden Nanopartikel über die Clathrin-vermittelte Endozytose aufgenommen [117]. Die Clathrin-vermittelte Endozytose ist sehr komplex und bei der Vesikelbildung sind eine Vielzahl von Proteinen beteiligt [44]. Die Ablösung des Vesikels von der Membran ist dabei von der GTPase-Aktivität abhängig [44].

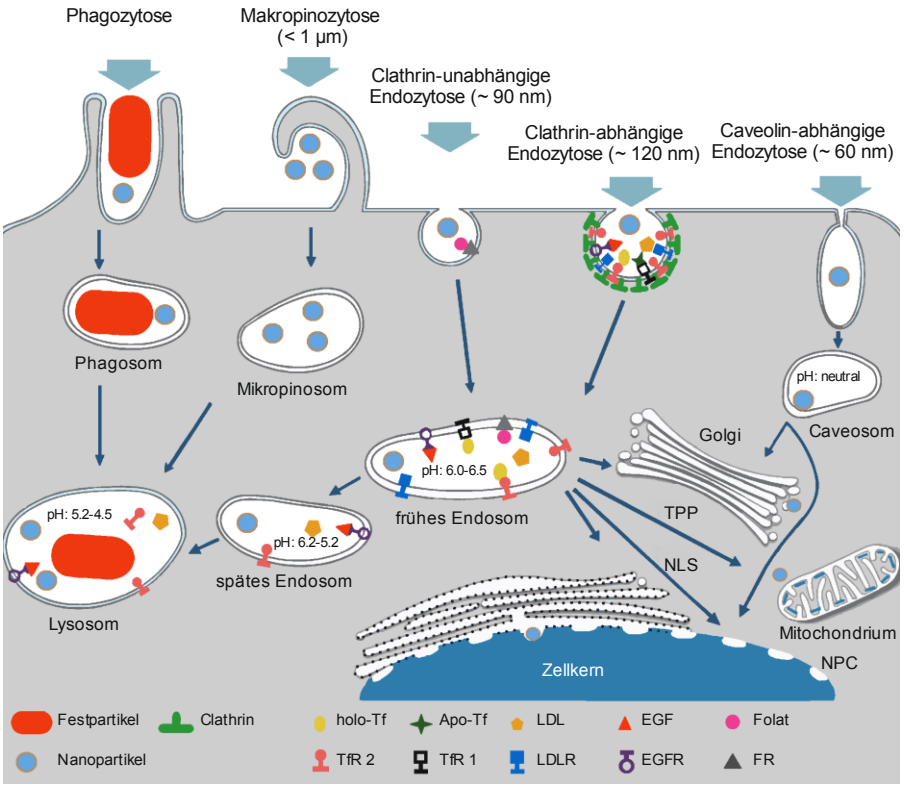

Fig. 2-2 Schematische Darstellung der verschiedenen Aufnahmewege von Nanopartikeln in die Zelle. Die Abbildung wurde modifiziert nach Yameen et al. (2014) [44]. Die Nanopartikel können über Phagozytose, Makropinozytose, Pinozytose, Clathrin-unabhängige Endozytose, Clathrin-vermittelte Endozytose und Caveolae-Endozytose in die Zelle gelangen. Abkürzungen: Epidermaler Wachstumsfaktor (EGF), EGF-Rezeptor (EGFR), Endoplasmatisches Retikulum (ER),Folatrezeptor (FR), Lipoprotein mit niedriger Dichte (LDL), LDL-Rezeptor (LDLR), Kernlokalisierungssignal (NLS), Kernpore (NPC), Transferrin (Tf), Transferrin-Rezeptor (Tfr), trans-proteomische Leitung (TPP).

Bei der Endozytose sind die Nanopartikel zunächst in den intrazellulären Vesikel eingeschlossen und können nur durch Verlassen des Vesikels in das Zytoplasma gelangen [3, 44]. Die Clathrin-vermittelte Endozytose wird vor allem für 100 nm große Nanopartikel bevorzugt, die positiv geladen sind [44]. Polylactid-Co-Polyethylene-Glykol-Nanopartikel [118] und SiO_2-Nanopartikel mit Isothiocyanat [119] wurden hauptsächlich über Clathrin-vermittelte Endozytose aufgenommen. Proteine und Ca^{2+}-Ionen, die an die Rezeptoren in der Membran binden, absorbieren häufig an Nanopartikel. Für ZnO-Nanopartikel wird daher die Rezeptor-gekoppelte Endozytose angenommen, so dass Lysosomen gebildet werden [115]. Der saure pH-Wert im Lysosom bewirkt die Hydrolyse von ZnO zu Zn^{2+}-Ionen [115]. Im Zytosol können die Ionen und Nanopartikel verschiedene Signalwege für den Zelltod induzieren [115]. Bakterielle Toxine und Oberflächenproteine gelangen vorwiegend über Clathrin-unabhängige Endozytose in die Zelle, bleiben in Lysosomen oder Endosomen, oder werden zum Golgi-Apparat oder zurück zur Zellmembran transportiert [44]. Bei der Caveolae-vermittelten Endozytose gelangen die Nanopartikel in die Caveolaen, die im Gegensatz zu den Lysosomen und den Endosomen ein neutrales Milieu aufweisen [117]. Die Caveolaen sind sackförmige Einbuchtungen, die eine typische Zusammensetzung aus Lipiden und Proteinen, vor allem dem Caveolin aufweisen [117].

Die Nanopartikel-Aufnahme in die Zelle hängt von der Ladung, der Form und auch von der Größe der Partikel ab [44]. Zusätzlich beeinflusst die Aggregation die Aufnahme, da je nach Aggregatform die Interaktion mit der Zellmembran begünstigt oder verschlechtert wird [3]. Generell zeigen diverse Studien, dass kleinere Nanopartikel eine höhere Aufnahmerate und eine höhere Toxizität aufweisen [3]. Über die Bildung von Poren in der Zellmembran können Partikel im Bereich von 1,2-22 nm in die Zelle gelangen [3]. Partikel mit einer Größe von 20-30 nm werden von Makrophagen über die Phagozytose besser aufgenommen als Partikel, deren Durchmesser im Bereich von 200-500 nm liegen [96]. Des Weiteren gelangen 20 nm-große Ag-Nanopartikel in das Zytosol von Lovo-Zellen (Dickdarmzellen) im Gegensatz zu 100 nm-großen [120]. Dabei lösen beide Nanopartikel-Größen unterschiedliche Abwehrmechanismen in der Zelle aus [120]. Während die 100 nm-großen Ag-Nanopartikel indirekt über die Serin/Threonin Proteinkinase (PAK) oder Mitogenaktivierte Proteinkinase (MAPK) zellulären Stress induzieren, wirken die 20 nm-großen Partikel direkt in der Zelle [120]. Insgesamt ist die Aufnahme von 50 nm großen Nanopartikeln besonders begünstigt, wobei je nach Zelltyp und Nanopartikel andere Aufnahmemechanismen festgestellt wurden [3, 121-124]. Die Aufnahme in den Zellkern kann generell nur für Nanopartikel kleiner als 39 nm erfolgen, da dies die Größe der Zellkernporen ist [44].

Neben der Größe spielt auch die Form der Nanopartikel bei der Aufnahme eine Rolle, hierbei zeigten gleich lange sphärozylindrische Nanopartikel eine bessere Integration in die Lipiddoppelschicht als kugel-, pyramiden-, stabförmige oder kubische Nanopartikel [3]. Die Partikel-Aufnahme von stäbchenförmigen organischen Nanopartikeln in HeLa-Zellen ist begünstigt im Vergleich zu kugelförmigen [125]. Obwohl das Volumen beider Partikel gleich ist, werden die asymmetrischen bevorzugt aufgenommen [125]. Außerdem beeinflussen dynamische Bedingungen sowie die Geometrie der Kapillaren welche Nanopartikel-Form begünstigt aufgenommen wird [3]. Im Herzkreislaufsystem von Mäusen verweilen 50 nm-kugelförmige Au-Nanopartikel, während stäbchenförmige Nanopartikel tief in das Tumorgewebe eindringen [126]. Computersimulationen berechnen für Nanopartikel mit einer anisotropen Form und asymmetrischen Oberflächenmodifikation zudem eine Aufnahmerate von 80 % [127]. Auch der Aufnahmemechanismus der Nanopartikel wird durch die Geometrie beeinflusst. Durch die Änderung des Kontaktwinkels zwischen Partikel und Membran werden längliche Partikel schlechter über Phagozytose aufgenommen als runde [44].

Nanopartikel liegen unter physiologischen Bedingungen selten frei vor, so dass an der Oberfläche Liganden angelagert sind. Die Art der Liganden, die Ladung, die Hydrophobizität sowie die Verteilung der Liganden beeinflusst die Aufnahme in die Zelle [3]. Während hydrophile Nanopartikel eher an der Membranoberfläche bleiben, gehen hydrophobe Nanopartikel in die Zellmembran [3]. Dieser Effekt konnte auch mittels der Simulation der Moleküldynamik von Fullerenen festgestellt werden. Hydrophobe Fullerene (C_{60}) aggregieren und diffundieren in die Zellmembran [128] während Hydroxyl-funktionalisierte Fullerene schlechter aufgenommen werden [129]. Durch eine definierte

(geordnete) Verteilung der Liganden kann die Aufnahme begünstigt sowie die Aggregatbildung der Nanopartikel vermieden werden [3]. Die Ladung der Nanopartikel spielt daneben eine weitere Rolle bei der Aufnahme.

Da die Membran von Säugetierzellen leicht negativ geladen ist, kann sie mit positiv geladenen Nanopartikeln in Wechselwirkung treten [130]. Nanopartikel können z.B. an negativ geladene Membranproteine oder die Heparansulfate der Polysaccharide binden und die Zellmembran schädigen [3]. Durch die Anlagerung an die Membran können diese Nanopartikel schlechter die Membran passieren [3]. Für kationische Au-Nanopartikel wurde eine moderate Toxizität beobachtet, wohingegen für negativ geladene Au-Nanopartikel kein Effekt beobachtet wurde [130]. Bei niedriger negativer Ladung von Au-Nanopartikeln wurde die Aufnahme über Membranporen und bei hoher Ladung die Aufnahme mit der Endozytose festgestellt [131]. Des Weiteren reicherten sich positiv geladene Nanopartikel in Mitochondrien von HeLa-Zellen an [44].

Wirkung von Nanopartikeln auf zellulärer Ebene

Generell wird die Toxizität der Nanopartikel durch deren charakteristische Eigenschaften wie Größe, Form, Ladung, Oberflächengröße und Funktionalisierung [9, 11, 94] sowie deren Aufnahmewege [132] bestimmt. Aus den toxikologischen Untersuchungen geht hervor, dass kleinere Partikel tendenziell eine toxischere Wirkung aufweisen als größere [94]. Bei Metall-Nanopartikeln können sich Metallionen ablösen, die einen zusätzlichen schädigenden Einfluss haben [2]. Die Aufnahme von ZnO-Nanopartikeln in die Zellen führt zur Bildung von schädigenden Zn^{2+}-Ionen im Zytoplasma und in den Mitochondrien [133]. Auch freigesetzte Ag-Ionen von Ag-Nanopartikeln können mit Thiolgruppen der vitalen Enzyme interagieren und die DNA-Replikation hemmen [9]. Auf zellulärer Ebene können Nanopartikel oxidativen Stress auslösen, der zu Schädigungen der DNA, Zellmembran, Proteine und Lipide, bis hin zum Zelltod führt [3, 134]. Die Expression von Stressmarkern wie Hämoxygenase-1, Thioredoxinreduktase, Glutathion-S-Transferase sowie Entzündungsmediatoren wie Interleukin-8 und Interleukin-6 kann dabei verstärkt sein [135]. Außerdem können an Nanopartikeln toxische, organische Liganden oder Endotoxine (Lipopolysaccharide) gebunden sein, die Entzündungen hervorrufen [43]. Die Wirkungen von TiO_2-Nanopartikeln werden in der Literatur kontrovers diskutiert. Während einige Studien keine Effekte von TiO_2-Nanopartikeln auf die Zellphysiologie feststellten [136-138], wurden geno- und zytotoxische Effekte sowie die Bildung von reaktiven Sauerstoffspezies detektiert [9, 135, 139, 140]. Zum Beispiel waren Anatase-TiO_2-Nanopartikel toxischer als Rutil-TiO_2-Nanopartikel [141, 142] und Polyacrylat-funktionalisierte TiO_2-Nanopartikel zeigten im Vergleich zu nichtmodifizierten kaum negative Effekte. Im Gegensatz zu den TiO_2-Nanopartikeln sind die toxischen Effekte von ZnO-Nanopartikeln auf Zellen vielfach bestätigt [9, 133, 143].

Potenziell ausgelöste Krankheiten durch die Exposition mit Nanopartikeln

Tierexperimente haben gezeigt, dass die Nanopartikel-Belastung und die Mortalitätsrate miteinander korreliert [144]. In der Lunge wurden durch die Inhalation von Nanopartikeln Entzündungsreaktionen ausgelöst, die auch chronisch werden können [145]. Des Weiteren wurden verschiedene Erkrankungen auf chronische, allergische oder infektiöse Prozesse zugeführt sowie die Verstärkung von bestehenden Krankheiten beobachtet [11]. Im Nanometermaßstab bewirken Partikel stärkere Entzündungsreaktionen in Rattenlungen als die größeren Partikel [96]. Dabei ist das Entzündungsrisiko von TiO_2-Nanopartikeln in der Lunge im Vergleich zu NiO sehr viel geringer [11]. ZnO-Nanopartikel lösten oxidativen Stress in der Lunge aus, der zu Verletzungen sowie Entzündungsreaktionen führte [146]. Einer Lungenentzündung folgt in der Regel eine Lungenfibrose [11]. Vor allem für CNT wurde gezeigt, dass eine Lungenfibrose und Granulombildung in Tierexperimenten ausgelöst werden konnte [11]. Dabei wird vermutet, dass die Makrophagen nicht in der Lage sind die langen CNT zu phagozitieren [147].

In-vivo-Studien über die Wirkung von Nanopartikeln auf die Haut gibt es derzeit noch kaum. UV-geschädigte Haut zeigte eine erhöhte Durchlässigkeit für carboxylierte Quantum Dots im Vergleich zu gesunder Haut [148]. Tierexperimente mit einwandigen CNTs (*Single-Wall Carbon Nanotubes* (SWCNT)) führten zu einer Hautverdickung [149], Fullerene spielten eine Rolle bei der Bildung von Hauttumoren [150] und CNTs führten zu einer Granulombildung [151]. Diverse Studien belegen zudem, dass nach oraler Aufnahme Au-, Ag-, ZnO- und TiO_2-Nanopartikel in das Gewebe diffundieren können [11]. Zusätzlich wurden Schädigungen der Leber, Nieren und Milz nach Exposition mit Cu-Nanopartikeln in Mäusen beobachtet [3].

Auch wenn derzeitige Studien über die Risiken auf das Herzkreislaufsystem fehlen, so wird doch stark angenommen, dass Nanopartikel einen Risikofaktor für Arteriosklerose darstellen, die durch verstärkte Blutplättchenaggregation und Entzündungen ausgelöst wird [11]. Die Aktivierung der Blutplättchen nach der Exposition mit Polystyrenlatex-Nanopartikeln und CNTs [152, 153] sowie von Fe_2O_3-Nanopartikeln [154] wurde gezeigt. Auswirkungen auf die Blut-Hirn-Schranke sowie die Blut-Plazenta-Schranke wurden in *in-vivo*-Experimenten beobachtet. Cu-, Ag- [155] und Al-Nanopartikel [156] erhöhen die Durchlässigkeit des Endothels des Kapillarsystems, so dass die Funktionalität der Blut-Hirn-Schranke geschädigt wird [157]. Außerdem zeigen Studien, dass einige Nanopartikel wie TiO_2 [158], Fullerene [159], Polystyrene [160] und SiO_2 [161] die Plazenta schädigen können.

Insgesamt wurden bereits in vielen *in-vitro* Experimenten sowie in Tierexperimenten die toxischen Wirkungen von einigen Nanopartikeln und das Auslösen von Krankheiten gezeigt. Ungeklärt ist jedoch, inwiefern die Übertragbarkeit auf den Menschen gegeben ist [11]. Zusammenhänge zwischen auftretenden Krankheiten und der Nanopartikelbelastung müssen untersucht werden. Ob z.B. die erhöhte Anzahl an Lungenkrebserkrankungen in Kohlebergwerken mit der Exposition mit Nano-

partikelstaub zusammenhängt, ist noch nicht bewiesen [162]. Derzeit fehlen eindeutige Hinweise, ob die Nanomaterialien auch im Menschen Krankheiten auslösen [11].

2.4 Toxikologische Analyse von Nanomaterialien

Trotz mehr als zehnjähriger Nanotoxikologie-Forschung sind die genauen Wirkmechanismen und Risiken von entwickelten Nanoprodukten nicht vollständig verstanden [96]. Der langfristige Erfolg der Nanotechnologie ist jedoch abhängig von der Entwicklung der Nanotoxikologie [96]. Innovationen im Bereich der *in-vitro*-Testung sind gefordert, um relevantere Ergebnisse als mit bisherigen Modellen erreichbar zu liefern. Zudem sollte es das Ziel sein, die enorm hohen Kosten der Tierexperimente zu senken. Im Jahre 2005 wurden weltweit für Tierexperimente zehn Milliarden Euro ausgegeben [43]. Hierfür wurden mehr als 100 Millionen Tiere eingesetzt, von denen 20 % für die Toxizitätstestung verwendet wurden [43]. In Deutschland wurden 2013 drei Millionen Tierexperimente durchgeführt, von denen 5 % für die Toxizitätstestung eingesetzt wurden [163]. Für eine umfassende Risikoeinschätzung der Nanopartikel bedarf es sorgfältiger Analysen. Faktoren, die die Toxizität der Nanopartikel beeinflussen, sind die Stabilität in physiologischen Medien, die Aggregat- und Agglomerat-Bildung, die Proteinhülle an der Nanopartikel-Oberfläche und die Anlagerung von Endotoxinen. Des Weiteren fehlen Detektionsmethoden der Nanopartikel zur Definierung eines relevanten Konzentrationsbereiches für die Testung. Zusätzlich müssen die eingesetzten Methoden, Zellen und Expositionszeiten standardisiert werden.

2.4.1 Herausforderungen bei der *in-vitro* Testung

Die toxikologische Untersuchung von Nanomaterialien birgt viele Herausforderungen. Zum einen ist die Definition und Klassifizierung, wie in Kapitel 2.2 bereits beschrieben, kritisch zu hinterfragen, zum anderen wird die Wirkweise von Nanomaterialien von vielen Faktoren bestimmt. Für die Analyse werden präzise, standardisierte und preiswerte Detektionsmethoden von Nanopartikeln in biologischen Proben wie Luft, Wasser oder Aerosolen benötigt [43, 96]. Aufgrund von fehlenden Daten ist das tatsächliche Risiko der Nanomaterialien nur eingeschränkt zu simulieren [97]. So ist z.B. die exakte Nanopartikel-Konzentration, die die Lunge erreicht, in *in-vivo* Studien nicht bestimmbar, da sie vom Nanopartikel-Gehalt in der Luft, dem inhalierten Volumen und der Größen-abhängigen Anreicherung in der Lunge abhängt [43]. Die Verwendung von realistischen und relevanten Konzentrationen bei der Toxizitätstestung der Nanopartikel ist daher schwierig zu definieren [43]. Häufig werden bei der Testung sehr hohe Konzentrationen eingesetzt, die auch die höchste anzunehmende Dosis im Falle eines Unfalls weit übersteigt [11].

Für die spätere Übertragbarkeit der Ergebnisse auf *in-vivo*-Experimente sollten zudem bei der *in-vitro*-Testung vergleichbare Konzentrationen verwendet werden [43]. Laut der OSHA entspricht eine Nanopartikel-Konzentration der Luft von 5 mg/m³ einer Belastung des menschlichen Lungengewebes von 3×10^{-5} bis 5×10^{-3} µg/h/cm² und einer Konzentration von 2 bis 300 Partikel/h/Epithelzelle [43]. Bei statischen *in-vitro*-Testungen kommt es jedoch zur Ablagerung von Nanopartikeln und somit zu

lokalen Konzentrationsänderungen, die *in vivo* in dem Maße nicht zu beobachten sind. Allerdings haben auch die gewonnenen Erkenntnisse aus Tierexperimenten nur eine bedingte Aussagekraft über die Wirkungen auf den Menschen, da sich z.B. die Lungenphysiologie und das Immunsystem der Labortiere von denen des Menschen signifikant unterscheiden [43].

Des Weiteren ist für toxikologische Untersuchungen eine detaillierte Charakterisierung der Nanopartikel notwendig. Während der Testung ändern sich die Eigenschaften der Nanopartikel, sei es durch Agglomeration, Dissoziation von Ionen, Oberflächenadsorption/-desorption, chemische Reaktionen oder Interaktionen mit anderen Materialen [96]. Bei der Toxizitätstestung liegen Nanopartikel nicht frei vor, sondern Proteine und andere kleine Moleküle wie Aminosäuren und Zucker adsorbieren an deren Oberfläche und bilden eine Hülle um den Partikel [3]. Während sich die innere Hülle innerhalb von Sekunden ausbildet und stark an die Nanopartikel anheftet, bildet sich die äußere Hülle sehr viel langsamer aus [3]. Insgesamt ist die Bildung der Proteinhülle ein dynamischer Prozess, so dass die Zusammensetzung der Hülle von der Umgebung abhängt [11]. Da die Proteinhülle eine entscheidende Rolle bei der Interaktion mit den Zellen spielt [3, 11], hängen die Auswirkungen der Nanopartikel auf Mensch und Umwelt auch von ihr ab [164].

Abhängig von der Medienzusammensetzung wurden unterschiedliche Effekte von SiO_2-Nanopartikeln beobachtet. Eine deutlich höhere Aufnahme von SiO_2-Nanopartikeln von A549-Zellen in serumfreien Medien im Vergleich zu Kultivierungen mit Serum wurde beobachtet [164]. Die SiO_2-Nanopartikel, die im Serum vorlagen, hatten dabei keinen schädigenden Einfluss auf die Zellen [164]. Außerdem können die angehefteten Proteine und kleinen Moleküle eine sterische Hinderung bei der Anbindung an den Membranliganden bewirken [3]. Dahingegen wurde die Interaktion mit dem Integrin-Rezeptor MAC-1 und die Aufnahme in die Zelle durch die Bindung von Fibrinogen an Au-Nanopartikeln begünstigt [40]. Zusätzlich können sich an die Nanopartikel Endotoxine anlagern, die Entzündungsreaktionen in Zellen auslösen und nur schwierig eliminiert werden können [165]. Auch unterschiedliche pH-Werte im menschlichen Organismus bewirken Änderungen der Nanopartikel-Oberfläche [162]. Diese Faktoren machen die toxikologischen Untersuchungen der Nanopartikel komplexer und sollten beim Nanopartikel-Design im medizinischen Bereich berücksichtigt werden.

Ein weiterer Faktor ist die Stabilität der Nanopartikel bei der Testung. Nanopartikel sind im Zellkulturmedium bei physiologischen Bedingungen selten stabil und tendieren in Abhängigkeit von ihrer Größe zur Aggregation und Agglomeration. Vor allem kleinere Nanopartikel neigen dazu schneller zu aggregieren, da die Anlagerung von Wassermolekülen die Ausbildung einer Hydrathülle erschwert [166]. Große Agglomerate sind dabei stabiler im Wasser als kleinere [166]. Die Agglomerate entstehen durch die Anlagerung von Partikeln, die durch z.B. Van-der-Waals-Kräfte zusammengehalten werden [11]. Die Aggregate sind dagegen viel fester mit kovalenten Bindungen zusammengehalten [11]. Der Grad der Aggregation und Agglomeration beeinflusst den hydrodynamischen Radius sowie die Oberflächengröße und somit auch die toxikologischen Eigen-

schaften [11]. Durch gezielte Funktionalisierung der Oberfläche kann die Stabilität von Nanopartikeln für die medizinische Anwendung erhöht werden [94]. Zudem gibt es Ansätze durch die Zugabe von biokompatiblen Stabilisatoren wie z.B. Seren oder Gummiarabikum die Stabilität der Suspension bei der *in-vitro*-Testung zu verbessern [167]. Für eine detaillierte Diskussion der Stabilität von Nanopartikel-Suspensionen sei auf Kapitel 3 verwiesen.

Neben den Eigenschaften der Nanopartikel spielen die Versuchsbedingungen eine entscheidende Rolle bei der Testung. Obwohl derzeit viele toxikologische *in-vitro* Untersuchungen vorliegen, mangelt es an der Vergleichbarkeit der Studien, so dass teilweise für die gleichen Nanomaterialien kontroverse Effekte gezeigt wurden [11]. Gründe dafür sind die fehlende Standardisierung der Versuchsbedingungen, die Variation der eingesetzten Zelltypen und Zytotoxizitätsmethoden sowie die Charakterisierung der Nanopartikel. Die Wahl der Zellen beeinflusst die Ergebnisse. Zwar liefern Zelllinien reproduzierbare Ergebnisse, aber diese unterscheiden sich im Gegensatz zu den Primärzellen deutlich von der Zellphysiologie *in vivo*. Für ZnO-Nanopartikel wurden in Abhängigkeit von den verwendeten Zellen unterschiedliche kritische Konzentrationen bestimmt [70]. Während bei Neuroblasten 100 µg/ml ZnO-Nanopartikel die Viabilität reduzierten, war dieser Effekt bei neuronalen Stammzellen bereits bei einer Konzentration von 12 µg/ml zu beobachten [70, 168, 169]. Des Weiteren kann die Wahl der Zytotoxizitätsmethode entscheidend sein, da einige Nanopartikel mit den Farbstoffen, die zur Detektion der Zellantwort eingesetzt werden, interagieren (siehe auch Kapitel 3). Zum Beispiel können Markermoleküle wie Lactatdehydrogenase (LDH) oder bestimmte Zytokine an Nanopartikel adsorbieren, so dass deren Gehalt in der Zelle für den Nachweis der Stoffwechselaktivitäten nicht genau ermittelt werden kann [165]. Insgesamt ist die Risikoeinschätzung eines Nanomaterials sehr komplex und aufwendig [96], da Ausgangsmaterial, Zwischen- und Endprodukt unterschiedliche Eigenschaften aufweisen können. Somit bedarf es sorgfältiger Analysen aller Entwicklungsstufen des Herstellungsprozesses der Nanomaterialien. Da die Produktion von Nanomaterialien stetig zunimmt, sind langfristig Hochdurchsatz-Testtechniken notwendig [94].

2.4.2 Modellsysteme zur Toxizitäts-Bestimmung

Der Bedarf an neuen Modellen und Testsystemen gerade im Bereich der *in-vitro*-Testung ist in den letzten Jahren enorm gestiegen. Die derzeitige Verwendung von klassischen zweidimensionalen Monokulturen für Wirkstoff- und Toxizitätstestung liefert kaum übertragbare Ergebnisse auf den menschlichen Organismus. Da Tierexperimente aus ethischen Gründen reduziert werden sollten und zudem auch häufig den menschlichen Stoffwechsel nicht gut nachahmen, ist die Entwicklung von alternativen Methoden gefordert. Besonders bei der Entwicklung von Wirkstoffen könnten erweiterte präklinische Modelle die Wirkstoffentwicklung deutlich verbessern. Eine Vielzahl an Wirkstoffvorläufern könnte mit relevanten Testsystemen effizient und schnell analysiert werden, ohne dass viele Tierexperimente benötigt werden würden. Außerdem können die Modelle bei der Risikoeinschätzung von Nanopartikeln eingesetzt werden. Die Verteilung im Organismus sowie die Simulation von

physiologischen Bedingungen sind dabei essentiell. Computermodelle können grundlegende Fragestellungen simulieren wie die Verteilung von Nanopartikeln sowie deren Aufnahme in die Zelle. Komplexe *in-vitro*-Modelle haben den Vorteil, dass sie relevantere Ergebnisse liefern und die natürlichen Bedingungen besser nachahmen können. Andererseits sind sie deutlich aufwendiger und teurer als die klassischen zweidimensionalen Kultivierungen. Ziel dieser neuen Technologien sollte es daher sein, die Kosten zu senken und das Hochdurchsatz-*Screening* zu ermöglichen. Nachfolgend sind die neuesten Testsysteme und Innovationen im Bereich der Nanopartikel-Untersuchung dargestellt und deren Perspektiven diskutiert.

2.4.2.1 Computersimulationen und einfache Modellsysteme

Neben den klassischen *in-vitro* und *in-vivo* Experimenten im Bereich der Wirkstoff- und Nanopartikel-Testung werden auch Computersimulationen entwickelt [3]. Mittels mathematischer Modelle können die Einflüsse von verschiedenen Faktoren simuliert werden, so dass Vorhersagen über das Verhalten von Nanopartikeln und deren Verteilung getroffen werden können [46]. Dabei spielen die Partikelladung, die Kräftekonstanten und die molekularen Wechselwirkungen wie die Van-der-Waals Kräfte eine entscheidende Rolle [3]. Während das CHARMM-Modell (*Chemistry at HARvard Macromolecular Mechanics*) die Wechselwirkungen jedes einzelnen Atoms berücksichtigt und somit viel detaillierter ist, werden im GROMOS-Modell (*GROningen MOlecular Simulation computer program package*) die Kräfte zwischen den Kohlenwasserstoffketten betrachtet und vereinfacht, so dass die Rechenkapazität verringert wird [3]. Bei der *Dissipative Particle Dynamic*s Methode (DPD) werden einzelne Atome zu Partikeln zusammengefasst [127]. Das Monte-Carlo-Modell oder die Molekül-dynamik werden genutzt, um das Passieren der Nanopartikel durch die Zellmembran zu analysieren [3]. Mittels mathematischer Modelle konnten die Partikelladung [131, 170], die Partikelform [3, 127], die Partikelgröße [3, 171], die Oberflächenfunktionalisierung [127, 172] und die Membransymmetrie [127] variiert und somit deren Einfluss auf die Nanopartikel-Aufnahme simuliert werden. Der Einfluss der Partikelladung auf die Zellaufnahme ist in Fig. 2-3 dargestellt. Die Interaktion mit der Zellmembran nimmt mit dem Anteil an positiver Ladung zu [170]. Positiv geladene Au-Nanopartikel können sich beispielsweise in die Membran einlagern und die Zellmembran zerstören [131, 170]. Hydrophobe und negative geladene Nanopartikel hingegen interagieren kaum mit der Zellmembran [131].

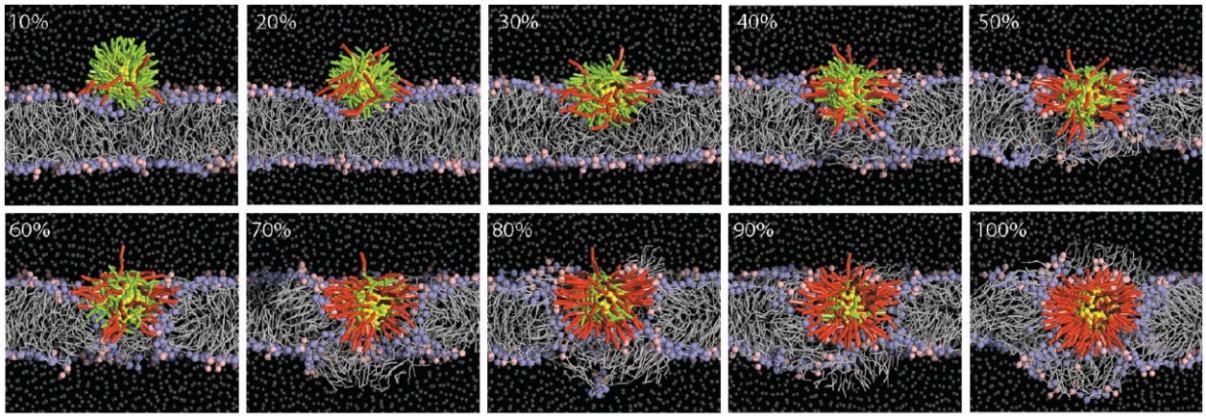

Fig. 2-3 Computeranimation zur Simulation der Interaktion einer negativen Doppelschicht bestehend aus Dipalmitoyl-Phosphatidyl-Choline (DPPC) und Diamitoyl-Phosphatidyl-Glycerol (DPPG) und Au-Nanopartikeln (gelb) mit unterschiedlich stark geladenen positiven Oberflächen, Quelle: [170]. Hydrophobe Liganden sind in grün und positiv geladene Liganden in rot dargestellt [170]. Der Anteil an positiver Ladung der Au-Nanopartikel ist dabei angegeben [170]. Mit zunehmender positiver Ladung der Nanopartikel steigt auch die Interaktion mit der Membran.

Mittels der DPD-Methode wurde gezeigt, dass die Bildung eines Nanopartikel-Ligand-Komplexes einen Einfluss auf die Effektivität der Aufnahme und deren Dauer hat [127]. Für kleinere Nanopartikel und Peptid-funktionalisierte Nanopartikel wurde ein passiver Transport durch die Membran prognostiziert [3, 172]. Des Weiteren werden die Modelle genutzt, um die Verteilung der Nanopartikel im Gefäßsystem zu simulieren. Stäbchenförmige Nanopartikel lagern sich dreimal so stark an die Blutgefäße an als kugelförmige [173] und akkumulieren vor allem hinter den Verzweigungen der Blutgefäße [171]. Zudem spielen die Orientierung zur Gefäßwand und die Nanopartikel-Größe eine Rolle [171].

Neben den Computermodellen dienen isolierte und vereinfachte Membranmodelle zur Aufklärung von Interaktionen der Nanopartikel und der Lipidschicht [3]. Der Phasenübergang von Luft zu Wasser in der Lunge kann damit untersucht werden [3]. Bei synthetischen Membranmodellen werden häufig Cholesterol, Phophorlipide, Shingolipide, Membranproteine und Polysacharide verwendet. Es werden Lipiddoppelschichten, Liposomen und Einfachschichten (Langmuir-Monolayer) analysiert [3]. Als Modellpartikel werden z.T. auch kleine Peptide verwendet [3]. Während die Langmuir-Monolayer den Übergang zwischen Luft und Wasser simulieren, wird das Passieren der Membran häufig an Liposomen untersucht [3]. Anhand von Langmuir-Monolayern, bestehend aus 1,2-Dipalmitoyl-sn-glycero-3-pjophocholin (DPPC) und Palmitinsäure konnte gezeigt werden, dass die Aufnahme von SiO_2-Nanopartikeln durch die Bildung von hydrophoben Nanopartikel-Lipid-Komplexen stattfindet [174]. Die Zusammensetzung des Lipidmonolayers wirkt sich auf die Interaktion der Nanopartikel mit den Lipidmolekülen aus, die wiederum entscheidend für das Passieren der Lipidschicht der Nanopartikel ist [175].

2.4.2.2 Zellbasierte Modellsysteme

Um die Komplexität der *in-vitro*-Toxizitätstestung zu erhöhen, soll der Einsatz von dreidimensionalen (3D) Zell- und Gewebekonstrukten anstelle von zweidimensionalen (2D) Kulturen etabliert werden.

Die Vorteile der 3D-Zellkultur gegenüber der 2D-Zellkultur werden in Kapitel 3 und Kapitel 5 detaillierter diskutiert. Die Strategien für die Bildung von 3D-Zellstrukturen sind verschieden. Durch Besiedelung der Zellen auf Gerüstsubstanzen wird ihnen eine definierte Struktur vorgegeben, wohingegen die Einkapselung der Zellen im Hydrogel flexiblere 3D-Konstrukte zulässt. Über die Regulation der mechanischen Eigenschaften des Gels können die Phänotypen der Zellen gesteuert werden [46], so dass z.B. Tumore generiert werden können [176]. Bei einem weiteren 3D-Modell werden durch spontane Zellaggregation Sphäroide gebildet. Da diese in Abhängigkeit von ihrer Größe einen apoptotischen/nekrotischen Kern aufweisen, werden sie häufig als Tumormodell eingesetzt [46]. Für eine ausführliche Diskussion über die Anwendung von Sphäroiden sei auf Kapitel 3 verwiesen.

Neben den 3D-Zellkultur-Modellen werden dynamische Bedingungen erzeugt, die die Blutzirkulation oder das Herzkreislaufsystem simulieren sollen. Denn obwohl 3D-Kultivierungen deutlich besser die Morphologie im menschlichen Gewebe nachstellen, fehlt der physiologische Scherstress. Des Weiteren wird der Gasaustausch und der Transfer von Nährstoffen und Stoffwechselprodukten verbessert [46]. Zur Simulation des physiologischen Flusses werden Mikrofluidik- [177-179], Makrofluidik- oder andere Strömungssysteme angewendet [177, 180]. Mit diesen Systemen können die Wirkstofffreisetzung sowie die Absorption, Verteilung und Eliminierung von Partikeln untersucht werden [178]. Unter dynamischen Bedingungen wurde z.B. die Bindung von liposomalen Nanopartikeln [181] und Anti-ICAM-1-funktionalisierten Partikeln untersucht [182]. Die Verteilung wurde von der Geometrie der Mikrokanäle beeinflusst und die Partikelbindung nahm mit steigender Flussgeschwindigkeit ab [182]. Vor allem durch die Mikrofluidik könnte zukünftig eine schnellere und effizientere Charakterisierung der Nanopartikel möglich werden [46]. Gao et al. entwickelten eine Mikrofluidikkammer, die eine Wirkstofftestung im hohen Durchsatz ermöglicht und die Analyse mittels Massenspektrometrie integriert (ESI-Q-TOF-MS) [183]. Im Mikromaßstab wird ein Konzentrationsgradient der Testsubstanz aufgebaut, der dann die Zellkulturen überströmt. Nachfolgend sind auf dem Chip Festphasenextraktionsäulen zur Aufreinigung der Proben integriert, die dann in der Massenspektroskopie analysiert werden können [183]. Zusätzliche Studien über die Effekte von Nanopartikeln unter dynamischen Bedingungen sind in Kapitel 6 beschrieben.

Eine weitere Strategie zur Erhöhung der Komplexität von *in-vitro*-Experimenten ist die Verwendung von Kokulturen statt Monokulturen, die häufig in Transwell®-Systemen kultiviert werden. Die Transwell®-Systeme werden zur Simulation von natürlichen Barrieren eingesetzt und weisen eine 10 µm dicke Membran aus Polyester oder Polycarbonat mit Porengrößen zwischen 0,4-3 µm auf [184]. Zusätzlich sind die charakteristischen Eigenschaften der Lunge wie das Immunsystem und die Gas-Flüssig-Phasen-Übergänge interessant. Mit Kokulturen aus Lungenepithelien und Makrophagen konnte das Immunsystem in der Lunge besser simuliert werden [112]. Makrophagen wiesen für die Epithelzellen eine Art Schutzfunktion vor den Nanopartikeln auf [112]. Außerdem wurde mit einer biologischen Gerüstsubstanz ein 3D-Modell zur Simulation der Schleimhäute der Atemwege mit

bronchialen Epithelzellen und Fibroblasten entwickelt [185]. Mit dem MucilAir™ System (Epithelix) oder dem EpiAirway-System (MatTek) kann die Inhalation von Nanopartikeln mit primären Bronchialepithelzellen in 3D nachgeahmt und chronische Effekte von Nanopartikeln analysiert werden [43, 186]. Auch Kokulturen von Leberzellen und Fibroblasten konnten für Langzeit-Analysen verwendet werden [46, 187]. Zudem kommen Kokulturen mit zwei oder drei verschiedenen Zelltypen für Blut-Hirnschranke-Modelle zum Einsatz, um die Permeabilität der zerebralen Kapillaren für Nanopartikel zu untersuchen. Häufig werden verschiedene Primärzellen wie Endothelzellen, Astrozyten und Perizyten miteinander kombiniert [188]. Alternativ wird auch die humane Zelllinie hCMEC/D3 als Blut-Hirn-Schranke-Modell verwendet [189].

2.4.2.3 Komplexe zellbasierte Modellsysteme

Besonders vielversprechend ist die *Organ-on-a-Chip*-Technologie, bei der komplexe 3D-Konstrukte und Kokulturen mit der Mikrofluidik kombiniert eingesetzt werden [46, 190]. Außerhalb des menschlichen Organismus können miniaturisiert eine Vielzahl von funktionalen Untereinheiten von Organen und Geweben und deren physiologische Umgebung nachgeahmt werden [190]. Dadurch werden neue Möglichkeiten für die Medikamententestung, Erforschung von Krankheiten sowie für die Nanotechnolgie geschaffen, da effektives *Screening* und eine hinreichende toxikologische Untersuchung derzeit die größte Herausforderung darstellen [191]. Die präklinischen Tierversuche sind sehr zeitaufwendig und teuer sowie können nicht immer die Situation im menschlichen Organismus vorhersagen [46]. Daher versagen viele Wirkstoffe nach der erfolgreichen präklinischen Studie in den ersten klinischen Anwendungen [46].

Zusätzlich müssen für eine umfassende Analyse der Nanopartikel-Wirkung auf den menschlichen Organismus Faktoren wie die Stabilität, der Transport, die Bindung an sowie die Aufnahme in die Zelle unter physiologischen Bedingungen erfolgen [46]. Bei den Standard-*in-vitro*-Testsystemen (2D, statisch) sind alle Zellen den gleichen Kultivierungsbedingungen im Brutschrank ausgesetzt, dabei unterscheidet sich der Sauerstoffgehalt und die Luftfeuchtigkeit in den verschiedenen Geweben im Organismus [190]. Hautzellen benötigen beispielsweise eine niedrige Luftfeuchtigkeit [190]. Zudem kann unter den Standardbedingungen die Struktur und Festigkeit der Oberfläche nicht variiert werden [190]. Die im Vergleich zu 2D-Experimenten aussagekräftigeren Ergebnisse der *Organ-on-a-Chip*-Technologie sollen dafür genutzt werden, um zelluläre Mechanismen aufzuklären sowie ein besseres Verständnis über die Organphysiologie zu erhalten [190]. Dabei können Lungenalveolen, kontrahierende Herzzellen, Nieren-, Darm- oder Leberstrukturen sowie Tumore geschaffen werden [190]. Des Weiteren können auch verschiedene Zellkulturkammern miteinander verbunden werden, so dass ein Kreislaufsystem von verschiedenen Organen simuliert werden kann [190]. Die Durchführung von Langzeit-Experimenten wird ebenfalls ermöglicht [190]. Vor allem das Gehirn und das Immunsystem sind einzigartig beim Menschen und lassen sich nicht ausreichend mit Tiermodellen repräsentieren [190]. Mit den *Organ-on-a-Chip*-Modellen kann zum Bespiel die Immunantwort von

Immunzellen nach Induktion von Bakterien untersucht werden [190]. Zudem können Krankheiten simuliert und die Wirkung von Wirkstoffen sowie von Nanopartikeln schnell, kostengünstig und effizient analysiert werden [190].

Bei der *Organ-on-a-Chip*-Technologie werden verschiedene Zelltypen auf kleine Strukturen (Chips) bestehend aus synthetischen Polymeren gebracht [190]. Dabei wird der Chip für die mikroskopische Detektion aus einem transparenten Material hergestellt und weist in der Regel eine Größe von 5 cm x 2 cm mit verschiedenen Kammern auf [190]. Die *in-vivo*-Mikroumgebung wird durch bestimmte Geometrien, Strukturen und Konzentrationsgradienten simuliert [46]. Über die Oberfläche können die Zellen gezielt differenziert werden, so dass die charakteristische Funktionsweise des Organs nachgeahmt werden kann [190]. Dabei werden synthetische Polymere, Silikone oder auch Alginate verwendet [190]. Die Materialien müssen dünn, flexibel und dehnbar sowie durchlässig für Sauerstoff und Nährstoffe sein [190]. Die Zellkulturoberfläche wird je nach Zelltyp variiert, so dass unterschiedliche Festigkeiten und Rauheiten geschaffen werden [190]. Während Knochengewebe hart ist, sind Muskel- und Hautgewebe viel weicher [190]. Außerdem werden in das Material häufig unterschiedlich große Poren integriert, die mit extrazellulären Proteinen beschichtet sein können, um Übergange zwischen der Luft- und der Wasser-Phase der Lungenalveolen zu kreieren [190].

Die Inhalation von Wirkstoffen und Nanopartikeln könnte zukünftig mit den *Lung-on-a-Chip*-Modellen untersucht werden. Kürzlich wurde bereits ein 2D-Modell vom Wyss Institut (*Wyss Institute for Biologically Inspired Engineering*, Harvard Universität, USA) entwickelt [190]. Dieses Modell dient derzeit auch als Vorlage für Darm- und Nieren-Modelle. Zwei Kammern sind durch eine poröse, flexible Membran voneinander getrennt und können unterschiedlich stark mechanisch gestreckt werden (siehe Fig. 2-4) [190]. Diese Membran wird beidseitig mit verschiedenen Zelltypen besiedelt. Während die Oberseite mit Lungenepithelzellen bedeckt und von Luft überströmt wird, wird die Unterseite mit Endothelzellen besiedelt, die mit synthetischem Blut durchflossen werden [190]. Durch die Poren in der Membran können bei einer induzierten bakteriellen Infektion der Luft Leukozyten aus der Blutbahn mit der Luft in Kontakt kommen [190]. Um die natürliche Bewegung der Lungenalveolen nachzuahmen, können die seitlichen Kammern aufgeblasen und entleert werden [190].

Mit dem Lungen-Modell wurden bislang die Wirkungen von SiO_2-Nanopartikeln und deren Aufnahme in die Lunge analysiert [192]. Die mechanische Stimulation begünstigt dabei die Aufnahme der Nanopartikel von den Zellen sowie den Transport in das mikrovaskuläre System [192]. Somit bewirkte die Exposition mit SiO_2-Nanopartikeln die Induktion von Entzündungsreaktionen der Lungen [192]. Gute Übereinstimmungen konnten dabei mit Mäuseexperimenten festgestellt werden [192]. Daneben wurde das Lungen-Modell zur Simulation eines Interleukin-2 induzierten Lungenödems eingesetzt, so dass entsprechende Wirkstoffe untersucht werden konnten [193].

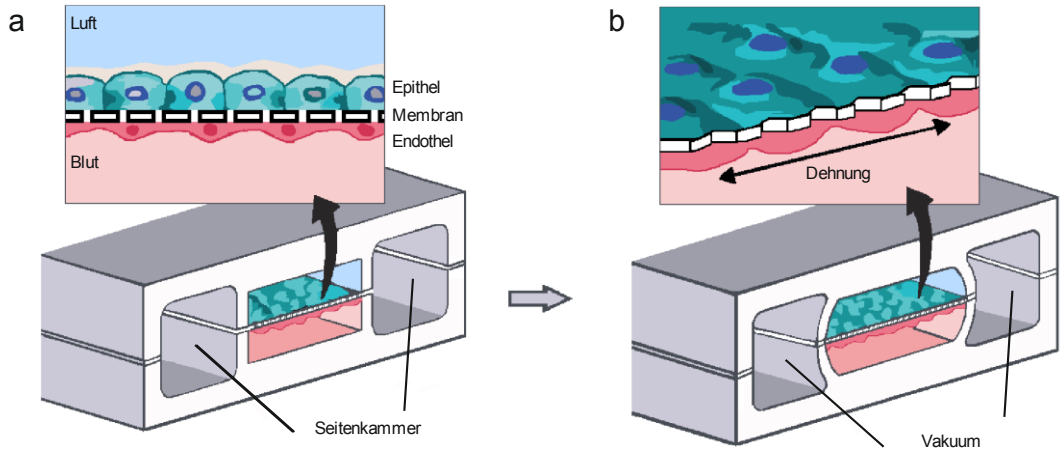

Fig. 2-4 Schematische Darstellung eines *Lung-on-a-Chip*-Modells entwickelt vom *Wyss Institute for Biologically Inspired Engineering* [190]. Lungenepithelienzellen (blau) sind auf der Oberseite der Membran besiedelt, während die untere Seite mit Endothelzellen bedeckt ist (rot). Zur Simulation der Lunge wird der obere Teil der Kammer mit Luft durchströmt wohingegen der untere Teil mit synthetischem Blut durchflossen wird [190]. Um die natürliche Bewegung der Lungenaveoloen nachzustellen, können die seitlichen Kammern aufgeblasen und entleert werden (b) [190]. Abbildung modifiziert nach Huh et al. (2010) [192].

Ein Hauptmerkmal der Lunge ist außerdem die große Oberfläche, wodurch ein hoher Gasaustausch erfolgen kann [194]. Mit dem in Fig. 2-5 dargestellten zelllosen Lungenmodell von Kniazeva et al. (2011) kann dieser hohe Gasaustausch simuliert werden [194]. Mehrere mikrofluide Blut-Gas-Doppelschichten, bestehend aus Silikonmatrix, werden parallel geschaltet [194]. In zukünftigen Lungenmodellen könnten diese beiden Modellsysteme kombiniert und zudem verschiedene Lungenzellen eingesetzt werden.

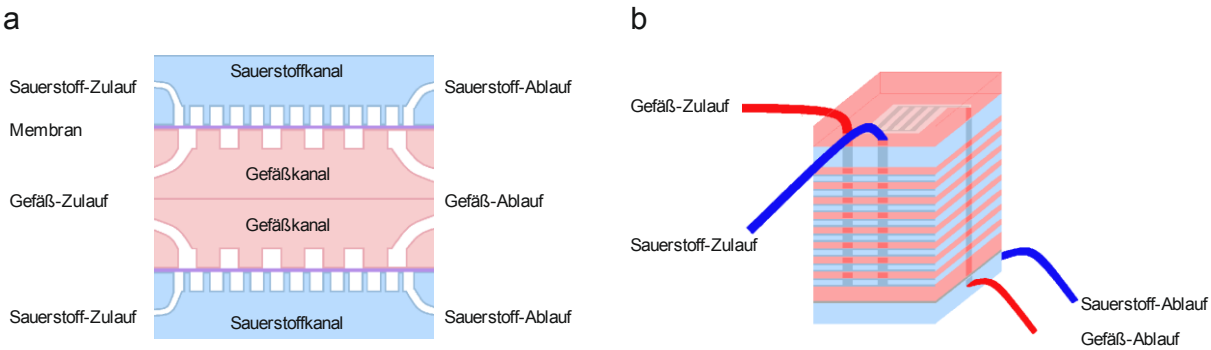

Fig. 2-5 Schematische Darstellung eines Lungenmodelles bestehend aus zehn Doppelschichten, zur Simulation des Gasaustausches, modifiziert nach Knieazeva et al. (2011) [194]. a) Querschnitt einer Doppelschicht aus Gefäß- und Gaskammern. Die Sauerstoffübertragung kann aus der Umgebung oder aus den angrenzenden Doppelschichten erfolgen. b) 10-fache Doppelschicht.

Da Nanopartikel und Wirkstoffe auch oral aufgenommen werden können, z.B. über die Nahrung, sind die Wirkungen auf den Gastrointestinaltrakt von Interesse. Analog zum *Lung-on-a-Chip*-Modell entwickelte das Wyss Institut ein *Gut-on-a-Chip*-Modell [190]. Darmepithelzellen (Caco-2 Zellen) werden auf einer porösen Membran aufgebracht und bei einem niedrigen Scherstress von 0,02 dyn/cm² kultiviert [195]. Das verwendete Polydimethylsiloxan (PDMS) hat den Vorteil, dass es transparent ist und eine hohe Flexibilität aufweist [196]. Unter dynamischen Bedingungen entwickeln die Darmzellen eine Polarität und es bilden sich darmzottenähnliche Strukturen [195]. Durch die erfolgreiche Kokultivierung mit den Darmbakterien (*Lactobacillus rhamnosus*) konnten die natürlichen Bedingungen

im Darm simuliert werden [195]. Des Weiteren gibt es Ansätze die 3D-Struktur der Darmzotten aufzubauen und somit ein alternatives Darm-Modell zu entwickeln. Dazu wurden Darmzellen Caco-2 auf einem miniaturisierten 3D-Hydrogel-Gerüst in der Form der menschlichen Darmzotten besiedelt [197]. Zukünftig könnten zusätzlich andere Zelltypen im Hydrogel eingekapselt werden, so dass weitere physiologische Bedingungen geschaffen werden [197]. Langfristig könnte dieses Modell zur Aufnahme von Wirkstoffen über den Gastrointestinaltrakt genutzt werden [197].

In der Leber werden vom Körper aufgenommene Stoffe und Toxine metabolisiert, so dass sich die Ausgangsstoffe ändern [190]. Untersuchungen von Au-Nanopartikeln auf isoliertem Lebergewebe aus Ratten sowie in *in-vivo*-Experimenten zeigten keine toxischen Effekte [198]. Isolierte Gewebestücke verlieren jedoch schnell ihre Funktionalität, so dass sie für Langzeit-Untersuchungen ungeeignet sind [46]. Weitere *Liver-on-a-Chip*-Modelle konnten die typischen Leberstrukturen simulieren. Nakao et al. (2011) entwickelten ein Modell bestehend aus einem Mediumkanal, einer Zellkulturkammer und einer Endothel-ähnlichen Barriere [199]. Neben dem Lungen-, Leber- und Darm-Modell gibt es auch Ansätze die Niere zu simulieren [46]. Der von Jang et al. (2013) entwickelte Nierentubulus ähnelt dem Aufbau der Lungen- und Darmmodelle. Die Membran wird von einer Seite mit Nierenepithelzellen besiedelt, die einem Fluidstrom ausgesetzt sind [200]. Mittels des Nierenmodells konnten ähnliche Ergebnisse bei der Untersuchung der Toxizität von Cisplatin wie unter *in-vivo*-Bedingungen erzielt werden [200].
Darüber hinaus werden Modelle entwickelt, um das Gefäßsystem im menschlichen Organismus zu simulieren [46] und die einzelnen Organeinheiten auf dem Chip miteinander zu verbinden [201]. Außerdem finden Gefäßmodelle Anwendung bei der Entwicklung von therapeutischen Nanopartikeln, die intravenös injiziert werden [46]. Mit den Gefäßmodellen können die Interaktionen der Nanopartikel mit anderen Blutkomponenten, die Überwindung von endothelialen Barrieren, die Aufnahme in die Zelle sowie der Einfluss der Partikelfunktionalisierung untersucht werden [46]. Zusätzlich werden Faktoren wie Scherstress, Sauerstoff und Nährstoffaustausch sowie der Abtransport von Stoffwechselprodukten realisiert [201]. In mikrofluiden Gefäßmodellen, die zwischen 1-100 µm groß sind [202], können physiologische Geometrien und Verzweigungen integriert werden, so dass Turbulenzen und unterschiedliche Scherstressraten simuliert werden können [46]. Dabei werden verschiedene Techniken für die Gefäßbildung verwendet, wie unter anderem die subtraktive Methode, die additive Methode, die Lithographie, das *Bioprinting*, die Funktionalisierung von Gerüstmaterialien sowie die Kokultuvierung [201]. Es werden bei der Gefäßneubildung Strukturen wie z.B. Kanäle aus den jeweiligen Materialien geschaffen, während bei der Vaskulogenese und bei der Angiogenese Zell-Zell-Interaktionen hergestellt werden, so dass eine Gefäßstruktur entsteht [201]. Als nichtabbaubare Substanzen dienen Silikon und PDMS und als biologisch abbaubare Materialien kommen Polylactid-co-Glycolid, Polyglycerol-Sebacat und Polycarobolacton zum Einsatz [201]. Die neueren Methoden verwenden dagegen Calcium Alginat, Agarose, Kollagen, Fibrin oder Polyethylen-Glycol-Diacrylat [201]. Anhand eines mikrofluiden Blutgefäß-Modells konnte gezeigt werden, dass SiO_2-

Nanopartikel zu einer vermehrten Aggregation von Blutplättchen führen, wobei die Viabilität der Blutplättchen nicht beeinträchtigt wird [203].

Innovationen sind zudem auch im Bereich der kardiovaskulären Testsysteme erforderlich [46]. Denn die Simulation des Herzens erfordert komplexe Systeme, damit die gleichmäßige Kontraktion des Herzmuskels durch elektrische und mechanische Stimulation simuliert werden kann [46, 190]. Erste Fortschritte und Erfolge im Bereich der *Heart-on-a-Chip*-Modelle konnten schon erreicht werden. Studien ergaben, dass die Intensität der Kontraktion der Herzmuskelzellen von der Steifheit der Matrix abhängt [46]. Da die Herzmuskelzellen weichere Materialien bevorzugen, soll die Zelladhäsion mit Hydrogel-Matrices [204] oder Fibronektin-Beschichtungen verbessert werden [46]. Zur Simulation der linken Herzkammer wurden die physikalischen Faktoren wie Druck, Ausdehnung und Frequenz kontrolliert. Embryonale Kardiomyzeten wurden auf einer dünnen Membran besiedelt und einem pulsartigen Fluss ausgesetzt, um die Zirkulation im Herzen zu simulieren [205]. In dem von Grosberg et al. (2011) entwickelten *Heart-on-a-Chip*-Modell wurden Herzmuskelzellen auf PDMS, das zuvor mit Fibronektin beschichtet wurde, besiedelt [206]. Die Zellen wurden elektromagnetisch stimuliert, so dass die Kontraktion des Herzens simuliert werden konnte [206]. Über die Intensität der Kontraktion des Herzens konnten Herzwirkstoffe wie zum Beispiel das Epinephrin getestet werden [206]. In einem weiteren Herzmodell kommen spezielle Zellkulturoberflächen zum Einsatz, die mit einem temperaturabhängigen Polymer, Polyisopropyl-Acrylamide beschichtet sind [207]. Wenn die Oberfläche mit Zellen vollständig besiedelt ist, wird die Temperatur reduziert. Dadurch ändert sich die Eigenschaft der Zellkulturoberfläche leicht, so dass sich die Zellen ablösen [207]. Im Unterschied zu einer enzymatischen Trypsinierung bleiben allerdings die Zellinteraktionen und die komplette Zellschicht erhalten. Diese kann dann auf eine neue Oberfläche transferiert werden. Bei der Überlagerung von mehreren Zellschichten konnte beobachtet werden, dass diese spontan anfangen zu pulsieren. Histologische Untersuchungen ergaben starke Übereinstimmungen mit den realen Herzstrukturen [207].

Zukünftig ist besonders die Kombination von verschiedenen Organen von Interesse. Erste Erfolge von *Multi-Organ-on-a-Chip*-Modellen wurden durch die Kokultivierung von Leberzellen und Fibroblasten in Transwells® bei dynamischen Bedingungen erreicht [208]. Nach 14-tägiger Kultivierung wurden unterschiedliche Sensitivitäten auf toxische Substanzen in der Kokultur und in den Einzelkulturen beobachtet [208]. Mit einem *Multi-Organ-on-a-Chip*-Modell, bestehend aus einer Kokultur aus Nervenzellen und Lebersphäroiden, konnten Langzeituntersuchungen von 2,5 Hexandion (Toxin) über zwei Wochen durchgeführt werden [209]. Die Kokultur war dabei sensitiver als die beiden einzelnen Kulturen [209].
Zur Simulation des menschlichen Organismus wurden 3D-Zellaggregate aus verschiedenen menschlichen Zelltypen wie C3A, A549, HK-2 und HPA über ein Mehrfachflusssystem miteinander verknüpft [210]. Die Wirkung von Substanzen kann damit simultan an mehreren Zelltypen

erfolgen [210]. Das langfristige Ziel der *Organ-on-a-Chip*-Technologie ist die Kombination von verschiedenen Orangen bis hin zum ganzen Organismus. In Fig.2-6 ist schematisch ein *Body-on-a-Chip*-Modell mit Lunge, Herz, Leber, Niere, Knochen, Darm und Leber dargestellt. Die einzelnen Organe sind über ein mikrofluides Gefäßsystem miteinander verbunden. Der Transport von Wirkstoffen und Nanopartikeln, die über die Lunge oder oral aufgenommen werden, könnte so untersucht werden.

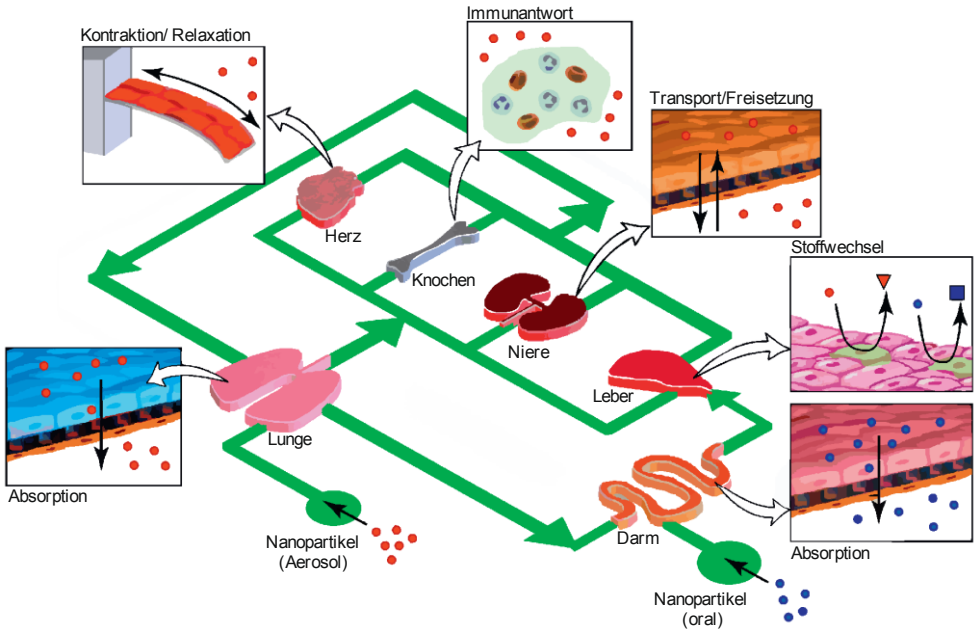

Fig. 2-6 Schematische Darstellung eines *Body-on-a-Chip*-Modells, modifiziert nach Huh et al. (2011) [196]. Die verschiedenen Organe werden in Mikrosystemen dargestellt und mit einem mikrofluiden System miteinander verknüpft. Die respiratorische und orale Aufnahme von Nanopartikeln sowie deren Metabolismus könnte damit in Zukunft simuliert werden. Das Modell integriert dabei die Absorption in der Lunge, die Immunantwort in den Knochen, die Transport- und Spaltungsvorgänge in der Niere sowie den Abbau in Leber und Darm. Zudem kann die Wirkung auf das Herz untersucht werden. [196]

Insgesamt sind die *Organ-on-a-Chip*-Modelle sehr vielversprechend sei es für die Wirkstoff- und Toxintestung oder auch im Bereich der regenerativen Medizin. Vor allem die von der OECD vorgeschriebenen Langzeit-Experimente für Chemikalien und Kosmetika könnten mit der neuen Technologie erfolgen [209]. Teilweise korrelierten die Nanopartikel-Untersuchungen der *Organ-on-a-Chip*-Experimente mit den *in-vivo*-Ergebnissen, allerdings können mit den bisherigen Lebermodellen noch keine reproduzierbaren Stoffwechsel von Wirkstoffen simuliert werden [46]. Es fehlen standardisierte Techniken und vergleichbare Organmodelle [46]. Ideal wäre ein modulares System, bei dem nur die Zelltypen verändert werden [46]. Zudem sollten mikrovaskuläre 3D-Zellkulturen, deren mikroskopische Detektion sowie die Analyse des Proteingehalts und ihrer Geneexpression etabliert werden [46, 190]. Auch die Kontrolle der Sauerstoff- und CO_2-Konzentration, des pH-Werts sowie die Flussrate in den Mikroinkubatoren ist zu optimieren [190]. Zusätzlich muss überprüft werden, ob die *in-vivo*-Bedingungen abgebildet werden und vor allem ob die gewonnenen Erkenntnisse auf den Menschen übertragbar sind.

3 Das hierarchische, zellbasierte Screening-System

3.1 Zusammenfassung

Die stetig wachsende Anzahl an Industrie- sowie Verbraucher-Nanoprodukten erfordert ein umfassendes Risikomanagement der neuen Materialien. Bei der Herstellung der Nanoprodukte kommen verschiedene Personengruppen in Kontakt mit den unterschiedlichen Vorstufen. Da sich die Eigenschaften der Nanomaterialien während ihres Lebenszyklus ändern können, sollten die Produkte in jeder Entwicklungsstufe untersucht werden. Die möglichen Wechselwirkungen mit den Menschen und der Umwelt sind zu analysieren. Derzeit fehlen jedoch einheitliche Richtlinien für die Testung von Nanopartikeln und Nanomaterialien. Für die *in-vitro*-Untersuchungen werden die Testsysteme der Wirkstoffe verwendet. Dabei weisen Nanopartikel andere Eigenschaften auf, die die Ergebnisse der Tests beeinflussen können. Die Stabilität der Nanopartikel im Zellkulturmedium ist z.B. nicht immer gegeben, die Nanopartikel können mit *Assay*-Komponenten interferieren oder eine Eigenfluoreszenz aufweisen. Vor allem Metalloxid-Nanopartikel können die Farbstoffe reduzieren, die bei den traditionellen Zytotoxizitättests eingesetzt werden, so dass falschpositive Ergebnisse die Folge sind. Des Weiteren kann die Eigenfluoreszenz einiger Nanopartikel das detektierte Signal beeinflussen. Zudem agglomerieren viele Nanopartikel im Zellkulturmedium bei einem neutralen pH-Wert. Form und Größe der Partikel werden dadurch verändert, so dass sich ihre Interaktionen mit den Zellen, wie z.B. deren Aufnahme in die Zelle, ändern.

Für eine relevante Risikobewertung der Nanopartikel müssen daher verschiedene Toxizitätstests an unterschiedlichen Zelltypen angewendet werden. Aufgrund der Vielzahl von Nanomaterialien und deren Vorstufen können jedoch nicht alle Materialien mit allen Methoden untersucht werden. Daher wurde ein zellbasiertes, iteratives *Screening*-System entwickelt, mit dem die Wirkung von einer großen Anzahl von Nanomaterialien auf verschiedene Zellsysteme untersucht werden kann (Veröffentlichung III, Kapitel 3). Zur Etablierung der Methoden des *Screening*-Systems wurden exemplarisch Zinkoxid- (ZnO), Titandioxid- (TiO_2) und Silber- (Ag) Nanopartikel als *Benchmark*-Partikel eingesetzt. Als Modellzelllinien wurden A549-Zellen sowie NIH-3T3-Zellen verwendet. Die Wirkungen der Nanopartikel auf unterschiedliche biologische Prozesse wie die Zellmorphologie, die Zellviabilität und die Genexpression von Biomarkern wie Interleukin 8 oder dem Hitzeschockprotein 70 wurden analysiert. Zusätzlich wurde untersucht, ob statt der Testung von Nanopartikelsuspensionen im Zellkulturmedium alternativ auch Nanopartikel-Beschichtungen getestet werden können. Dadurch sollen mögliche Stabilitätsprobleme der Nanopartikel vermieden werden.

Das entwickelte *Screening*-System ist in ein *Pre-*, *Fine-* und *Complex-Screening* unterteilt. In dem *Pre-Screening* werden einfache Methoden mit allen Materialien durchgeführt, während die Komplexität der Methoden vom *Fine-* bis zum *Complex-Screening* zunimmt und nur für ausgewählte Materialien angewendet wird. Im *Pre-Screening* werden die Wirkungen auf die Zellviabilität und die

Zellmorphologie untersucht. Nanomaterialien werden aussortiert, die im *Pre-Screening* bereits signifikante Effekte aufzeigen. Mit den verbleibenden Materialien werden im *Fine-Screening* sensitivere Methoden eingesetzt, die einen breiten Wirkungsbereich der Nanopartikel auf die Zellen abdecken. Etwaige Fehlinterpretationen der Ergebnisse, bedingt durch die optischen, elektrischen oder chemischen Eigenschaften der Nanopartikel, sollen durch die Anwendung von verschiedenen Detektionsmethoden wie Mikrokopie, Absorption, Fluoreszenz, Lumineszenz und Impedanz minimiert werden. Informationen werden erhalten über den Energiestoffwechsel, die Art des Zelltods, die Proliferation, die Genexpression, DNA-Schädigungen und Zelladhäsion nach der Exposition mit den Nanomaterialien. Des Weiteren kann die Nanopartikel-Aufnahme und die Erzeugung von reaktiven Sauerstoffspezies untersucht werden.

In Abhängigkeit von der späteren Anwendung der Nanomaterialien ergeben sich unterschiedliche Gefahren für den Menschen und verschiedene Aufnahmemöglichkeiten in den Organismus. Im vorgestellten *Screening*-System kommen daher verschiedene Zelllinien zum Einsatz, wie Fibroblasten, Lungen-, Leber-, Nieren- oder Darm-Zellen. Die Zelllinien weisen unterschiedliche Sensitivitäten und Zelltyp-spezifische Verhalten auf und liefern reproduzierbare Ergebnisse. Zusätzlich zu den Zelllinien werden vor allem im *Complex-Screening* auch Primärzellen eingesetzt, die besser der Zellphysiologie *in vivo* entsprechen. Um die Komplexität der Zellkulturen für die *in-vitro*-Testung von Nanopartikeln zu erhöhen, werden im *Complex-Screening* zudem auch dreidimensionale (3D) Zellkulturen anstelle der zweidimensionalen (2D) Kulturen angewendet. Die Zell-Zell-Wechselwirkungen und die extrazelluläre Matrix *in vivo* können somit besser nachgeahmt werden. Des Weiteren sollen dynamische Bedingungen das Strömungsverhalten von Blut- und Herzkreislauf imitieren. Außerdem kann der Abtransport von Stoffwechselprodukten erfolgen und eine homogene Nanopartikel-Konzentration im Medium erreicht werden. Durch Kombination beider Zellsysteme können Langzeitanalysen durchgeführt werden. Da diese Modelle sehr viel komplexer sind, werden diese nur mit ausgewählten Nanomaterialien durchgeführt.

Zunächst wurde das *Pre-Screening* aufgebaut, in dem die Wirkungen der Nanopartikel auf die Zellviabilität und die Zellmorphologie untersucht werden. Für die Entwicklung des *Screening*-Systems wurde zunächst die Sensitivität der Zellmorphologie-Studien für die *in-vitro*-Testung von Nanopartikeln analysiert. Die Untersuchung der Zellmorphologie stellte eine wichtige Methode für die Detektion der Nanopartikel-Effekte auf die Zellen dar. Morphologie-Änderungen nach der Exposition mit ZnO-Nanopartikel konnten in 2D-Kulturen als auch in 3D-Hydrogelsystemen beobachtet werden. Fehlinterpretation von anderen Toxizitätstests, bedingt durch Wechselwirkungen der Nanopartikel mit den *Assay*-Komponenten, könnten durch zusätzliche Morphologie-Studien minimiert werden. Bei einigen Zellsystemen wie dem 3D-*Scaffold*-Modell sind jedoch nur aufwendige Rasterelektronenmikroskopie-Aufnahmen möglich. Eine methodische Herausforderung bei der *in-vitro*-Testung von Nanopartikeln ist die Herstellung von stabilen wässrigen physiologischen Nanopartikel-Suspensionen,

da viele Nanopartikel bei diesen Bedingungen agglomerieren. Alternativ zu der Untersuchung von Nanopartikel-Suspensionen konnte demonstriert werden, dass auch Beschichtungen analysiert werden können. Hierbei kann das Zellwachstum auf beschichteten Oberflächen sowie die Wirkung von herausgelösten Nanopartikeln bestimmt werden.

Im *Fine-Screening* wird unter anderem zur Genexpressionsanalyse die quantitative *PCR* eingesetzt werden. Dazu wurde die Expression von Interleukin-8 (Il-8) als Biomarker für Entzündungsreaktionen und vom Hitzeschockprotein 70 (Hsp 70) als Biomarker für eine oxidative Stressreaktion nach der Exposition mit den beiden Nanopartikel-Suspensionen analysiert. In beiden Ziellinien wurde nach der ZnO-Nanopartikel-Exposition eine erhöhte Il-8-Expression detektiert, aber nicht für TiO_2-Nanopartikel. Für Hsp 70 wurde dagegen nur bei den A549-Zellen eine Zunahme der Expression durch ZnO-Nanopartikel beobachtet. Außerdem wurde die *Electric-Cell-Substrate-Impedance-Sensing* (ECIS)-Methode angewendet, um die Wirkungen der Nanopartikel online zu verfolgen. Direkt nach der Zugabe der ZnO-Nanopartikel wurde eine Abnahme des Impedanz-Signals festgestellt, bedingt durch eine verminderte Zelladhäsion. Für TiO_2-Nanopartikel wurde dieser Effekt nicht beobachtet.

Für das *Complex-Screening* wurden verschiedene 3D-Zellkulturmodelle auf deren Anwendbarkeit für die Testung von Nanopartikeln analysiert. Bei dem 3D-*Scaffold*-Modell werden die Zellen auf einer 3D-Gerüstsubstanz besiedelt, wohingegen beim 3D-Hydrogel-Modell die Zellen im Hydrogel eingekapselt werden. Im dritten, dem 3D-Sphäroid-Modell, werden Zellaggregate gebildet, so dass keine zusätzlichen Hilfsmaterialien benötigt werden (Veröffentlichung VII, Kapitel 5). In Abhängigkeit vom verwendeten 3D-Modell sind unterschiedliche Zytotoxizitätstests geeignet. Mit den drei 3D-Zellkulturmodellen wurden unterschiedliche kritische Konzentrationen für ZnO-Nanopartikel bestimmt. Daher sollte bei der Wahl des im *Complex-Screening* angewendeten 3D-Modells die spätere Anwendung des Nanomaterials berücksichtigt werden. Je nach 3D-Modell können unterschiedliche Aspekte der Zell-Zell-Interaktion simuliert werden. Während mit dem Sphäroid-Modell Zell-Zell-Kontakte und natürliche Diffusionsbarrieren, wie sie *in vivo* vorliegen, simuliert werden können, ist es möglich, mit dem 3D-*Scaffold*-Modells Organstrukturen zu erstellen. Mittels des transparaten 3D-Hydrogel-Modells können die Zell-Zell-Kontakte mikroskopisch detektiert werden.

Mit dem entwickelten *Screening*-System kann prozessbegleitend, d.h. während der Herstellung der Nanomaterialien die Toxizitätstestung der Vorstufen erfolgen. Durch die hierarchische Struktur ist es hoch effizient, kostenminimierend und der Einsatz von Tierexperimenten kann reduziert werden. Je nach Anwendung können Nanopartikel-Suspensionen oder die Stabilitäten von Nanopartikel-Beschichtungen und Nanokompositen analysiert werden.

Das beschriebene *Screening-System* (Veröffentlichung III) wurde während der Dissertation für verschiedene Anwendungsbereiche eingesetzt.

Bei der Risikobewertung von Metall-Nanopartikeln sollte berücksichtigt werden, dass sich Ionen ablösen und einen schädlichen Einfluss auf die Zellen haben könnten. Für die weitere Entwicklung des *Screening*-Systems wurden daher in Veröffentlichung VI (Kapitel 4) die Wirkung von Nanopartikeln und deren Ionen auf verschiedene Zelltypen separat überprüft. Als *Benchmark*-Nanopartikel kamen hier Ag-Nanopartikel bzw. Ag^+-Ionen zum Einsatz. Im *Pre-Screening* wurde die Zellviabilität mittels des MTT-Tests analysiert und die Zellmorphologie untersucht. Als Methoden des *Fine-Screenings* wurden zur Analyse der Zelladhäsion die ECIS-Messung und zur Zelltod-Bestimmung der LDH-Test sowie der Caspapse 3/7-Test angewendet. Mit den ausgewählten Methoden des *Pre-* und *Fine-Screenings* konnten Unterschiede in der Wirkung der Nanopartikel und der Ionen auf die Zellen ermittelt werden. Die Methoden sind daher für das *Screening*-System geeignet. Im Vergleich zu den Ag^+-Ionen waren die Ag-Nanopartikel wesentlich toxischer. Des Weiteren wurden unterschiedliche Zelltod-Mechanismen festgestellt. Während die Partikel die Apoptose einleiteten, führten Ionen zu nekrotischem Verhalten.

Des Weiteren spielt die Aufnahme der Nanopartikel in die Zelle eine entscheidende Rolle (siehe auch Kapitel 2.3), so dass diese Interaktion mit der Zelle auch im *Screening*-System zu überprüfen ist. Bisher wurde die Aufnahme in die Zelle mikroskopisch mittels Transmissionselektronenmikroskopie (TEM) oder für fluoreszierende Nanopartikel, wie Quantum Dots oder Fluoreszenz-markierte Nanopartikel, mittels Fluoreszenzmikroskopie beobachtet. Die TEM-Aufnahmen sind dabei aufwendig und erfordern eine lange Probenvorbereitung. Bei der Fluoreszenzmikroskopie müssen einige Nanopartikel mit Fluoreszenzfarbstoffen markiert werden, wodurch sich ihre charakteristischen Eigenschaften ändern können. Zudem sind beide Methoden qualitativ und nicht quantitativ, da nur wenige Zellen untersucht werden. Für ein repräsentatives *Screening* von einer Vielzahl von Nanopartikeln sind diese Methoden daher nicht geeignet. Für das *Screening*-System wurde daher eine alternative Testmethode zur Detektion der Nanopartikel-Aufnahme untersucht.
Die Durchflusszytometrie stellt eine gute Alternative dar, mit der über das Seitwärtsstreulicht die Granularität der Zellen detektiert werden kann. Es ist anzunehmen, dass durch die Nanopartikel-Aufnahme die Granularität der Zellen zunimmt. Eine Markierung der Nanopartikel mit Fluoreszenzfarbstoffen ist dadurch nicht notwendig. Um diese Methode für den Einsatz im *Fine-Screening* zu etablieren, wurde die Aufnahme von TiO_2-Nanopartikeln in A549-Zellen und NIH-3T3-Zellen überprüft. Das detektierte Seitwärtsstreulicht (SSC) nahm in Abhängigkeit von der eingesetzten TiO_2-Nanopartikel-Konzentration zu. Damit werden bei höheren Konzentrationen mehr TiO_2-Nanopartikel in die Zelle aufgenommen bzw. adsorbieren an der Zellmembran. Bei einer TiO_2-Nanopartikel-Konzentration von 50 µg/ml war bei den NIH-3T3-Zellen eine Sättigung erreicht. Außerdem stieg bei den NIH-3T3-Zellen das SSC-Signal in Abhängigkeit von der Expositionsdauer der TiO_2-Nanopartikel (50 µg/ml) an. Für die A549-Zellen hingegen wurde diese kontinuierliche, zeitabhängige

Zunahme des SSC-Signals nicht beobachtet. Die beiden Zelllinien variieren demnach in der Aufnahme der TiO_2-Nanopartikel. Die Veröffentlichung dieser Ergebnisse ist derzeit in Vorbereitung.

Des Weiteren wurde das *Screening*-System im Rahmen der Dissertation für die Herstellung von Aluminiumoxid-Nanokompositen, die bei Sanitärkeramiken eingesetzt werden sollen, angewendet (Veröffentlichung I, Kapitel 7). Die toxikologische Analyse der Ausgansmaterialien, Zwischenprodukte sowie der entwickelten Nanokomposite erfolgte prozessbegleitend. Um eine hydrophobe Nanokomposit-Oberfläche für einen *Easy-to-Clean*-Effekt zu erreichen, wurden die Nanopartikel-Größe sowie die eingesetzte –Konzentration variiert. Nanokomposite mit einem Feststoffgehalt von 4 % mit Partikelgrößen von 120 nm oder 130 nm wiesen optimale mechanische Eigenschaften auf und waren nicht toxisch für die Zellen.

Die in der Veröffentlichung VII (Kapitel 5) etablierten 3D-Sphäroid-Modelle, die im *Complex-Screening* eingesetzt werden, wurden für die Toxizitätstestung von CdTe/CdS/ZnS (Kern/Schale/Schale) Quantum Dots (QD) angewendet (Veröffentlichung IV, Anhang A1). Hierfür wurde die Wirkung der QD auf humane mesenchymale Stammzell-Sphäroide untersucht. Die QD wurden dabei während sowie nach der Sphäroid-Bildung hinzugegeben und die Zellantwort untersucht. Analog zu den Ergebnissen in Kapitel 5 konnte eine Korrelation der Sphäroid-Durchmesser in Abhängigkeit von den toxischen QDs festgestellt werden. Mittels des ATP-Tests wurden signifikante Unterschiede zwischen 2D- und 3D-Zellkulturen beobachtet. Die 2D-Zellkulturen reagierten sensitiver auf die QD als die 3D-Zellkulturen. Die Ergebnisse der Publikation bestätigen, dass die etablieren 3D-Sphäroid-Modelle für das *Screening*-System essentiell sind.

Das entwickelte *Screening*-System ist jedoch nicht nur auf die Testung von Nanomaterialien beschränkt. Für die Zulassung von Wirkstoffen und Medizinprodukten sind *in-vitro*-Untersuchungen erforderlich. Die Methoden des *Screening*-Systems wurden genutzt, um erste Einschätzungen über die *in-vitro*-Toxizität des Medizinproduktes 4DryField® PH der Firma PlantTec Medial zu untersuchen. Das Medizinprodukt ist aufgrund seiner hohen Wasserabsorption für die Blutstillung zertifiziert. Außerdem verhindert es Verwachsungen (Veröffentlichung V, Anhang A2). Die *in-vitro*- und *in-vivo*-Biokompatibilität des neuen Polysaccharids 4DryField® PH wurde überprüft. Dabei zeigten die Polysaccharide *in vitro* auf die beiden Tumorzelllinien A549-Zellen (humane Lungenepithel) und L929-Zellen (Mäuse-Fibroblasten) keine zytotoxische Wirkung. Die *in-vivo*-Studien an Ratten belegten verträgliche Dosen von bis zu 1,09 g/kg Körpergewicht. Darüber hinaus wurden keine negativen Auswirkungen auf das allgemeine Wohlbefinden der Tiere bedingt durch das 4DryField® PH festgestellt. Die Biokompatibilität des 4DryField® PH ist somit gegeben.

Zusätzlich kann das *Screening*-System für die Biokompatibilität-Testung von Materialien angewendet werden, die in der Biomedizin eingesetzt werden. Hier können Implantate, Schrauben, Werkzeuge sowie 3D-Gerüstsubstanzen analysiert werden. Zur Herstellung dieser Komponenten könnte zukünftig

das 3D-Druckverfahren genutzt werden, da es eine hohe Flexibilität aufweist und je nach Anwendung komplexe Geometrien und Strukturen hergestellt werden können. Verwendete Materialien müssen vor dem Einsatz im menschlichen Organismus *in vitro* auf ihre Biokompatibilität umfangreich getestet werden. Im Rahmen der Dissertation erfolgte die Biokompatibilitäts-Testung von verschiedenen Polyamid-Pulvern (PA 12, PA 12 UV) (Veröffentlichung IX und X, Anhang A3 und A4). Hierfür wurde die Wirkung auf die Suspensionszellen CHO-K1, die adhärenten A549-Zellen und die NIH-3T3-Zellen sowie die Hefe-Kulturen (*Saccharomyces cerevisiae*) analysiert. Das bereits zertifizierte PA 12 Material sowie das bisher nicht zertifiziere PA 12 UV Material waren biokompatibel. Für das PA 12 UV Material wurde zudem ein besseres Zellwachstum beobachtet. Für die Hefe-Kultivierung kamen Well-Platten mit 23 verschiedenen Well-Geometrien zum Einsatz. Dabei wurde mit der quadratischen Well-Geometrie die höchste optische Dichte erreicht und somit das Wachstum der Hefe-Kultur begünstigt. Die Sauerstoffzufuhr wurde hier verbessert. In der Veröffentlichung konnte gezeigt werden, dass mit dem 3D-Druckverfahren komplexe Kulturgefäße hergestellt werden können, die für den Laborbedarf geeignet sind. Es können zeiteffizient neue Prototypen designt werden, die an die individuellen Anforderungen der Prozesse und der Organismen angepasst werden können. Hierbei können verschiedene Well-Platten, Schüttelkolben-Verschlüsse mit integrierten Luer-Anschlüssen und Filterhalterungen für selbst entwickelte Membran-Reaktor-Systeme hergestellt werden.

3.2 Iterative Cellular Screening System for Nanoparticle Safety Testing

Franziska Sambale[1], Frank Stahl[1*], Ferdinand Rüdinger[1], Dror Seliktar[2], Cornelia Kasper[3], Detlef Bahnemann[1,4], Thomas Scheper[1]

[1] Gottfried Wilhelm Leibniz University Hanover, Institute for Technical Chemistry, Callinstr. 5, 30167 Hanover, Germany
[2] Technion - Israel Institute of Technology, Faculty of Biomedical Engineering,Haifa 32000, Israel
[3] University of Natural Resources and Life Science (Boku), Institute of Applied Microbiology, Muthgasse 18, 1190 Vienna
[4] Laboratory "Photoactive Nanocomposite Materials", Saint-Petersburg State University, Ulyanovskaya Str. 1, Peterhof, Saint-Petersburg, 198504 Russia

* Corresponding author: Frank Stahl, phone number: 049 511 762 2968, Stahl@iftc.uni-hannover.de

Published in Journal of Nanomaterials, Volume 2015 (2015), Article ID 691069, DOI: 10.1155/2015/691069. Reprinted with kind permission from Journal of Nanomaterials

3.2.1 Abstract

Nanoparticles have the potential to exhibit risks to human beings and to the environment; due to the wide applications of nanoproducts, extensive risk management must not be neglected. Therefore, we have constructed a cell-based, iterative screening system to examine a variety of nanoproducts concerning their toxicity during development. The sensitivity and application of the various cell-based methods were discussed and proven by applying the screening to two different nanoparticles: Zinc oxide and titanium dioxide nanoparticles. They were used as benchmarks to set up our methods and to examine their effects on mammalian cell lines. Different biological processes such as cell viability, gene expression of interleukin-8 and heat shock protein 70, as well as morphology changes were investigated. Within our screening system, both nanoparticle suspensions and coatings can be tested. Electric cell impedance measurements revealed to be a good method for online monitoring of cellular behavior. The implementation of three-dimensional cell culture is essential to better mimic *in vivo* conditions. In conclusion, our screening system is highly efficient, cost minimizing and reduces the need for animal studies.

Keywords: Nanoparticles, screening, *in vitro* assays, 3D cell culture, gene expression, impedance measurement, coating

3.2.2 Introduction

Nanoparticles have been used in many applications over the last decades such as cosmetics, medicine, and paints. In 2012 more than 100 products containing nanoparticles were available [211]. However, the constantly-increasing amount of industrial as well as consumer nanoproducts requires reliable and extensive risk management, as interactions with human beings and the environment grow more frequent. Various public exposure paths are possible [165], but up to now no standardized guideline for nanoparticle and nanomaterials testing exists [211, 212]. Currently for nanoparticle testing *in vitro*, only the commonly-used assays which are validated for drug testing are available. However, nanoparticles differ significantly from normal chemicals [165] and can interfere with the assays [165, 211-213].

In particular, oxidized nanoparticles are able to reduce assay dyes, causing them to underestimate cytotoxicity by overestimating cell viability [214]. Furthermore, a key challenge of *in vitro* nanoparticle safety testing is determining the stability of nanoparticles in biological media. For a plurality of nanoparticles, stable nanoparticle suspensions exhibit an acid pH value and/or contain different stabilizing agents. Thus, adding nanoparticles for *in vitro* cytotoxicity assays directly to the physiological aqueous culture media often results in nanoparticle aggregation and agglomeration [165, 215, 216].

While these limitations in nanoparticle cytotoxicity measurements are known, as long as alternative assays have not been investigated careful examinations of the results are needed. Furthermore, when choosing a method for nanoparticle testing it must be excluded that false-positive results can be misinterpreted. Nevertheless, for nanoparticle cytotoxicity studies *in vitro,* cell-exposure studies can yield the first evidence of their potential risk. These tests offer the advantages to be simple and to clarify the primary mechanism [211]. Additionally, these methods are rapid, cheaper and more reproducible than *in vivo* systems [211]. Thus, *in vitro* studies are often used before animal studies are applied. However, there are concerns about whether the results of these studies can really predict *in vivo* cell behavior. A comparison study of the effects of TiO_2 nanoparticles demonstrated a good correlation between acute toxicity measurements of *in vitro* and *in vivo* tests based on the steepest slopes of dose response curves [217]. Moreover, Kim et al could identify a higher cytotoxicity of nano-sized SiO_2 as compared with micro-sized particles *in vitro* as well as *in vivo* [218].

To improve the prediction of *in vivo* effects a set of *in vitro* assays investigating different mechanism is needed [218]. As *in vitro* assays cannot mimic real tissue conditions also more complex *in vitro* models like three-dimensional (3D) cell culture models could bridge the gap between classical two-dimensional (2D) *in vitro* models and *in vivo* studies.

The development of consumer nanomaterials implies long optimization procedures resulting in the formation of plenty of precursors and intermediates. All these materials may pose risks to human beings and the environment. All these materials must be tested for toxicity, especially with regards to the Occupational Safety provision and consumer protection. However, the number of *in vitro* cytotoxicity assays currently available is huge, consequently, all of these assays cannot be applied for all precursors, intermediates and products. Moreover, animal studies are ethically controversial and therefore limited. Thus, a broad and complex study can often not be performed because the bottlenecks are *in vitro* cell-based toxicity tests and *in vivo* animal studies which are very time-consuming and costly.

Therefore, the aim of our study was the development of an *in vitro* hierarchical nanoparticle screening system to examine any kind of nanoparticles concerning their toxicity. First, the structure of the screening system is presented in general. Next is a separate section of the pre-, fine- and complex-screening where the sensitivity and difficulties of the cytotoxicity assays are discussed. The

application of the methods in each screening level was proven exemplary with two different nanoparticles. This screening system includes different cytotoxic assays and complex cell culture systems such as a three-dimensional cell culture or dynamic cultivation to increase the relevance of *in vitro* assays. As nanoparticle suspension testing has limitations regarding the cell culture, we studied whether similar results can be obtained with nanoparticle suspensions and with coating experiments, respectively. According to the possible nanoparticle incorporation into the human organism, we used human lung carcinoma A549 cells (respiratory tract) and murine fibroblasts NIH-3T3 cells (skin). As a benchmark-system for the development of the screening system we investigated the effects of ZnO-NP and TiO_2-NP on mammalian cell lines. These two nanoparticle types have been used in different applications and their influence on 2D monolayer cultures has been analyzed previously. "For ZnO-NP cytotoxic effects have been published [212, 219-221] while the cytotoxicity of TiO_2-NP is still a point of discussion. Some studies have reported non-toxic effects for TiO_2-NP [222, 223] whereas other studies investigated cytotoxic effect of TiO_2-NP [223-225]. In the present study both nanoparticles were screened with the developed screening-system.

3.2.3 Materials and Methods

3.2.3.1 Nanoparticles

In this study ZnO-NP (with 0.1% Ru) were used, which were synthesized and characterized by Bloh et al. (2012, 2014) [226, 227]. The ZnO-NP have a Brunauer–Emmett–Teller (BET) surface of 6.54 m²/g and a particle size of 50 ± 10 nm (X-ray) [226]. ZnO-NP exhibited an average hydrodynamic diameter (dynamic light scattering) of 41± 5 nm in water, 190 ± 3 nm in Dulbecco's Modified Eagle Medium (DMEM) and 106 ± 11 nm in the standard culture medium (mean ± standard derivation) [228]. The TiO_2-NP (Hombikat XXS 700) were obtained from Sachtleben, Duisburg, Germany exhibiting a primary particle size of 7 nm (REM) in the anatase form according to the data sheet. The hydrodynamic diameter of TiO_2-NP was published by Sambale et al. (2015) [228]. In water TiO_2-NP have a diameter of 79 ± 25 nm, in DMEM 142 ± 29 nm and in the culture medium 118 ± 28 nm [228].

3.2.3.2 Cell Culture

A549 human lung carcinoma cells (DSMZ no.: ACC 107) and NIH-3T3 mouse fibroblasts cells (DMSZ no.: ACC 59) were purchased from the German Collection of Microorganisms and cell cultures (DSMZ). Both cell lines used here were cultivated in Dulbecco's Modified Eagle's medium (DMEM) (D7777 Sigma-Aldrich, Steinheim, Germany) supplemented with 10% fetal calf serum (FCS) and 100 µg/ml antibiotics (penicillin/streptomycin) in a humidified environment at 37°C/ 5% CO_2. Every 3 or 4 days cells were sub-cultivated when the cultures reached 70-80% confluence. The passage number of all used cells was less than 20.

3.2.3.3 3D Cell Culture

For 3D cell cultures, two different 3D cell culture models were performed. 20,000 cells were seeded on each side of a round scaffold of 1 mm thickness and 7 mm diameter via pipetting (matriderm®, Medskin Solution Dr. Suwelack AG, Germany). The scaffolds were placed in a 24-well-plate and were incubated at 37°C/ 5% CO_2 for 72 h to allow the cells to adhere and to build a 3D structure. Afterwards, the cells were treated in triplicates with different concentrations of ZnO-NP or TiO_2-NP in the cell culture medium for 24 h. As a second model, cell encapsulation in a semi-synthetic PEG-fibrinogen-based hydrogel (Faculty of Biomedical Engineering, Technion, Haifa, Israel) was investigated. Here, 1 ml hydrogel (fibrinogen concentration of 8 mg/ml) contains 1 x 10^6 cells and 10 µl photoinitiator (10% (w/v) in 70% ethanol). For generating defined hydrogel constructs, 50 µl of the hydrogel-cell-mixture were added to a 6 mm silicon gasket (Grace Bio-Labs silicone gasket for ProPlate® microarray system, Sigma-Aldrich, USA). Covalent cross-linking of the hydrogel was performed with UV light (6 W, 365 nm, VL-6L, Vilber Lourmat, France) for 2 min. Then, each hydrogel construct was placed in a 24-well plate containing 500 µl cell culture medium. Additionally, hydrogel constructs without cells were used as controls. To allow the cells to adhere in the hydrogel, to proliferate and to be connected to a 3D network the cells were incubated for 48 h before nanoparticle exposure for 24 h was performed.

3.2.3.4 Nanoparticle Testing

According to their doubling time a defined number of cells were seeded for each cell line. The A549 cells exhibit a doubling time of 40 hours, whereas NIH-3T3 cells exhibit a doubling time of 20 hours. For 2D cell culture experiments 8,000 A549 cells/well and 6,000 NIH-3T3 cells/well were seeded in 96-well plates (Sarstedt AG) and different exposure methods of ZnO-NP and TiO_2-NP were investigated. Suspension: For nanoparticle testing in suspension an aqueous nanoparticle suspension was diluted with cell culture media. The cells were cultured for 24 h in 100 µl standard culture medium before nanoparticle treatment and were exposed to different concentrations of nanoparticles for 24 h (triplicates). Coating: For coating experiments cells were seeded directly on nanoparticle coatings (triplicates) and cell viability was determined after 48 h. Extracts: In order to analyze wheatear nanoparticles were entered solution from the nanoparticle coatings, extracts were prepared according to the ISO standard 10993-12:2012 (Biological evaluation of medical devices – Part 12: Sample preparation and reference materials) [229]. Therefore, 3 cm²/ml cell culture medium were added to the nanoparticles coatings (different concentration in triplicates) and they were placed in an incubator at 37°C and 5% CO_2 for 24 h. Then standard culture medium was replaced to extract medium, and cells were cultured for a further 24 h in the incubator.

3.2.3.5 Cell Morphology

The effect of ZnO-NP and TiO_2-NP suspension on cell morphology in 2D and in 3D cell culture (hydrogel) was examined by phase contrast microcopy (Olympus IX 50, Olympus Corporation, Tokio, Japan) after cells were exposed to nanoparticles for 24 h.

3.2.3.6 Cell Viability

After nanoparticle exposure the cell viability was determined using either the CTB analysis (CellTiter-Blue® Cell Viability Assay, Promega, Madison, USA) or the MTT assay (Sigma-Aldrich, Munich, Germany). The MTT assay is based on the reduction of the yellow tetrazolium dye MTT to the insoluble blue formazan by metabolic active cells [230]. To perform the MTT assay the cell culture medium was removed from each well and 100 µl (2D cell culture)/300 µl (3D scaffolds) of 10% MTT solution (90 µl DMEM, 10 µl MTT stock solution (5 mg/mL phosphate buffered saline) were added to each well and incubated for 4 h at 37°C/ 5% CO_2. Afterwards 100 µl (2D cell culture)/200 µl (3D scaffolds) sodium dodecyl sulfate (SDS Solution) (1 g SDS in 10 ml 0.01 M HCl) was added to each well and samples were incubated for a further 18 h. To ensure that the formazan was released completely from the scaffold, the samples were shaken at a speed of 700 rpm. The absorption signal at 570 nm/630 nm was determined using a microplate reader (Bio-Rad, Munich, Germany) to quantify the results. Scaffolds without cells were used as background controls.

Comparable to the MTT assay, the CTB assay is based on the reduction of the blue resazurin to purple resorufin by metabolically active cells monitored via fluorescence. For the 3D hydrogel cell cultures 100 µl CTB stock solution was added to achieve a final concentration of 10% CTB solution and the dye was incubated for 18 h at 37°C/ 5% CO_2. Samples with hydrogel and different nanoparticle concentrations but without cells were used as background control. The fluorescence signals at an extinction wavelength of 544 nm and an emission wavelength of 590 nm were determined using a microplate reader (Fluoroskan Acent, Thermo Fisher Scientific Inc., Waltham, USA). For both assays the absorption/fluorescence signals of cell-free controls with different nanoparticle concentration were determined to prevent misinterpretations of the assays.

3.2.3.7 Electric Cell-Substrate Impedance Sensing

Electric Cell-Substrate Impedance Sensing (ECIS) measurements were performed to monitor the cellular behavior online. Therefore, cells were grown on 8W1E (8 well 1 electrode) ECIS slides (Applied BioPhysics, USA). Each of the eight wells contains an electrode covered with a gold film, used to apply an alternating current (AC) signal. Cell attachment, cell spreading, and cell morphological changes affect the measured electrode impedance which can be detected by ECIS™ Model 1600R (Applied BioPhysics, USA). Initially, each slide was equilibrated over night with 400 µl of standard culture medium. Then, the medium was removed and 125,000 cells (A549 cells or NIH-3T3 cells) in 400 µl standard culture medium were seeded per well. One well remained cell-free as reference. After approximately 48 h the cells had grown to confluence and the impedance signal was

stable. ZnO-NP or TiO_2-NP suspension in culture medium was added to the cells at least in duplicates at a concentration of the calculated half maximal inhibitory concentration (IC_{50}) value. In addition, at least two wells were filled with standard culture medium as a control while to the cell-free well nanoparticles were added at the same concentration. The impedance signal was monitored during the entire time of the measurement.

3.2.3.8 Quantification of the expression levels of il-8 and hsp70 mRNA

The quantification of the expression of *il-8* and *hsp70* genes was analyzed with quantitative real-time PCR (qPCR). In a T75 culture-flask 25,000 cells/cm² of A549 cells or NIH-3T3 cells were incubated at 37°C for 24 h until the cells were exposed to ZnO-NP or TiO_2-NP at a concentration of the IC_{50} value for 24 h. NIH-3T3 cells were exposed to 20 µg/ml ZnO-NP/TiO_2-NP and A549 cells to 40 µg/ml. Afterwards, the total RNA was isolated by using the RNeasy® Plus Mini Kit (QIAGEN, Hilden, Germany) following the manufacturer's instructions and the RNA concentration was measured at 260 nm by Nanodrop ND-1000 (Peqlab Biotechnologie GmbH, Germany). For cDNA synthesis 2 µg of RNA, 3 µl oligo (dt) primers (poly d(T) 12-18 Primer, Roth, Germany) in a total volume of 27 µl (add with ddH_2O) were incubated at 65°C for 5 min and then held at 4°C for 1 min. Then, 8 µl M-MLV RT 5 x Buffer (Promega, USA), 4 µl dNTPs (dNTP set, Thermo Scientific, USA) and 1 µl M-MLV Reverse Transcriptase (Promega, USA) were added and the mixture was incubated at 37°C for 1 h. The qPCR was performed with a reaction volume of 25 µl, containing 0.5 µl (0.2 µM) of each of the forward and reverse primers (see Tab. 3-1), 25 ng cDNA template and 12.5 µl IQ™ SYBR® Green Supermix (Bio-Rad, USA).

Tab. 3-1 Sequences of the primers used in qPCR.

Gene name	Gene Bank accession No. (NCBI GenBank)	Location (bp)	Expected size of PCR amplicon (bp)	Sequence (5'-3')
GAPDH	NM_002046.3	880-900 1005-984	126	F: AAGGTGGTGAAGCAGGCGTCG R: AATGCCAGCCCCAGCGTCAAAG
HPRT	NM_000194.2	650-669 897-916	267	F: AAGCTTGCTGGTGAAAAGGA R: AAGCAGATGCCCACACAACT
For A549 cells				
IL-8	NM_000584.3	221-240 351-332	131	F: CAGTTTTGCCAAGGAGTGCT R: AATTTCTGTGTTGGCGCAGT
Hsp70 (HSPA1A)	NM_005345.5	2049-2068 2186-2166	138	F:GTGTAACCCCATCATCAGCG R: CAATCTTGGAAAGGCCCCTAA
For NIH-3T3 cells				
IL-8	NM_011339.2	338-357 447-428	110	F: GAATTTCCACCGGCAATGAA R: TCCCGAATTGGAAAGGGAAA
Hsp70 (HSPA1A)	NM_010478.2	2141-2161 2244-2225	104	F: CATCGAGGAGGTGGATTAGAG R: ACCTTGACAGTAATCGGTGC

The measurements were carried out on an iQ5 Multicolor Real-Time PCR Detection System (Bio-Rad, USA) and all samples were run in triplicates. In addition, the efficiency of each primer pair was determined using serial dilution of the cDNA template. PCR reactions were performed at 95°C for 3

min followed by 40 cycles of 95°C for 10 sec and of 57°C for 20 sec. The data (comparative threshold (ct) values) were analyzed using the Gene Expression Analysis for iCycler iQ® Real-time PCR Detection System (Bio-Rad, USA). Glyceraldehyde 3-phosphate dehydrogenase (GAPDH) and hypoxanthine-guanine phosphoribosyltransferase (HPRT) were used as endogenous control genes to normalize the expression of the target genes. Therefore, the expression levels of *hsp70* and of *il-8* are expressed as n-fold differences relative to the reference genes.

3.2.3.9 Data and statistical analysis

For the determination of the IC_{50} value dose-response-curves were fitted to the data obtained by the MTT or the CTB assay using OriginPro 8.5.0 SR1 (nonlinear curve fitting, growth/sigmoidal, DoseResp). The data shown are from at least three independent experiments triplicates ($n \geq 3$). The ANOVA one-way analysis (OriginPro 8.5.0 SR1) was performed for statistical analysis and a significant effect was reported at * $p<0.05$.

3.2.4 Results and discussion

3.2.4.1 Development of a Cellular Screening System

In our recent study we have constructed and validated a cell-based, hierarchical screening system in order to realize the analysis of a variety of nanoparticles and nanomaterials under defined and reproducible conditions (Fig. 3-1). For this purpose, the published scheme for biomaterials in tissue engineering by Bruns et al. (2007) served as a template for our screening system for nanoparticles [231]. The idea of the screening system is that toxicity measurements are done during the course of nanomaterial development. The screening system is divided into the pre-, fine, and complex screening (Fig. 3-1). In the pre-screening simple methods are used for all materials, whereas more complicated techniques for fine and complex screening which are applied only to selected materials. Especially in fine screening, the assays cover various impact areas on the cells.

After each screening step cells exhibiting a significant variation as compared to non-treated cells are identified ($p< 0.05$, ANOVA one way). Materials causing such significant variations are not further investigated and rejected, whereas the remaining nanomaterials are subjected to further analyses. Continuous communication (feedback) between the process chain and the screening system is essential in order to optimize nanoparticle development and associated safety testing. Feedback should be given with regards to the toxicity and particle properties in order to select nanomaterials which are profitable and which should be further analyzed. Thus, the hierarchical structure facilitates making decisions as to which nanomaterials need complex, costly investigations or *in vivo* studies thus avoiding unnecessary testing of the remaining nanomaterials. Finally, only nanomaterials which pass the whole screening system without significant side-effects can reach the application level. Thus, our screening system is highly efficient, cost minimizing and reduces animal studies.

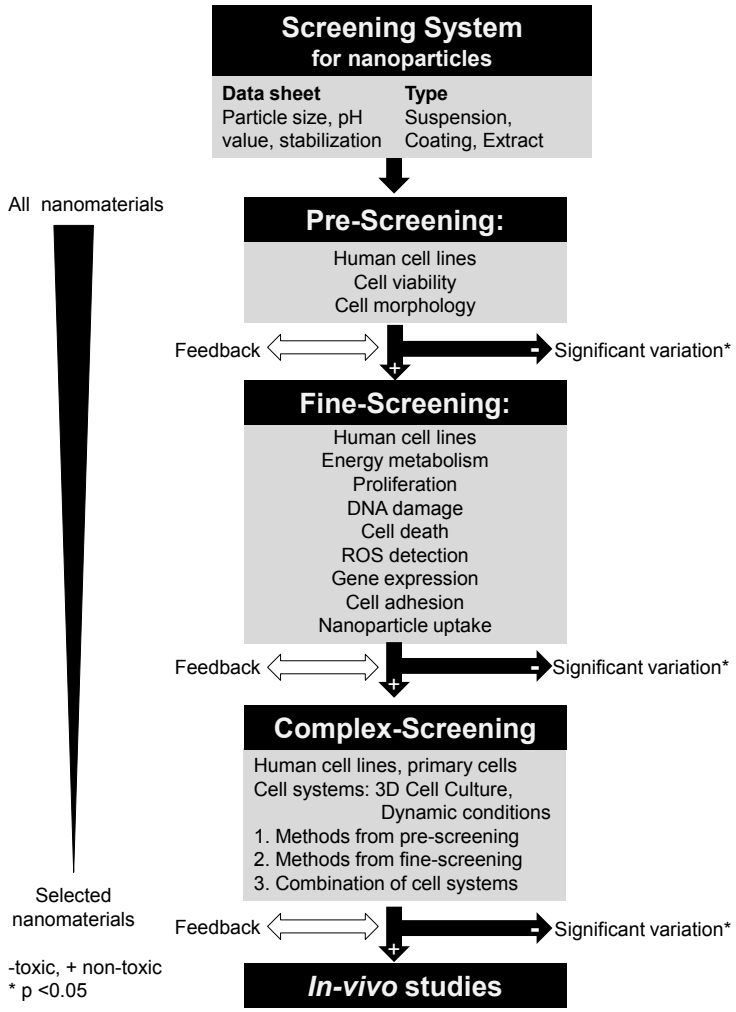

Fig. 3-1 Hierarchical cell-based screening-system for nanoparticle safety testing. The screening-system is divided in pre-, fine- and complex-screening and allows examining of a variety of nanoparticles during nanoproduct development. Pre-Screening is performed with all nanomaterials whereas complex cell systems are only applied to selected nanomaterials.

Before nanoparticles or nanomaterials can be analyzed in the screening system, a thorough characterization is needed. Therefore, a data-sheet is required which provides information about the size, the surface modification, the zeta potential, the aqueous stability, and the sterilization methods. According to the data-sheet information and the desired application of the nanomaterials, one specific type of nanoparticle testing is applicable such as suspension, coating, or extraction (detailed description is given below). For the evaluation of the nanoparticle screening system, two different, commonly-used kinds of nanoparticles were selected: ZnO-NP and TiO_2-NP. While the focus in this study has been on short-term nanoparticle exposure investigations, long-term conditions can also be tested in this complex-screening layout.

Concentrating on the desired application of the nanoparticles and on their potential absorption into the human organism different cell lines were selected for the pre- and for the fine-screening. The main absorption routes are via skin, via respiratory tract, and via gastrointestinal tract [211]. The skin, being the largest organ [211], provides a large target surface for nanoparticles. Recent studies have reported the penetration of nanoparticles [211] through the skin tissue which means investigations of *in vitro*

skin test systems are needed. In addition, nanoparticles can be inhaled and can be absorbed by pulmonary alveoli [211, 217]. Moreover, via the gastrointestinal tract nanoparticles can reach the liver and accumulate there [211]. With regard to the described adsorption routes, a matrix of relevant cell lines is required to identify cytotoxic effects of nanoparticles *in vitro* because various cell lines display different sensitivities and cell responses [211, 232].

To avoid cell-type specific behavior it is important to use different cell lines. Therefore, commonly used cell lines such as A549 cells (lung model) and NIH-3T3 cells (skin model) have been applied here. The use of mammalian cell lines in the screening system has the advantage that they provide reproducible results as cells are uniform, standardized, and well-characterized. Thus, cell lines provide the first evidence concerning the toxicity of the nanomaterials.
However, using standardized cell lines bears the disadvantage that their cell behavior cannot be easily transferred to *in vivo* conditions because they are often immortalized or isolated from tumors [215]. In addition, the proliferation rate of immortalized cell lines is often higher than that of *in vivo* cells [215]. Therefore, in the screening system primary cells and complex cell systems are examined to better mimic real tissue conditions in a human organism. These cell systems are three dimensional (3D) cell cultures where cells can develop more *in vivo*-like cell-cell-interactions and an extracellular matrix [233, 234]. Secondly, dynamic conditions are performed to mimic, for instance, the blood-stream. Both cell systems can finally be combined for a higher complexity and to perform long term exposure analysis. Since these models require much more complex settings, they are used only with selected nanomaterials in complex-screening.

3.2.4.2 Pre-Screening: Morphology Studies and Comparison of Nanoparticle Suspensions, Coatings and Extract Medium

Morphology studies of A549 cells and NIH-3T3 cells exposed to ZnO-NP and TiO_2-NP in 2D and 3D cell cultures

For in vitro studies 2D cell culture is needed in the pre-screening because it allows high-throughput screening. Thus, different nanoparticles, nanoparticle concentrations and various cell types can be tested in parallel. The pre-screening reduces the huge amount of nanomaterials obtained from the process chain to a more manageable number. Decisions have to be made which nanomaterial requires further investigation in the fine- or complex screening. The impact of the cell viability after nanoparticle exposure indicating cytotoxic effects is analyzed with commonly used assays such as the MTT, the CTB or the WST-1 (4-[3-(4-iodophenyl)-2-(4-nitrophenyl)-2H-5-tetrazolio]-1,3-benzene disulfonate) assay. With all three assays, comparable results can be produced and they differ only in their sensitivity. Besides these viability measurements, morphology studies are applied in the pre-screening. Cell morphology studies are important to support the results obtained with cytotoxicity assays, especially with regards to potential interference by the nanoparticles on the assay compounds.

Some harmful effects can be identified via cell morphology changes, so in these cases false-positive results may be detected.

To validate the significance of cell morphology studies for screening cytotoxic effects of nanoparticles, A549 and NIH-3T3 cells were treated with ZnO-NP or TiO_2-NP, respectively. In addition, the cells were grown in 2D as well as in 3D. For 3D cell cultures the cells were encapsulated in a hydrogel. The cell morphology of non-treated and treated cells was observed. The specific IC_{50} value calculated from the viability results for both cell lines and with both cell systems were displayed. In Fig. 3-2 the cell morphology of NIH-3T3 (c) and A549 cells (g) grown in 2D and treated with ZnO-NP were shown.

In the standard culture media the NIH-3t3 cells exhibited their characteristic contact arms to their neighboring cells (Fig. 3-2, a, b). ZnO-NP treated NIH-3T3 cells at the IC_{50} value changed their morphology turning smaller and rounder, characteristic of dead cells. At higher nanoparticle concentrations they became detached from the surface. For A549 cells grown in 2D, the control cells had a triangular shape and became round when ZnO-NP were added (IC_{50} value) (Fig. 3-2, e). In 3D the NIH-3T3 cells displayed the same changes as observed in the 2D cell culture (Fig. 3-2, b). In the hydrogel NIH-3T3 cells are highly networked (Fig. 3-2, b). At the IC_{50} value the cells turned round (Fig. 3-2, d). On the contrary, A549 cells grown in the hydrogel were round in the standard culture media as well as in the ZnO-NP treated media (Fig. 3-2, f, h). Thus, no significant differences in their morphology could be revealed. For TiO_2-NP no reduction in the viability was determined and both cells lines did not show any morphology changes (data not shown).

In summary, the morphology studies should be regarded as an important tool in the nanoparticle safety screening system. In some cases, however, the viability assay is not enough to pre-screen the nanoparticles accurately. In this context, for *in vitro* drug testing Quent el al. have reported an overestimation of the viability of daunorubicin-treated cells determined by the MTT assay [213]. The morphology study clearly displays the release of detached cells indicating cell death whereas the MTT was still reduced in the cells [213]. In our study, ZnO-NP morphology changes of NIH-3T3 cells could be observed in 2D as well as in the 3D hydrogels. Also for A549 cells grown in 2D the toxic effect of ZnO-NP was determined by the cell morphology studies. However, for A549 cells growing in hydrogel this method failed to identify toxic effects. Here, no changes in the morphology of the A549 cells after adding ZnO-NP to the culture were observed while the cell viability assay showed a significant reduction at this concentration (Tab. 3-1). Furthermore, different 3D cell culture models based on cell aggregation (spheroids), cell encapsulation (hydrogel), and cell adhesion on scaffolds are currently used to mimic a 3D environment. In particular the scaffold model hinders morphology studies as scaffolds are not transparent. In conclusion, morphology studies can support other cytotoxic assay but can only detect specific impacts of nanoparticle exposure.

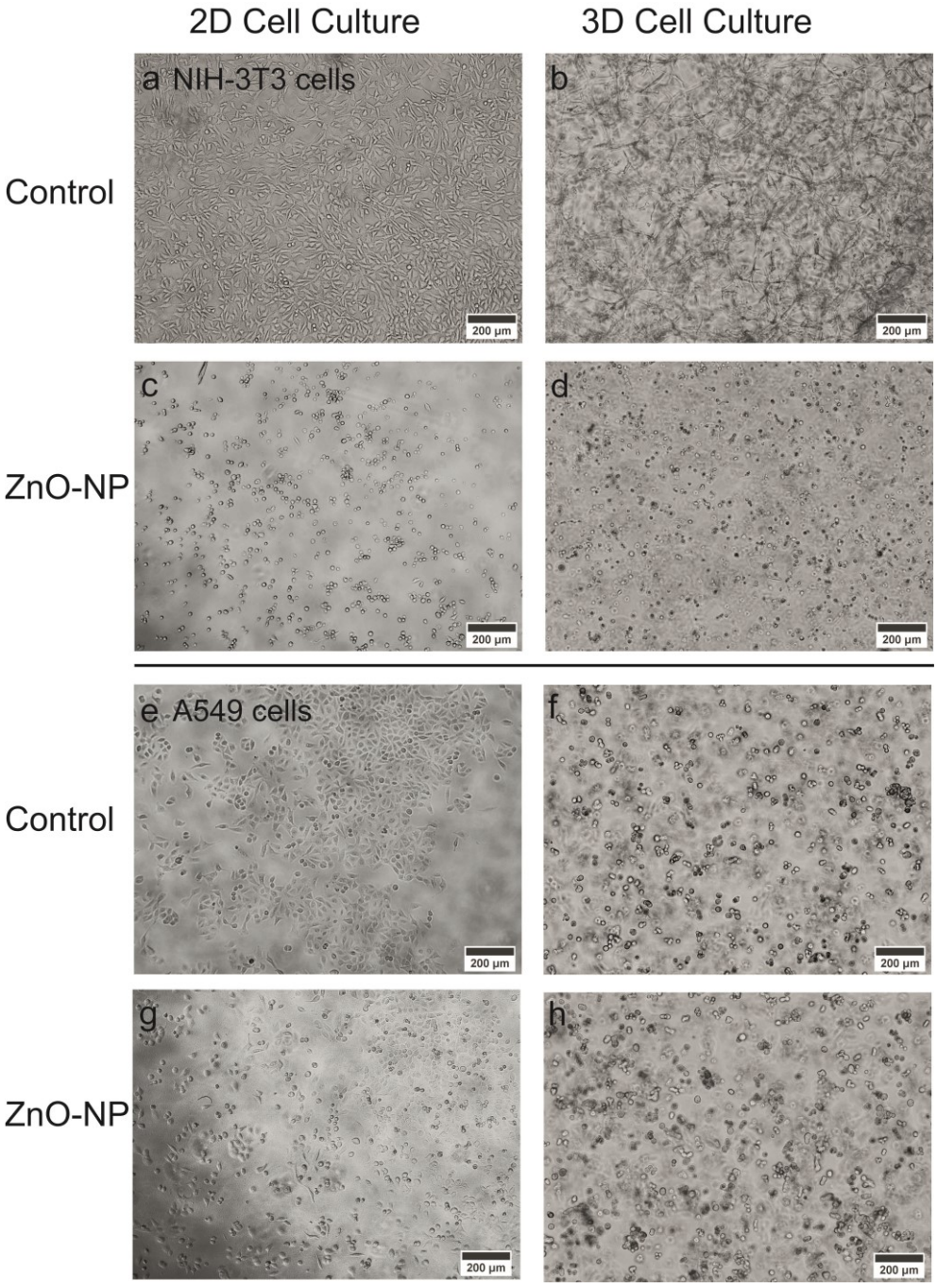

Fig. 3-2 Morphology studies of NIH-3T3 cells (a-d) and A549 cells (e-h) grown on 2D monolayers (a, c, e, g) or encapsulated in a hydrogel (3D cell culture) (b, d, f, h). NIH-3T3 cells were cultivated in standard culture medium (a, b) or were treated with 10 µg/ml ZnO-NP in 2D (c) and in 3D (d). For A549 cells 40 µg/ml ZnO-NP were added in 2D (g) and 300 µg/ml ZnO-NP in 3D (h). The A549 control cells cultivated in standard culture medium were displayed in e, f. Morphology changes after ZnO-NP exposure were observed in 2D for both cell lines whereas in 3D effects were only determined for NIH-3T3 cells.

Cell viability measurements of A549 cells and NIH-3T3 cells exposed to ZnO-NP and TiO_2-NP in suspension, extract medium or on coatings.

For *in vitro* nanoparticle safety testing, the methodological challenge is the preparation of stable, aqueous, physiological, nanoparticle suspensions because nanoparticles often agglomerate in biological media. As reported by Jones et al. (2009) these nanoparticle aggregation can affect several nanoparticle properties such as size and cellular uptake [215]. Currently, different dispersion protocols

and various biocompatible stabilizers were examined for generating stable nanoparticle suspensions [115, 216]. Protocols have thus been developed for the dispersion of nanoparticles in FCS using various centrifugation steps [216], in culture media, [216] or in an aqueous suspension [115]. Only with gum arabic as a stabilizer was the ZnO-NP suspension found to be stable for more than five days [115]. In this study alternative *in vitro* techniques were developed and validated to avoid the described problems with nanoparticle suspensions. We studied whether similar cell viability results can be obtained with nanoparticle suspensions, extract medium, and coatings. For this purpose both cell lines were seeded on nanoparticle coatings and viability measurements were carried out. Additionally, extract media from TiO_2-NP and ZnO-NP coatings, respectively, were prepared according to the ISO 10993–12:2012 standard for medical devices and subsequently used for the treatment of the cells [229]. Thereby, we wanted to monitor whether nanoparticles are dissolved from the coatings thus influencing the viability of the cells.

For TiO_2-NP no significant reduction in the viability of either cell lines tested was observed for all three methods (see supporting information, Fig. 3-8). On the other hand, the viability of the cells was reduced by ZnO-NP in a dose-dependent manner. In Fig. 3-3 the viability of ZnO-NP suspensions, coatings, and extract medium exposure to NIH-3T3 and to A549 cells is displayed. In addition, in Tab. 3-2 the IC_{50} value of the viability measurements are summarized.

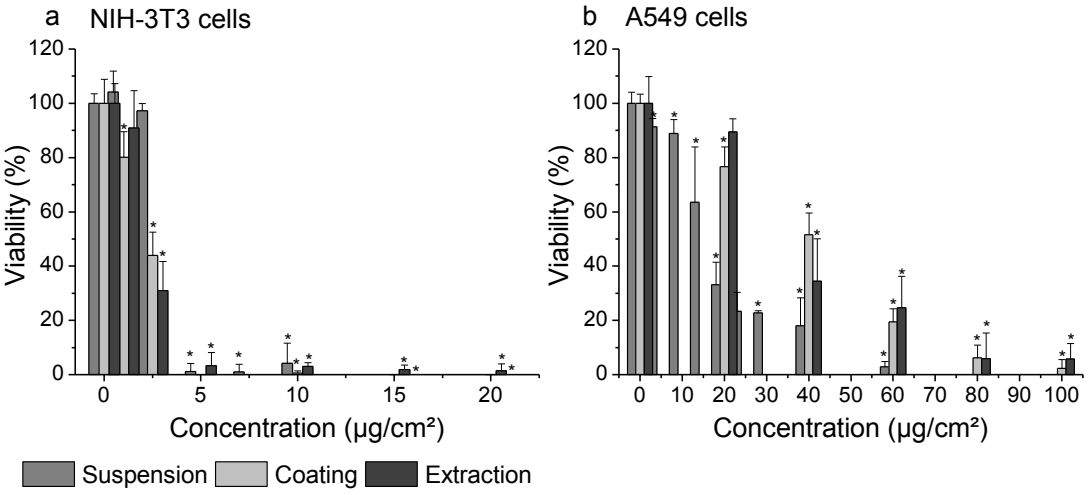

Fig. 3-3 Viability of NIH-3T3 cells (a) and A549 cells (b) after ZnO-NP exposure determined with the MTT assay. The cells were treated with nanoparticle suspension, coating or extract medium. The signals of untreated cells were set as 100%. Data points are means ± SD for $n \geq 3$.* $p<0.05$.

Tab. 3-2 Calculated IC_{50} value of NIH-3T3 cells and A549 cells treated with ZnO-NP suspensions, coatings or extract medium (MTT assay). For A549 cells the IC_{50} value for nanoparticle suspensions is twice lower as compared with the respective coatings. Data points are means ± SD for n ≥ 3

	IC_{50} value [µg/cm²]	
	NIH-3T3 cells	**A549 cells**
Suspension	3 ± 1	18 ± 5
Coating	2 ± 1	31 ± 8
Extract medium	2 ± 2	30 ± 8

For ZnO-NP toxic effects were detected with all three methods and with both cell lines performing the MTT assay. NIH-3T3 cells were found to be more sensitive to ZnO-NP than A549 cells, thus different cell lines apparently show a different sensitivity to nanoparticles. The NIH-3T3 cells exhibited the same IC_{50} value for ZnO-NP suspensions, coatings, and extract medium. On the contrary, the IC_{50} value determined for ZnO-NP suspensions in A549 cells was found to be half the IC_{50} value determined with the coating experiments. Therefore, instead of suspension testing for the identification of toxic nanoparticles, coating analysis can be a good alternative, especially for nanoparticles which agglomerate in standard culture media. For the coating and extract medium results no differences in the IC_{50} values were observed for either cell line. Thus, the determined reduction in the cell viability is apparently caused by the release of ZnO-NP from the coating. Our results clearly demonstrate that ZnO-NP exposure induces a decrease of the cell viability indicating toxic effects.

Obviously, nanoparticle effects to human cell lines can be either investigated with stable suspensions, with coatings, or with extract medium. The choice of strategy depends on the nanoparticle properties as well as the desired application of the nanoproduct. While for some nanoparticles a stable aqueous suspension in the cell culture medium can be produced, other nanoparticles agglomerate under these conditions. When evaluating the potential risk of nanoparticles to human beings, it should be considered that nanoparticles often may not reach the human organism as individual nanoparticles but rather as nanoparticle agglomerates. In *in vitro* studies, proteins present in the media often adsorb to the nanoparticles [165] thus affecting the cell response of the nanoparticle treatment. The same effect may take place in the human organism. However, nanoparticle agglomerate analysis can make sense, e.g., to predict the *in vivo* cell behavior. On the contrary, for the *in vitro* investigation of nanoparticle effects in the respiratory tract, stable nanoparticle suspensions are required. Inhaled particles with diameters below 2.5 µm can reach the pulmonary alveoli and can be absorbed [217]. For any nanoparticle test system it is therefore important to consider the relevance for human health effects [235].

As an alternative technique for nanoparticle *in vitro* testing we performed the coating method. However, the proliferation rate of adherent cells can be affected by nanostructured surfaces. Several studies have demonstrated that the surface roughness of the cell culture plates influences the cellular

behavior [236-238]. Therefore, the stability of certain nanoparticle coatings (nanomaterials, nano composites) and the effect of potentially solved nanoparticles to the human organism may be more relevant. Thus, the preparation of extract media is the chosen strategy for certain nanomaterial applications such as for medical devices, window glasses, or sanitation. Comparable with our extract experiments, Paddle-Ledinek et al. (2006) have used this method before to test wound dressings coated with nanoparticles [239]. In the present study, it could be shown that non-stable nanoparticle coatings require particular care during the testing process. Hence, measurements of the toxic effect of ZnO-NP with suspensions, coatings, and with the extraction method demonstrated that extract testing is an alternative indirect method to investigate the cytotoxicity of nanomaterials.

In summary, the nanoparticle screening system introduced here is capable of analyzing suspensions, coatings, as well as coating extractions regarding the respective application of the nanomaterials. Moreover, the analysis of the extract also monitors the stability of the coating.

3.2.4.3 Fine-Screening: Gene Expression Analysis and ECIS Measurements of A549 cells and NIH-3T3 cells Exposed to ZnO-NP and TiO_2-NP

Following the pre-screening assays, fine-screening tests were performed to provide higher sensitivity and to yield detailed information concerning the cells responses induced by the nanoparticle exposure. To avoid potential misinterpretations resulting from, e.g. possible interferences of nanoparticles with the assay components, different methods based on fluorescence or luminescence are used here in the fine-screening. Additionally, several positive and negative controls are needed. Moreover, for an accurate *in vitro* nanoparticle fine-screening, various biological effects of the nanoparticles were analyzed. The energy metabolism in the cells can, for example, be investigated with adenosine triphosphate (ATP). For cell death analysis, the release of lactate dehydrogenase (LDH) indicates necrosis and the caspase activity or the annexin V-FITC/PI assay indicating apoptosis can be performed. Changes in the proliferation rate of the cells can be detected with the bromodeoxyuridine (BrdU) assay which is based on the integration of BrdU, a chemical analogue of the nucleoside thymidine. BrdU can be detected by labeled antibodies and indicates the proliferation rate of the cell. Moreover, DNA damage in cells caused by the exposure to nanoparticles can be observed by the alkaline microelectrophoresis (comet assay). Also, the generation of reactive oxygen species (ROS) induced by nanoparticles can be determined, thus demonstrating stress for the cells. A commonly-used assay for the ROS detection is the DCF assay. In addition, nanoparticles may also affect the gene regulation, so the expression of selected marker genes can be quantified using real-time-PCR or microarray analysis. Molecular markers can, for instance, be mitosis markers, heat-shock proteins, interleukins, or apoptosis markers. While all the described methods are endpoint assays, the Electric Cell-Substrate Impedance Sensing (ECIS) measurement provides online data. Cell morphology changes such as cell rounding or surface detachment can be detected immediately after the addition of nanoparticles [165]. In addition, no additional compounds are required for this alternative technique, minimizing thus false positive results [240].

In our study, we investigated the effects of ZnO-NP and TiO_2-NP on the gene expression using real-time PCR analysis. We selected two established biomarkers: *il-8* indicating inflammation [241, 242] and *hsp70* indicating oxidative stress responses [243, 244]. In NIH-3t3 cells (Fig. 3-4, a) as well as in A549 cells (Fig. 3-4, b), the *il-8* mRNA level was increased when cells were exposed to ZnO-NP. Furthermore, ZnO-NP-induced *hsp70* expression in A549 cells (Fig. 3-4, b). On the contrary, exposing NIH-3T3 cells and A549 cells to TiO_2-NP did not lead to higher levels of the investigated biomarkers. The real-time PCR results clearly demonstrated that ZnO-NP induce inflammation in both invested cell lines and additionally oxidative stress in A549 cells. Several studies confirmed our investigation. In human bronchial epithelial cells, for example, ZnO-NP exposure increased the expression of *il-8* mRNA [241] as well as the protein level [241, 245]. Also, *il-8* mRNA secretion has been used for identifying cytotoxic effects of other nanoparticles, such as carbon nanotubes and polystyrene nanoparticles [246]. Exposure of TiO_2-NP to kreatinocytes [216], human monocytes, and lung epithelial cells [244] did not cause inflammation. Furthermore, for TiO_2-NP an increase of the *il-8* gene expression in A549 cells was only achieved at unrealistically high concentration (400 µg/cm²) with regard to *in vivo* conditions [242]. However, *in vivo* studies with mice demonstrated that TiO_2-NP induce increased levels of several interleukins such as *il-8* mRNA [247] [248].

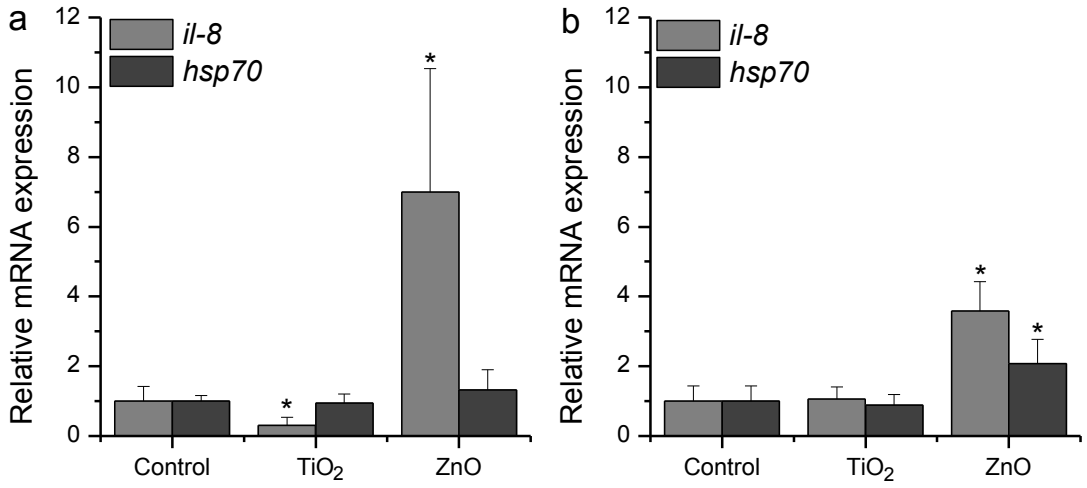

Fig. 3-4 Relative mRNA expression of *il-8* and *hsp70* from NIH-3T3 cells (a) and A549 cells (b) upon treatment ZnO-NP or TiO_2-NP for 24 h. NIH-3T3 cells were exposed to 20 µg/ml and A549 cells to 40 µg/ml ZnO-NP or TiO_2-NP. Data points are means + SD for $n \geq 4$. Significant differences versus the control group are indicated in the figure (ANOVA, One way). * $p<0.05$.

The second chosen biomarker, *hsp70,* was already validated for investigation of the effect of several nanoparticles. *Hsp70's* virtues include that is a very sensitive biomarker for cellular stress responses, is well characterized [249, 250], and precludes false protein-folding [251]. The toxic effect of silver nanoparticles was determined *in vivo* by an increased level of *hsp70* mRNA [252, 253] and of Hsp70 protein [249] indicating oxidative stress. Furthermore, Cu-NP [250], carbon-black nanoparticles [254] and CdSe/ZnS nanoparticles [255] induced *hsp70* expression. While in our study ZnO-NP exposure lead to a higher *hsp70* expression in A549 cells, this effect was not observed for NIH-3T3 cells. According to Chen et al. (2012), NIH-3T3 cells exhibited a lower heat shock response than other cell

lines, thus the sensitivity to nanoparticle response detection was reduced [251]. In addition, different cell lines revealed a variance in their exposure time-course response [251]. For TiO_2-NP no significant changes of *hsp70* expression relative to the control cells were observed for Thp-1 cells (human monocytes) or for NCI-H292 cells (human lung epithelial cells) [244] but not for other cell lines such as NIH-3T3 cells or HepG2 cells [251]. On the contrary, the *hsp70* expression in mice (*in vivo*) was down-regulated after TiO_2-NP exposure [247, 248]. Presumably, a *hsp70* reduction could indicate a detoxification process of the cells [248].

ECIS was used for online monitoring of nanoparticle effects in the cells by the ECIS measurements. Instead of endpoint measurements, cellular response to nanoparticle addition can be observed directly and no additional dye is needed. Thus, interferences of assay compounds with nanoparticles can be minimized. The results of the impedance measurements of NIH-3T3 cells (Fig. 3-5, a) and of A549 cells (Fig. 3-5, c) cultivated with ZnO-NP were compared with the control cells.

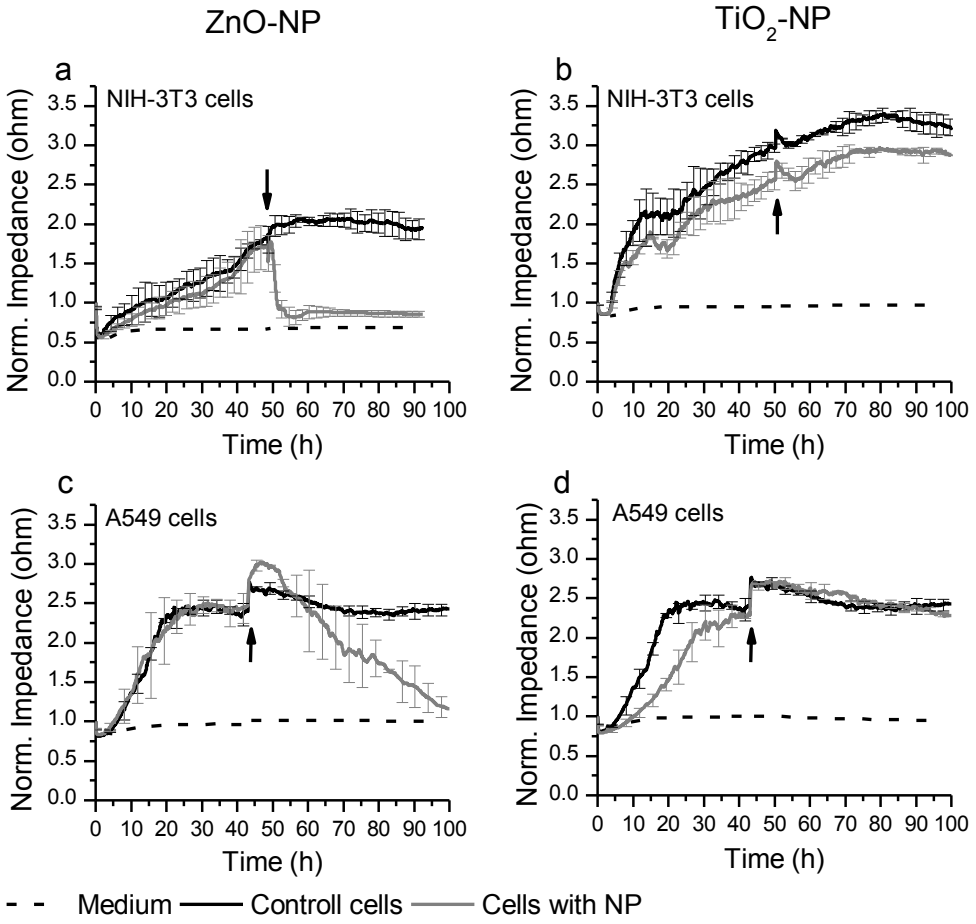

Fig. 3-5 Electric Cell-Substrate Impedance Sensing of NIH-3T3 cells (a, b) and A549 cells (c, d) to monitor nanoparticle toxicity. The cells were grown to confluence before nanoparticle exposure. Dynamic changes in the impedance signal of NIH-3T3 cells to 0 and 20 µg/ml suspensions of ZnO-NP (a) or TiO_2-NP (b) are displayed. For A549 cells the effect of 40 µg/ml of ZnO-NP (c) and TiO_2-NP (d) were investigated. Cell-free medium with nanoparticles were used as reference. The measurements were performed with a 16 kHz ac source. The time point for nanoparticle addition is indicated with the black arrow. Data points are means ± SD for $n \geq 3$.

After addition of ZnO-NP to the cells, the impedance signal dropped immediately for the NIH-3T3 cells. Interestingly, for A549 cells the impedance signal increased after ZnO-NP addition during the

first 10 h before it decreased again. The cells treated with ZnO-NP lost their cell-cell interaction, became smaller and were detached from the surface. The decrease of the impedance signal indicated the cell death, thus ZnO-NP exhibited a toxic effect to the cells. The slight increase of the impedance signal for A549 cells after ZnO-NP addition had been already reported by Seiffert et al.(2012) [240]. Such an effect cannot be explained with proliferation as A549 cells have doubling times of 24 h, thus another cellular response must have occurred [240]. For TiO_2-NP no changes in the impedance signal were revealed with both cell lines (Fig. 3-5, b, d) indicating no cellular changes. Also, the impedance of a cell-free control did not change. Thus, the nanoparticles themselves did not affect the impedance signal.

ECIS measurements have previously been used for cytotoxicity analysis of nanoparticles. A significant decrease in the impedance signal indicating cytotoxicity was determined for ZnO-NP as well as for CuO-NP but not for TiO_2-NP [240]. Furthermore, the calculated IC_{50} value determined with the viability assay was found to be comparable with the one determined by the cell-impedance measurements after 24 h [240]. For anatase TiO_2-NP no significant cytotoxic effect was observed [256, 257] and for rutile TiO_2-NP only at high concentrations (IC_{50} value >200 µg/ml) [256, 258]. Therefore, the effect of TiO_2-NP on the cellular behavior appears to be dependent on the particle size as well as on the shape.

In our study during the fine-screening stage, TiO_2-NP was not found to cause a significant variation either in the gene expression analysis or in the ECIS measurements. Thus, these particles should be further analyzed in the complex-screening mode.

3.2.4.4 Complex-Screening: Comparison of Cell Viability of A549 cells and of NIH-3T3 Cells Exposed to ZnO-NP and TiO_2-NP in 2D and in Different 3D Cell Culture Models

The complex-screening is performed for the remaining nanomaterials not exhibiting any clear toxic effects during the fine-screening to apply more extensive *in vitro* methods. As currently-used 2D cell culture models have several limitations [234, 259], 3D cell culture systems are employed here. The cells were grown in a more physiological cell environment to better predict the cellular behavior in the organism. The 3D cell culture exhibits a higher complexity compared to the conventional 2D cell culture and is more expensive. Currently, different models have been developed to enable *in vitro* 3D cell growth such as cell spheroids, cell encapsulation in hydrogel [260], or cell adhesion on scaffolds.

Secondly, the bloodstream can be mimicked by cells growing under continuous flow conditions (2D cell culture). Here, a shear stress is applied to the cells during nanoparticle exposure. Therefore, to realize both aspects in the complex-screening, it is divided into three sections (Fig. 3-1). In the first section the methods used in the pre-screening are performed on either a 3D cell culture model or under continuous flow conditions. Afterwards in section 2, the methods of the fine-screening are performed. Finally, after the nanoparticles have been tested separately in the cell culture systems a combination of 3D cell culture and continuous flow conditions should be performed (section three). In contrast to the

previously described methods, long term exposure analysis can also be investigated hereby. These experiments provide more relevant results, so *in vivo* studies should follow when no significant variation is detected. Thus, the complex-screening can bridge the gap between the cell-based *in vitro* testing and the *in vivo* studies, thereby reducing the amount of animal studies can be reduced.

In our study we compared different 3D cell culture models and their applicability for the investigation of nanoparticle toxicity. NIH-3T3 cells and A549 cells were seeded on collagen scaffolds or were encapsulated in a hydrogel. The scaffold model as well as the encapsulation of cells in the hydrogel was developed within the present study. For both of these 3D cell culture models we have optimized parts of the procedure like the cell density and incubation for cell growth and the assay performance. The composition of the semi-synthetic PEG-fibrinogen-based hydrogel mix was tuned to create a defined structure and enable cell growth. The cells were treated with different concentrations of ZnO-NP or TiO_2-NP and the viability of the cells was determined. In addition, the two 3D cell culture models were compared with the already-published data for cell spheroids [228]. As described above, not all assays can be combined with all cell culture systems. The viability assays differ in the solubility of the detection-dye. Whereas the MTT assay generates an insoluble product, the reagent used in the CTB assay is soluble. In our study we preferred the CTB assay to measure the viability of the cells grown in the hydrogel because no additional solution step was needed for detection. On the other hand, for the cells grown on the collagen scaffold, diffusion limitations of the reactive dye may affect the results. To avoid only cells on the outer scaffold surface metabolizing the dye, we used the MTT assay instead. Here, the formed blue formazan was trapped in the cells once MTT was metabolized. Thus, the MTT was able to reach the cells inside of the scaffolds as well and the viability of all living cells can be revealed. For a better comparison of the 3D cell culture results, the two assays were performed with the 2D cell culture as well. Fig. 3-6 displays the viability of both cell lines after ZnO-NP exposure determined with the CTB assay or the MTT assay. The cells were encapsulated in hydrogel, seeded on scaffolds or cultured on 2D monolayers.

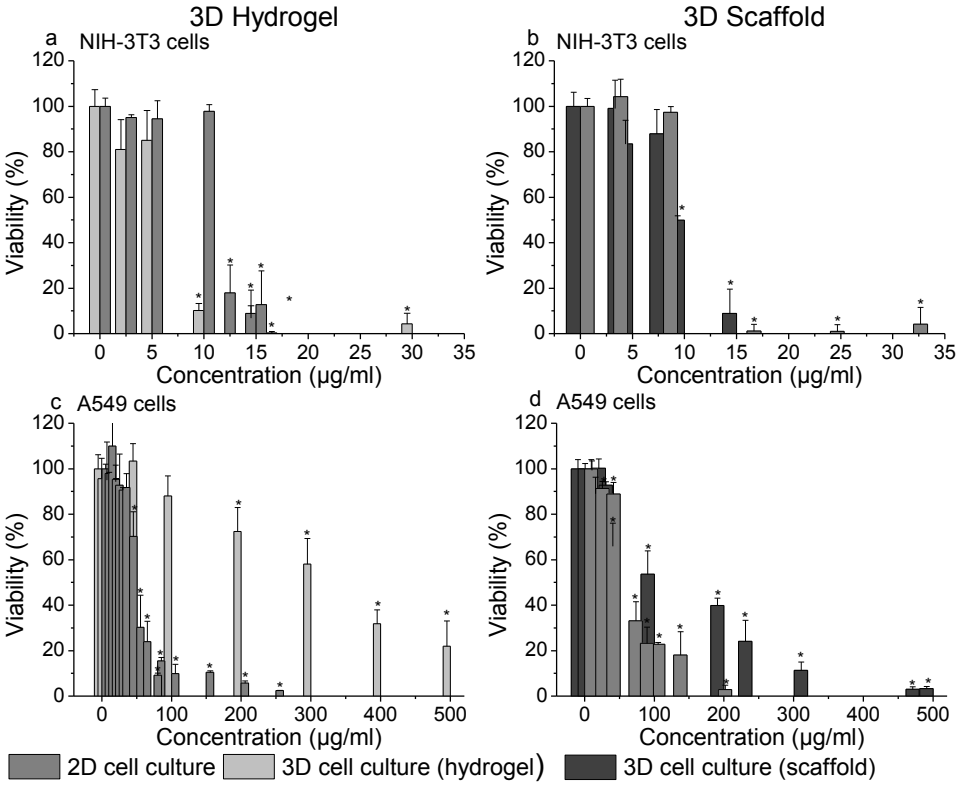

Fig. 3-6 Viability of NIH-3T3 cells (a, b) and A549 cells (c, d) after ZnO-NP exposure determined with the CTB assay (a, c) or the MTT assay (b, d). The cells were encapsulated in hydrogel (a, c), seeded on scaffolds (b, d) or cultured on 2D monolayers. The signals of untreated cells were set as 100%. Data points are means ± SD for $n \geq 3$. *$p<0.05$

In Tab. 3-3 the calculated IC_{50} value for ZnO-NP in the 2D cell culture as well as in the 3D cell culture models are summarized for A549 and for NIH-3T3 cells. Additionally, the spheroid results from our previous study are listed to allow a comparison of all three 3D cell culture models [228]. Again ZnO-NP reduced the viability of the cells in a dose-dependent manner in the 2D as well as in the 3D cell cultures. The results of the two different cell viability assays did not show a significant difference for the 2D cell culture. The choice of the viability assay for cells growing in 3D is dependent on the used 3D model. For the 3D scaffold model the MTT assay and for 3D hydrogel the CTB assay gave solid results. According to the IC_{50} value the NIH-3T3 cells were more sensitive to the ZnO-NP than the A549 cells. For NIH-3T3 cells only minor differences in the IC_{50} values were observed, but for A549 cells in the hydrogel a more than fivefold higher IC_{50} value was determined. Also, the value for the scaffold model was found to be higher. However, the spheroid model displayed a slightly lower IC_{50} value in comparison to the 2D monolayer culture [228].

Tab. 3-3 Comparison of calculated IC_{50} values for ZnO-NP of 2D cell culture and different 3D cell culture models. NIH-3T3 cells and A549 cells were attached on collagen scaffolds, encapsulated in hydrogel or aggregated in spheroids to grow in 3D. After exposure to ZnO-NP the viability of the cells was determined using either the MTT assay or the CTB assay. Values are means ± SD for n ≥ 3. * Data were already published by Sambale et al 2015 [228].

	Viability assay	**IC_{50} value [µg/ml]**	
		NIH-3T3 cells	**A549 cells**
2D	MTT	10 ± 3	58 ± 16
2D*	CTB	15 ± 6	54 ± 12
3D Scaffold	MTT	11 ± 2	75 ± 18
3D Hydrogel	CTB	7 ± 3	328 ± 13
3D Spheroids*	CTB	9 ± 1	42 ± 13

For TiO_2-NP no significant reduction was observed in 2D as well as in 3D (hydrogel and scaffold model) with either cell line (Fig. 3-7). Interestingly, in our previous study we observed that TiO_2-NP induced the formation of several smaller spheroids [228].

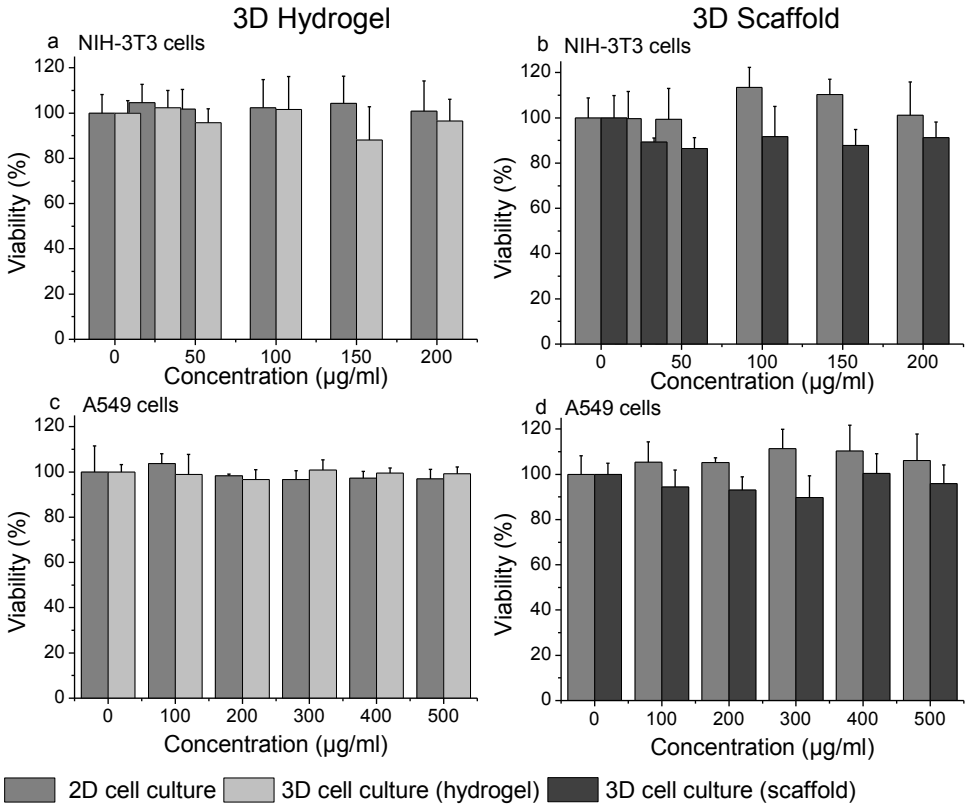

Fig. 3-7 Viability of NIH-3T3 cells (a, b) and A549 cells (c, d) after TiO_2-NP exposure determined with the CTB assay (a, c) or the MTT assay (b, d). The cells were encapsulated in hydrogel (a, c), seeded on scaffolds (b, d) or cultured on 2D monolayers. The signals of untreated cells were set as 100%. Data points are means ± SD for n ≥ 3.

Differences of 2D and 3D cell cultures for toxicity testing have already been reported in literature. Controversial results showed increased, decreased or equal cell sensitivity in 3D cultures when compared to 2D monolayers [233, 261]. Lee and colleagues showed a reduced toxic effect in HepG2 spheroids for cadmium telluride (CdTe) and gold nanoparticles in comparison to the 2D cell culture [262]. Drug screening analysis of aflatoxin B1, amiodarone, valproic acid, and chlorpromazine with HepaRG spheroids [233] and of staurosporine and chlorambucil with HCT116 spheroids [261] demonstrated differences in their half maximal effective concentration (EC_{50}) value for 2D and 3D cell

cultures. In our study we discerned A549 cells in the hydrogel to be less sensitive to ZnO-NP than the cells in 2D. In recent studies it was shown that gold nanoparticles can bind to hyaluronic acid hydrogel, thus limiting the cell-nanoparticle interaction [263]. However, for NIH-3T3 cells no significant difference in the sensitivity of 2D cells or 3D hydrogel model cells was observed. Thus, limitations of nanoparticle penetration through the hydrogel can be excluded. In addition, Xu et. al. also demonstrated that cells grown in hyaluronic acid hydrogel were less sensitive to doxorubicin-loaded polymer nanoparticles than cells grown on 2D monolayers [264].

In summary, the three 3D cell culture models provide different critical concentrations *in vitro* for ZnO-NP. Therefore, for a solid prediction for the later *in vivo* studies the suitability of the 3D model and the later application of the tested nanomaterial has to be in the focus. With spheroids limitations of nutrients, oxygen and other metabolites present in tumor tissues can be investigated [259]. Thus, spheroids are interesting for tumor modeling. This 3D model can be used for nanoparticle development for tumor therapies and nanomedicine. In contrast, the hydrogel and the scaffold 3D model are more representative to mimic real tissue conditions in the human organism. Formation of model tissues and organs could be realized [259]. These models can find applications to clarify nanoparticle risks and to support industrial nanoparticle development.

3.2.5 Conclusions

We have constructed a hierarchical cell-based screening system for nanomaterial development, which is divided in pre-, fine- and complex-screening. Therefore, a set of high-throughput cytotoxicity assays as well as complex cell culture models such as 3D cell culture or dynamic cultivation were integrated. In future work, the screening-system could also be extended to long-term studies using a bioreactor. In addition, other nanoparticles will be screened as well. Initially, in the current study we focused on ZnO-NP and TiO2-NP because they are frequently used in many applications. In our future studies we will extend our investigations with a large set of different nanoparticles. Therefore, other nanoparticles will be screened as well. Regarding the later application, the effects of the nanoparticles can be examined in suspension, coating or in extract media. A high amount of nanomaterials can be analyzed extensively, so that only for selected nanoparticles the application of *in vivo* studies is needed. Indeed, *in vivo* studies cannot be replaced but can be significantly reduced applying our screening-system. As cases studies, the effects of zinc oxide (ZnO-NP) and titanium dioxide nanoparticles (TiO_2-NP) were screened. ZnO-NP revealed cytotoxic effects to mammalian cells in 2D cell culture as well as in 3D cell culture thus reducing cell viability, and inducing inflammation and oxidative stress. On the contrary, for TiO_2-NP no significant variation was observed with the used methods. We clearly demonstrated that assays have limitations that and the choice of the cell line may affect the results. In comparison to NIH-3T3 cells, A549 cells were less sensitive to the investigated nanoparticles and did not adhere to the 3D hydrogels. While microscopic detection of morphology changes was solid in 2D cell cultures, this method was critical in 3D cell cultures to identify toxic nanoparticles. Electric Cell-

Substrate Impedance Sensing measurements provide an excellent method for the non-invasive online monitoring of cellular responses to nanoparticles and was hence placed in the fine-screening part of the overall assay. Interferences of dyes with the nanoparticles can be excluded.

In conclusion, the developed screening-system can bridge the gap between constantly-increasing nanotechnology and comprehensive risk assessment to define safety provisions for workers and customers.

Conflict of Interests

The authors declare that there is no conflict of interests regarding the publication of this paper.

Acknowledgment

This work was supported by the European Regional Development Fund (EFRE Project "Nanokomp", grant number: 60421066). We acknowledge support by Deutsche Forschungsgemeinschaft and Open Access Publishing Fund of Leibniz Universität Hannover.

3.2.6 Supporting Information

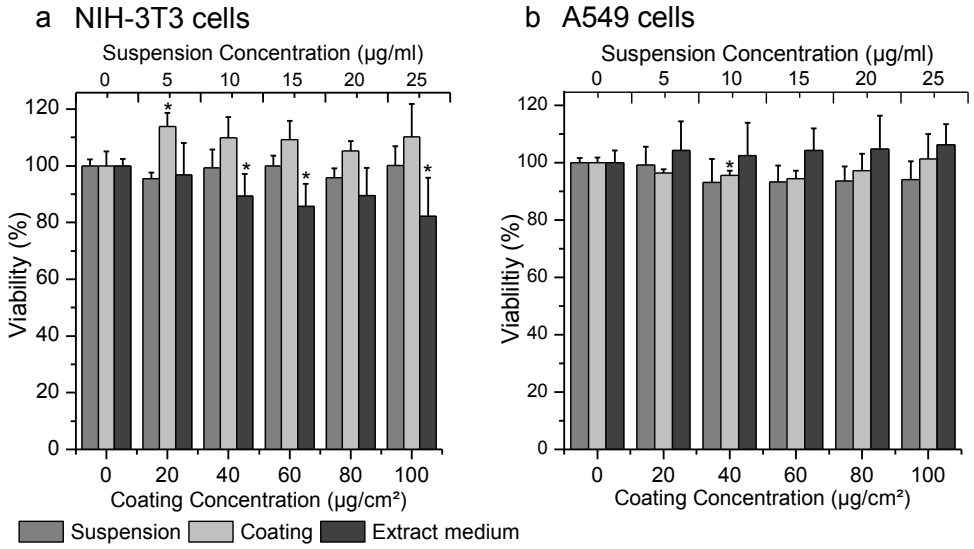

Fig. 3-8 Viability of NIH-3T3 cells (a) and A549 cells (b) after TiO2-NP exposure determined with the MTT assay. The cells were treated with nanoparticle suspension, coating or extract medium. The signals of untreated cells were set as 100%. Data points are means ± SD for $n \geq 3$.

4 *Pre-Screening* und *Fine-Screening* von Silber-Nanopartikeln

4.1 Zusammenfassung

Für die Entwicklung des *Screening-Systems* wurden neben ZnO- und TiO_2-Nanopartikeln auch Ag-Nanopartikel eingesetzt. Ag-Nanopartikel weisen aufgrund ihrer antimikrobiellen Wirkung ein breites Anwendungsspektrum auf. Bedingt durch die vielfältigen Einsatzbereiche sind die Effekte der Ag-Nanopartikel detailliert zu untersuchen. Bisher wurde in diversen Studien die Toxizität von Ag-Nanopartikeln auf Bakterien, Algen und Säugerzellen demonstriert. Wie in Kapitel 2.3 beschrieben, können sich jedoch bei Metall-Nanopartikeln die Ionen ablösen und einen schädigenden Einfluss aufweisen. Daher sollte bei der Untersuchung von Metall-Nanopartikeln die Wirkung der Nanopartikel gegen die der Ionen abgegrenzt werden.

Die Methoden des *Pre-* und *Fine-Screenings* wurden verwendet, um die Effekte von Ag-Nanopartikeln und Ag^+-Ionen auf Zellen zu analysieren. Neben Ag-Nanopartikeln wurde das Silbersalz ($AgNO_3$) in gleicher Konzentration wie Ag^+-Ionen bei einer vollständigen Dissoziation in der Ag-Nanopartikel-Suspension vorliegen würden, untersucht. Es wurden verschiedene Zelllinien wie die NIH-3T3-Zellen, die A549-Zellen, die HepG2-Zellen und die PC-12–Zellen (Rattennebennieren-Zelllinie) eingesetzt. Im *Pre-Screening* wurden die Effekte der Nanopartikel und der Ionen auf die Zellmorphologie sowie die Zellviabilität mittels des MTT-Tests untersucht.

Bei dem MTT-Test handelt es sich um eine photometrische Endpunktmethode, mit dem die Proliferation und die Viabilität der Zellen bestimmt werden kann. Sie basiert auf der Umsetzung des gelben Tetrazoliumsalzes MTT in das blaue, kristalline Formazan (3-(4,5-Dimethylthiazol-2-yl)-2,5-Diphenylformazan) durch die metabolische Aktivität von vitalen Zellen. Zudem wurden verschiedene Methoden des *Fine-Screenings* angewendet, um detaillierte Informationen bezüglich des Wirkmechanismus zu erhalten. Hierbei wurde die ECIS-Methode eingesetzt, die eine Online-Analyse der Auswirkung auf z.B. die Zelladhäsion ermöglicht. Des Weiteren wurden zwei Methoden zur Detektion der Zelltodmechanismen für das *Screening-System* erprobt. Mittels des *CytoTox-ONE™ Homogeneous Membrane Integrity Assay* (Promega, Madison, USA) können Störungen der Membranintegrität untersucht werden, die ein Anzeichen für nekrotische Zellen sind. Bei der Kultivierung von Zellen mit toxischen Substanzen können Schäden in der Zellmembran durch die Freisetzung des zytoplasmatischen Enzyms Laktatdehydrogenase (LDH) detektiert werden. Das Assay basiert auf der Umsetzung von Laktat zu Pyruvat durch das freigesetzte LDH, wodurch das Coenzym NAD^+ zu NADH reduziert wird. Im Folgenden wird dann durch den Katalysator Diaphorase Wasserstoff auf das blaue Resazurin übertragen und somit zum violetten Resorufin umgesetzt. Dabei ist die Menge des entstandenen Resorufins proportional zu der Anzahl an nekrotischen Zellen. Als zweites wurde das *Apo-One® Homogenous Caspase 3/7 Assay* (Promega, Madioson, USA) als Methode des *Fine-Screenings* eingesetzt, das apoptotischen Zelltod detektiert. Mit dem Assay wird die Aktivität von

Caspase 3/7 ermittelt, die bei der Apoptose in Säugerzellen entscheidend ist. Das Assay basiert auf der Spaltung des nicht fluoreszierenden Substrates Z-DEVD-R110 zu dem fluoreszierenden Rhodamin R-110 durch Caspase 3/7.

Der im *Pre-Screening* verwendete MTT-Test zeigte eine Konzentrations-abhängige Abnahme der Viabilität nach der Exposition mit verschiedenen Ag-Nanopartikel- bzw. Ag^+-Ionen-Konzentrationen. Mittels der Ergebnisse konnten die Dosis-Wirkungskurven jeweils für jede Zelllinie erstellt und die spezifischen Kenngrößen wie IC_{50}-, NOAC (*No Observed Adverse Effect Concentration*)- und TLC (*Total Lethal Concentration*)-Wert bestimmt werden. Dabei wiesen die untersuchten Zelllinien eine unterschiedliche Sensitivität auf. Während z.B. die A549-Zellen für die Nanopartikel einen IC_{50}-Wert von 10 ppm (µg/ml) aufwiesen, lag dieser bei den HepG2-Zellen bei 6 ppm und bei den NIH-3T3-Zellen sowie den PC-12-Zellen bei 4 ppm. Bei den NIH-3T3-Zellen wird zudem deutlich, dass der toxische Dosisbereich sehr klein ist, da bei 3 ppm Ag-Nanopartikel kein Effekt beobachtet wurde, jedoch bei 4 ppm 50 % der Zellen nicht mehr lebensfähig waren. Generell sind die Ag-Nanopartikel im Vergleich zu den Ag^+-Ionen für alle untersuchten Zelllinien wesentlich toxischer. Die IC_{50}-Werte für die Ag^+-Ionen waren für die A549-Zellen siebenfach, für die HepG2-Zellen 16fach, für die NIH-3T3-Zellen 18fach und für die PC-12-Zellen fünffach höher als die IC_{50}-Werte, die für die Ag-Nanopartikel bestimmt wurden. Die unterschiedlichen Zell-Sensitivitäten sind bedingt durch die Zelltyp-spezifischen Eigenschaften wie beispielsweise die Nanopartikel-Aufnahmerate oder die Stoffwechselaktivität der Zellen. Mit den Ergebnissen konnte bestätigt werden, dass die toxische Wirkung der Ag-Nanopartikel überwiegt.

Zusätzlich zu den Viabilitätstests wurde im *Pre-Screening* die Zellmorphologie untersucht. Hierbei konnten Morphologie-Änderungen der Zellen beobachtet werden. Während mit Standard-Kulturmedium die Zellen eine konfluente Zellschicht ausbildeten, wurden nur wenige Zellen nach der Ag-Nanopartikel-Exposition auf der Kulturoberfläche beobachtet. Bei höheren Konzentrationen lösten sich die Zellen von der Kulturoberfläche ab. Die verbleibenden Zellen waren zudem kleiner als die unbehandelten Zellen. Diese Morphologie-Änderung ist ein Indikator für den apotpotischen Zelltod. Die Art des Zelltods wurde daher mit den Methoden des *Fine-Screenings* überprüft.

Nachfolgend wurde die ECIS-Methode im *Fine-Screening* angewendet. Direkt nach Zugabe der Ag-Nanopartikel nahm das Impedanz-Signal ab. Bei der zellfreien Kontrolle wurde hingegen das Impedanz-Signal nicht durch die Nanopartikel-Zugabe beeinflusst. Die Signalabnahme zeigt die unmittelbare toxische Wirkung der Ag-Nanopartikel auf die Zellen. Sie resultiert durch das Ablösen der Zellen, das mikroskopisch bestätigt werden konnte. Zur Bestimmung des Zelltods wurden im weiteren Verlauf des *Fine-Screenings* die LDH-Freisetzung und die Caspase3/7-Aktivität in den A549-Zellen nach der Exposition mit Ag-Nanopartikeln oder Ag^+-Ionen analysiert. Dabei konnten Unterschiede für die Nanopartikel und die Ionen festgestellt werden. Die Ag^+-Ionen führten zu einer erhöhten LDH-Freisetzung ins Medium, die auf Membranschäden der Zellen zurückzuführen ist und

nekrotischen Zelltod aufzeigt. Da dieser Effekt bei den Nanopartikel-behandelten Zellen nicht beobachtet wurde, liegt hier eine andere Art des Zelltods vor. Die Caspase 3/7-Aktivätit in den Zellen war durch die Ag-Nanopartikel im Zellkulturmedium deutlich erhöht, so dass der apoptosische Zelltod bestätigt wurde. Die Ag-Nanopartikel werden von den Zellen aufgenommen, lagern sich an Zellorganelle oder an die DNA und können deren Funktion beeinträchtigen. Des Weiteren induzieren die Ag-Nanopartikel die ROS-Bildung, die einen oxidativen Stress für die Zellen darstellt. Aufgrund dieser Auswirkungen der Nanopartikel wird in der Zelle der programmierte Zelltod (Apoptose) eingeleitet.

Insgesamt waren die ausgewählten Methoden des *Pre-* und *Fine-Screenings* geeignet, um die toxische Wirkung der Ag-Nanopartikel zu detektieren und diese von der der Ag^+-Ionen zu unterschieden. Des Weiteren konnte gezeigt werde, dass mit dem *Pre-Screening* erste Vorkenntnisse über die Wirkung der Nanopartikel bzw. der Ionen ermittelt werden können. Die gewonnenen Erkenntnisse können die Methodenauswahl im nachfolgenden *Fine-Screening* unterstützen. Mittels des *Pre-Screenings* konnte der Dosis-Bereich der beiden Substanzen bestimmt werden und durch die Zellmorphologie-Änderungen erste Hinweise auf den möglichen Zelltod aufgezeigt werden. Bei Metall-Nanopartikel lösen sich häufig Metallionen ab, die schädigend auf die Zellen wirken könnten [2]. Dennoch wiesen die Ag-Nanopartikel eine deutlich höhere toxische Wirkung auf als die Ag^+-Ionen. Dabei konnten im *Fine-Screening* für Ag-Nanopartikel ein apoptotischer und für die Ag^+-Ionen ein nekrotischer Zelltod ermittelt werden. Auch der im *Fine-Screening* ermittelte Zelltod-Mechanismus bestätigt, dass die toxische Wirkung auf die Zellen vorrangig durch die Ag-Nanopartikel und nicht durch die Ag^+-Ionen verursacht wird.

4.2 Investigations of the Toxic Effect of Silver Nanoparticles on Mammalian Cell Lines

Franziska Sambale[1], Stefanie Wagner[1], Frank Stahl[1*], Renat R. Khaydarov[2], Thomas Scheper[1], Detlef W. Bahnemann[1]

[1] Institute of Technical Chemistry, Leibniz University Hannover, Callinstr.5, 30167 Hannover
[2] Institute of Nuclear Physics, Tashkent, Uzbekistan
*Email: stahl@iftc.uni-hannover.de, Telephone: +49 511 762 2968

Published in Journal of Nanomaterials, Volume 2015 (2015), Article ID 136765, DOI: 10.1155/2015/136765. Reprinted with kind permission from Journal of Nanomaterials

4.2.1 Abstract

Silver nanoparticles are widely used for many applications. In this study silver nanoparticles have been tested for their toxic effect on fibroblasts (NIH-3T3), on a human lung adenocarcinoma epithelial cell line (A-549), on PC-12-cells, a rat adrenal pheochromocytoma cell line, and on HEP-G2-cells, a human hepatocellular carcinoma cell line. The viability of the cells cultivated with different concentrations of silver was determined by the MTT assay, a photometric method to determine cell metabolism. Dose-response curves were extrapolated and IC_{50}, Total Lethal Concentration (TLC), and No Observable Adverse Effect Concentration (NOAEC) values were calculated for each cell line. As another approach, Electric-Cell-Substrate-Impedance-Sensing, an automated method to monitor cellular behavior in real-time was applied to observe cells cultivated with silver nanoparticles. To identify the type of cell death the membrane integrity was analyzed by measurements of the lactate dehydrogenase releases and by determination of the caspase 3/7 activity. To ensure that the cytotoxic effect of silver nanoparticles is not traced back to the presence of Ag^+ ions in the suspension, an Ag^+ salt ($AgNO_3$) has been examined at the same concentration of Ag^+ present in the silver nanoparticle suspension that is assuming that the Ag particles are completely available as Ag^+ ions.

4.2.2 Introduction

Recently nanotechnology has revolutionized the technological progress and is predicted to be one of the key technology of the 21st century [265]. Nanoparticles are defined with a particle size between 1 and 100 nm. Compared to their bulk counterparts, nanoparticles exhibit different physical and chemical properties. Many properties that are found to change in the nanoscale, for example, physical characteristics, surface area, magnetic, mechanical, optical as well as chemical properties such as reactivity, thermal properties, etc. Because of their new properties many of these newly developed nanomaterials are already used in different industries. Typical application fields are, for example, optics, photocatalysis, automotive industry, water and air treatment, fabrics, cosmetics, and health products. [265]

Silver has been known for its antibacterial effect for a long time [266]. In ancient Greece, Rome, and Macedonia, silver was used to control infections. Nowadays, silver is used for many bactericidal applications, e.g., wound healing [267], water treatment [268], and flower preservation [269]. Other

application fields of silver nanoparticles include catalysis [270], optics [271, 272], electronics [273], and various other areas of science and technology. Currently the most effective application for silver nanoparticles appears to be their usage as antibacterial/antifungal agent [274, 275]. The manufacturing of bactericidal cotton fibers containing silver nanoparticles for textile industry [276, 277], is of great interest, because ordinary cotton fabrics provide an excellent environment for microorganisms [278]. Further applications for silver nanoparticles are paints, for example, nanosilver-based paint should prevent the growth of algae on outside walls [279].
However, at present concerns have been raised concerting the environmental impact of nanoparticles and the possible human exposure. Nanomaterial risk assessment is mainly influenced by the mobility of nanoparticles [265]. In addition, due to the large surface area of nanoparticles pollutants can be adsorbed to nanoparticles. During nanomaterials development accumulation of nanoparticles in the ground water or in the air can occur [265]. As nanoparticles such as silver nanoparticles can be absorbed by plants or other living organism, the particles can be reach the food chain [265]. There are a lot of publications reporting the results of investigations of the antibacterial effect of silver nanoparticles. Sotiriou and Pratsinis examined the antibactericidal activity of silver ions and nanosilver particles and reported that the bactericidal activity against gram negative *Escherichia coli* bacteria is dominated by Ag^+ ions and not by the silver nanoparticles themselves [280]. Fabrega et al. investigated the effect of colloidal Ag nanoparticles at different pH values in the presence of Suwannee River humic acids (SRHA) against Pseudomonas fluorescens SBW25 and observed a toxic effect at a concentration of 2000 ppm without SRHA at pH 9 [281]. The effect of silver nanoparticles on aquatic organisms has also been investigated by different research groups [282, 283]. Until ten years ago it was assumed that silver is non-toxic to mammalian cells, except for argyria, a blue coloration of the skin, caused by colloidal silver [284].

The main nanoparticle uptake possibilities into the human body were via the skin, via the respiratory tract or the gastrointestinal tract [265]. Thereby, nanoparticle size, shape, and surface modification play an important role in the distribution in the organism. Nanoparticles absorbed via the respiratory tract can reach the lymph stream and the blood circulation [285]. Some studies showed that nanoparticles are able to pass through the blood-brain-barrier [286] and through cell membranes [287, 288], and can thus deposit in organs and interact with biological systems.

It has been shown that silver nanoparticles can induce a toxic response of different mammalian cell lines [289-293]. Hence silver nanoparticle exposure resulted in a decreased viability or the release of lactate dehydrogenase in rat liver cells [292], in mouse germline stem cells [291], in human fibroblasts [294], and in rat adrenal cells [295]. Chairuangkitti et al. investigated *in vitro* toxic effects of silver nanoparticles on human lung carcinoma (A-549) cells and reported a clear relationship to the generation of reactive oxygen species [289]. Kawata et al. investigated the toxic effect of silver nanoparticles in comparison to silver ions and polystyrene nanoparticles which are known as nontoxic

nanomaterials to HEP-G2 cells. They contributed the toxic effect to both; the nanosize of these particles as well as to the ionic form Ag^+ [296]. AshaRani et al. investigated the cytotoxic and genotoxic effect of silver nanoparticles on human cells. Their results indicated mitochondrial dysfunction as well as induction of reactive oxygen species (ROS) by Ag-nanoparticles which result in DNA damage and chromosomal aberrations [297]. The induced toxic effects of silver nanoparticles can be divided into ROS-dependent and ROS-independent pathways [289].

Because silver nanoparticles are used in many application fields and previous studies showed the possible hazardous effects of these materials it is important to investigate the toxic action more intensely. Therefore, we have investigated the toxic effect of silver nanoparticles and silver ions on four commonly used cell lines, concentrating on the possible exposure options to the organism. The viability of the cells cultivated in the presence of different concentrations of Ag nanoparticles and Ag^+ ions was measured employing the MTT assay, a well established photometric method to determine the cell metabolism. Dose-response curves were extrapolated from these data and Total Lethal Concentration (TLC), No Adverse Effect Concentration (NOAEC), and IC_{50}-values were calculated. Electric-Cell-Substrate-Impedance-Sensing (ECIS), an automated method to monitor cell behavior in real-time, was also carried out. To investigate the cell death the caspase 3/7 activity assay was performed.

4.2.3 Materials and Methods

4.2.3.1 Silver Nanoparticles and Silver Ions

The silver nanoparticles used for the cytotoxic tests were synthesized by the Institute of Nuclear Physics, in Tashkent, Uzbekistan. They were liberated from pure silver electrodes via 12 V battery-operated constant current generators. The apparatus used for silver ion generation has been described previously [298]. The water-based colloidal silver solution was obtained by a recently reported three-stage process based on the electroreduction of silver ions in water [299]. The concentration of silver nanoparticles and ions in solution was determined by neutron activation analysis (NAA) [300]. Samples were irradiated in the nuclear reactor of the Institute of Nuclear Physics (Tashkent, Uzbekistan). The product of nuclear reaction $^{109}Ag(n,\gamma)^{110m}Ag$ has the half-life $t_{1/2} = 253$ days.

Through measurements of the intensity of gamma radiation with an energy of 0.657 MeV and 0.884 MeV emitted by ^{110m}Ag. A Ge(Li) detector with a resolution of about 1.9 keV at 1.33 MeV the silver concentration was determined. A 6144-channel analyzer were used for recording gamma-ray quanta. The silver nanoparticles used in the study were characterized by Khaydarov et al. and obtained a primary particle size of 7 ± 3 nm (TEM) [299]. As reference for the cytotoxic testing a silver ion suspension was used ($AgNO_3$) at the same total Ag concentration.

4.2.3.2 Dynamic Light Scattering Measurements

To measure the hydrodynamic diameter and the distribution of the silver nanoparticles in water, dynamic light scattering (DLS) measurements were performed. Suspensions (1 ml) with a concentration of 10 ppm in water were prepared and then measured with a Malvern Zetasizer Nano-ZS (Malvern Instruments, UK). Each measurement was repeated three times to enable the calculation of a standard deviation.

4.2.3.3 Cell Culture

Four different cell lines were cultivated: HEP-G2-cells, NIH-3T3-cells, PC-12-cells, and A-549 cells. HEP-G2-cells are human hepatocellular carcinoma cells (DMSZ no.: ACC 180), NIH-3T3 cells are mouse fibroblasts (DMSZ no.: ACC 59), PC-12 cells are rat adrenal pheochromocytoma cells (DSMZ no.: ACC 159), and A-549 cells are human lung carcinoma cells (DSMZ no.: ACC 107). All cell lines were cultivated in Dulbecco's Modified Eagle's medium (DMEM) (D7777 Sigma-Aldrich, Steinheim, Germany) supplemented with the respective serum (Tab. 4-1) and 1% antibiotics (penicillin/ 100 U/ml and streptomycin/ 100 µg/ml) in a humidified environment at 37°C / 5% CO_2. After three to four days the cells had grown to approximately 70% confluence. Afterwards, they were detached with trypsin and cultured in a new cell culture flask.

Tab. 4-1 DMEM, additives, and cell number per well used for the experiments. (fetales calf serum (FCS), horse serum (HOS), Newborn Calf Serum (NCS).

Cell line	DMEM additives	Doubling time	Cell number per well
A-549	10% FCS	40 h	8.000
NIH-3T3	10% FCS	20 h	6.000
PC-12	10% HOS, 5% NCS, 1% Sodium pyruvate, 1% L-glutamine	50-60 h	10.000
HEP-G2	10% FCS	50-60 h	10.000

4.2.3.4 Cultivation with Nanoparticle Addition

Depending on the doubling times, the cells were seeded a defined number of cells (see Tab. 4-1) in a 96-well plate and were incubated for three days. At day four the medium of each well was removed and 200 µl of the different nanoparticle suspensions in varying concentrations in the cell culture medium were added to the wells. The cells were cultivated for three more days after which the viability of the cells was determined by the (3-(4,5-dimethylthiazol-2-yl)-2,5-diphenyl-tetrazolium-bromid)-assay. Moreover the caspase 3/7 activity was measured with the Apo-ONE® Homogeneous Caspase-3/7 Assay (Promega, USA) or the lactate dehydrogenase release was determined with the CytoTox-ONETM Homogeneous Membrane Integrity Assay (Promega, USA)

4.2.3.5 Cytotoxicity Test Methods

MTT-ASSAY

The viability of the cells was analyzed by the MTT assay (Sigma-Aldrich, Steinheim, Germany). This assay is based on the reaction of the tetrazonium ring by mitochondrial dehydrogenase enzymes and leads to an insoluble blue reaction product [301]. Firstly, the medium was removed from each well. Secondly, 100 µl of fresh medium and 10 µl of MTT solution (5 mg/ml PBS, sterile) were added to each well and incubated for 4 h at 37°C / 5% CO_2. After incubation of the dye 100 µl of 10% SDS in 0.01 M HCl were added and the plates were further incubated for 24 h. The determination of the transmission signals at 570/630 nm was performed using a microplate reader (Bio-Rad, Munich, Germany). Each measurement was repeated three times independently in quintuple to calculate the standard error. Statistical analysis was performed using the student t-test.

Electric-Cell-Substrate-Impedance-Sensing

ECIS is an automated method to monitor cellular behavior. Cells are grown on electrodes covered with a gold film and an alternating current (AC) signal is applied. As cells attach and spread upon these electrodes, their insulating membranes block and constrain the current flow resulting in measured variations in the electrode impedance. Any changes in the environment that result in morphological changes of the cells alter the current paths and can be readily detected by the ECIS™ Model 1600R (Applied BioPhysics, USA). To implement this experiment, one 8W1E (8 well 1 electrode) ECIS slide was incubated for about 24 h with cell culture medium, with each well of the slide being filled with 400 µl of medium. Afterwards, the medium was removed and 125,000 A-549-cells cells in 400 µl were seeded per well, two electrodes remained cell-free as reference. When the impedance signal was stable, the cells had grown to confluence, the medium was removed and 400 µl of the silver nanoparticle suspension in the culture medium at a concentration of 10 ppm were added to the wells. For each analysis, two wells were filled with the same suspension and three wells were filled with cell culture medium without nanoparticles as a reference. The impedance signal is monitored during the entire time of the measurement which is terminated when the signals do not change anymore.

Dose-response-curves

From the results obtained from the MTT assay, dose-response-curves were plotted for the determination of the "No Observable Adverse Effect Concentration" (NOAEC), the Inhibitory Concentration (IC_{50}) and the Total Lethal Concentration (TLC) values. For this the normalized cell viability (viability of cells in normal culture medium = 1) was plotted as a function of the logarithm of the particle or rather the ion concentration in ppm. The theoretical dose-response curves were extrapolated using the following equation:

$$y = 1 - \frac{1}{1 - e^{a(b-x)}} \quad (1)$$

with a = curve slope, b = IC_{50} value [ppm] and x being the absorbance values expressed as percentage cell viability.

NOAEC values were determined with y being 95 % of the maximum response on the normalized cell viability employing the following equation:

$$NOAEC = \mathrm{b} - \frac{\ln(19)}{\mathrm{a}} \quad (2)$$

TLC values were determined with y being 5 % of the maximum response on the normalized cell viability with the following equation:

$$TLC = \mathrm{b} - \frac{\ln(\frac{1}{19})}{\mathrm{a}} \quad (3)$$

Caspase 3/7-activity

The cells were cultivated in 96-well plates. The caspase 3/7 activity was measured with the Apo-ONE® Homogeneous Caspase-3/7 Assay (Promega, USA). To perform this test 100 µl of the Apo-ONE® Caspase 3/7 Reagent were added to each well of the 96-well plate. The plate was shaken for 1 minute at 400 rpm and was then incubated at 22 °C. Every 10 minutes the fluorescence with an excitation wavelength of 485 nm and an emission wavelength of 538 nm was measured with the Fluoroskan Ascent (Thermo Electron Corporation). Three independent experiments were performed to calculate the standard error.

Lactate dehydrogenase assay (LDH)

The cells were cultivated in 96-well plates. The membrane integrity of the cells was analyzed by the CytoTox-ONE™ Homogeneous Membrane Integrity Assay (Promega, USA). To perform the assay 100 µl medium from each well were transferred into a new well of a 96-well plate. This plate was incubated for 20 minutes at 22°C. Afterwards, 100 µl of the CytoTox-One™ reagent were added to each plate. Then the plate was shaken and the fluorescence with an excitation wavelength of 560 nm and an emission wavelength of 590 nm was measured with the Fluoroskan Ascent (Thermo Electron Corporation).

4.2.4 Results

4.2.4.1 DLS Measurements

To identify the diameter of the silver nanoparticles used for the cytotoxicity measurements DLS measurements of the particles at Ag concentrations of 10 ppm in water were carried out (Fig.4-1). In water Ag-NP obtained a hydrodynamic diameter of 70 ± 5 nm (mean ± standard derivation).

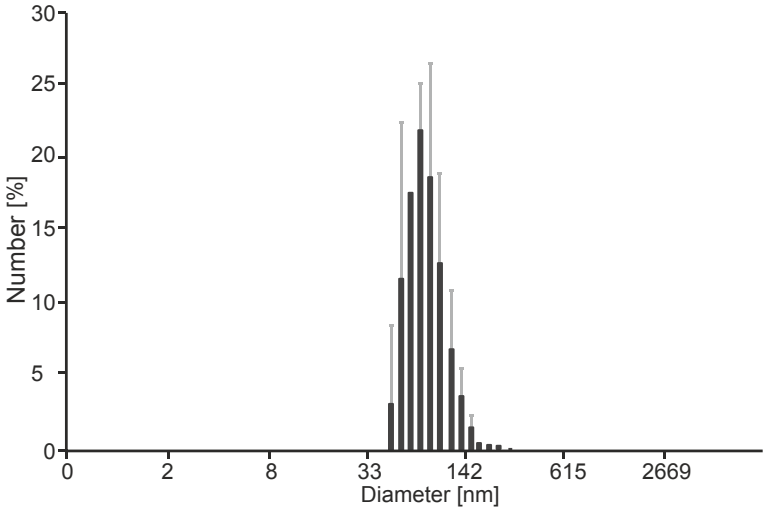

Fig. 4-1 DLS measurements of silver nanoparticles at a concentration of 10 ppm in water.

4.2.4.2 Dose-Response-Curves and Cytotoxicity Data

The first experiment was to measure the viability of the four different cell lines exposed to the silver nanoparticles and to the silver ions at different concentrations via the MTT assay. Fig. 4-2 shows the dose-response curves of the four different cell lines: A-549, NIH-3T3, HEP-G2, and PC-12 cells cultivated in presence of silver nanoparticles and of silver ions, respectively, after 72 h exposure. The results of the MTT assay were extrapolated using formulas (1) to (3).

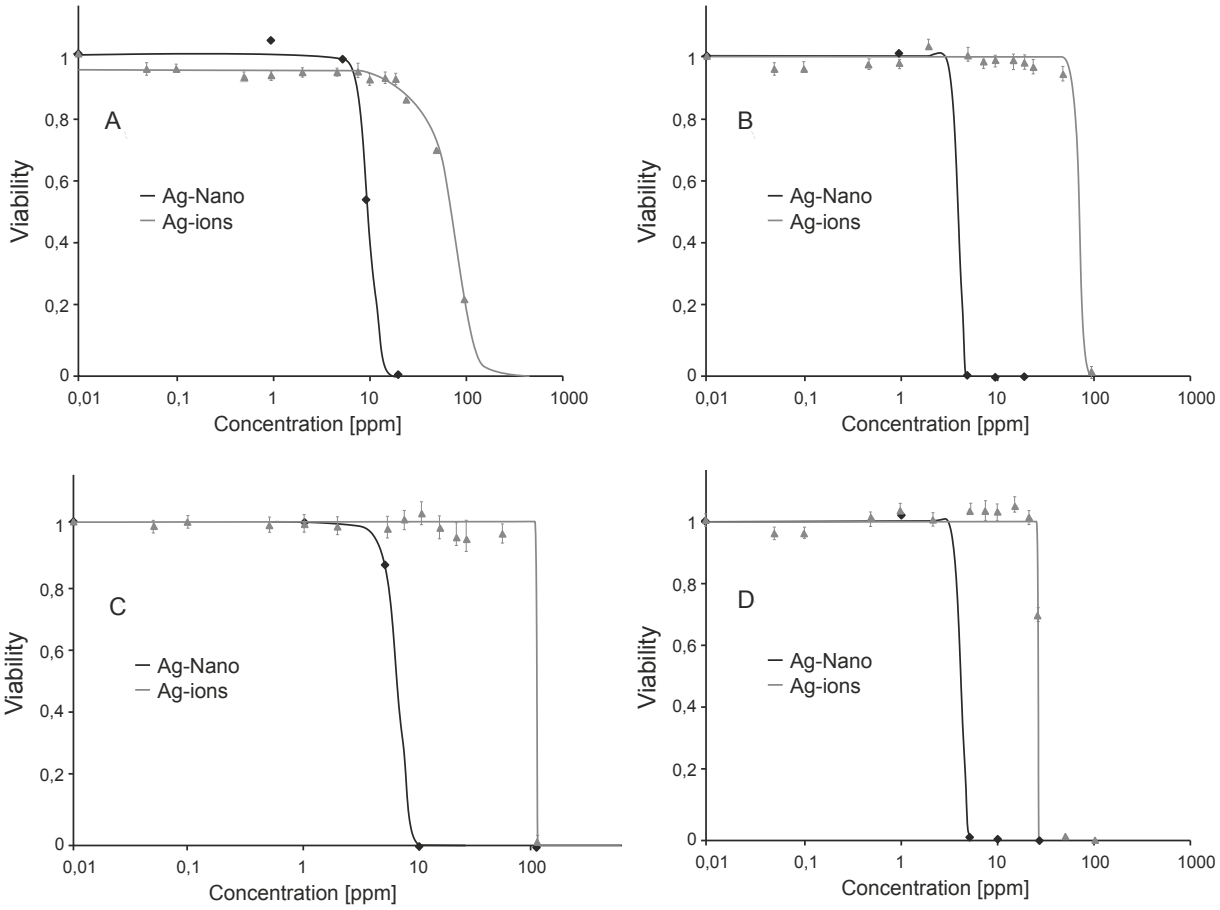

Fig. 4-2 Viability (± SEM) and extrapolated dose-response curves of A-549-cells (A), NIH-3T3-cells (B), HEP-G2-cells (C), and PC-12-cells (D) cultivated with silver nanoparticles and silver ions, respectively.

In Tab. 4-2 the thus calculated IC_{50} (Inhibitory Concentration), TLC (Total Lethal Concentration) and NOAEC (No Observable Adverse Effect Concentration) values for the different cell lines cultivated with silver nanoparticles and with silver nitrate are shown.

For all cell lines the decrease of the viability is much higher by cultivation in the presence of silver nanoparticles than by cultivation with silver ions (Fig. 4-2). For all cell lines the IC_{50} values by cultivation in the presence of silver nanoparticles are similar ranging from 4 ppm for the NIH-3T3 and PC-12 cells to 10 ppm for the A-549 cells, whereas the slopes of the dose-response curves are varying considerably more, resulting in respective differences in the TLC and NOAEC values. The values calculated for the silver ions differ drastically from those obtained for the silver particles; here the range for the IC_{50} values is between 25 ppm for the PC-12 cells and 97 ppm for the HEP-G2 cells. The slopes of the curves differ in the same way resulting in a rather narrow toxic dose range between 94 ppm and 99 ppm for the HEP-G2 cells, whereas the toxic dose range for the A-549 cells is quite wide, i.e., between 19 ppm and 144 ppm.

Tab. 4-2 NOAEC-, IC_{50}-, and TLC-values for A-549, NIH-3T3, HEP-G2, and PC-12 cells cultivated with silver nanoparticles and silver ions, respectively.

	Silver nanoparticles [ppm]			**Silver ions [ppm]**		
	NOAEC	**IC_{50}**	**TLC**	**NOAEC**	**IC_{50}**	**TLC**
A-549	6	10	14	19	72	144
NIH-3T3	3	4	5	59	72	86
HEP-G2	4	6	9	94	97	99
PC-12	3	4	5	24	25	26

A-549 cells were chosen for the impedance measurements of cells cultivated in the presence of particles. These experiments were performed verify the cytotoxicity results obtained from the MTT assay and the dose-response curves.

Fig. 4-3 shows the ECIS of A-549 cells cultivated with silver nanoparticles at the IC_{50} concentration of 10 ppm in the cell culture medium, the cell growth in normal culture medium as well as the impedance signal of a cell-free-electrode as a reference. The ECIS measurements allows online-monitoring of the nanoparticle effects to the cells. The impedance signal of the electrodes seeded with cells and cultivated with nanoparticles in the culture medium decreases immediately after addition of the particles, indicating a morphology change of the cells on the electrodes or a detachment of cells from the electrode surface, respectively.

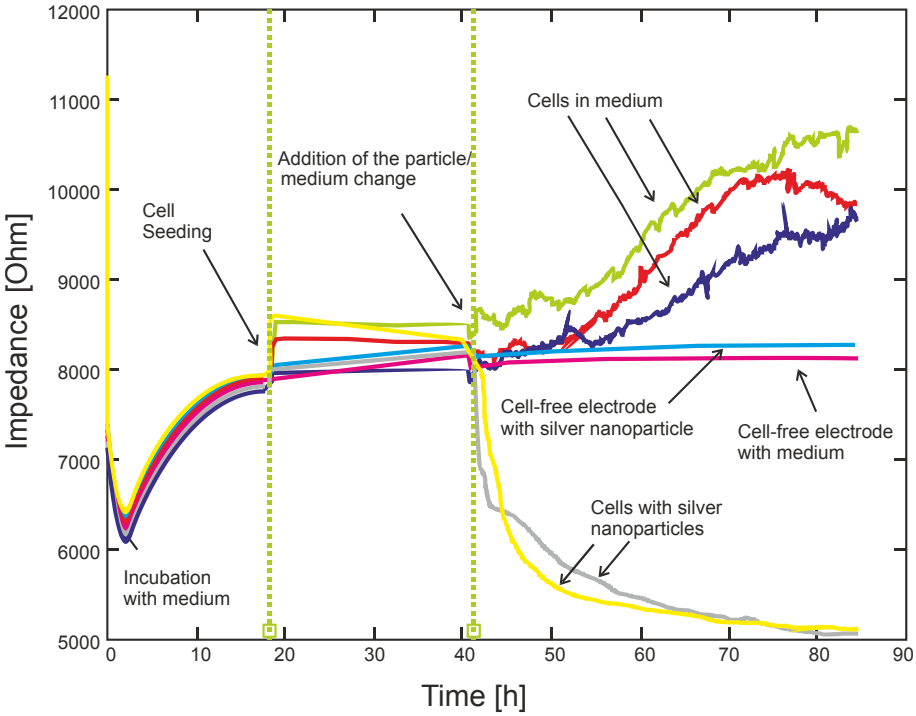

Fig. 4-3 Electric Cell-Substrate Impedance Sensing of A-549 cells with addition of silver nanoparticles at a concentration of 10 ppm. Cell-free medium with and without silver nanoparticles were used as reference and cells in standard medium as control.

The micrographs of the A-549 cells cultivated on the electrodes in normal medium and with 10 ppm silver nanoparticles in the medium after the impedance measurements, respectively, are shown in Fig. 4-4. The micrographs confirm the decrease of the impedance signal indicating a morphology change of the cells. Moreover, a lower number of cells is found on the ECIS electrode cultivated in the presence of silver nanoparticles in the culture medium as compared with the electrode cultivated in normal culture medium. The treated cells exhibit a more spherical shape in comparison with the untreated cells.

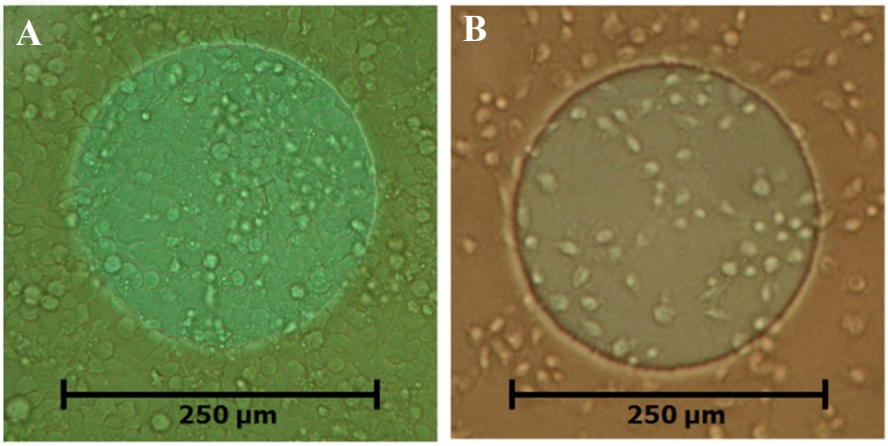

Fig. 4-4 Phase contrast micrographs of A-549-cells on an Electric-Cell-Substrate-Impedance-Sensing electrode (8W1E) in normal culture medium (A) and 48 h after addition of silver nanoparticles at a concentration of 10 ppm to the culture medium (B).

4.2.4.3 Determination of Cell Death

To determine cell death, i.e., to distinguish between apoptosis and necrosis, LDH measurements and caspase 3/7 activity measurements were performed using A-549 cells. For these experiments concentrations were chosen exhibiting a toxic response in the dose-response curves of the A-549 cells. The IC_{50} value of A-549 cells cultivated with silver nanoparticles was determined to be 10 ppm; hence this concentration was used for the determination of the cell death. For the silver ions a concentration of 50 ppm was employed for the determination of the caspase 3/7 activity.

In Fig. 4-5 the caspase 3/7 activity of A-549 cells cultivated with addition of 10 ppm silver nanoparticles in the culture medium and with 50 ppm silver ions as well as the activity of untreated cells in normal culture medium is shown. Cells cultivated with silver nanoparticles show a much higher caspase 3/7 activity than untreated cells. The caspase 3/7 activity of cells cultivated with silver ions at a concentration of 50 ppm is slightly lower than that of untreated cells.

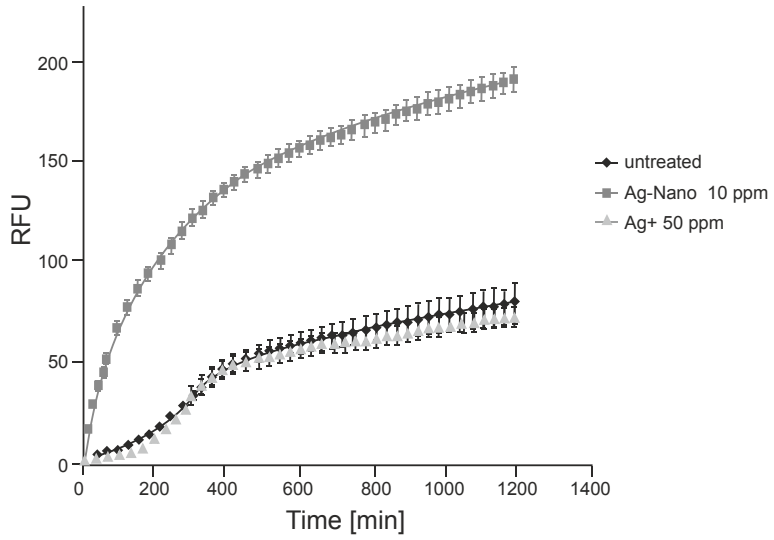

Fig. 4-5 Caspase 3/7 activity of A-549-cells cultivated with silver nanoparticles at a concentration of 10 ppm, with silver ions at a concentration of 50 ppm, and for untreated cells during a cultivation period of 20 h. Data are shown as the mean ± SEM of three independent experiments.

Fig. 4-6 displays the LDH release of the cell culture supernatant of A-549-cells cultivated in normal cell culture medium (untreated cells), with addition of 10 ppm silver nanoparticles, and with 10 ppm of silver ions. There is no LDH release in the cell culture supernatant of A-549 cells cultivated with silver nanoparticles at a concentration of 10 ppm evincing that the cell membranes are not destroyed. By cultivation of A-549 cells with 10 ppm of silver ions in the medium there is a LDH release in the culture supernatant which is, however higher than in the supernatant of untreated cells. This indicates that the membranes are destroyed and the cells die due to necrosis.

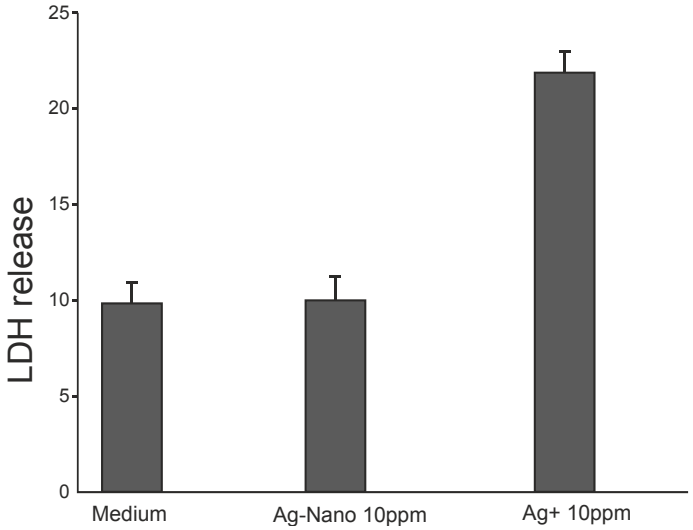

Fig. 4-6 LDH release of the cell culture supernatant of A-549-cells cultivated with silver nanoparticles at a concentration of 10 ppm and with silver ions at a concentration of 10 ppm as well as for untreated cells after a cultivation period of 24 h. Data are shown as the mean ± SEM of five independent experiments.

4.2.5 Discussion

DLS measurements of particle suspensions in water (Fig. 4-1) revealed that the hydrodynamic particle diameter of 70 ± 5 nm. Presumably, the hydrodynamic diameter of Ag nanoparticles in the culture medium could be smaller. Other studies have previously reported and confirmed the nanoparticle stabilization by proteins and sera contained in the medium [302-304]. The results obtained from the viability data of the MTT assay could be good described with the extrapolated dose-response curves (Fig. 4-2).

The calculated IC_{50}, TLC and NOAEC values are different for each cell line ranging from 3 ppm to 144 ppm. The most sensitive cells expressing a toxic response caused by silver nanoparticles are PC-12 and NIH-3T3 cells; here, IC_{50} values as low as 4 ppm have been determined, whereas the IC_{50} value for the A-549 cells is about 10 ppm. However, in comparison with the sensitivity of the cell lines cultivated in presence of silver ions the variation in the toxic doses is not very high. When cultivating the cells with silver ions IC_{50} values between 25 ppm for the PC-12 cells and 97 ppm for the HEP-G2 cells have been determined. For each cell line investigated here, the IC_{50}, TLC and NOAEC values are in the same range. Adding 3 ppm silver nanoparticles to NIH-3T3 cells has no effect, however, upon the addition of 4 ppm almost 50% of the cells were not viable anymore and once 5 ppm of silver nanoparticles were present in the culture medium only 5% of the cells were viable, confirming that the range of the toxic doses is very small. The results obtained also show that the toxic effect is not mainly caused by the silver ions but rather by silver nanoparticles for all tested cell lines. This effect has previously been observed in sea urchin *Paracentrotus lividus* [305].

Braydich-Stolle et al. (2005) investigated the toxic effect of 15 nm sized silver particles and a soluble silver salt (silver carbonate) on C18-4 cells, and did not observe any toxic effect for the silver ions in the investigated concentration range [291]. The EC_{50} values for the particles calculated from the MTS assay are found to be 8.75 µg/ml (8.75 ppm) while for the silver ions they are as high as 408 µg/ml (408 ppm) [291]. In the present study higher toxicity of silver ions (IC_{50}-values between 25 ppm and

97 ppm) was observed, however, the EC_{50} values for the silver particles are found to be in the same range for the cell lines studied here (IC_{50} values between 4 ppm and 10 ppm).

Hussain et al. (2005) investigated the toxic effect of silver nanoparticles with different sizes on BRL3A rat liver cells [292]. The EC_{50} value for the silver particles with a diameter of 100 nm was reported to be 19 ± 5.2 µg/ml (19 ± 5.2 ppm) while for particles with a size of 15 nm an EC_{50} value of 24 ± 7,5 µg/ml (24 ± 7,5 ppm) has been determined [292]. These toxicity values are slightly lower than those found here, but in the same range. On the contrary, Haase et al. (2012) reported an IC_{50} value of 110 µg/ml (110 ppm) for peptide coated silver nanoparticles with a diameter of 20 nm [302].Kawata et al. (2009) investigated the toxic effect of silver nanoparticles with a size of 7-10 nm of silver carbonate and of polystyrene nanoparticles (as reference) to HEP-G2 cells [296]. They observed a decrease in cell viability by addition of 2 mg/l (2 ppm) of the silver nanoparticles to the cells.Both, the cultivation with polystyrene as a non-toxic nanoparticle reference and with silver ions in the concentration range between 0.1 mg/l and 3 mg/l showed no toxic effect [296]. Our results indicate that there is a toxic effect of silver nanoparticles on HEP-G2 cell when adding concentrations exceeding 4 ppm.

The ECIS of A-549 cells cultivated with silver nanoparticles at a concentration of 10 ppm and the reference cell growth in normal medium shown in Fig. 4-3 confirm the toxicity of silver nanoparticles. It is obvious that the impedance signal decreases directly after addition of 10 ppm of silver nanoparticles. That indicates that the toxic effect occurs immediately after the addition of the nanoparticles. In the absence of cells the impedance signal is not influenced by the nanoparticles as shown in Fig. 4-3. The signal of a cell-free electrode with nanoparticles showed the same impedance signal as the cell-free electrode incubated with only medium.

The micrographs of the electrodes taken after the ECIS experiment (Fig. 4-4) confirm these results. The electrode seeded with cells in normal culture medium (Fig. 4-4 (A)) showed a confluent cell layer of A-549 cells which in the ECIS measurement was observed as a high impedance signal. The electrode with cells cultivated for 48 h with silver nanoparticles at a concentration of 10 ppm only showed a few cells on the electrode surface corresponding to a low impedance signal in the measurement. Apparently the dead cells detached from the electrode surface and because of that the impedance signal decreased. The cells which remained attached to the electrode surface exhibited changes in morphology and were found to be smaller than untreated cells which can be regarded as an indicator for apoptosis. Similar morphological changes of cells cultivated in the presence of silver nanoparticles at a concentration of 10 µg/ml were observed by Braydich-Stolle and co-workers [291]. The IC_{50} value of A-549-cells cultivated with silver nanoparticles calculated from the dose-response curves is 10 ppm, thus ECIS showed a good correlation with these results.

To determine the kind of cell death LDH release and caspase3/7 activity measurements were carried out with A-549 cells cultivated with silver nanoparticles and of silver ions. As shown in Fig. 4-6, there was no LDH release in the cell culture supernatant of the A-549 cells cultivated with silver nanoparticles at a concentration of 10 ppm, whereas the overlap of cells cultivated with silver ions showed much more LDH release which is similar to that observed for untreated cells. This indicates that cell death induced by cultivation with nanoparticles is not related to necrosis, since the cell membranes remain intact. Untreated cell culture also contains cells which due to mechanical interferences are necrotic. Braydich-Stolle et al. also found no significant LDH release in C18-4 cells cultivated with different concentrations of silver nanoparticles in the concentration range between 5 µg/ml and 100 µg/ml (5 and 100 ppm) [291]. Measurements of the caspase 3/7 activity of A-549 cells cultivated with silver nanoparticles at a concentration of 10 ppm and with silver ions at a concentration of 50 ppm, (Fig. 4-5) revealed a much higher activity of caspase 3/7 in cells cultivated with the particles as compared to cells cultivated in cell culture medium alone or with addition of 50 ppm silver ions. That indicates that the A-549 cells are undergoing apoptosis by cultivation with silver nanoparticles, whereas the cells cultivated with silver ions do not exhibit apoptosis but rather show necrosis.

The mechanism of cell death is clearly different when cultivation is performed in the presence of nanoparticles or ions, leading to the conclusion that the toxic effect of silver nanoparticles to A-549 cells is indeed not caused by the silver ions. Moreover; these results are supported by the dose-response curves as well as by the calculated IC_{50} values.

4.2.6 Conclusions

The toxic effect of silver nanoparticles on four different mammalian cell lines has been investigated studying the mitochondrial activity and employing the Electric-Cell-Substrate-Impedance-Sensing (ECIS) method. As reference, Ag^+-ions were used at the same concentration as the Ag-atoms present in the particles.

Based upon the results of the MTT assay, dose-response curves were extrapolated and IC_{50}, TLC, and NOAEC values were calculated. The results showed that silver nanoparticles are considerably more toxic than silver ions. Depending on the cell line the respective values were found to be between 5 (PC-12 cells) and 18 (NIH-3T3-cells) times higher.

The results from ECIS measurements indicate that the toxic effect of the silver nanoparticles occurs immediately after addition of the silver nanoparticle suspension. Measurements of LDH release of the cell culture supernatant of cells cultivated with nanoparticles or ions, respectively, showed no release for cells cultivated with the particles but LDH release for the ions. Cells cultivated with toxic doses of nanoparticles or ions, respectively, showed caspase 3/7 activity for the nanoparticles but no activity for the ions. Clearly, the mechanism of cell death is different when cultivations are carried out with silver

particles or with ions. Cells cultivated in the presence of particles apparently suffer apoptosis while cells cultivated with ions die due to necrosis.

Acknowledgements

This work was supported by the German Federal Ministry of Education and Research (BMBF Project "HelioClean", grant number: 03X0069F). For constructive discussions Prof. Cornelia Kasper is gratefully acknowledged.

5 *Complex-Screening*: Dreidimensionale Zellsysteme

5.1 Zusammenfassung

Für die Risikobewertung der Nanomaterialien werden verbesserte Strategien für die *in-vitro*-Nanopartikel-Testung gefordert. Im *Complex-Screening* sollen daher dreidimensionale Zellsysteme verwendet werden. Derzeitige Standard-*in-vitro*-Testsysteme für Toxin-, Wirkstoff- und Nanopartikel basieren auf zweidimensionalen (2D) Kulturen. In den 2D-Zellkulturen sind die Eigenschaften wie Zellmorphologie, Zellfunktion, Zellantworten und Zell-Zell-Interaktionen nicht vergleichbar mit denen im menschlichen Organismus. Die Zellen sind z.B. mit der einen Seite an die Zellkulturoberfläche adhäriert, während die andere Zellseite dem Nanopartikel enthaltenen Medium ausgesetzt ist. Interaktionen mit anderen Zellen erfolgen nur über den Zellrand mit den benachbarten Zellen. In 2D-Kulturen wurden bisher toxische Effekte für verschiedenen Nanopartikel beobachtet. Die Übertragbarkeit dieser Ergebnisse auf die Wirkung im menschlichen Organismus ist jedoch fraglich und muss überprüft werden. Im natürlichen Gewebe bilden Zellen dreidimensionale (3D) Strukturen aus, so dass bestimmte Zell-Zell-Interaktionen und eine extrazelluläre Matrix entstehen. Um 3D-Zellwachstum *in vitro* zu ermöglichen, können Zellen auf einer Gerüststruktur anwachsen, in Gelen eingekapselt werden oder es können Zellaggregate (Sphäroide) gebildet werden. Bei den Sphäroiden sind die Größe und die Zellpackungsdichte entscheidend für den Nährstofftransport und die Zell-Zell-Interaktionen. Da größere Sphäroide mit einem Durchmesser größer als 600 µm häufig Nährstoff- und Gaslimitierungen aufweisen und daher einen apoptotischen/nekrotischen Kern haben, stellen Sphäroide besonders geeignete Modelle dar, um die Zell-Zell-Kontakte und natürliche Diffusionsbarrieren zu simulieren.

Die 3D-Zellsphäroide wurden für die *in-vitro* Testung von Nanopartikeln untersucht, um die Mikroumgebung der Zellen den Bedingungen im menschlichen Organismus anzupassen. Die Wirkungen von Nanopartikeln auf 3D-Sphäroide wurden mit der auf 2D-Kulturen verglichen. Da Zinkoxid (ZnO)-Nanopartikel und Titandioxid (TiO_2)-Nanopartikel die in der Nanotechnologie am häufigsten eingesetzten Nanopartikel sind, wurden diese exemplarisch untersucht. Als Ziellinien wurden die A549-Zellen (Lunge) und die NIH-3T3-Zellen (Haut) verwendet. Zudem wurde überprüft, ob bei den gebildeten Sphäroiden eine Diffusionslimitierung der Nanopartikel vorliegt und somit die Zellen im Kern der Sphäroide mit den Nanopartikeln nicht in Kontakt kommen. Die Nanopartikel wurden daher direkt während sowie nach der Sphäroid-Bildung hinzugegeben und die Zellantwort untersucht. Die Einflüsse der Nanopartikel auf die Viabilität der Zellen sowie die Morphologie der Sphäroide wurden analysiert. Zusätzlich wurde die Sphäroid-Bildung auch online mikroskopisch verfolgt und es wurden Zeitraffervideos erstellt. Es wurden zwei verschiedene Zellviabilitättests, das *CellTiter-Blue® Cell Viability Assay* (Promega, Madison, USA) sowie das *CellTiter-Glo® Luminescent Cell Viability Assay* (Promega, Madison, USA) miteinander verglichen und deren Anwendung für die 3D-Sphäroide überprüft. Der CTB-Test beruht auf der Reduktion des blauen

Resazurins zum violetten Resorufin durch metabolisch aktive Zellen. Das fluoreszierende Reduktionsprodukt Resorufin wird detektiert, so dass indirekt die Menge an lebenden Zellen in der Kultur bestimmt wird. Beim ATP-*Assay* wird die Viabilität über die intrazelluläre ATP-Menge bestimmt. Zur Quantifizierung des ATPs werden die Zellen lysiert und am Luminometer die Luciferase-Reaktion von Luciferin zu Oxyluciferin in der Gegenwart von Magnesium, ATP und Sauerstoff verfolgt.

Die A549-Zellen bildeten lockere Zellaggregate, wohingegen die NIH-3T3-Zellen eine kompakte 3D-Sphäroid-Struktur aufwiesen. Anhand der mikroskopischen Aufnahmen wurde ersichtlich, dass die Sphäroid-Bildung bereits nach sechs Stunden abgeschlossen war. Bei den Viabilitätstests wurden unterschiedliche Verhältnisse zwischen Signal und Hintergrundsignal festgestellt. Die Sensitivität des ATP-Tests war im Vergleich zum CTB-Test höher. Beim CTB-Test wurde das Resazurin vorrangig von den Zellen, die an der Hülle der Sphäroide angesiedelt sind, umgesetzt. Die Diffusion des Resazurins zu den im Inneren der Sphäroide liegenden Zellen ist eingeschränkt. Da für den ATP-Test die Sphäroide zunächst lysiert werden, werden hier die Diffusionslimitierungen des *Assay*-Farbstoffes minimiert. Vor allem die Viabilität der kompakten Sphäroide der NIH-3T3-Zellen konnte daher mit dem ATP-Test präziser bestimmt werden.

In Abhängigkeit von der Konzentration beeinflussen die ZnO-Nanopartikel die Viabilität der Zellen in 2D sowie in 3D. Die 3D-Sphäroide aus A549-Zellen waren im Vergleich zu den in 2D-kultivierten Zellen empfindlicher gegenüber den ZnO-Nanopartikeln. Bei den NIH-3T3-Zellen wurden dagegen keine signifikanten Unterschiede in der Empfindlichkeit gegenüber den ZnO-Nanopartikeln zwischen 2D- und 3D-Kulturen beobachtet. Die TiO_2-Nanopartikel (maximale Konzentration von 150 µg/ml) zeigten keine Wirkung auf die Viabilität beider Zelllinien in 2D. Auch die TiO_2-Nanopartikel-Exposition von vollständig ausgebildeten Sphäroiden hatte keinen signifikanten Einfluss auf die Viabilität.

Der Zeitpunkt der Nanopartikel-Exposition bei der Sphäroid-Bildung beeinflusst außerdem die Morphologie der Sphäroide sowie die Signale der Vibilitätstests. Während die Morphologie der Sphäroide nach abgeschlossener Sphäroid-Bildung bei unterschiedlichen Nanopartikel-Konzentrationen unverändert war, wurden bei zeitgleicher Sphäroid-Bildung und Nanopartikel-Exposition Morphologieänderungen beobachtet. Mit steigender ZnO-Nanopartikel-Konzentration nahm der Durchmesser der Sphäroide von beiden untersuchten Zelllinien zu. Die A549-Zellen, die direkt mit den ZnO-Nanopartikeln exponiert wurden, waren im Vergleich zu denen in den gebildeten Sphäroiden sensitiver. Die toxischen ZnO-Nanopartikel bewirkten den Verlust der Zell-Zell-Kontakte. Bei der direkten Zugabe von TiO_2-Nanopartikeln bildeten sich mehrere kleine Sphäroide anstelle eines einzelnen Sphäroids. Die Anzahl der Sphäroide korrelierte dabei mit der TiO_2-Nanopartikel-Konzentration. Bei den NIH-3T3-Zellen wurde zudem eine Zunahme des Fluoreszenz- bzw. des Lumineszenz-Signals der kleinen Sphäroide bei steigender TiO_2-Nanopartikel-Konzentration

detektiert. Bei dem anderen Sphäroid-Modell wurden diese Effekte nicht beobachtet. Die TiO_2-Nanopartikel haben einen Einfluss auf die Zell-Zell-Wechselwirkungen, die für die Sphäroid-Bildung entscheidend ist. Das Oberflächen-Volumen-Verhältnis ist bei kleineren Sphäroiden besser, so dass mehr Zellen an der Sphäroid-Hülle vorhanden sind, die Farbstoffe umsetzen können.

Insgesamt bestätigen die Ergebnisse die Bedeutung der 3D-Zellkulturstudien zur Risiko-Einschätzung von Nanopartikeln, da einige Effekte nicht in der 2D-Zellkultur beobachtet werden können. Die Wirkungen der Nanopartikel auf Zell-Zell-Interaktionen können mittels 3D-Modellen besser simuliert werden, als mit 2D-Kulturen. Auch die Wahl der Zelllinie sowie der Zeitpunkt der Nanopartikel-Zugabe beeinflusst die Ergebnisse. Die 3D-Zellaggregate eigenen sich dabei vor allem um die Diffusion von Nanopartikeln in kompakte Gewebestrukturen im menschlichen Organismus zu simulieren. Mit den zweiten 3D-Sphäroid-Modell, bei dem die Nanopartikel-Zugabe während der Sphäroid-Bildung erfolgt, können dagegen die Effekte auf die Zell-Zell-Wechselwirkungen analysiert werden. In Abhängigkeit von der späteren Anwendung der Nanopartikel ist das entsprechende 3D-Modell zu wählen.

5.2 Three Dimensional Spheroid Cell Culture for Nanoparticle Safety Testing

Franziska Sambale[1], Antonina Lavrentieva[1*], Frank Stahl[1], Cornelia Blume[1], Meike Stiesch[2], Cornelia Kasper[3], Detlef Bahnemann[1], Thomas Scheper[1]

[1] Gottfried Wilhelm Leibniz University Hanover, Institute for Technical Chemistry, Callinstr. 5, 30167 Hanover, Germany
[2] Medical School Hannover, Carl-Neuberg-Straße 1, 30625 Hannover, Germany
[3] University of Natural Resources and Life Science (Boku), Institute of Applied Microbiology, Muthgasse 18,1190 Vienna

*Corresponding author: Antonina Lavrentieva, phone number: 049 511 762 2955, lavrentieva@iftc.uni-hannover.de

Reprinted from *Journal of Biotechnology* 205 (2015) 120–129, DOI: 10.1016/j.jbiotec.2015.01.001 with kind permission from Elesevier.

5.2.1 Abstract

Nanoparticles are widely employed for many applications and the number of consumer products, incorporating nanotechnology, is constantly increasing. A novel area of nanotechnology is the application in medical implants. The widespread use of nanoparticles leads to their higher prevalence in our environment. This, in turn, raises concerns regarding potential risks to humans. Previous studies have shown possible hazardous effects of some nanoparticles on mammalian cells grown in two-dimensional (2D) cultures. However, 2D *in vitro* cell cultures display several disadvantages such as changes in cell shape, cell function, cell responses and lack of cell-cell contacts. For this reason, the development of better models for mimicking *in vivo* conditions is essential.

In the present work, we cultivated A549 cells and NIH-3T3 cells in three-dimensional (3D) spheroids and investigated the effects of zinc oxide (ZnO-NP) and titanium dioxide nanoparticles (TiO_2-NP).The results were compared to cultivation in 2D monolayer culture. A549 cells in 3D cell culture formed loose aggregates which were more sensitive to the toxicity of ZnO-NP in comparison to cells grown in 2D monolayers. In contrast, NIH-3T3 cells showed a compact 3D spheroid structure and no differences in the sensitivity of the NIH-3T3 cells to ZnO-NP were observed between 2D and 3D cultures. TiO_2-NP were non-toxic in 2D cultures but affected cell-cell interaction during 3D spheroid formation of A549 and NIH-3T3 cells. When TiO_2-NP were directly added during spheroid formation in the cultures of the two cell lines tested, several smaller spheroids were formed instead of a single spheroid. This effect was not observed if the nanoparticles were added after spheroid formation. In this case, a slight decrease in cell viability was determined only for A549 3D spheroids. The obtained results demonstrate the importance of 3D cell culture studies for nanoparticle safety testing, since some effects cannot be revealed in 2D cell culture.

Keywords: spheroids; *in vitro* cytotoxicity testing; mammalian cells; zinc oxide nanoparticles; titanium dioxide nanoparticles; 3D cell culture

5.2.2 Introduction

Interest in nanoparticle research has increased dramatically over the last decades due to the wide range of applications of nanoparticles in everyday objects such as sun screens and paints. Nanoparticles are

also intensively studied as possible candidates for the coating of medical implants. Such coatings can reduce the risk of bacterial contamination and can improve implant biocompatibility. Since nanoparticle safety issues are not fully clarified, further investigations are needed to characterize the effects of nanoparticles on human health and the environment. Nanotoxicological, nanotherapeutics and drug screening studies are still primarily based on two dimensional (2D) cell culture or, in the later stages, on complex animal *in vivo* models [306]. Although 2D cell culture is a robust, well-established and reproducible technique of *in vitro* testing, the use of 2D cultures often yields results with large discrepancies relative to *in vivo* animal models. This is not surprising, since 2D cell culture represents an environment, remarkably distinct from the *in vivo* situation, where the majority of tissues are three-dimensional (3D) [262, 307, 308].

In the last few years, many new drugs have been withdrawn during animal trials because previous *in vitro* toxicity testing failed to identify their hazards [309]. 2D cell cultures cannot represent the complex native tissue environment with the extracellular matrix (ECM) and the totality of intercellular interactions which are very important for cell physiology and behavior [306, 308]. Moreover, gene expression analysis of diverse cell lines has revealed hundreds of genes which are expressed differently in 2D and in 3D cultures [308, 310]. Therefore, various 3D models have been developed to better mimic the conditions and properties of *in vivo* tissue [311]. In this regard, *in vitro* studies of nanoparticles effects in a 3D cell culture model seem to be more appropriate compared to 2D monolayer systems, since toxicity results can be more strongly influenced by the cell microenvironment [233, 261].

Spheroids (cell aggregates) represent a simple 3D system since no scaffold or supporting material is required for 3D cell growth [307]. It has been shown that cellular adhesion regulates cell migration, proliferation and apoptosis in spheroids [308]. Different techniques are used to generate spheroids such as hanging drop or low-attachment plates [312]. The size of the cell aggregates (spheroids) plays a crucial role and impacts cell responses [307, 313]. Small-sized spheroids do not display the complexity of real tissue, whereas larger spheroids demonstrate diffusion limitations for oxygen and nutrients [313]. These limitations often induce necrotic core formation and reduce the viability of the cells [313]. In addition, various cell types show differences in their cell packing density [314]. Some cells form very compact structures whereas others display low cell density in aggregates [314, 315]. Literature suggests that the ideal size for spheroids ranges from 100 µm to 600 µm [262, 313-316]. The spheroid critical size can vary, depending on cell type and cell packing density, thus a separate investigation for each cell line used is recommended. In cell spheroids, the ECM and the dense cell packing act as transport barriers, hindering nanoparticle penetration to the spheroid core [317] and only a subset of the cells are exposed to the tested substance (e.g. nanoparticles) [262]. Moreover, the penetration of nanoparticles in spheroids can be limited by nanoparticle-cell interaction [316].

Zinc oxide (ZnO) and titanium dioxide nanoparticles (TiO_2-NP) are widely used for many applications. For ZnO-NP several cytotoxic effects have been reported on different cell types in 2D, whereas only a few studies have been published in 3D. It was reported that ZnO-NP decreased cell viability [219, 221, 318-321], induced oxidative stress [220, 318], lead to DNA damage [318, 322] and induced apoptosis [322, 323]. In contrast to ZnO-NP, the toxicity of TiO_2-NP is still a point of discussion. The differences in the reported results of TiO_2-NP toxicity may occur due to the divergence in used cells, size of nanoparticles and applied assays [223]. Several working groups revealed toxic effects of TiO_2-NP such as induced generation of reactive oxygen species (ROS) [324], up-regulated apoptosis markers [325] and decreased cell viability [326-328]. In addition, genotoxic effects of TiO_2-NP on NIH-3T3 cells were detected by the comet assay at the highest dose of 1.000 µg/ml TiO_2-NP [223]. Other groups reported absence of toxic effects of TiO_2-NP in 2D cultures [216, 219, 222, 329].

In few published studies on the effects of nanoparticles in 2D and 3D cell cultures particles were added after spheroid formation. Kim et al. (2014) revealed similar cell proliferation of A549 cells in 2D and 3D cell cultures treated with ZnO-NP, whereas molecular markers for oxidative stress were significantly reduced only in 2D cell culture [330]. Cell viability in C6 rat glioma spheroids was not decreased in the presence of TiO_2-NP [331]. Lee and colleagues showed a reduced toxic effect in HepG2 spheroids for cadmium telluride (CdTe) and gold nanoparticles in comparison to the 2D cell culture [262]. Interestingly, the EC_{50} values obtained for some drugs in 3D cell culture were in the same range as those obtained in *in vivo* experiments [233]. This clearly demonstrates that *in vitro* 3D nanoparticle safety testing could bridge the gap between conventional 2D cell cultures and complex animal studies [306]. By using valid *in vitro* models which mimic the complexity of tissues, the number of whole-animal studies can be minimized [332] and costs can be reduced [261, 306]. Although being very advantageous for simulating the *in vivo*-like cell microenvironment, 3D cell cultures still need further improvement and validation, since viability assays were initially established for monolayer 2D cell culture [307, 308]. Moreover, the influence of the size and density of cell aggregates, as well as the effect of the time point of drug or nanoparticles application during spheroid formation need further investigation.

The skin and the respiratory tract are important pathways of possible nanoparticle adsorption into the human organism. Therefore, in the present work we used two model cell lines - human lung carcinoma A549 cells and murine fibroblasts NIH-3T3 cells. ZnO-NP and TiO_2-NP were chosen as nanoparticle models because both nanoparticles are extensively used for different applications and their effects on 2D monolayer cultures has been described in the literature. Cytotoxic effects of ZnO-NP were reported for both A549 [219, 220] and NIH-3T3 cells [221] in 2D cultures. TiO_2-NP were shown to be non-toxic to NIH-3T3 cells [222, 223] and to A549 cells [222]. Some working groups, however, reported toxic effects of TiO_2-NP on A549 cells [325, 327] in 2D cell cultures. The aim of this work was to

study the influence of the time point of application of nanoparticles on the cell viability in 3D spheroids. In addition, a validation of two different cell viability assays for such cultivation systems was carried out.

5.2.3 Material and Methods

5.2.3.1 Cell Culture

Both used cell lines A549 human lung carcinoma cells (DSMZ no.: ACC 107) and NIH-3T3 mouse fibroblasts cells (DMSZ no.: ACC 59) were purchased from the German Collection of Microorganisms and cell cultures (DSMZ). All cell lines were cultivated in Dulbecco's Modified Eagle's medium (DMEM)(D7777 Sigma-Aldrich, Steinheim, Germany) supplemented with 10% fetal calf serum (FCS) and 100 µg/ml antibiotics (penicillin/streptomycin) in a humidified environment at 37°C/ 5% CO_2. Cells were sub-cultivated every 3 or 4 days when the cultures reached 70-80% confluence. All used cells had a passage number of less than 20.

5.2.3.2 Nanoparticles

TiO_2-NP (Hombikat XXS 700) were obtained from Sachtleben, Duisburg, Germany. According to the data sheet the primary particle size of TiO_2-NP is 7 nm (REM) in the anatase form. The ZnO-NP (with 0.1% Ru) used for the cytotoxicity tests were synthesized and characterized by Bloh et al. (2012, 2014) [226, 227]. For the ZnO-NP a BET surface of 6.54 m²/g were measured with a particle size of 50 ± 10 nm (X-ray) by Bloh et al [226]. To measure the hydrodynamic diameter and the distribution of the ZnO-NP and TiO_2-NP in water and in the used cell culture media, dynamic light scattering measurements were performed. Suspensions (1 ml) with a concentration of 500 µg/ml in water and in cell culture medium were prepared and then measured with a Malvern Zetasizer Nano-ZS. Each measurement was repeated three times to enable the calculation of a standard deviation.

5.2.3.3 Nanoparticles Testing

A549 cells and NIH-3T3 cells in 2D cell culture (96-well plates, Sarstedt AG) and in 3D spheroids (96-well plates, ultra-low attachment, Corning AG) were exposed to different concentrations of ZnO-NP and TiO_2-NP for 24 h. For the monolayer culture, 8.000 A549 cells/well or 6.000 NIH-3T3 cells/well were initially seeded in a 96-well plate and were cultured 24 h in 100 µl culture medium before nanoparticle treatment. For the spheroids, two different exposure methods were performed. In the first model, similar to the 2D cell culture, the cells were equilibrated for 24 h in a standard culture medium to aggregate and form a spheroid. Afterwards, different concentrations of nanoparticles were added and the cells were incubated for 24 h (with equilibration (w. eq)). In the second model, the cells were seeded in the 96-well-plate directly with nanoparticles in the culture media and cells were grown for 48 h. Here, microtissue formation occurred in the presence of nanoparticles. In both spheroid models, 2.500 cells/well were seeded and grown in 150 µl cell culture medium.

5.2.3.4 Microscopy and Spheroid Diameter

Images were taken of all spheroids using a microscope (Olympus, IX50, Olympus Corporation, Tokio, Japan) with a camera (Olympus SC30, IX-TVAD, Toxio, Japan). The *cellSens* Software (cellSens Standard 1.7.1, Olympus) was used to measure the spheroid area. We assumed that all spheroids have a round shape, and therefore the diameter of the spheroids was determined from their area. The shown data are from at least three independent experiments which were done in triplicates (mean with standard derivation) ($n \geq 3$).

5.2.3.5 CTB Analysis

CTB analysis (CellTiter-Blue® Cell Viability Assay, Promega, Madison, USA) was performed according to the manufacturer's protocol for the 2D monolayer and was optimized for the 3D cell culture. The CTB assay is based on the reduction of the blue resazurin to purple resorufin by metabolically active cells. The reaction can be monitored via fluorescence measurements and indicates indirectly the amount of viable cells in the culture. For the 2D cell cultures at first medium was removed from each well and 100 µl of 10% CTB solution (90 µl DMEM, 10 µl CTB stock solution) were added to each well and incubated for 2 h at 37°C/ 5% CO_2. For the spheroids, 40 µl medium was left in each well and 110 µl of CTB/DMEM solution was added to get a final concentration of 10% CTB in DMEM. Here, the cells were incubated for 20 h at 37°C/ 5% CO_2. The fluorescence signals at an extinction wavelength of 544 nm and an emission wavelength of 590 nm were determined using a microplate reader (Fluoroskan Acent, Thermo Fisher Scientific Inc., Waltham, USA). The intensity of the measured fluorescence signal was proportional to the cell number in 3D spheroids (supporting information, Fig. 5-7). Each measurement was repeated at least three times in triplicates to calculate the standard derivation.

5.2.3.6 ATP Analysis

Adenosine triphosphate (ATP) analysis (CellTiter-Glo® Luminescent Cell Viability Assay, Promega, Madison, USA) was performed according to the manufacturer's protocol for the 2D monolayer and was optimized for the 3D cell culture. The ATP assay is based on the quantification of the amount of intracellular ATP which correlates with the number of metabolically active (viable) cells. For this assay, the cells were lysed and the ATP was detected by the luciferase reaction of beetle luciferin to oxyluciferin in the presence of Mg^{2+}, ATP and molecular oxygen (Promega, USA). For the 2D cell cultures, the medium was removed and 100 µl of 50% CellTiter-Glo® solution (50 µl DMEM, 50 µl CellTiter-Glo® stock solution) was added. For the spheroids, 40 µl medium was left in each well and 110 µl of CellTiter-Glo®/DMEM solution was added to get a final concentration of 50% CellTiter-Glo® in DMEM. The 2D culture was shaken for two minutes with 300 rpm and luminescence was recorded 10 minutes after reagent addition. For microtissues in 3D culture, the plate was shaken for 5 minutes with 300 rpm and luminescence was recorded 30 minutes after reagent addition. The

luminescence signals were measured with Perkin Elmer Wallac Victor 2v Multilabel HTS Counter 1420.

5.2.3.7 Data and Statistical Analysis

With the data obtained by the CTB assay and the ATP assay, dose-response-curves (nonlinear curve fitting, growth/sigmoidal, DoseResp) were fitted with OriginPro 8.5.0 SR1 for the determination of the half maximal inhibitory concentration (IC_{50}). To accomplish this, the normalized cell viability was plotted as a function of the logarithm of the particle. The shown data are from at least two independent experiments which were done in triplicates ($n \geq 3$). Statistical analysis was performed using the analysis of variance (ANOVA, one way) (OriginPro 8.5.0 SR1). A significant effect was reported at * $p<0.01$.

5.2.4 Results

5.2.4.1 Characterization of Nanoparticles

The hydrodynamic diameter of both nanoparticle types was measured by dynamic light scattering (DLS). ZnO-NP exhibited an average hydrodynamic diameter of 41± 5 nm in water, 190 ± 3 nm in DMEM and 106 ± 11 nm in the standard culture medium (mean ± standard derivation). For TiO_2-NP the average diameter was 79 ± 25 nm in water, 142 ± 29 nm in DMEM and 118 ± 28 nm in the culture medium.

5.2.4.2 Difference in IC_{50} values Obtained by CTB and ATP Assays for Various Nanoparticles

Effect of ZnO-NP

Exposure of the cells (A549 and NIH-3T3) to ZnO-NP caused decrease of cell viability in a concentration-dependent manner. Decreased cell viability was observed in both cell lines in 2D and in 3D cell cultures, revealing a toxic effect of ZnO-NP (Fig. 5-1). For the 2D monolayer, a half maximal inhibitory concentration (IC_{50} value) of 15 ± 6 µg/ml for the NIH-3T3 cells and 54 ± 12 µg/ml for A549 cells were determined using the *Cell Titer Blue* (CTB) assay (Tab. 3-1). In comparison to the 2D monolayer, the IC_{50} values obtained for the spheroids with the CTB assay were lower. The NIH-3T3 spheroids with and without equilibration (w/o eq) demonstrated the lowest IC_{50} value. All calculated IC_{50} values were summarized in Tab. 3-1. Differences in the sensitivity of NIH-3T3 cells in 2D and 3D cell cultures obtained with the CTB assay could not be observed with the ATP assay. For 2D and 3D cell culture, the IC_{50} values determined with the ATP assay were comparable equal. In contrast, the A549 cells displayed a lower cell resistance to the ZnO-NP toxicity in the spheroids if compared to 2D cultures in both assays. For the CTB and the ATP assay, the signal-to-background-ratio for untreated cells was calculated (supporting information, Fig. 5-8). The viability of the cells cultured in a 2D monolayer can be determined with both assays but the ATP assay has a higher sensitivity. However, the CTB assay gives a very low signal-to-background-ratio for the NIH-3T3 spheroids, whereas the

ATP assay gives a higher ratio. In comparison, the signal-to-background-ratio for the CTB assay for the spheroids of A549 cells was similar to the ratio given for 2D monolayer cultures.

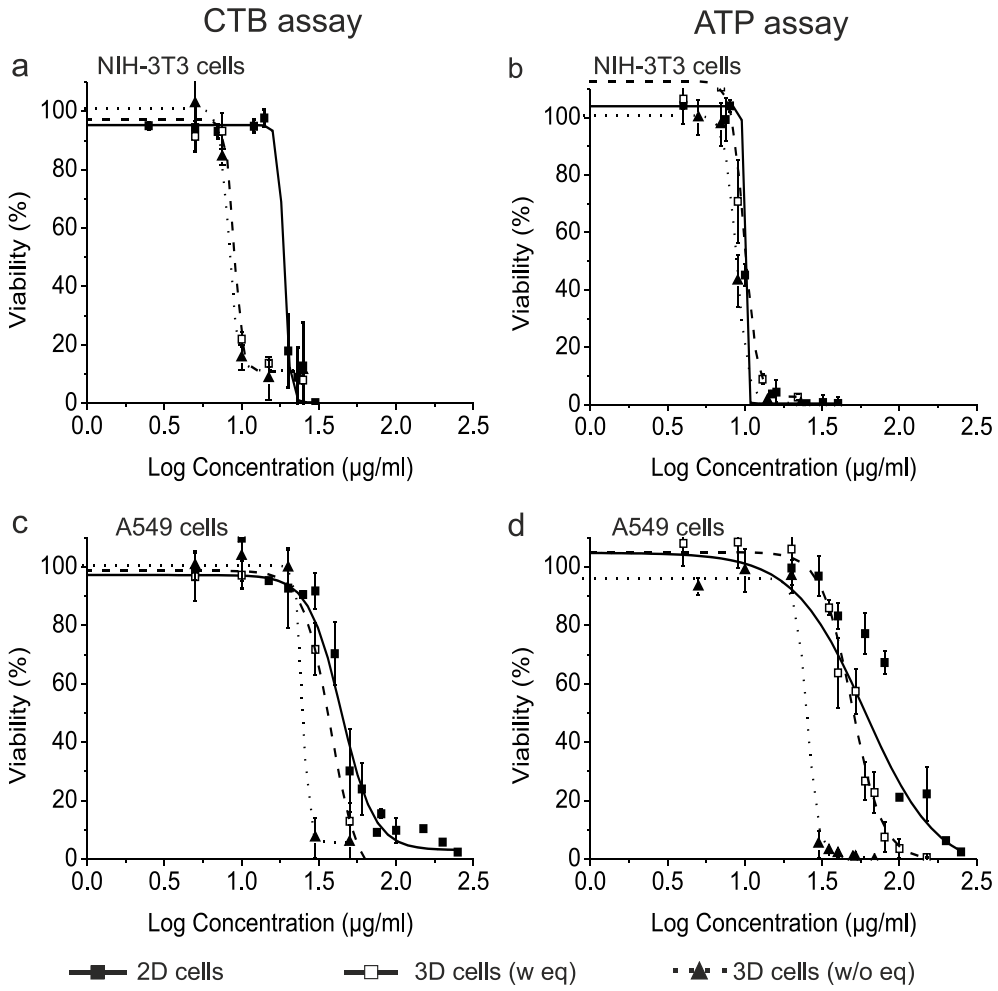

Fig. 5-1 The viability of NIH-3T3 cells (a, b) and the A549 cells (c, d) determined by the CTB and the ATP assays. The figures show the extrapolated dose-response curves of NIH-3T3 cells (a, b) and A549 cells (c, d) cultivated with ZnO-NP in 2D and 3D. Data points are means ± SD for n ≥ 3

Tab. 5-1 Inhibitory Concentration (IC_{50} value) for NIH-3T3 cells and A549 cells cultivated with ZnO-NP in 2D and 3D cell cultures (w eq= with equilibration, w/o eq= without equilibration). Data are presented as mean ± SD. Significant differences versus control group are indicated in the table (ANOVA, One way). * $p<0.01$

	NIH-3T3 cells: IC_{50} value [µg/ml]		**A549 cells: IC_{50} value [µg/ml]**	
	CTB assay	**ATP assay**	**CTB assay**	**ATP assay**
2D Cell Culture	15 ± 6	11 ± 2	54 ± 12	64 ± 9-
3D Cell Culture Spheroid w eq	9 ± 1	10 ± 2	42 ± 13	45 ± 8*
3D Cell Culture Spheroid w/o eq	10 ± 1	10 ± 1	24 ± 5*	24 ± 8*

Effect of TiO_2-NP

Parallel to the toxic ZnO-NP, TiO_2-NP were tested in 2D and in 3D cell culture systems. Here, both CTB and ATP assay give the same results. For the 2D cell culture, no decrease of the viability of both NIH-3T3 cells and A549 cell lines was revealed by exposure to TiO_2-NP (Fig. 5-2). Moreover, for the NIH-3T3 cells no significant toxic effect could be observed for spheroids with equilibration (w eq)

determined both with the CTB and the ATP assay (Fig. 5-2 a, b). On the contrary, the metabolic activity of the cells in spheroids without prior equilibration delivers an increase up to 350% higher fluorescence signal (CTB assay) with 150 mg/µl TiO_2-NP in the medium (Fig. 5-2 a). A slight decrease of the metabolic activity of the A549 cells was investigated for spheroids with equilibration. Hence, the TiO_2-NP influenced the viability of A549 cells grown in 3D spheroids (Fig. 5-2 c, d). Interestingly, for spheroids without equilibration, the viability determined with the ATP assay decreased only for 25 µg/ml TiO_2-NP in the medium. For TiO_2-NP concentrations higher than 50 µg/ml no decrease of cell viability was observed.

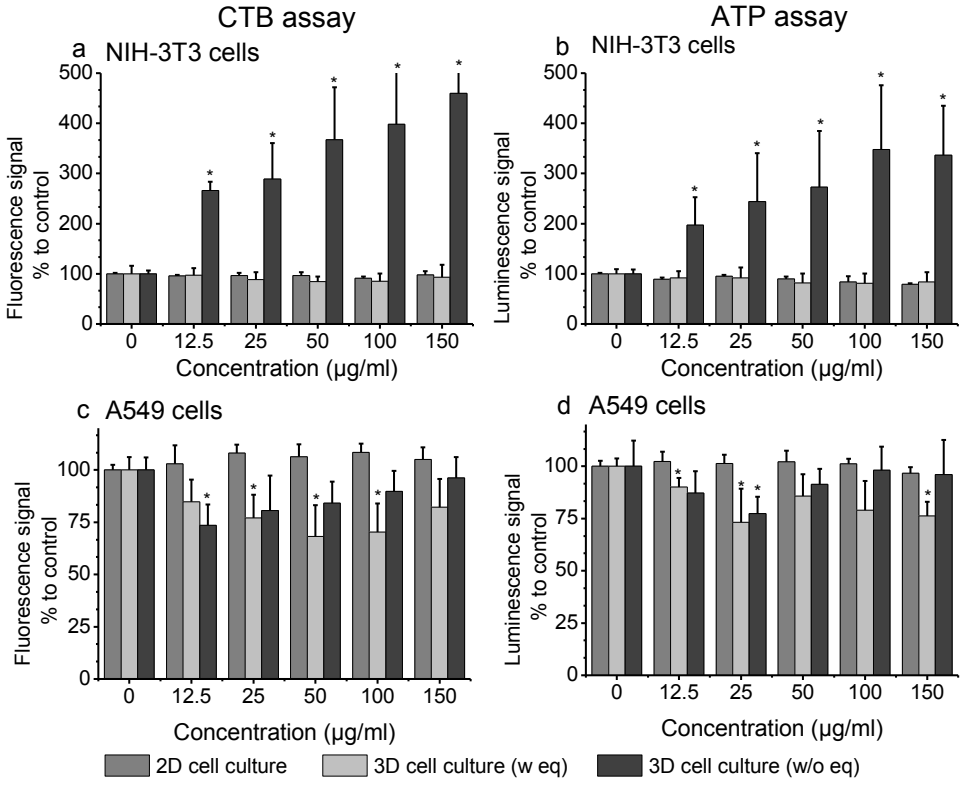

Fig. 5-2 Viability of NIH-3T3 (a, b) and A549 cells (c, d) treated with TiO_2-NP determined by the CTB assay (a, c) and the ATP assay (b, d). The metabolic activity of cells cultured without nanoparticle is used as 100% fluorescence/luminescence signal control. Data points are means + SD for $n \geq 3$. Significant differences versus control group are indicated in the figure (ANOVA, One way). * $p<0.01$.

5.2.4.3 Morphology of 3D NIH-3T3 and A549 Cell Cultures Exposed to ZnO-NP and TiO_2-NP

The morphology of NIH-3T3 and A549 spheroids exposed to ZnO-NP and TiO_2-NP is shown in Fig. 5-3 and Fig. 5-4. A significant difference in cell packing density was revealed for both cell lines. NIH-3T3 cells demonstrated a compact spheroid structure (Fig. 5-3, Fig. 5-4) whereas A549 cells had a lower cell density (arranged as loose aggregates) (Fig. 5-3, Fig. 5-4). In addition, the spheroid diameter for both cells lines was different, although the same cell number was used. After duration of 6 h, spheroid formation is nearly completed for both cell lines (supporting information, Fig. 5-9). The influence of nanoparticles on spheroid morphology was investigated.

ZnO nanoparticles

Fig. 5-3 shows the morphology of spheroids of NIH-3T3 cells and A549 cells treated with ZnO-NP with and without equilibration. Fig. 5-3 a-f represents the NIH-3T3 spheroid morphology after ZnO-NP treatment with: (a, d) 0 µg/µL, (b, e) 10 µg/µL and (c, f) 15 µg/µL. The diameter of spheroids with equilibration (w eq) stayed constant after 24 h exposure to nanoparticles (Fig. 5-3 a-c). Also, after an exposure time of up to 72 h no significant changes in the diameter of the spheroids could be observed (data not shown). The morphology of the spheroids without equilibration is shown in Fig. 5-3 d-f. Here, the spheroids' observed diameter increases depending on the ZnO-NP concentration. Similar results were observed with the A549 cells which are displayed in Fig. 5-3 g-l. Without previous equilibration (w/o eq), the diameter of the A549 spheroids is increasing in correlation with the amount of ZnO-NP. Measured diameters of the spheroids for both methods are shown in Fig. 5-5. For NIH-3T3 cells, the spheroid diameter of the untreated cells was 319 ± 36 µm and for the A549 cells 684 ± 46 µm.

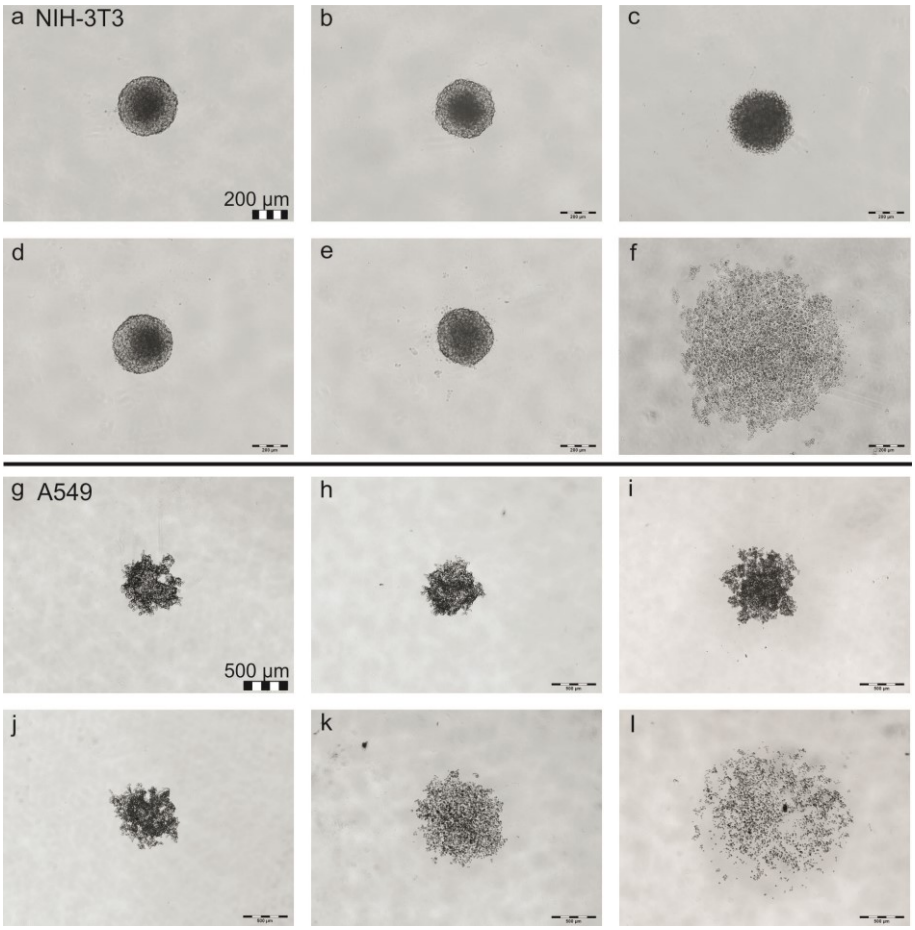

Fig. 5-3 Morphology of spheroids of NIH-3T3 cells and A549 cells treated with ZnO-NP with equilibration (a-c, g-i) and without equilibration (d-f, j-l). The figures display the difference of the two methods of ZnO-NP exposure. In figure a, d NIH-3T3 cells were grown in standard medium whereas in b, e 10 µg/ml and in c /f 15 µg/ml ZnO-NP were added to the culture (scale bar= 200 µm). In figure g, j A549 cells were grown in standard medium whereas in h, k 20 µg/ml and in i, l 40 µg/ml ZnO-NP were added to the culture (scale bar= 500 µm).

TiO_2 nanoparticles

The effect of TiO_2-NP on spheroid formation and morphology was also studied. Analogue to the ZnO-NP methodology, the same two exposure models were compared. In agreement with the results from the ZnO-NP, the spheroid diameter with equilibration stays constant for NIH-3T3 cells (Fig. 5-4 a-c) and A549 cells (Fig. 5-4 g-i). Interestingly, the effects of TiO_2-NP to spheroids without prior equilibration were different than those of ZnO-NP. Here, instead of an increasing diameter of spheroids exposed to higher nanoparticle concentrations in the culture medium, the cells formed smaller spheroids (Fig. 5-4 d-f, Fig. 5-4 j-l). This observation was made for both cell lines. Fig. 5-6 shows the amount of spheroids per well and their diameters for both cell lines and different nanoparticle concentrations. The higher the concentration of the TiO_2-NP, the larger is the number of spheroids per well and smaller the spheroid diameter (Fig. 5-6).

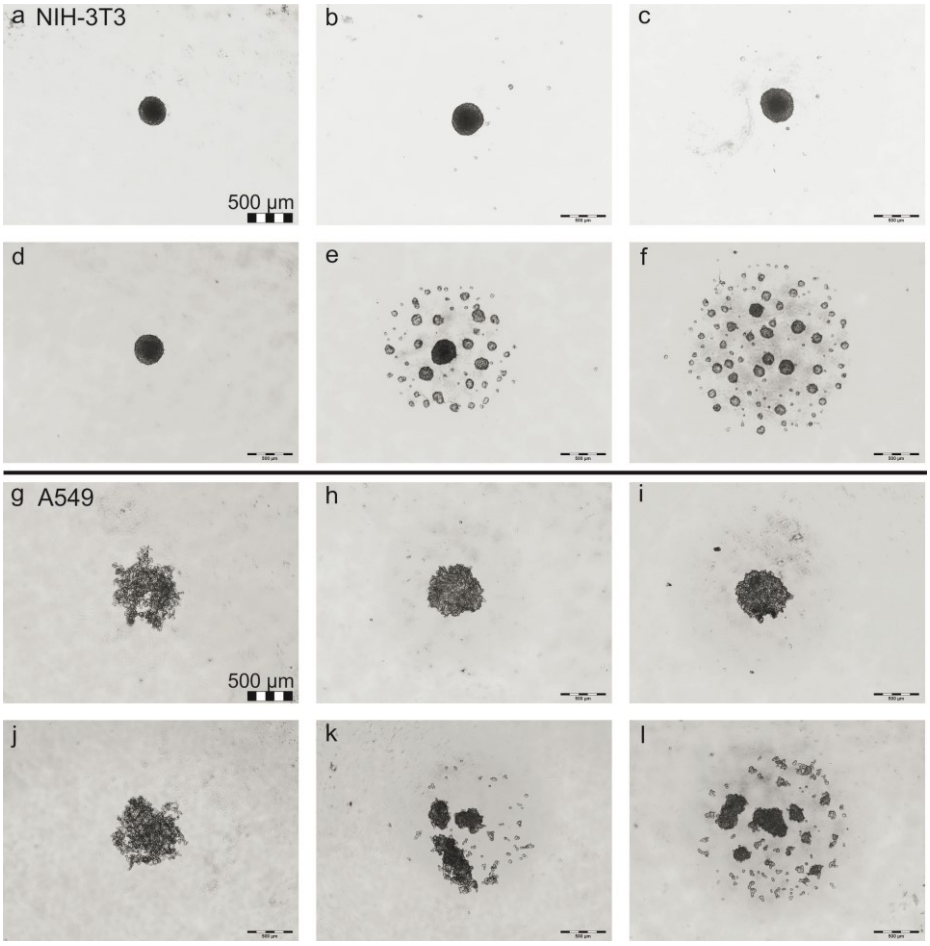

Fig. 5-4 Morphology of spheroids of NIH-3T3 cells and A549 cells incubated with TiO_2-NP with equilibration (a-c, g-i) and without equilibration (d-f, j-l). The figures display the difference of the two methods of TiO_2-NP exposure. In figure a, d NIH-3T3 cells were grown in standard medium whereas in b, e 25 µg/ml and in c, f 50 µg/ml TiO_2-NP were added to the culture (scale bar= 500 µm). A549 cells were grown in standard medium (g, j), with 25 µg/ml (h, k) and with 50 µg/ml TiO_2-NP (i, l) (scale bar= 500 µm).

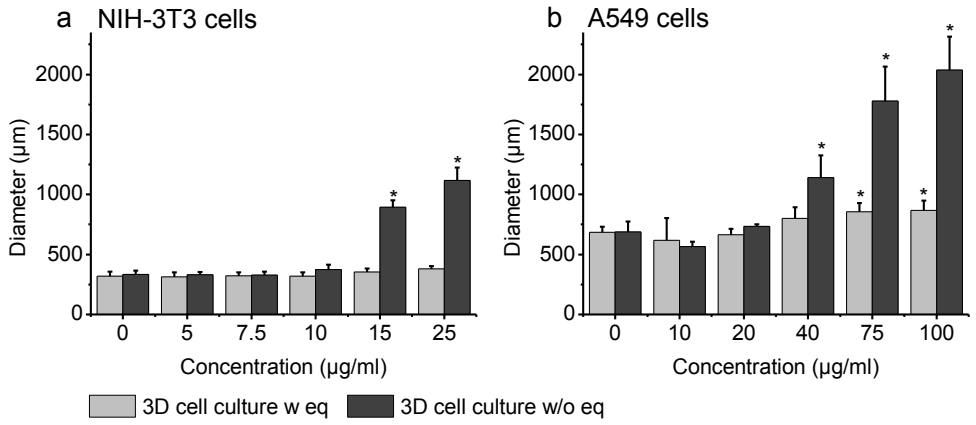

Fig. 5-5 Comparison of spheroids of NIH-3T3 cells (a) and the A549 cells (b) with (w eq) and without equilibration (w/o eq). The figures show the diameters of the NIH-3T3 spheroids (a) and A549 spheroids (b). For spheroids without equilibration the increase of the diameter correlates with the ZnO-NP concentration. This effect could be observed with both cell lines. Data points are means + SD for n ≥ 3). Significant differences versus control group are indicated in the figure (ANOVA, One way). * p<0.01

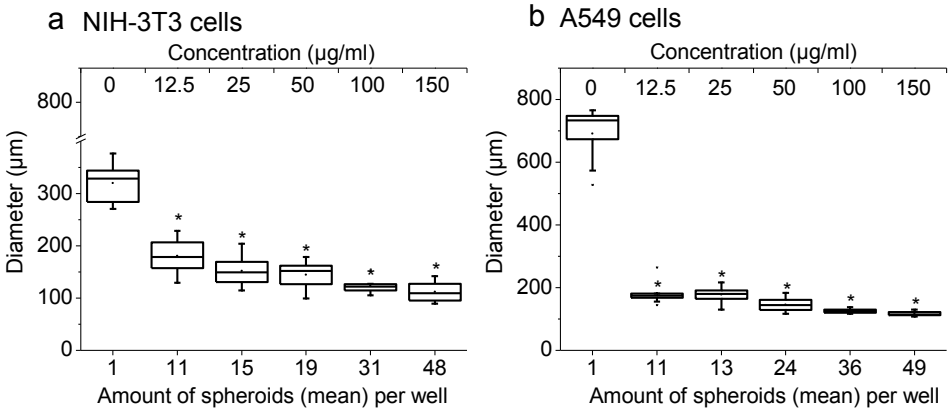

Fig. 5-6 Correlation of spheroid diameter and the amount of spheroids per well after TiO_2-NP addition. The figures show the diameters of the NIH-3T3 spheroids (a) and A549 spheroids (b) without equilibration. Data points are means ± SD for n ≥ 3). Significant differences versus control group are indicated in the figure (ANOVA, One way). * p<0.01

5.2.5 Discussion

In this study we compared the effects of ZnO-NP and TiO_2-NP to a 2D monolayer and a 3D spheroid cell cultures. 3D cell spheroids of A549 cells and NIH-3T3 cells were cultivated in order to approach *in vivo* tissue microenvironment and investigated as an advanced model for *in vitro* nanoparticle testing. On one hand, spheroid size and the cell packing density (cell-cell interaction) could play an important role in nanoparticle safety testing by introducing nutrient transport limitation and cell-cell interaction *in vitro* complexities. On the other hand, the spheroid formation time (equilibration time) before exposure to nanoparticles could influence the cell response and the outcome of the cell viability assays. Cells grown in a 2D monolayer are attached on one side to the plastic cell culture flask bottom, while they are exposed to the medium with tested nanoparticles from the other side; contact with other cells occurs only at the periphery (cell edges). The cells in spheroids display a complex heterogeneous model with cell-cell communications, a gradient of oxygen, nanoparticle concentration and pH value [261]. For this reason we compared two different exposure models for nanoparticle testing in

our work using 3D spheroid cell cultures. We varied the time for spheroid formation before adding nanoparticles. In the first model, the cells were allowed to form spheroids prior nanoparticle exposure (with equilibration (w eq)), while in the second model, the cells were treated with nanoparticles directly without prior equilibration (w/o eq).

ZnO-NP

Toxic ZnO-NPs were chosen in order to study the difference between 2D and 3D cell culture systems. With the help of CTB and ATP assays, a toxic effect of ZnO-NP was revealed for NIH-3T3 cells and A549 cells, because the viability of the cells decreased in correlation with the nanoparticle concentration. The results of the *in vitro* cytotoxicity of ZnO-NP also clearly shows differences in the sensitivity of the two chosen cell lines to this nanoparticle. In addition, the calculated IC_{50} value of the A549 cells in the 2D monolayer culture was two-times higher than that of the NIH-3T3 cells. These differences in the sensitivity of the cells were also revealed by Kroll et al. (2011) with $BaSO_4$ nanoparticles [232]. The toxic effect of ZnO-NP determined with the CTB and the ATP assay correlates with the increasing diameter of the spheroids without prior equilibration. This effect can be explained by the loss of cell-cell contacts as a result of the toxic effect of ZnO nanoparticles. For spheroids with equilibration, the diameter remained constant. Indeed, Lee et al. (2009) did not observe significant morphological changes for toxic cadmium telluride nanoparticles [262]. Therefore, the time for spheroid formation before nanoparticle addition influences the cell response.

According to the signal-to-background-ratio of the CTB and ATP assay for the NIH-3T3 cells, the ATP assay is more suitable for measuring the viability of NIH-3T3 spheroids because it provides a higher sensitivity. For the ATP assay, the cell spheroids were lysed before detection of ATP. Thus, diffusion limitations of the dye were minimized. Indeed, Lee et al. (2009) also revealed a higher activity in 2D than in 3D for the MTT assay [262]. However, for a diameter of ≥ 500 µm this cell viability assay still could be verified [315]. The CTB assay underestimates the viability of the NIH-3T3 cells in a spheroid due to the high cell packing density, compact spheroid structure, and corresponding resazurin diffusion limitations. In addition, the metabolic activity and the proliferation rate of NIH-3T3 cells grown in spheroids are regulated by cell-cell interactions [308]. Moreover, the proliferation rate is reduced in spheroids [262]. Thus, the ATP assay with valid signal-to-background values gives more significant results, especially for NIH-3T3 cells. Here, the cells (spheroids) are disrupted and the ATP amount was quantified, since the number of cells correlates with the amount of ATP.

The A549 cells showed a lower cell-cell interaction in their spheroids and were looser packed. Presumably, diffusion limitations are minimized in these spheroids and, therefore, the metabolic activity of the core cells can be detected. As a result, both CTB and ATP assays give reasonable results for A549 cells. In addition, the spheroid structure and the spheroid morphology play a critical role in the choice of the viability assay [315]. Different cell types have different cell-cell interactions

which influence their behavior in a 3D cell culture [315]. No significant difference in the IC_{50} value could be observed with the ATP assay between the 2D monolayer and 3D NIH-3T3 cell cultures. Interestingly, the A549 cells are more sensitive to the ZnO-NP in 3D cell culture compared to cultivation in the 2D monolayer. Moreover, spheroid formation time (equilibration) before nanoparticle addition has an effect on the sensitivity of A549 cells. A549 cells without equilibration (w/o eq) are more sensitive compared to cells with equilibration (w eq). This effect indicates that the fully formed cell-cell contacts and the synthesis of extracellular matrix in the spheroids with equilibration all seem to have a protective function against nanoparticle toxicity for the cells. Thus, less cells are exposed to the toxic nanoparticles. Moreover, the dead cells on the shell act as an additional physical barrier [262]. Furthermore, in A549 spheroids with equilibration a nanoparticle concentration gradient still exist.

TiO_2-NP

The effects of TiO_2-NP on 2D and 3D cell cultures were investigated. NIH-3T3 cells and A549 cells grown in a 2D monolayer did not show a change in their metabolic activity after TiO_2-NP treatment. For the NIH-3T3 cells neither the CTB assay, nor the ATP assay revealed a cytotoxic effect of TiO_2-NP. Interestingly, addition of TiO_2-NP to the NIH-3T3 cells directly during spheroid formation leads to formation of numerous small spheroids. In NIH-3T3 cells, higher CTB and ATP assay signals were obtained for TiO_2-NP treated spheroids when compared to control 3D cultures. This could be caused by higher surface-to-core cell numbers. In smaller spheroids, more cells are located on the surface of the spheroid which leads to easier dye access and faster resazurin metabolization. Moreover, smaller spheroids have higher proliferation rates on the surface since cells have less contact inhibition.

Further, A549 cells were studied in order to reveal the influence of cell culture conditions on cell response. TiO_2-NP caused stronger cytotoxic effect in 3D spheroids than in monolayer cultures. In the 2D monolayer no decrease in cell viability was observed while in A549 spheroids the viability drops slightly in the presence of TiO_2-NP. At a TiO_2-NP concentration of 25 µg/ml (and higher concentrations) the viability of A549 cells dropped to 73 ± 16% (ATP assay). A cytotoxic effect for these concentrations, however, was not observed for NIH-3T3 cells. This could be explained by differences in the packing densities (cell-cell interaction) between A549 and NIH-3T3 cells. Cell adhesion and, consequently, diffusion rates (limitations) can significantly affect cytotoxicity itself or cytotoxicity readouts. We observed a low packing density and a loose spheroid structure for the A549 cells which was caused by lower cell-cell interaction. On the contrary, NIH-3T3 cells form very compact spheroids, demonstrating stronger cell-cell interactions.

Similar to NIH-3T3 cells, A549 cells form smaller spheroids during NP treatment without equilibration. Also remarkable in A549 cells, TiO_2-NP concentrations below 25 µg/ml induces slight decreases in viability whereas higher concentrations do not show any effect. One explanation could be that for the A549 cells the small spheroids of A549 cells display similar behavior as cells in a 2D

monolayer, due to the loss of the cell-cell interaction complicity. In comparison to the ZnO-NP, the nontoxic TiO_2-NP have a different effect on spheroids without prior equilibration. Toxic ZnO-NP causes the increase of spheroid diameter with increased nanoparticle concentrations. Apoptotic and necrotic cells lose their ability to generate a stable extracellular matrix and adhere to their neighbor cells. In contrast, TiO_2-NP cause a formation of smaller spheroids instead of one large spheroid. This effect could be observed with both cell lines.

The obtained results underline the importance of 3D *in vitro* testing because the effects of TiO_2-NP could not be observed in 2D monolayers (data not shown). The TiO_2-NP which are nontoxic for 2D cell culture, influence spheroid formation in both tested cell lines which could be caused by lower cell-cell interactions of treated cells. In general, cell adhesion is very important for cell behavior and indicates the first cell response to a tested material [326]. Hence, cellular adhesion regulates cell migration, proliferation and apoptosis [308]. Indeed, changes in the expression of cell adhesion molecules (integrin, N-catherin, connexin and pannexin), or their direct or indirect blocking can influence the cell-cell interaction and cell aggregation in spheroids and result in tissue morphology changes [307].

Shinto et al. (2012) demonstrated that the exposure of carboxyl-modified polystyrene (PS-COOH) nanoparticles reduces the adhesion of cells to microsphere surfaces which was measured with the help of atomic force microscopy (AFM) [333]. Because the melanoma cells, used in this study, express several adhesion receptors from the integrin family, the authors proposed a nonspecific COOH-integrin interaction [333]. Therefore, the nanoparticles act as a nonspecific competitive inhibitor which results in a reduction of the microsphere-cell adhesion [333]. In addition, TiO_2-NP affects the cell adhesion of mesenchymal stem cells (MSC) in dependence of the particle size [326]. The amount of the adhesion protein vinculin was lower in cells exposed to larger TiO_2-NP (196 nm) [326]. Furthermore, gene expression studies with TiO_2-NP in 2D cell culture with HaCaT cells have shown an overexpression of the matrix metallopepitdases (MMP-9 and MMP-10) [334]. These enzymes are involved in the degradation of the ECM components and the ECM remodeling [334]. Moreover, the authors found that TiO_2-NP induce a higher expression of cell adhesion molecules such as fibronectin and intergrin [334]. They propose that inflammation could be induced in cells after exposure to TiO_2-NP. The inflammation is caused by the absence of an intact ECM due to the overexpression of metallopeptidases [334].

The studies of the authors Fujita, Horie et al.(2009) have been performed with 2D cell culture, but their results are in agreement with our investigations of TiO_2-NP in spheroids. Our study is the first which varied the spheroid initiation time and demonstrated a significant difference in spheroid morphology as a result of the different time points of nanoparticle application. Further studies are needed to investigate the effects of TiO_2-NP on cell adhesion in more detail.

5.2.6 Conclusions

Our study reports the importance of 3D *in vitro* cell cultures systems for nanoparticle safety testing. Here, we compared the effect of toxic ZnO-NP and non-toxic TiO_2-NP to A549 and NIH-3T3 cell lines, grown in a 2D monolayer and in spheroids. Moreover, the formation time of the spheroids before nanoparticle addition was varied. We determined cell viability with the Cell Titer Blue assay and the ATP assay and compared their performance for spheroid viability measurements. It was found that for spheroid analysis, the ATP assay gives more significant results, especially for NIH-3T3 cells. We revealed that spheroid structure and spheroid morphology play a critical role in the readouts of the viability assays. For NIH-3T3 cells a compact 3D spheroid structure was observed, while A549 formed looser aggregates. Therefore, besides assays based on metabolic activities, cell morphology monitoring, as well as spheroid size could be used as a tool for cytotoxicity measurements.

ZnO-NP displayed a toxic effect on both cell lines, with higher sensitivity of the NIH-3T3 cells. Similar inhibitory concentrations of ZnO-NP were obtained for NIH-3T3 cells in 2D and 3D cell culture using the ATP assay. In contrast, the A549 cells were more sensitive to the ZnO-NP in 3D spheroids compared to 2D monolayers. In addition, treatment with TiO_2-NP caused a minor decrease in A549 cell viability in 3D spheroids, while no toxic effect was observed in 2D cell cultures.

Furthermore, spheroid formation time before nanoparticle addition influences the cell response and the spheroid morphology. For spheroids without equilibration, we revealed a correlation in the spheroid diameter (spreading of the cell in low-attachment wells) with increasing ZnO-NP concentration. Under the same conditions, nontoxic TiO_2-NP have caused formation of smaller spheroids and increased spheroid amount per well for both tested cell lines. Since this effect cannot be observed in monolayer cultures, 3D culture systems provide additional information about the effect of nanoparticles or other tested substances on cell physiology and intercellular interactions.

Acknowledgement

This work was supported by the European Regional Development Fund (EFRE Project “Nanokomp”, grant number: 60421066) and by the BIOFABRICATION FOR NIFE (initiative, which is financially supported by the Lower Saxony ministry of Science and Culture and the Volkswagen Stiftung). Marline Kirsch and Timon Harries are gratefully acknowledged for assistance in the laboratory work.

5.2.7 Supporting Information

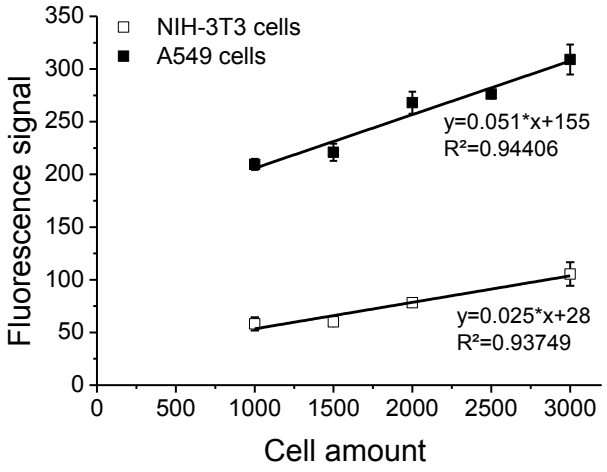

Fig. 5-7 Intensity of the measured fluorescence signal and cell number of 3D NIH-3T3 and A549 cells spheroids.

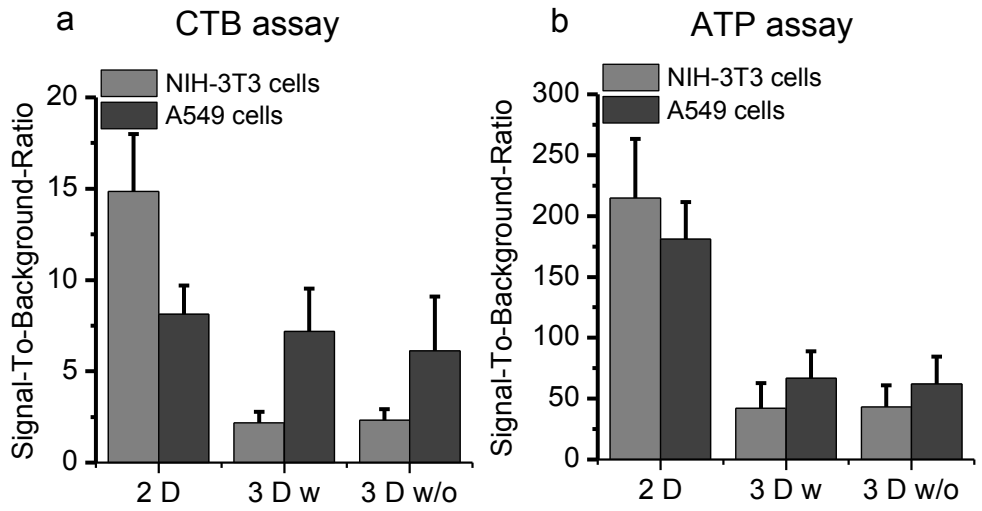

Fig. 5-8 Signal-To-Background-Ratio of the CTB (a) and the ATP assay (b) for NIH-3T3 cells and A549 cells.

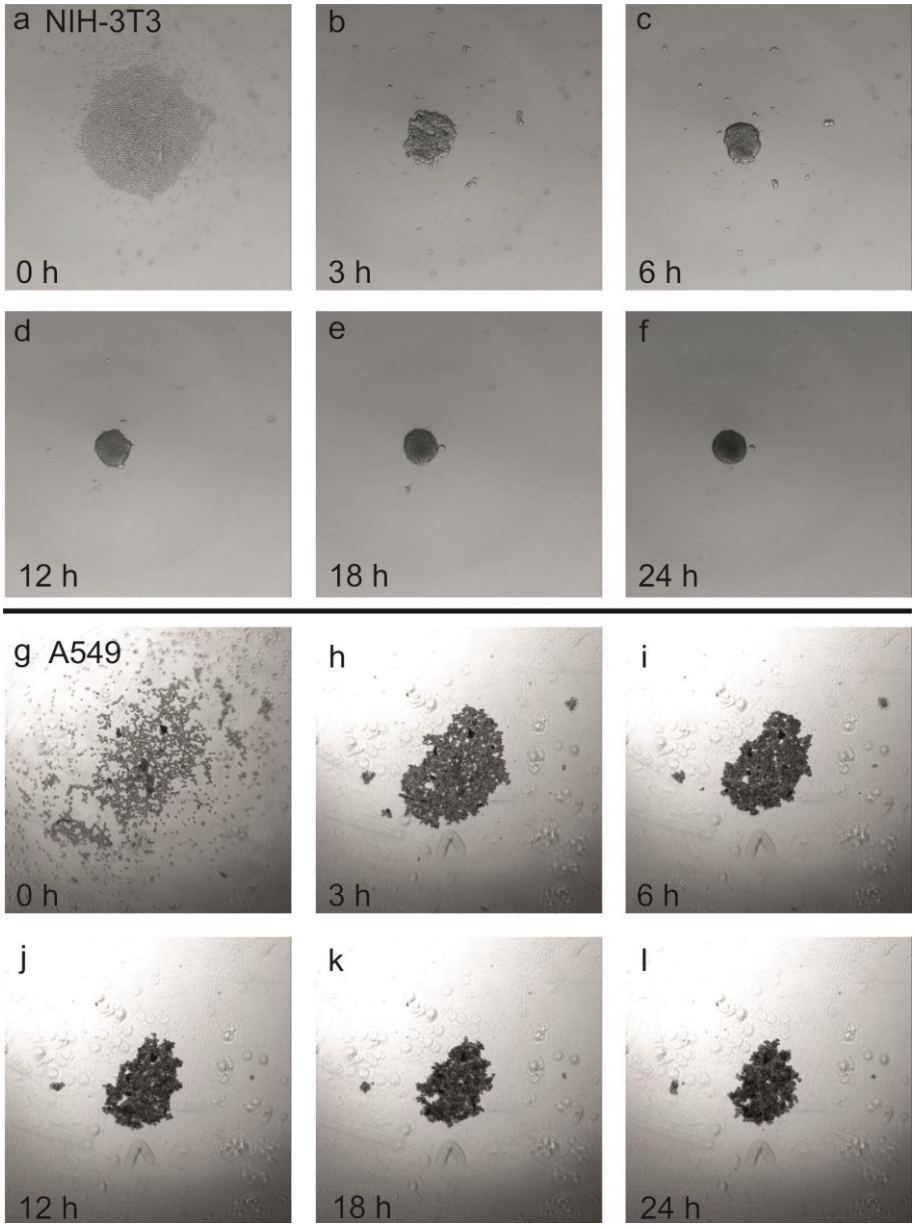

Fig. 5-9 Morphology of spheroid formation of NIH-3T3 cells and A549 cells after 24 h.

Time lapse videos

Video 1: Spheroid Formation of NIH-3T3 cells for 24 hours (control cells), objective 4x, 2 frame/min (LumaScope 600, Etaluma)

Video 2: Spheroid Formation of NIH-3T3 cells for 24 hours with 50 µg/ml titanium dioxide nanoparticles, objective 4x, 2 frame/min (LumaScope 600, Etaluma)

6 *Complex-Screening:* Dynamische Kultivierungsbedingungen

6.1 Zusammenfassung

Im *Complex-Screening* sollen neben den dreidimensionalen Zellsystemen auch dynamische Kultivierungsbedingungen zum Einsatz kommen. Für die bessere Übertragbarkeit von *in-vitro*-Untersuchungen auf den menschlichen Organismus sollte zukünftig die Komplexität von *in-vitro*-Experimenten erhöht werden. Derzeit erfolgen *in-vitro*-Tests für Nanopartikel überwiegend unter statischen Bedingungen. Dabei können Nanopartikel über respiratorische, orale oder dermale Aufnahmewege in das Gefäß- und Blutsystem gelangen. Dort wirkt eine kontinuierliche Strömung auf die Zellen und die Nanopartikel. Zudem kann ein kontinuierlicher Austausch von Gasen, Nährstoffen und Stoffwechselprodukten erfolgen und die Nanopartikel werden homogen verteilt. Bei der statischen Kultivierung hingegen kann es zu Ablagerungen von Nanopartikeln kommen, so dass teilweise lokal höhere Konzentrationen vorliegen. Verschiedene Faktoren wie die Zell-Nanopartikel-Interaktion, die Nanopartikel-Aufnahme, die Verteilung im Medium sowie der Transport zur Zelle können durch dynamische Kultivierungsbedingungen beeinflusst werden. Unterschiede in der Exozytose- und Endozytoserate von Nanopartikeln wurden unter Perfusion bereits beobachtet [335]. Außerdem hat die kontinuierliche Strömung einen Einfluss auf die Zellphysiologie, die Zell-Zell-Wechselwirkung und die Zellantwort. Der Scherstress kann zu Änderungen der Zellmorphologie, Zelladhäsion, Membranstabilität und Membransteifigkeit führen. Im menschlichen Organismus sind verschiedene Zelltypen, wie die Lungenepithelzellen, vaskuläre Zellen und Endothelzellen permanent einem kontinuierlichem Fluss oder einer mechanischen Stimulation ausgesetzt. Vor allem Endothelzellen werden durch dynamische Kultivierungen beeinflusst.

Die Simulation der physiologischen Strömungsbedingungen stellt daher einen wichtigen Parameter für die Wirkstoff- und Nanopartikel-Testung dar. Derzeit wird der Einsatz von dynamischen Systemen für die *in-vitro*-Testung erprobt. Hierbei werden verschiedene Mikro- und Makrofluid-Systeme sowie andere Strömungssysteme entwickelt. Dabei werden entsprechend den *in-vivo*-Gefäßen mikrofluidische Geometrien in der Größe von 0,01 mm (Kapillaren) bis hin zu 0,5-15 mm (Arterien und Venen) benötigt [182]. Zur Herstellung der Strukturen könnte zukünftig auch das 3D-Druckverfahren eingesetzt werden. Die verwendeten Materialien müssen vorher auf Biokompatibilität überprüft werden (Veröffentlichungen IX und X). Die Kombination von 3D-Druckverfahren und Mikrofluid-Systemen könnte eine schnelle und effiziente Charakterisierung der Nanopartikel unter dynamischen Bedingungen ermöglichen.

Bisher wurden nur wenige Zytotoxizitätsuntersuchungen von Nanopartikeln unter Perfusion durchgeführt. Im Rahmen dieser Dissertation wurden daher die Wirkungen von Zinkoxid (ZnO)- und Titandioxid (TiO_2)-Nanopartikeln jeweils unter statischen und dynamischen Bedingungen untersucht. Da Nanopartikel zunächst mit der Lunge und der Haut in Kontakt kommen, wurde die Wirkung auf

Lungen (A549-Zellen)- und Fibroblasten (NIH-3T3-Zellen) analysiert. Hierbei wurden die Zellviabilität, Zellmorphologie und Zelladhäsion bestimmt. Zur Bestimmung der Viabilität der Zellen wurde der Adenosintriphosphat (ATP)-Test angewendet. Die Menge des detektierten ATPs in den Zellen gibt dabei Rückschlüsse auf die Stoffwechselaktivität der Zellen. Zusätzlich wurde die *Electric Cell-Substrate Impedance Sensing* (ECIS)-Methode eingesetzt, um online die Effekte der Nanopartikel-Exposition und der Strömungsbedingungen zu analysieren.

Die Zellmorphologie der beiden Zelltypen wurde unterschiedlich stark von dem angewendeten Scherstress beeinflusst. Während die NIH-3T3-Zellen sich in Fließrichtung des Mediums anordneten, blieb die Morphologie der A549-Zellen nach dynamischer Kultivierung unverändert. Bei den A549-Zellen waren hingegen kleine Vesikel innerhalb der Zellen zu beobachten. Sowohl in der statischen als auch in der dynamischen Kultur verminderte die ZnO-Nanopartikel-Exposition die Zellviabilität. Zudem wurde das Ablösen der Zellen in Abhängigkeit von der Dosis beobachtet. Dieser Effekt konnte mittels ECIS-Messung unmittelbar nach der Zugabe der Partikel detektiert werden. Im Vergleich zu den statischen Zellkulturen reagierten die dynamischen Kulturen empfindlicher auf die ZnO-Nanopartikel. Die kritische Nanopartikel-Konzentration wird demnach von den Kultivierungsbedingungen bestimmt. Im Gegensatz zu den ZnO-Nanopartikeln beeinflussten die TiO_2-Nanopartikel weder in der statischen noch in der dynamischen Kultur die Viabilität der Zellen. Die Orientierung der NIH-3T3-Zellen in Fließrichtung wurde nach TiO_2-Nanopartikel-Exposition jedoch nicht beobachtet.

Insgesamt sind statische Kultivierungen nicht ausreichend, um die Effekte der Nanopartikel auf die Zellen zu detektieren. Mit dynamischen Kultivierungsbedingungen kann die physiologische Zellumgebung besser simuliert und es können relevantere Ergebnisse als mit statischen Kultivierungsbedingungen erzielt werden. Des Weiteren kann mit den dynamischen *in-vitro*-Experimenten ein grundlegendes Verständnis der Zell-Nanopartikel-Interaktion gewonnen werden, das mit komplexen Tierexperimenten teilweise nicht erreicht werden kann. Außerdem könnte der Einsatz von Tierversuchen minimiert werden. Zukünftig könnte die Kombination von dynamischen Kultivierungsbedingungen und 3D-Zellwachstum die Langzeittestung ermöglichen. Die dynamische Kultivierung wird daher im *Complex-Screening* angewendet.

6.2 *In Vitro* Toxicological Nanoparticle Studies under Flow Exposure

Franziska Sambale[1*], Frank Stahl[1], Detlef Bahnemann[1,2], Thomas Scheper[1]

[1] Gottfried Wilhelm Leibniz University Hanover, Institute for Technical Chemistry, Callinstr. 5, 30167 Hanover, Germany
[2] Laboratory "Photoactive Nanocomposite Materials", Saint-Petersburg State University, Ulyanovskaya Str. 1, Peterhof, Saint-Petersburg, 198504 Russia

*Corresponding author: Franziska Sambale, Email: sambale@iftc.uni-hannover.de, Telephone: +49 511 762 2966, Fax: +49 511 762 3004

Reprinted from *Journal of Nanoparticle Research* (2015)17:298:p. 1-12, DOI 10.1007/s11051-015-3106-2 with kind permission from Springer.

6.2.1 Abstract

The use of nanoparticles is becoming increasingly common in industry and everyday objects. Thus, extensive risk management concerning the potential health risk of nanoparticles is important. Currently, *in vitro* nanoparticle testing is mainly performed under static culture conditions without any shear stress. However, shear stress is an important biomechanical parameter. Therefore, in this study a defined physiological flow to different mammalian cell lines such as A549 cells and NIH-3T3 cells has been applied. The effects of zinc oxide and titanium dioxide nanoparticles, respectively, were investigated under both static and dynamic conditions. Cell viability, cell morphology, and adhesion were proven and compared to the static cell culture. Flow exposure had an impact on the cellular morphology of the cells. NIH-3T3 cells were elongated in the direction of flow and A549 cells exhibited vesicles inside the cells. Zinc oxide nanoparticles reduced the cell viability in the static and in the dynamic culture; however, the dynamic cultures were more sensitive. In the static culture and in the dynamic culture titanium dioxide nanoparticles did not affect cell viability. In conclusion, dynamic culture conditions are important for further *in vitro* investigations and provide more relevant results than static culture conditions.

Keywords: Mammalian cells, zinc oxide nanoparticles, titanium dioxide nanoparticles, physiological flow, shear stress

6.2.2 Introduction

Since the use of nanotechnology is constantly increasing across diverse applications, nanoparticle safety characterization becomes more and more important. Currently, many everyday products such as sprays include nanoparticles that could be absorbed by the respiratory system [336]. A toxicological assessment of all chemicals is required according to the REACH (Regulation, Evaluation, Authorization, Restriction of Chemicals, 1907/2006) regulation [336]. However, animal studies are limited to a low number of assessments and are; time consuming, costly, and ethically controversial [336]. In addition, commonly applied two dimensional *in vitro* investigations for drug or nanoparticle screening [337] cannot reflect the complexity of the human organism [336]. Thus, recently alternative screening strategies have been developed to achieve an improved mimicking of the *in vivo* environment in *in vitro* experiments.

Three dimensional (3D) cell cultures provide more relevant cell environments for cell growth and cell-cell interactions compared to the two dimensional (2D) monolayer cell cultures. Secondly, nanoparticles inhaled or absorbed from consumer products could reach the vascular system and the bloodstream [338]. The simulation of physiological flow is important and increases the comparability with *in vivo* conditions for nanoparticle risk management, but also for *in vitro* drug studies [178, 259]. Especially, the physiological flow plays an important role in nano-medicine, because nano-carrier binding, transport [179, 182], and drug delivery in the human body [177, 181, 259] can be affected. Moreover, receptor-nanoparticle binding [182, 339], stability of liver specific drugs [340], and drug safety [178] should first be tested in *in vitro* perfusion systems. The complexity of the organism may sometimes hinder an exact quantification of the particle delivery in animal studies [182].

Another advantage of dynamic test conditions is the superior distribution of nutrients, waste products, and test substances within the cell culture [337, 341]. Under static culture conditions accumulation of toxic waste products can cause oxidative stress [259]. Moreover, in static cell culture experiments the sedimentation of nanoparticles has been reported [341], resulting in a local increase of the nanoparticle concentrations [337]. Homogenous dispersion of nanoparticles and prevention of sedimentation are advantages of flow exposure conditions [337]. In addition, nanoparticle dispersion under physiological flow may affect the cell-nanoparticle-interaction and the nanoparticle uptake via the cells. Differences of the exocytosis and the endocytosis rate of nanoparticles by cells have been observed upon perfusion [335]. In addition to the nanoparticle distribution the effect of the physiological flow on the cell response is important. Many cell types such as lung epithelial cells, vascular cells, and endothelial cells are permanently exposed to continued flow or mechanical stimuli under physiological conditions in the human organism [259, 335]. The mechanical stress caused by blood circulation or by the vascular system cannot be induced in the static 2D cell cultures [259, 341]. However, various studies have demonstrated that, in particular, endothelial cells are highly affected by flow exposure [342]. Physiological flow can affect the cellular behavior [234, 259] as well as the cell-cell interactions [342]. Shear stress leads to cell morphology modification [259, 343, 344], cell adhesion changes [342] as well as membrane disruption and stiffness [342]. Moreover, impacts of mechanical stimuli on cell function [343, 344], cell metabolism [343], and protein expression [342, 344] have been reported.

Since dynamic cell conditions significantly impact the cellular response as well as the nanoparticle or drug distribution, *in vitro* nanoparticle studies under flow exposure provide more relevant predictions for an *in vivo* cell response [177, 180, 259, 337, 338]. Therefore, a mechanical stress methodology for nanoparticle risk management and future drug development is needed [179] in order to minimize animal studies [178]. As so far only a few nanoparticle cytotoxicity studies under perfusion have been performed, the focus of the present study was the comparison of nanoparticle exposure under dynamic and under static conditions. Therefore, the effects of two widely applied types of nanoparticles were studied. Titanium dioxide (TiO_2-NP) and zinc oxide nanoparticles (ZnO-NP) were investigated to

provide better insights into the cytotoxic effects of nanoparticles. Both nanoparticles find applications in cosmetics, sunscreens or paints [16]. Previously, the cytotoxic effects of these two types of nanoparticles have been investigated under static culture conditions revealing toxic effects for ZnO-NP (significant effect at 3-70 µg/ml) [219-221] but not for TiO_2-NP (100 µg/ml) [222, 223]. The present study concentrates on the main absorption routes of nanoparticles into the human organism, i.e., the effects to lung and to skin cells have been modeled. Therefore, A549 cells (human alveolar basal epithelial cells) and NIH-3T3 cells (fibroblasts) were selected. Lung cells in their physiological environment are especially exposed to mechanical stress via breathing and blood circulation. Recently, A549 cells were cultured under perfused conditions using the Cultex® Radial Flow System [336]. In the present study, differences in the metabolic activity of the cells were obtained by the adenosine triphosphate (ATP) assay. Moreover, the cell morphology after flow exposure and nanoparticle addition was investigated. In addition, electric cell-substrate impedance sensing (ECIS) was applied to monitor the online cytotoxic effects under flow conditions, especially its impact on the cell adhesion.

6.2.3 Material and Methods

6.2.3.1 Cell culture

In this study A549 human lung carcinoma cells (DSMZ no.: ACC 107) and NIH-3T3 mouse fibroblasts cells (DMSZ no.: ACC 59) were used. Both cell lines were purchased from the German Collection of Microorganisms and cell cultures (DSMZ). Cells were cultivated in Dulbecco's Modified Eagle's Medium (DMEM) (D7777 Sigma-Aldrich, Steinheim, Germany) supplemented with 10% fetal calf serum (FCS) and 100 µg/ml antibiotics (penicillin/streptomycin) in a humidified environment at 37°C/ 5% CO_2. When the cultures reached 70-80% confluence the cells were sub-cultivated approximately every three days. All used cells obtained a passage number less than 20.

6.2.3.2 Nanoparticles

The TiO_2-NP (Hombikat XXS 700) were kindly provided by Sachtleben GmbH, Duisburg, Germany. Their primary particle size was 7 nm (scanning electron microscopy) in the anatase form according to the data sheet. The hydrodynamic diameter of TiO_2-NP in water was 79 ± 25 nm, 142 ± 29 nm in DMEM and 118 ± 28 nm in the culture medium (mean ± standard derivation) determined with dynamic light scattering [345]. The PDI value of TiO_2-NP in water was 0.156 ± 0.013 nm, 0.650 ± 0.052 nm in DMEM and 0.605 ± 0.052 nm in the culture medium. Bloh et al. (2012, 2014) synthesized and characterized the hexagonal ZnO-NP (with 0.1% Ruthenium) used in this study [226, 227]. They reported a BET surface of 6.54 m^2/g and a particle size of 50 ± 10 nm (X-ray) [226]. In addition, the hydrodynamic diameter of ZnO-NP was 41 ± 5 nm in water, 190 ± 3 nm in DMEM and 106 ± 11 nm in the standard culture medium (mean ± standard derivation) [345]. The PDI value of ZnO-NP in water was 0.153 ± 0.007 nm, 0.617 ± 0.081 nm in DMEM and 0.552 ± 0.118 nm in the culture medium.

6.2.3.3 Nanoparticle Testing

Initially, 100,000 cells/channel were seeded in microchannels with a growth area of 0.6 cm² and a channel height of 0.4 mm (µ-Slide VI$^{0.4}$, tissue culture treated, Ibidi GmbH, Munich, Germany). The cells were cultivated in the channel for 24 hours at 37°C/ 5% CO_2 to achieve a confluent cell layer before dynamic cultivation. Afterwards, the medium was removed and fresh medium containing different concentrations of ZnO-NP or TiO_2-NP were added for the static experiments. Therefore, the aqueous nanoparticle suspension (10 mg/ml) was diluted with cell culture medium. The cells were exposed to the nanoparticles for 24 hours. For flow exposure experiments each channel of the µ-Slide was connected to tubes and a 5 ml medium reservoir containing various concentrations of nanoparticles. To achieve a final shear stress of 10 dyn/cm², the flow rate was increased stepwise using a peristaltic pump (IDEX Health & Science Ismatec® Reglo ICC). At first, 2 dyn/cm² was applied for one hour, then 5 dyn/cm² for another hour before 10 dyn/cm² was approached for 22 hours.

6.2.3.4 Cell viability Assay

For the determination of the cell viability the adenosine triphosphate (ATP) analysis (CellTiter-Glo® Luminescent Cell Viability Assay, Promega, Madison, USA) were performed according to the manufacturer's protocols. Therefore, the cells were lysed to determine the amount of intracellular ATP. The ATP yield was detected indirectly by a luciferase reaction in the presence of Mg^{2+}, ATP and molecular oxygen (Promega, USA). After 24 hours nanoparticle exposure in the medium was renewed and 50% CellTiter-Glo® solution (50 µl DMEM, 50 µl CellTiter-Glo® stock solution) was added to each channel. For the CTB assay the cells were incubated for 1 hour at 37°C/ 5% CO_2. The cells were shaken for two minutes at 300 rpm. After incubation of the 50% CellTiter-Glo® solutions for 10 minutes the luminescence signal was detected (Perkin Elmer Wallac Victor 2v Multilabel HTS Counter 1420). The signal intensities of the assay correlates with the number of viable cells and metabolically active cells in the culture. The displayed data were taken from at least three experiments. For statistical analysis, the ANOVA one way was performed (ANOVA, one way, OriginPro 8.5.0 SR1). Significant differences were considered when $p<0.05$.

6.2.3.5 Electric Cell-Substrate Impedance Sensing

Electric cell-substrate impedance sensing (ECIS) was carried out using ECIS™ Model 1600R (Applied BioPhysics, USA). Therefore, 200,000 cells/channel of ECIS Flow array with a growth area of 2.5 cm² and a channel height of around 0.35 mm (1E channel µ-Slide with 8 x 1 electrodes, Applied BioPhysics, USA, comparable to the µ-Slide I$^{0.4}$ Luer) in 200 µl standard culture medium were seeded. Flow exposure was applied when cells had grown to confluence and the impedance signal stayed stable. The shear stress was increased stepwise to 10 dyn/cm² using a peristaltic pump (IDEX Health & Science Ismatec® Reglo ICC). For ZnO-NP exposure, 5 µg/ml was selected for NIH-3T3 cells and 40 µg/ml for A549 cells indicating approximately the half inhibitory concentration. In addition, for TiO_2-NP a concentration of 100 µg/ml was used. The cellular activity was permanently monitored by

measuring the impedance at multiple frequencies and applying an alternating current. Phase contrast microscopy (Olympus IX 50, Olympus Corporation, Tokio, Japan) of the cells grown on the ECIS electrode was performed after flow exposure and after static cultivation.

6.2.4 Results

6.2.4.1 Investigation of Cell Morphology

The morphologies of NIH-3T3 cells and A549 cells cultivated in static or dynamic cell culture conditions are displayed in Fig. 6-1. Besides flow exposure, the cells were treated with ZnO-NP or TiO_2-NP.

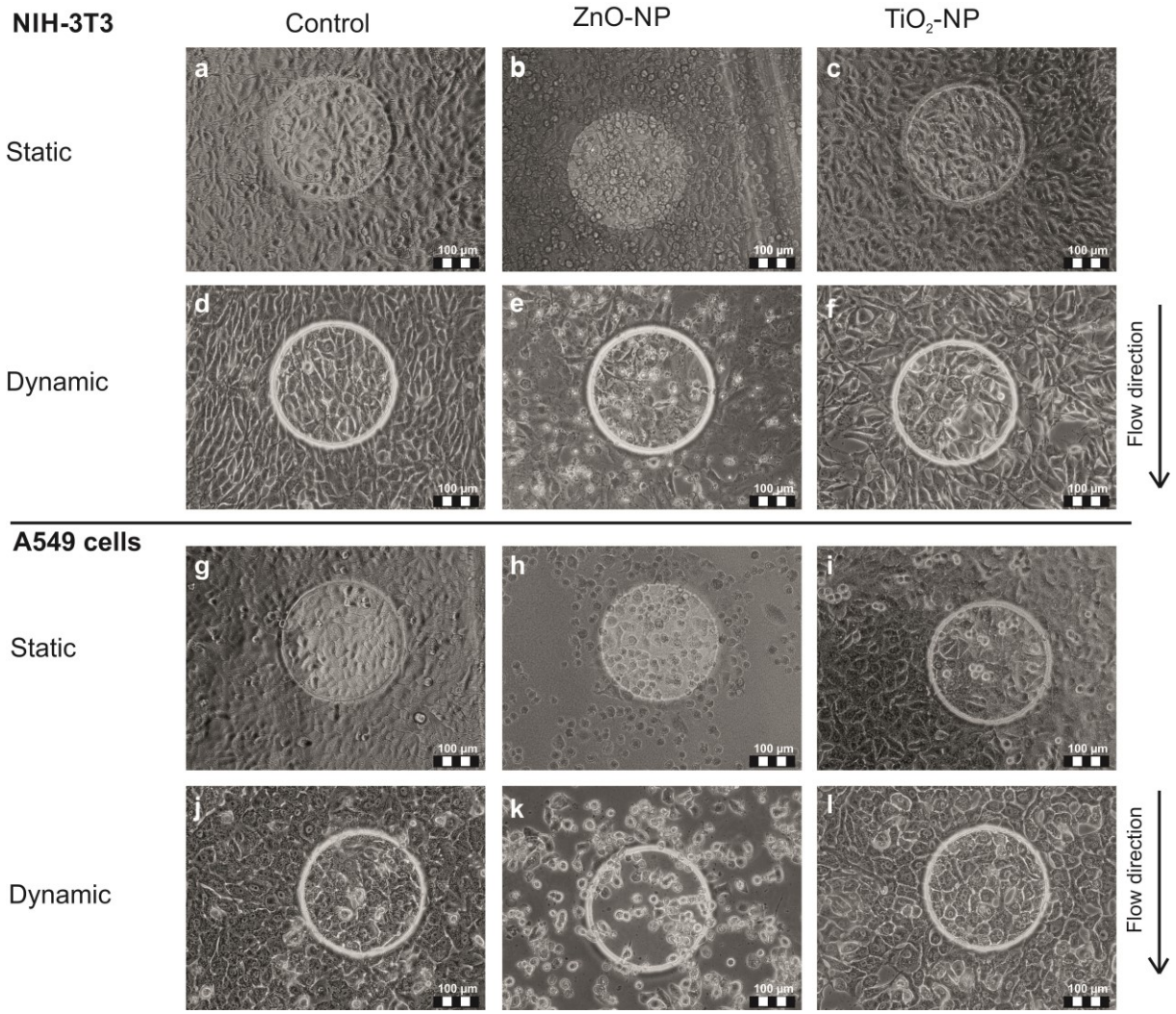

Fig. 6-1 Micrographs of NIH-3T3-cells (a-f) and A549 cells (g-l) on an electric cell-substrate impedance sensing electrode in normal culture medium (a, d, g, j), 48 h after addition of ZnO-NP (b, e, h, k) or TiO_2-NP (c, f, I, l) to the culture medium under static condition (a-c, g-i) and under flow exposure (d-f, j-l). NIH-3T3 cells were exposed to 5 µg/ml and A549 cells to 40 µg/ml ZnO-NP. Both cell lines were exposed to 100 µg/ml TiO_2-NP. The cells under flow exposure were exposed to a shear stress of 10 dyn/cm².

In comparison to the static culture the NIH-3T3 control cells were elongated in the flow direction (Fig. 6-1, d). For A549 cells no significant differences in the cell morphology were observed both under static and under flow conditions (Fig. 6-1 g, j). Under dynamic conditions A549 cells were not

elongated in the flow direction (Fig. 6-1 j). However, small vesicles were detected inside the control cells as well as inside the TiO_2-NP treated cells. ZnO-NP exposure to NIH-3T3 cells and to A549 cells revealed cell rounding and cell detachment. For NIH-3T3 cells 5 µg/ml of ZnO-NP were added to the static and to the dynamic culture. Also, the same initial cell amount was seeded, after ZnO-NP treatment less adhered cells were detected in the dynamic culture in comparison to the static culture (Fig. 6-1 b, e). For A549 cells 40 µg/ml ZnO-NP led to cell shrinkage and cell rounding under both conditions (Fig. 6-1 h, k). TiO_2-NP exposure to A549 cells cultured under perfusion did not result in any morphology changes (Fig. 6-1 l). The NIH-3T3 cells were not straightened in a certain direction after TiO_2-NP exposure and under dynamic conditions (Fig. 6-1 f).

6.2.4.2 Comparison of Static and Dynamic Cell Culture

Initially, the effect of dynamic culture conditions was investigated in the absence of nanoparticles (Fig. 6-2). No significant difference in viability was determined under static or dynamic conditions for both cell lines investigated.

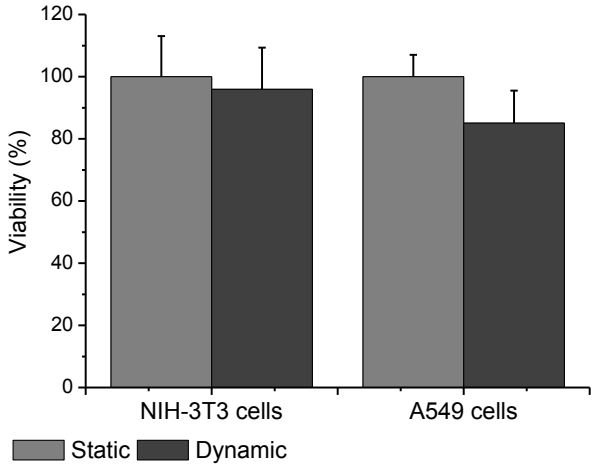

Fig. 6-2 Comparison of the viability of NIH-3T3 cells and A549 cells under static or dynamic culture conditions, determined with the ATP assay. The cells were cultivated in standard culture medium. Data points are means ± standard derivation.

After cell treatment with different concentrations of ZnO-NP or TiO_2-NP, the cell viability was determined using the ATP assay. In Fig. 6-3 the viability results of both cells lines after nanoparticle exposure at different concentrations with and without shear stress are displayed. ZnO-NP reduced the cell viability of A549 cells or NIH-3T3 cells in a dose-dependent manner in static and dynamic conditions (Fig. 6-3 a, c). Both cell lines were found to be more sensitive to ZnO-NP in the dynamic culture as compared with the static culture. In comparison the A549 cells the NIH-3T3 cells were more influenced by the flow exposure. Besides ZnO-NP, the effects of TiO_2-NP exposure under flow conditions were investigated. In the static culture and in the dynamic culture, TiO_2-NP concentrations up to 100 µg/ml did not induce any significant changes in the cell viability, as obtained with the ATP assay (Fig. 6-3 b, d).

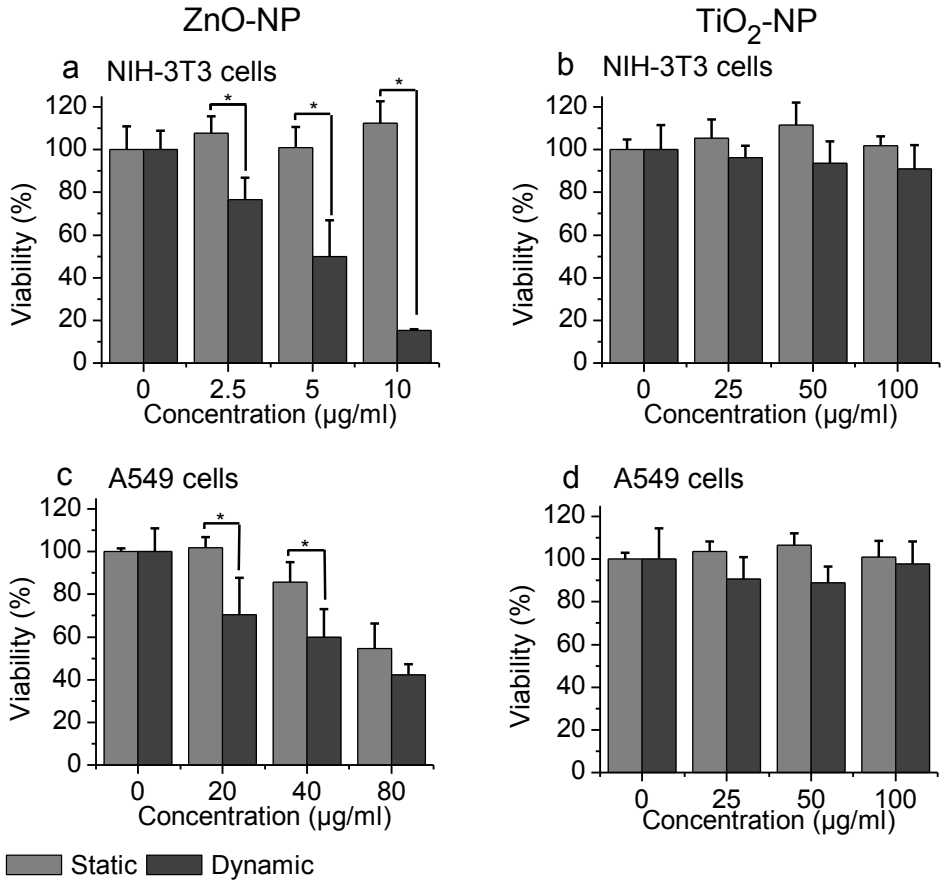

Fig. 6-3 Viability of NIH-3T3 cells (a, b) and A549 cells (c, d) after 24 h ZnO-NP (a, c) or TiO_2-NP (b, d) exposure, determined with the ATP Assay. Cells cultured in standard culture medium were set as 100%. Data points are means ± standard error ($3 \leq n \leq 6$). *p <0.05 ANOVA one way test, static vs. dynamic condition.

6.2.4.3 Impedance Measurements

Appling the ECIS measurements the nanoparticle effects in the cells can be monitored online whereas the ATP assay provides only endpoints data. ECIS measurements under flow exposure were performed with both cell lines and with ZnO-NP as well as with TiO_2-NP (Fig. 6-4). Initially, the cells were grown under static conditions before nanoparticle exposure and shear stress application. The impedance signal of the untreated NIH-3T3 cells stayed constant after flow induction whereas the signal of the A549 cells increased, especially within the first 10 hours. For ZnO-NP 5 µg/ml were applied for NIH-3T3 cells and 40 µg/ml for A549 cells and for TiO_2-NP the highest concentrations used in this study were added. After the ZnO-NP addition, the cells impedance signal was reduced immediately (Fig. 6-4 a, c). TiO_2-NP initially induced an increasing impedance signal in A549 cells (Fig. 6-4 d). For the NIH-3T3 cells the impedance signal stayed constant (Fig. 6-4 b). However, the impedance signal of a cell free control indicated that the nanoparticles themselves did not change he signal [346].

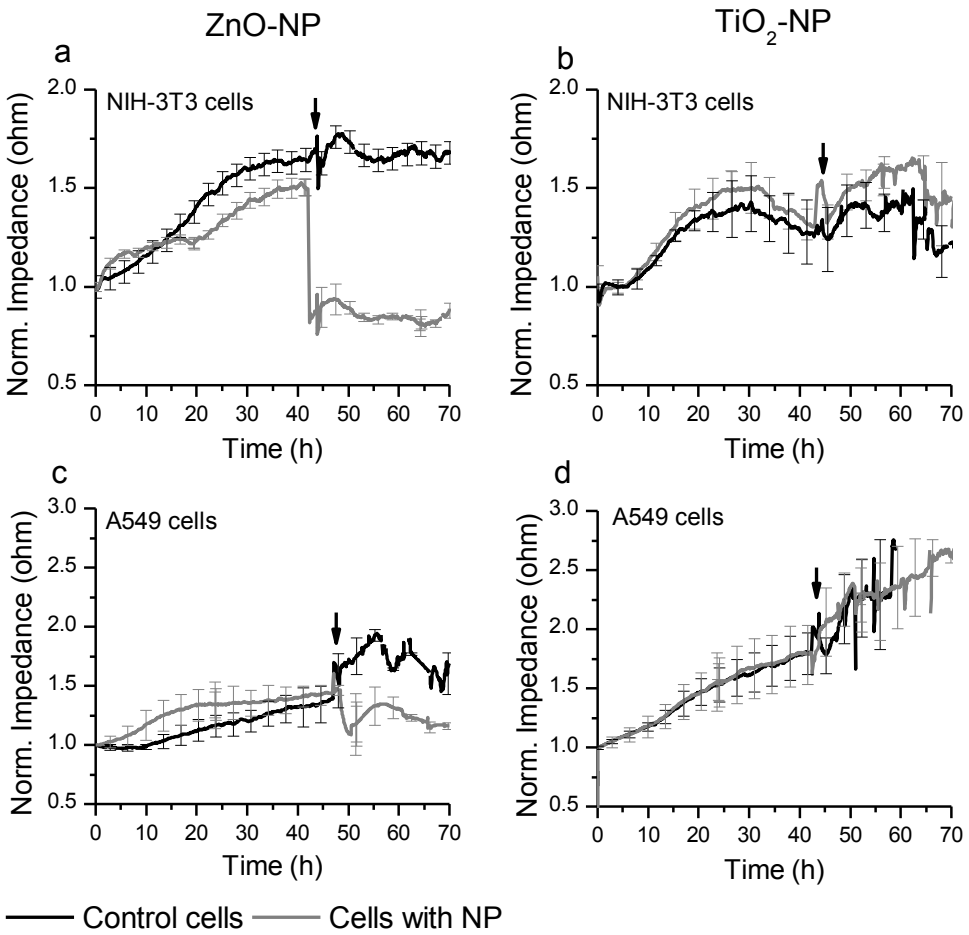

Fig. 6-4 Normalized impedance signal of NIH-3T3 cells (a, b) and A549 cells (c, d) under perfusion and with/without nanoparticle exposure (16 kHz). Before shear stress was applied cells were grown to confluence under static condition. The black arrow indicates the time point where flow exposure and nanoparticle treatment begun. To NIH-3T3 cells 5 µg/ml ZnO-NP suspension and to A549 cells 40 µg/ml was added. For TiO_2-NP a nanoparticle concentration of 100 mg/ml was applied to both cell lines. In addition, a shear stress was applied to cells cultivated in standard medium at the black arrow (control cells). Data points are means ± standard derivation.

6.2.5 Discussion

According to the literature, nanoparticle toxicity is dependent on the nanoparticle material and the nanoparticles' characteristic properties. Decksakulthorn et al. compared the IC_{50} value of ZnO and TiO_2-NP on A549 cells [347]. Both nanoparticles had a particle size of 70 nm. Whereas for ZnO-NP an IC_{50} value of 50 ppm was calculated, a value of 2700 ppm was determined for TiO_2-NP [347]. Thus, in this study, the nanoparticle material is the crucial factor for the nanoparticle toxicity. The higher solubility of ZnO-NP in the culture medium compared to TiO_2-NP could be one reason for the higher cytotoxicity of ZnO-NP [133]. However, the importance of Zn^{2+} ions for ZnO-NP cytotoxicity has been controversially discussed in the literature and needs further investigation [133, 348-350].

Furthermore, Li et al. 2010 investigated the cytotoxic effects of different-sized ZnO-NP on SMCC-7721 cells [351]. In their study, no size-dependent effect was determined for particle sizes in the range of 20-100 nm. However, for smaller ZnO-NP a greater intracellular ROS production for ZnO-NP of 4 nm has been observed by Hanley et al. 2009 than for 20 nm particles [352]. An identical degree of toxicity was revealed for different shaped ZnO-NP [353].

Zhang et al have investigated the impact of different particle sizes on the cytotoxic effect of TiO_2-NP. In general, the cell viability after TiO_2-NP exposure was not altered greatly [354]. However, the characteristic TiO_2-NP structure plays an important role on their toxic effects (Zhang et al. 2012). In their study, 25 nm anatase TiO_2-NP induced a higher toxicity than 5 and 100 nm, whereas 100 nm rutile TiO_2-NP displayed the lowest [354].

Besides the characteristic properties of the nanoparticles, the culture conditions of the *in vitro* experiments play an important role in determining the effects of toxicity. Therefore, in the present study, the influence of culture conditions on the cytotoxicity of nanoparticles was investigated. To provide more relevant results, a physiological flow to the cells has been applied for the nanoparticle toxicity testing in the present study. Depending on the organ and on the tissue in the human organism the shear stress ranges from 0.1-20 dyn/cm² [181, 342, 344]. For instance, *in vivo* cells in the microvascular system are exposed to 4-20 dyn/cm² [342], whereas leukocytes binding to the endothelium occurs at 1-6 dyn/cm² [181]. Recently, in *in vitro* experiments 2-8 dyn/cm² were applied to endothelial cells (HUVEC) [181, 342], 3 dyn/cm² to HeLa cells [339], and 3-9 dyn/cm² to NIH-3T3 cells [355]. Therefore, in the present study a shear stress of 10 dyn/cm² was applied to the cells which is the mean of the shear stress in the organism. In addition, ZnO-NP or TiO_2-NP were added to the cell culture medium. Cell viability, cell morphology, and adhesion were measured and compared to the respective values obtained with static cell cultures.

Comparison of static and dynamic cell cultures

In the present study the effect of dynamic culture conditions to NIH-3T3 cells and A549 cells was analyzed in detail. Since the cell morphology of NIH-3T3 cells significantly changed under flow exposure, the perfusion had an impact on this cell line. The respective micrograph (Fig. 6-1) shows that NIH-3T3 cells cultured in standard medium were elongated along the direction of flow. However, the NIH-3T3 cells are still well connected to their neighboring cells both in static and dynamic culture. On the contrary, no impact on the growth direction of A549 cells was observed. In the static cell culture as well as in the dynamic cell culture the A549 cells obtained the same shape.

Recently, morphology changes have been observed for various cells such as fibroblasts [259, 356], endothelial cells [259, 335, 342], and myofibroblasts [259]. Fibroblasts are effected more strongly by mechanical stimulations than A549 cells (epithelial cells) [356]. For A549 cells no significant differences were obtained after short-term stimulation for 10 minutes whereas within the cell-layer of fibroblasts extended extracellular spaces and cell free zones were apparent [356]. Perfusion or other mechanical stimuli had an impact on the cytoskeleton structure. The actin fiber in HUVEC cells (endothelial cells) was organized in the flow direction and, the cells spread in that direction [335, 342]. However, endothelial cells were still highly connected to their neighboring cells when being stretched [335]. Compared to the stretched HUVEC cells, cells in the static culture were more

quadratic [335]. Investigations on A549 cells under shear stress displayed a higher expression of proto-oncogene c-fos which leads to activation of a signal cascade for matrix remodeling [343].

The cell viability of both cell lines was not effected by flow exposure. Currently, little is known about the influence of shear flow on the viability and proliferation of cells [357]. Hattori et al. observed only slight increase in cell viability of HUVEC cells under shear stress conditions (1-10 dyn/cm²) compared to static culture conditions [358]. One explanation for slightly improved viability could be the washing out of dead cells by the perfused culture medium [358]. In addition, investigations by Freese et al. 2014 demonstrated that stretch conditions did not affect the cell viability of HUVEC cells [335].

In addition to morphology studies and viability, online monitoring of the cellular behavior after flow and nanoparticle exposure using ECIS measurements was performed here. The specific advantage of this method is that the impact on cell adhesion can be measured in real-time instead of at the endpoint. Cell migration, cell growth, morphological changes, and apoptosis can be affected by cell adhesion [344]. For the control cells the impedance signal stayed constant for NIH-3T3 cells indicating that flow exposure did not affect the cell adhesion of these cells. On the contrary, an increased impedance signal for A549 cells was detected after flow exposure. Since this effect was not seen for NIH-3T3 cells, a better nutrients supply and/or removal of waste products in the dynamic culture can be neglected as a suitable explanation for this difference. Moreover, the doubling time of A549 cells is 24 hours, thus the increasing impedance signal cannot be explained with proliferation [240]. Cell migration can also not be an explanation because no significant morphology change was revealed for A549 cells. However, previously with static cell cultures, an increase of the impedance signal was observed as well but only after ZnO-NP addition [240, 346]. This indicates that increasing impedance signals of A549 cells could be either induced by toxic substances or by convection stimuli. In addition, a certain cellular behavior of A549 cells can be considered as an initial stress response. Interestingly, whereas ZnO-NP exposure led to cell shrinkage and cell detachment of A549 cells, such an effect was not determined after flow exposure with standard medium. In general, the cellular stress response depends on external factors and on the cell type [359]. Furthermore, protective or destructive mechanisms can also be induced [359]. Cell shrinking and blistering were found to be indicators of apoptosis [359].

Effects of ZnO-NP on the cells

For ZnO-NP harmful impacts were observed on static cultures as well as on dynamic cultures. Cell shrinkage and cell detachment were induced for both cell lines dose-dependently clearly indicating a cytotoxic effect of ZnO-NP. The Impact of nanoparticles on the cell morphology has been investigated by Mahto et al. (2010) [337]. Cell detachment, cell shrinkage, and the formation of apoptosis structures were noted after the exposure of quantum dots to fibroblasts under flow exposure conditions [337]. These morphology changes were similar to the results presented in a dose-dependent

manner. However, in the static cultures the number of detached cells was higher as compared to the dynamic cultures for NIH-3T3 cells. Furthermore, immediately after ZnO-NP addition and the application of flow exposure the cell impedance decreased for both cell lines. This effect can be explained by cell detachment and cell shrinking. Changes of the cell adhesion can be monitored by impedance measurements. Thus, destroyed binding of adhesion proteins to the cells revealing cell detachment can be detected [355]. Recently, ECIS measurements have been performed to determine nanoparticle toxicity in static cell cultures. Cytotoxic effects of ZnO-NP in static cell cultures have thus been proven with impedance measurements [240, 346].

The A549 cells cultured under flow condition seem to be more sensitive to the stress, since for the control cells the above described initial impedance increase was not observed for ZnO-NP treated A549 cells in the dynamic culture. Thus, the proposed initial stress response could not be observed because the A549 cells were “double stressed”. The comparison of the sensitivity to ZnO-NP demonstrated higher cell viability for the static cell cultures than for the dynamic cultures for both cell lines. Thus, cells exposed to a physiological flow were more sensitive to the ZnO-NP. The perfusion therefore has an impact on the cellular responses. Cytoskeleton remodeling and rearrangement of adhesion proteins occur under shear stress [355].

Previously, the impact of shear stress on the cellular response has been demonstrated in different studies. Endothelial cells exposed to silver nanoparticles under flow conditions in a bioreactor were more sensitive than in a static culture [338]. In addition, toxicity testing of acetaminophen (as a model drug) to liver cells indicated a greater sensitivity of dynamic cell cultures compared to static controls [340]. For silica nanoparticles no significant difference in the cytotoxicity to endothelial cells was observed for 30-nm particles between static and cyclic stretch conditions while for 70-nm particles dynamic cell viability decreased [335]. In stretched HUVEC cells neither Il-8 secretion nor cell lysis were induced in comparison to the control cells indicating that cell stress induction or inflammation did not occur [335].

Furthermore, various studies have reported a lower cellular sensitivity when mechanically stimulated. Flow conditions had an impact on the nanoparticle distribution [181, 337, 341], the binding to cells [182, 335, 339, 341] and the uptake by cells [335, 341]. Fibroblasts (BALS/3T3 fibroblasts) exposed to quantum dots under flow conditions exhibited a higher resistance compared to the static cell culture due to QD settlement in the static culture which increased the local nanoparticle concentration [337]. In addition, gold nanoparticles affected the cell viability in static HUVEC cell cultures but not in the dynamic ones [341]. Large gold nanoparticle aggregates on the cell surface and lower nanoparticle concentration in the medium were obtained in the static cell cultures [341]. In addition, the nanoparticle uptake by HUVEC cells was 10-fold higher compared to the flow conditions [341]. Under stretched conditions the endocytosis rate could decrease and the exocytosis rates might increase [335]. The effect of nanoparticle binding under shear stress exposure is discussed

controversially in the literature. Theoretical models proposed a lower probability of particle adhesion [182], thus, binding of liposomal VHP-conjugated nanoparticles would be reduced with increasing shear stress [181]. However, drug cancer studies employing L-tyrosine polypholsphate nanoparticles targeted with folic acid displayed a 10-fold greater attachment to HeLa cells under flow conditions [339].

Effects of TiO_2-NP on the cells

Investigations of TiO_2-NP with both cell lines in the static cell cultures did not show an effect on the cell viability as determined with the ATP assay. Thus, TiO_2-NP were found to be non-toxic to the cells in static cultures. The cell morphology of A549 cells was not significantly changed after TiO_2-NP exposure; however, inside the cells small vesicles were observed. Recently, the formation of intracellular vesicles after aluminum oxide nanoparticle exposure has been observed in Chinese Hamster Ovary cells (CHO-K1 cells) as well [360]. Therefore, the vesicle formation could be also reveal the nanoparticle uptake [360]. Exposure of TiO_2-NP induced increased impedance signals for A549 cells but not for NIH-3T3 cells. This increase in the impedance signal could be explained by a higher granularity of the cells. Recently, ECIS measurements have been performed for the determination of nanoparticle toxicity in static cell culture. Under static conditions for anatase TiO_2-NP no impact on the impedance signal was revealed [240, 256, 257, 346]. The morphology studies on NIH-3T3 cells revealed that cells exposed to TiO_2-NP under flow conditions were not elongated in the flow direction in comparison to the untreated cells. Presumably, TiO_2-NP are assumed to hinder cytoskeleton remodeling of NIH-3T3 cells under flow conditions. However, the cell viability and the cell impedance was not affected by TiO_2-NP exposure. On the contrary, a toxic effect was revealed for TiO_2-NP treated endothelial cells under flow conditions [338].

6.2.6 Conclusions

Significant differences in the cellular behavior of NIH-3T3 cells and A549 cells under flow exposure have been demonstrated. In addition, the results of nanoparticle *in vitro* studies were affected by physiological flow conditions inducing shear stress. Flow exposure to fibroblasts (NIH-3T3 cells) induced cell structure remodeling and elongation in the flow direction. The cell morphology of A549 cells only changed slightly in comparison to the static culture. Zinc oxide nanoparticles (ZnO-NP) were found to be toxic to the cells inducing dose-dependent cell detachment and decreasing cell viability. In comparison to the static cell cultures the dynamic cultures were more sensitive to ZnO-NP. The critical inhibitory concentration of nanoparticles depends on the culture conditions. On the contrary, titanium dioxide nanoparticles (TiO_2-NP) did not affect cell viability or cell morphology. However, TiO_2-NP presumably hinder the cell remodeling of NIH-3T3 cells under flow exposure. In the A549 cell cultures numerous small vesicles were noted in the control cells as well as in TiO_2-NP treated cells under flow exposure. The different cellular response under flow conditions demonstrates that some effects cannot be observed under static conditions. In addition, the applied flow rates and the

cell lines used in *in vitro* flow exposure studies clearly have an impact on the cytotoxicity of nanoparticles. Dynamic cell cultures can mimic *in vivo* conditions much better, and therefore the role of *in vitro* investigations with flow conditions will be increasingly important in the future. Long-term toxicity screening can be especially enhanced employing dynamic cell cultures rather than static models.

Acknowledgments

This work was supported by the European Regional Development Fund (EFRE Project "Nanokomp", grant number: 60421066). Detlef Bahnemann kindly acknowledges support by the project "Establishment of the Laboratory of Photoactive Nanocomposites Materials" (No. 14.750.31.0016) supported by a Grant from the Government of the Russian Federation.

Conflict of interest The authors declare that they have no conflict of interest.

7 Anwendung des *Screening-Systems* für die Entwicklung von nanopartikulären Schichten

7.1 Zusammenfassung

In diesem Kapitel wird die prozessbegleitende Anwendung des *Screening*-Systems für die Entwicklung von Nanokompositen beschrieben. Insbesondere nanopartikuläre Beschichtungen haben in den letzten Jahren an Bedeutung gewonnen. Durch den Einsatz von Nanopartikeln sollen z.B. superhydrophobe oder selbstreinigende Oberflächen kreiert werden. Diese könnten bei Sanitäranlagen angewendet werden. Für die Herstellung von Nanokompositen müssen die Strategien für das Dispergieren der Nanopartikel sowie für ihre Formulierung und Charakterisierung aufeinander abgestimmt werden. Neben der Entwicklung von optimierten Oberflächeneigenschaften müssen jedoch auch etwaige Gesundheitsrisiken der Vorläufer und Produkte analysiert werden. Nanopartikel könnten sich von den Oberflächen ablösen und somit z.B. beim Baden mit dem Menschen in Kontakt kommen. Zudem könnten sie über das Abwasser in die Umwelt gelangen. Um das Risiko der Nanopartikel und der daraus hergestellten Nanokomposite beurteilen zu können, sollten nicht nur die Endprodukte sondern auch deren Vorläufer toxikologisch untersucht werden. Auf diese Weise können zum einen die erforderlichen Schutzmaßnahmen für die Mitarbeiter festgelegt werden. Zum anderen können bei bedenklichen Zwischenprodukten frühzeitig alternative Strategien entwickelt werden, so dass letztendlich Herstellungskosten reduziert werden könnten.

Mit dem entwickelten *Screening*-System, beschrieben in Kapitel 3, wird die prozessbegleitende toxikologische Analyse der Nanokomposite für die Anwendung im Sanitärbereich möglich. Somit können etwaige Risiken der Vorstufen der Nanoprodukte überprüft werden. Verschiedene Parameter wie Nanopartikel-Größe und -Konzentration in den Nanokompositen wurden variiert, mit dem Ziel gute mechanische Eigenschaften sowie einen hydrophoben *Easy-to-Clean*-Effekt zu erzeugen. Schmutz und Kalk sollen an den Oberflächen schlecht anhaften. Für die Herstellung der Nanokomposite wurden Aluminiumoxid (Al_2O_3)-Nanopartikel zunächst im Lösungsmittel dispergiert. Die Dispersion wurde anschließend für verschiedene Vinylester/Polyester-Harz-Formulierungen verwendet, aus denen die Beschichtungen hergestellt wurden. Charakteristische Eigenschaften wie die Benetzbarkeit, Härte und Toxizität wurden untersucht. Die Zytotoxizität der eingesetzten Al_2O_3-Nanopartikel wurde in wässriger Suspension und in der Formulierung analysiert. Die Nanokomposite wurden auf deren Stabilität überprüft, indem Extrakte entsprechend der ISO-Norm 10993-12: 2012 für medizinische Geräte gewonnen wurden. Der Einfluss der Nanopartikel-Suspensionen sowie der Extrakte auf die Zellviabilität von A549-Zellen (Lungenepithelzellen) sowie HepG2-Zellen (Leberkarzinomzellen) wurde untersucht.

Mit dem eingesetzten Dispergierverfahren konnten Suspensionen mit unterschiedlichen Partikelgrößen-Verteilungen und -Konzentrationen hergestellt werden. Dabei konnten Abhängigkeiten zwischen den ermittelten Eigenschaften der Nanopartikel-Formulierung und den späteren Beschichtungseigenschaften identifiziert werden. Kleinere Partikelgrößen (105-130 nm) und Feststoffgehalte von 4-5 % in den Nanokompositen führten zu höheren Kontaktwinkeln. Je höher der Kontaktwinkel, desto hydrophober ist die Oberfläche und desto besser ist deren selbstreinigende Eigenschaft. Die toxikologischen Untersuchungen zeigten, dass Al_2O_3-Nanopartikeln im Zellkulturmedium keinen Einfluss auf die Viabilität der A549- und HepG2-Zellen hatten. Für die Nanokomposite wurde eine relativ geringe zytotoxische Wirkung beobachtet, die von Partikelgröße und Feststoffgehalt abhing. Die ermittelten optimalen Partikelgrößen und Feststoffgehalte, mit denen hydrophobe Eigenschaften erzielt werden, wurden mit den toxikologischen Untersuchungen bestätigt. Als besonders stabile Nanokomposite erwiesen sich Formulierungen mit einem Feststoffgehalt von 4 %. Nanokomposite mit Partikelgrößen von 120 nm oder 130 nm zeigten zudem im Gegensatz zu 200 nm großen Partikeln keine Wirkung auf die Zellviabilität. Des Weiteren wurde keine Abhängigkeit zwischen der Rauheit und dem Kontaktwinkel der Beschichtungen festgestellt. Dahingegen wurde eine Korrelation zwischen Zellviabilität und Oberflächenrauheit ermittelt. Um zusätzlich die Härte der Formulierung zu verbessern, ist der Styrolgehalt in der Grund-Harzformulierung zu reduzieren. Analog verringerte sich die Zellviabilität mit steigender Stryolkonzentration in der Formulierung, da das Styrol eine toxische Wirkung aufweist.

Das *Pre-Screening* des entwickelten *Screening*-Systems zur Untersuchung von Nanokompositen im Sanitärbereich konnte erfolgreich angewendet werden. Durch Charakterisierung der Nanokomposite wurden Partikelgröße und Feststoffgehalt bezüglich der Beschichtungseigenschaften optimiert. Bereits in der früheren Prozessphase konnten diese Nanokomposite mit den optimierten Parametern auf deren toxikologische Wirkung untersucht werden. Die weitere Produktentwicklung wird demnach nach derzeitigem *Screening*-Stand aus toxikologischer Sicht empfohlen.

Bemerkung

Das nachfolgende Manuskript wird eingereicht. Die Arbeiten erfolgten im Rahmen des Forschungsvorhabens „Nanokomp“. Das Dispergieren der Nanopartikel sowie die Herstellung und Charakterisierung der Nanokomposite wurden von Frau Jutta Hesselbach, Institut für Partikeltechnik, Technische Universität Braunschweig durchgeführt (Fig. 7-1, Fig. 7-2, Fig. 7-3, Fig. 7-4, Fig. 7-5, Fig. 7-6, Fig. 7-7, Fig. 7-11 a). Im Rahmen der Dissertation wurden prozessbegleitend die Zwischenprodukte auf deren toxikologische Wirkung analysiert.

7.2 Surface and Mechanical Properties of Nanoparticulate Resin Coatings and their Toxicological Characterization

Franziska Sambale[1] and Jutta Hesselbach[2], Benedikt Finke[2], Carsten Schilde[2], Frank Stahl[1], Detlef Bahnemann[1], Thomas Scheper[1], Arno Kwade[2]

[1] Gottfried Wilhelm Leibniz Universität Hannover, Institute for Technical Chemistry, Callinstr. 5, 30167 Hanover, Germany
[2] Technische Chemie Braunschweig, Institute for Particle Technology, Volkmaroder Str. 5, 38104 Braunschweig, Germany

Submitted to Journal of Nanoparticle Research on 19th of August 2015.

7.2.1 Abstract

In this study a process chain to produce and characterize nanoparticulates, hydrophobic resin coatings were investigated for sanitary applications. Because nanocomposites might have a potential risk to the human organism and the environment, not only the manufacturing process but also the achievable product properties were examined. Also, toxicological investigations in regards to the used nanoparticle sizes and solids contents were carried out by investigating the impact of aluminum oxide nanoparticles on lung cells (A549 cells) and liver cells (HepG2 cells). Results included showed that by using modified alumina the product properties could be improved and that alumina particles were non-toxic. However, cell viability was slightly affected by the nanocomposite extracts depending on the applied particle size and concentration in the nanocomposites.

Keywords: Nanocomposite coating, nanoparticles, Biocompatibility, mammalian cell lines, nanotoxicology

7.2.2 Introduction

Currently, nanoparticles improve the properties of diverse products and find applications in medicine textile industry [6], cosmetics [5], food [4], agricultural sectors [4], military [112], and other industrial areas [112]. In particular, the processing of nanoparticulate coatings has gained importance in recent years [361, 362]. The particles are used to improve the surface concerning targeted properties, e.g. to achieve superhydrophobic or self-cleaning coatings [363, 364]. However, concerns have been raised regarding the impact of nanoparticles on the environment and the human body. Nanoparticles can be released in the wastewater of industry or washing machines, reach the ground water and accumulate in the environment [365]. In addition, seawater is exposed to titanium dioxide nanoparticles applied in sunscreens of tourists [1]. For the next years an exponential increase in the nanoparticle concentration in the sediments, sludge and soil in the environment is anticipated [366]. Because the permanent exposure of nanomaterials to the environment is known, investigations of the interaction of nanoparticles, organism, and biological compounds are very important. Therefore, *in vivo* and *in vitro* toxicological studies are needed to identify the risk for human health and the environment.

The application of nanocomposites in sanitary facilities requires carful risk management. Nanoparticles could be solved from the facility surfaces and could be absorbed by the human body

and/or reach the environment by the wastewater. Moreover, the entire process chain for producing such products presents a substantial risk of injury to human health. Thus, in the present study, the whole process chain was investigated to produce and characterize nanoparticulate composite coatings for applications in sanitary area. The main targets of this work has been to generate a surface with sufficient mechanical properties and a hydrophobic easy-to-clean-effect so that dirt and lime do not adhere strongly and can be easily removed from the surface [367]. Furthermore, the cytotoxicity of Al_2O_3-nanoparticles was investigated in this study to ensure the toxicological impact is low. Currently, the effects of Al_2O_3-nanoparticles aggregates on different organisms have been a point of disagreement in the literature. Whereas in most studies no significant impact on the cell metabolism was revealed [1, 2, 4, 19], metabolic stress response has been observed after Al_2O_3-nanoparticle exposure [3, 20, 21].

At first, alumina nanoparticles were dispersed in a solvent to produce a master batch, which should be used for different vinylester /polyester resin formulations. Following this step, the coatings were produced and finally characterized with regard to the formulation parameters. Beside wettability, roughness and hardness, and the toxicological properties were investigated. According to the ISO Standard 10993-12:2012 for medical devices [229] extracts of nanocomposites were prepared and the impacts on different mammalian cells were investigated. Previously, the ISO Standard has been used for *in vitro* biocompatibility testing of various substances like polymers for orthopedic implants [368], silver nanoparticles [369], or hydrophilic polymers [370] for wound dressing, denture materials [371], and bone cement [372]. Since nanoparticles or other toxic compounds could reached the respiratory tract, in the present study the effects on human lung epithelial A549 cells were investigated. In addition, the liver plays an important role in detoxification of incorporated substances, thus, human hepatocellular carcinoma HepG2 cells were also used.

7.2.3 Material and Method

7.2.3.1 Material

Pyrogene alumina was used as nanoparticle material having a primary particle size of 13 nm and a specific surface of 100±15 m^2/g, according to the manufactures data sheet. Two kinds of Al_2O_3-nanoparticles were acquired commercially as a dry powder: one without any modification and a second with an octylsilane modification to have a hydrophobic character. The alumina particles were dispersed in styrene by the addition of stabilizing additives from the Companies Byk Chemie and BÜFA Composite Systems GmbH & Co. KG. For the production of the nanocomposite coatings the previously prepared suspension was combined with a vinyl ester / polyester resin and a peroxide as a curing agent, both acquired from BÜFA Composite Systems GmbH & Co. KG. For the toxicological characterization cell lines A549 human lung carcinoma cells (DSMZ no.: ACC 107) and human hepatocellular carcinoma HepG2 cells (DMSZ no.: ACC 180) were used and purchased from the German Collection of Microorganisms and cell cultures (DSMZ).

7.2.3.2 Dispersing Process

Due to the solvent styrene, the selection of a suitable dispersing machine was limited. For this reason the Al_2O_3-nanoparticles were dispersed with both, an ultrasound sonotrode UW 2200 Sonopuls from Bandelin Electronics and a vertical ball mill. In the latter the particle agglomerates are dispersed by shear and compression stresses by the grinding media. The mill was constructed at the institute for particle technology for dispersing of nanoparticles in demanding media with the aim to manufacture nanocomposite materials. Fig. 7-1 shows the special design of the mill.

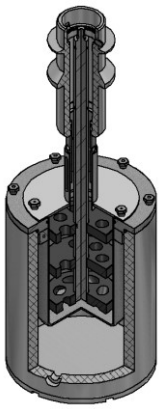

Fig. 7-1 Vertical stirred Media mill

The mill was built as a modification of an existing dissolver (Dispermat AE 03, VMA_Getzmann).The choice of materials (stainless steel and Polyamide 6G) and the double-wall grinding chamber for cooling allow the usage of critical solvents such as styrene. The volume of the grinding chamber, which was used in the present study was V_{GC} =970 ml, so that two out of three perforated disks, consisting of cast polyamide with a diameter of 950 mm were covered by the grinding media and suspension. For the dispersing step, yttrium-stabilized zirconia with a diameter of about 200 µm and 500 µm (SiLibeads, Sigmund Lindner GmbH) as well as alumina (Saint-Gobain) with a diameter of 400 µm were used at a filling ratio of 60 vol%.

The screening of a suitable stabilizer and its concentration was carried out by monitoring sedimentation and agglomeration effects via examination of the transmission and backscattering profiles of a laser beam scanning along the vertical axis of a sample cell (Turbiscan LabExpert from Formulaction) and measuring the particle size (aggregate size) with a diluted sample by dynamic light scattering (Nanophox, company Sympatec GmbH), which was also used for characterization of the dispersing progress. For the particle sizes measurements the samples were diluted with 2- Butanone.

7.2.3.3 Coating and Characterization Methods

Using a doctor blade (ZUA 2000, company Zehntner GmbH) a carrier foil was coated with the resin formulation at a set wet film thickness of 750 µm. After a curing time of about 12 hours at room temperature the coatings were tempered at 80°C for 4 hours without the carrier foil and the surface, which was faced to the foil, was then used to characterize the coating properties. The contact angles were determined by using a drop shape analyzer (DSA 100 from KRÜSS) where a drop with a volume

of 6 µl was generated automatically over the sample and deposited on the coating surface. The contact angle then was evaluated by adapting the drop on a conic section equation. Each drop was measured five times and for one surface the measurements were repeated with in total five drops, so that the result is the mean value of 25 evaluated drops. The roughness was measured *via* confocal laser microscope (VK 9700 from Keyence). To vary the roughness of the surface the coatings were treated by a grinding disc (Knuth Rotor from Struers). Selected samples were treated further by polishing with a diamant suspension (BioDIAMANT Liquid blue from Heraeus Kulzer GmbH). Images of the cross section and dispersed particles were done with a Scanning Electron Microscope (LEO 1550 of company Carl Zeiss) and the amount of alumina on the surface was analyzed by an Energy Dispersive X-ray Spectroscopy (QX 400, company Bruker). Nanoindentation (TI900, company Hysitron, Inc.) was used to characterize the mechanical properties of the coatings. Several mechanical properties of the coatings were investigated via force controlled indentation by a Berkovich-tip. The statistical certainty was ensured by making 40 measurements per sample [373].

7.2.3.4 Toxicological Characterization: Cultivation of the Cells and Testing Method

The cell lines were cultivated in Dulbecco's Modified Eagle's medium (DMEM)(D7777 Sigma-Aldrich, Steinheim, Germany) supplemented with 10% fetal calf serum (FCS) and 100 µg/ml antibiotics (penicillin/streptomycin) in a humidified environment at 37°C/ 5% CO_2. When the cultures reached 70-80% confluence the cells were sub-cultivated every 3 or 4 days. All used cells had a passage number of less than 20.

Nanocomposites extracts were prepared according to the recommendation of the ISO 10993-12:2012 (Biological evaluation of medical devices – Part 12: Sample preparation and reference materials) for toxicological characterization [11]. The coatings with embedded nanoparticles were sterilized by UV light for 30 minutes. Afterwards, 3 cm² /ml standard cell culture medium were added to the nanocomposites and were placed in an incubator at 37°C/ 5% CO_2 for 24 hours at a shaking speed of 160 rpm. Additionally, cell culture medium without any nanocomposites was incubated for 24 hours as well as a reference. Initially, 10.000 A549 cells/well or 15.000 HepG2 cells/well were seeded in 96-well plates (Sarstedt AG) and were cultivated at 37°C/ 5% CO_2 for 24 hours before nanoparticle exposure. The medium was gently removed and fresh medium containing different concentration of an aqueous Al_2O_3-NP suspension or extracts were added. The cells were exposed to the nanomaterial for 24 hours before cell viability was determined.

The cell viability was determined using the CellTiter-Blue® Assay (CellTiter-Blue® Cell Viability Assay, Promega, Madison, USA). The metabolic activity of the cells can be monitored by the reduction of the blue resazurin to purple resorufin via fluorescence measurements. Thereby, the metabolic activity correlates with the amount of viable cells in the cell culture. The assay was performed according to the manufacturer's protocol. The medium was removed and 100 µl of 10% CTB solution (90 µl DMEM, 10 µl CTB stock solution) were added to each well and incubated for

2 hours at 37°C/ 5% CO_2. The fluorescence signals at an extinction wavelength of 544 nm and an emission wavelength of 590 nm were determined using a microplate reader (Fluoroskan Acent, Thermo Fisher Scientific Inc., Waltham, USA). Each measurement was repeated at least three times in triplicates to calculate the standard deviation. The presented data are from at least three independent experiments which were performed in triplicates ($n \geq 3$). The ANOVA (ANalysis Of Variance) one way analysis was performed for statistical analysis (ANOVA, one way, OriginPro 8.5.0 SR1). The p value is used for testing the statistical hypothesis that the means of two populations (treated vs. untreated) are equal [374]. Significant differences between treated and untreated cells were reported at * $p<0.01$ (ANOVA, one way).

7.2.4 Results and Discussion

7.2.4.1 Preparation of the Styrene Based Nanosuspension

Fig. 7-2 (a) below, shows an example for the dispersing process of both ultrasonification and stressing between grinding beads to particle sizes less than 200 nm. Since in most dispersion processes a dispersion limit or a balance between dispersion and reagglomeration exists, a typical relation between median particle size and specific energy input was observed for both devices. This typical dispersion progress is described in literature by several dispersion or grinding kinetics [375, 376]. For dispersing the Al_2O_3-nanoparticles in the vertical stirred media mill the grinding media was varied, regarding size and material. The resultant stress energy transferred by the grinding media to the product particles can be described using a value for the kinetic energy of the grinding media according to the model of Kwade [377-379]. In case of stressing single particles by compression and shear stress between grinding media the stress energy is proportional to the third power of the grinding media diameter, the grinding media density and the second power of the tip speed. In Fig. 7-2 (a) the median particle sizes $x_{50,3}$ are shown as function of the specific energy input [380] for solids contents of 20 wt.%.

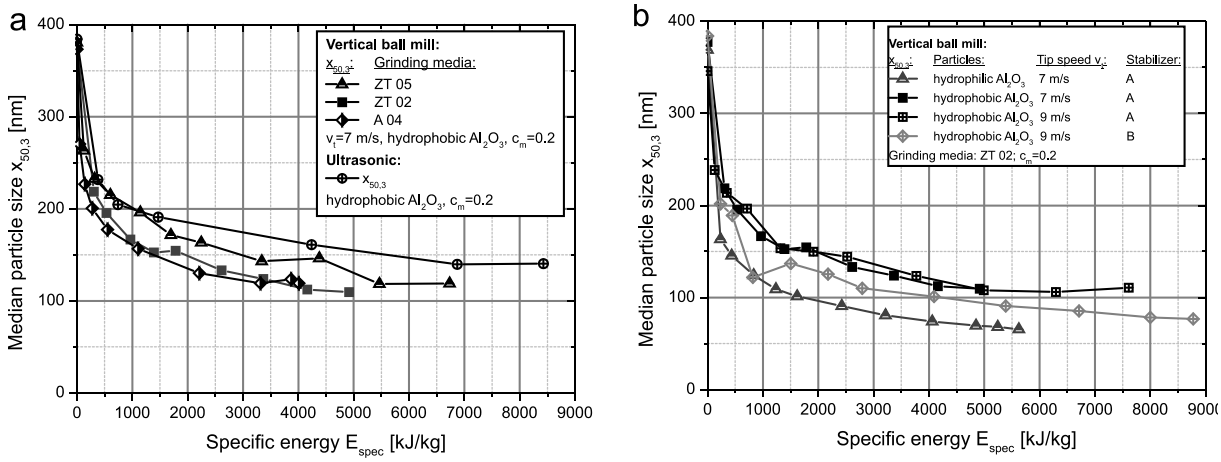

Fig. 7-2 Median particle size $x_{50,3}$ depending on the specific Energy E_{spec} for varying grinding media (a) and modification of the particles (b).

In general, for each particulate product an optimal stress energy exists [376, 377]. Due to the reduced strength of aggregated and agglomerated particles compared to single grains or crystals, this optimum

stress intensity is comparatively low for most dispersion processes [381]. Hence, a decrease in grinding media size and density leads to increasing dispersion efficiency. Moreover, small grinding media diameters lead to higher stress numbers, and thus, to a high dispersion efficiency. To investigate the dispersing process in more detail, unmodified alumina was also dispersed in styrene. As can be seen in Fig.7-2 (b) the highest product fineness could be achieved with the unmodified hydrophilic alumina particles. A reason could be that the interactions between the particles are weaker and therefore easier to overcome or the particles are less stable and reagglomeration takes place. Additionally the stabilizer might link better and/or faster to the particle surface.

In order to enhance the product fineness of the suspensions with the modified alumina to sizes below 100 nm, other stabilizers were investigated. The dispersing experiment was repeated and as it is shown in Fig.7-2 (b) the hydrophobic particles could be dispersed with the suitable stabilizer to sizes below 100 nm, too. In order to reach a higher stress number and shear stress, the solids content has been also increased to 30 wt. % additionally, but the stress energy of the used grinding media (ZT02) has not been sufficient due to viscous dampening of the high suspension viscosity [382]. So, only particle sizes of about 130 nm could be achieved in the master batch with 30 wt. %.

Fig.7-3 shows SEM-pictures of the dispersed particles, dried to a powder (a1 and b1) and processed into coatings (a2 and b2, cross section of the coating). As the result of the different dispersing processes the particles have different morphologies. The particles stressed by grinding media have lost their original fractal morphology obtained from pyrolysis and were compressed into a spherical shape, which has been shown already in [383]. Moreover, the pictures show an acceptable particle distribution in the coating.

In this study the entire process chain was investigated. In the coating step it had to be concluded that the new stabilizer B (see Fig. 7-3, b) was not suitable for the resin system. Even the coatings did not harden and remained liquid after an extended curing time. Due to the insufficient hardening of the coatings with stabilizer B, suspensions with stabilizer A had to be used for the characterization of wettability, mechanical and cytotoxic coating properties shown in the following. Via the dispersing processes, suspensions with different particle size distributions and solids content could be produced and investigated in the subsequent coating process.

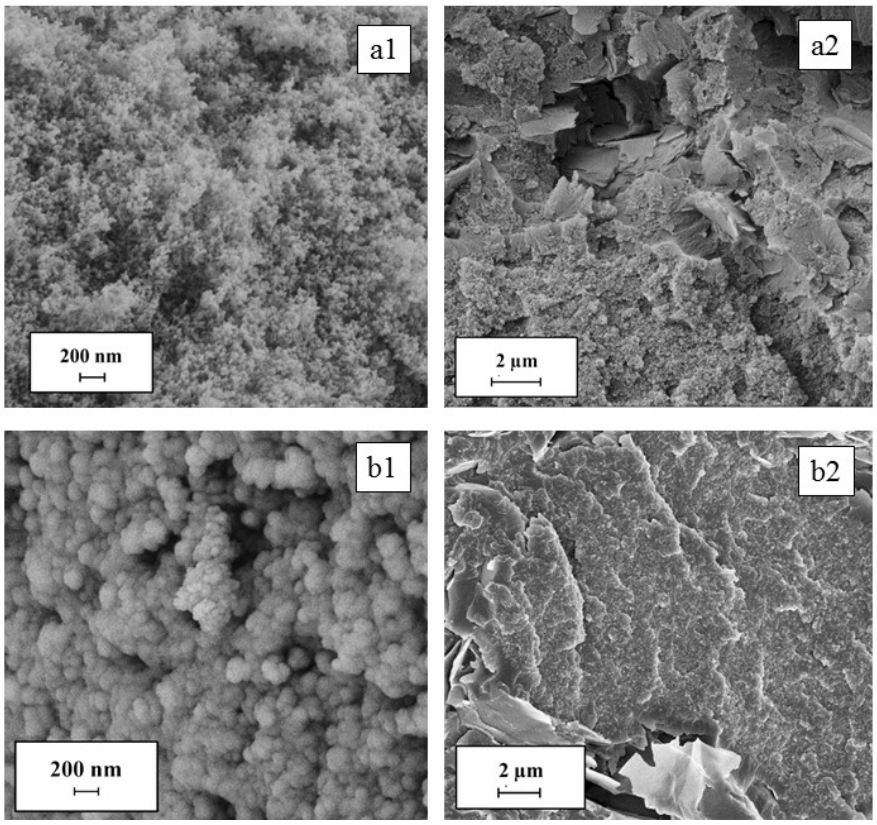

Fig. 7-3 SEM-pictures of the stressed particles by ultrasonic (a1 and a2) and by grinding media (b1 and b2), dried to a powder (a1 and b1) and the cross section of the coating with the processed particles (a2 and b2).

7.2.4.2 Characterization of the Coating Wettability and Mechanical Properties

The produced master batch (chapter 7.2.4.1) was combined with the polyester resin formulation. Apart from the particle sizes, the solids content was varied within the coating formulations. In the following, the coating without nanoparticles is referred as reference and the coating with additional styrene, which resembles the amount of styrene which is approximately added to the coating formulation by using the nanoparticulate master batch, is referred as reference 2, with coating Fig. 7-4 shows the results of the contact angle measurements in dependence of particle sizes (b) and solids content (a).

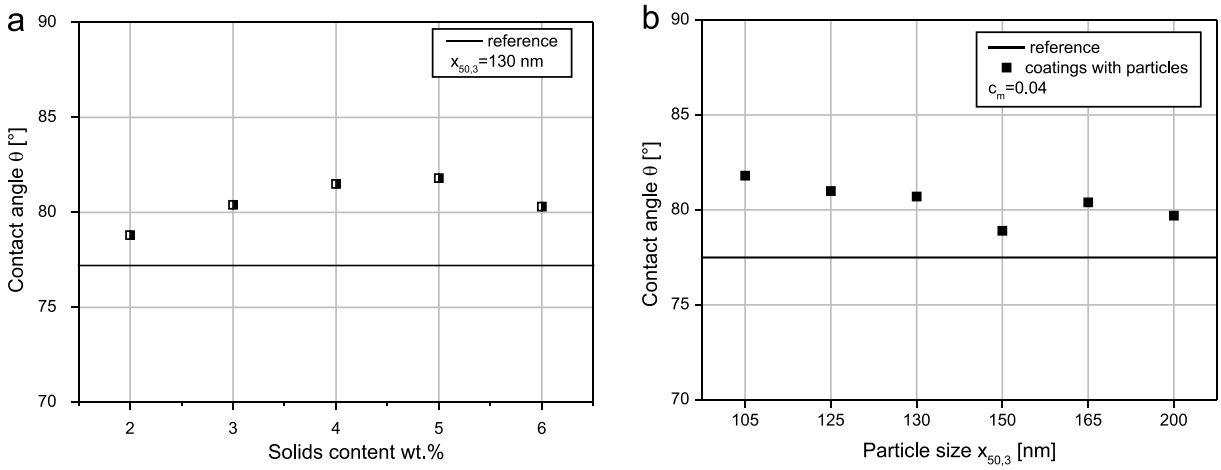

Fig. 7-4 Contact angles depending on the coatings by varying the solids content (a) and the particle sizes (b).

The mean contact angle increases with higher solid content and decreasing particle size. The latter can be explained mainly by the higher specific surface of the particles and thus, higher interactions by the

hydrophobic surface modification. The smaller contact angle of the coating with the content of 6 wt. % compared to 5 wt. % could be a result of a higher formulation viscosity and therefore a more inhomogeneous distribution of the particles within the coating. As described in the literature, the contact angle can be influenced by the surface roughness [384, 385]. For that reason, the measured contact angles are shown in Fig. 7-5 as a function of the surface roughness.

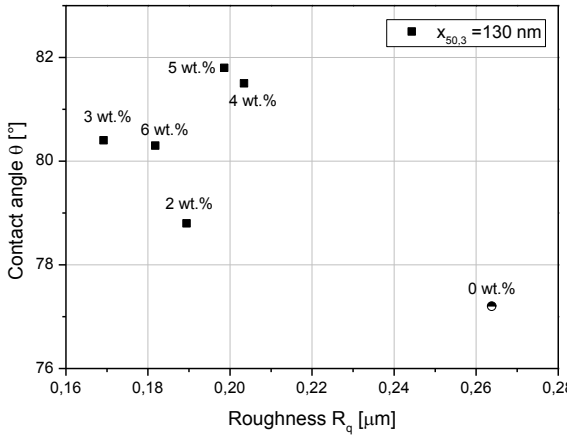

Fig. 7-5 Contact angle as a function of the surface roughness for the different solids contents

The coatings show no clear dependence between the roughness and the contact angle. The reference has a roughness of approximately 0.26 µm, so generally the roughness is reduced by the addition of the particle suspensions by less than 0.1 µm, as Fig. 7-6 proves. But in order to examine it more closely, the coatings were treated by polishing and sharpening the surfaces to achieve various states of roughness on the surface. Afterwards the contact angles were determined and the results are plotted in Fig. 7-6 (a) in dependence on the roughness.

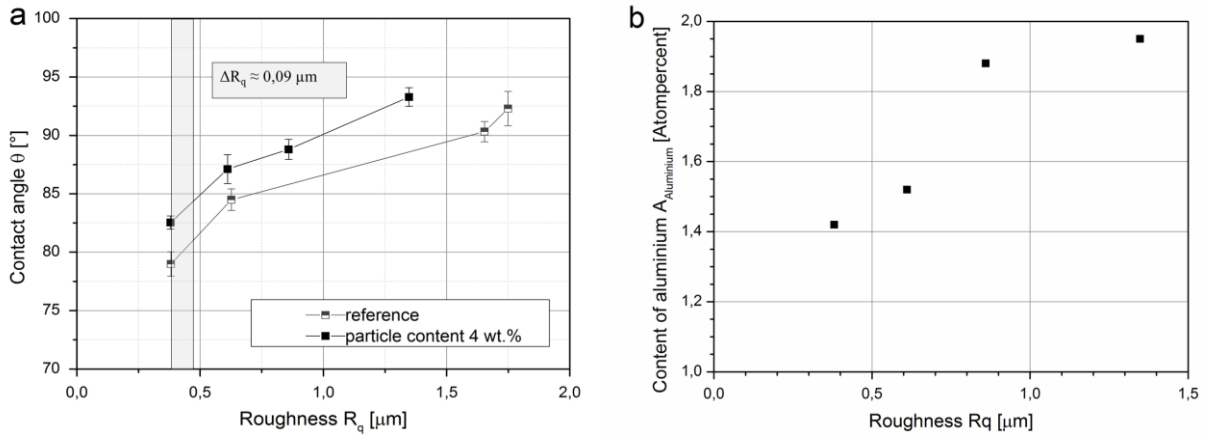

Fig. 7-6 Contact angles of the treated coatings as a function of the roughness (a) and the amount of alumina by EDX (b)

With increasing roughness of the coating surfaces the contact angle increases. Though, the differences in the roughness of the coatings due to the addition of the particles are much smaller than the differences achieved by mechanical surface treatment. It can therefore be concluded that the roughness of the nanoparticulate coatings in this study has no significant influence on the contact angle. It can also be seen in Fig.7-6 (a), that the contact angles of the treated nanoparticulate coatings are much

higher than the reference coatings. The analyses with the EDX shows that there is much more aluminium detected on the surface after surface treatment. This is an important point for the industrial application, because after producing the coatings, the surface will often be treated, too, and if the surface is worn out in the application the effect will more likely increase.

In addition to the wettability, the influence of the particle size and concentration in the coatings on mechanical properties, e.g. hardness, is an important point for application. Fig.7-7 displays the cumulative distribution of the individual hardness measurements for the samples with particle sizes of $x_{50,3}$ = 105 nm and $x_{50,3}$ = 130 nm at a constant particle content of 4 wt.% (a) and different solids contents (b) Moreover, there is the second reference coating (reference 2) with the higher amount of styrene than the reference included in the diagram.

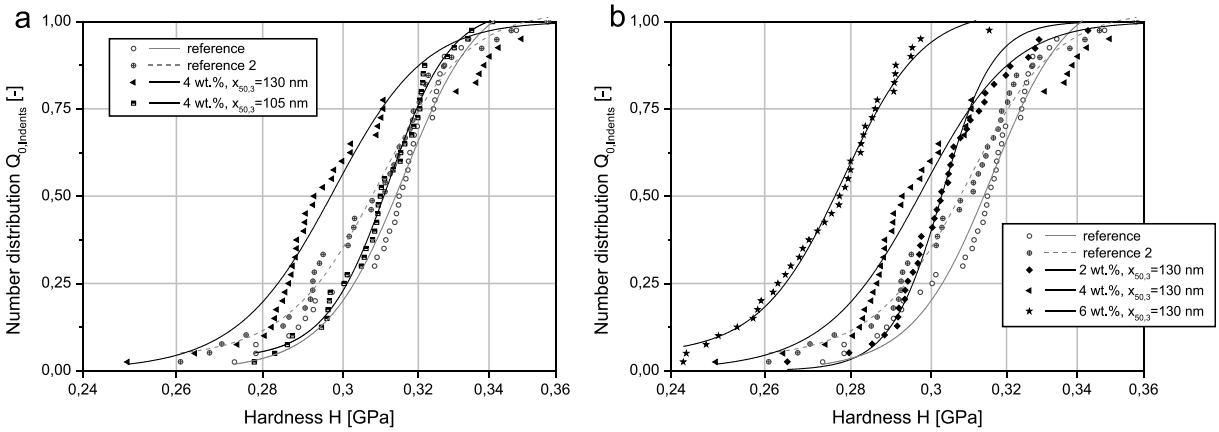

Fig. 7-7 Distribution of the individual indents for the coatings with particle sizes (a) and solids contents (b)

Overall the additional styrene and higher particle content in the coating lead so less-desirable mechanical properties. The latter could be the result of an increasing number of imperfections which induces lower hardness. The use of smaller particles leads to an increase in the hardness and the curve is shifted to higher values. Influences of the particle size and the mechanical properties could be seen in other composites, too [386]. However, the diminished mechanical properties by using a master batch could be reduced by using smaller particles and adapting the basic resin formulation. It may therefore be possible to enhance the coating to produce a higher hardness than the reference and it shows further the importance of a sufficient dispersing and stabilization process to the product properties.

7.2.4.3 Effects of Aluminum Oxide Nanoparticles Suspension on Cell Viability

Firstly, the impact of Al_2O_3-nanoparticle aqueous suspension on the cell viability was investigated. Therefore, Al_2O_3-nanopartcicles were added directly to the standard cell culture medium Fig.7-8 displays the results of the cell viability measurements of A549 cells and HepG2 cells after Al_2O_3-nanoparticles exposure for 24 hours. In both cell lines the cell viability was not affected by Al_2O_3-nanoparticles indicating no cytotoxic effect.

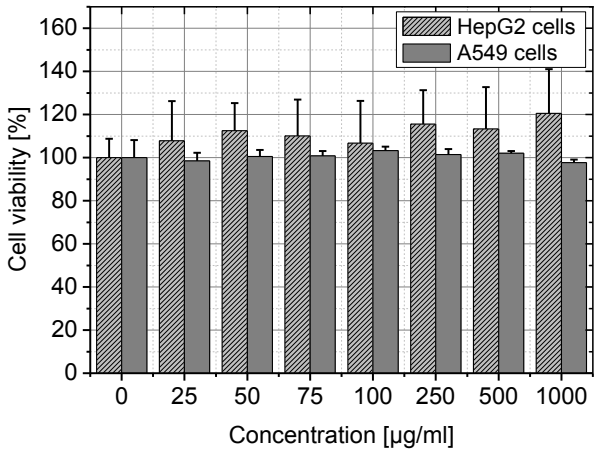

Fig. 7-8 Cell viability of A549 cells and HepG2 cells treated with different concentrations of Al_2O_3-NP in the cell culture media for 24 hours. The fluorescence signal of untreated cells was set as 100% viability. Data points are means ± standard derivation of three independent experiments.

Recently, a very low cytotoxic effect of Al_2O_3-NP has been demonstrated by various groups. The cell viability of L929 and BJ cells were not affected by Al_2O_3-NP in concentrations up to 400 µg/ml and no apoptotic or necrotic cells were detected in the cell culture after exposure [6]. In addition, the Al_2O_3-NP were non-toxic for the cocultures of human aleveloar macrophages U937 cells and A549 cells [112]. Moreover, Al_2O_3-NP showed only low or no toxic effect when exposed to human microvascular endothelial cells [5]. No significant effect on the cell viability, the membrane leakage for lactate dehydrogenase, the generation of reactive oxygen species or the mRNA expression of inflammation markers was detected after 100 µg/ml Al_2O_3-NP 24 hours exposure [5]. Rate alveolar macrophages were not affected by 40 nm- Al_2O_3-NP exposure even at high concentration of 250 µg/ml [290]. However, Al_2O_3-NP can penetrate into the cells in a dose-dependent manner [6], and are entrapped in intracellular vesicles or are located in the cytoplasm [167, 360]. On the contrary, stem cells were more sensitive to Al_2O_3-NP exposure. Oxidative stress responses induced by Al_2O_3-NP and internucleosomal condensation have been observed for human mesenchymal stem cells [4]. The gene expression levels of oxidative stress marker like cytochrome P450 1A and cytochrome P450 reductase were increased in a dose-dependent manner of Al_2O_3-NP [4]. Moreover, a significant decrease of the cell viability was observed for human mesenchymal stem cells at 200 µg/ml (40%) [4], for Chinese Hamster Ovary cells (CHO-K1 cells) at higher concentrations of 25 µg/ml [360], and for A549 cells at 100 µg/ml [167].

7.2.4.4 Influence of Particle Size and Concentration in the Nanocomposite on Cell Viability

In Fig.7-8 the results of the cell viability measurements of A549 and HepG2 cells after exposure with nanocomposite extracts for 24 hours are displayed. The applied concentrations of modified Al_2O_3-NP and particle sizes in the nanocomposite were varied. The concentration of modified Al_2O_3-NP in the nanocomposite had an influence on the cell viability of both investigated cell lines. After both cell lines were exposed with the extracts obtained from the nanocomposite, the cell viability was significantly decreased for 2%, 3%, 5%, and 6% but not for 4% modified Al_2O_3-NP concentration

(Fig.7-9, a). In addition, the particle size of modified Al_2O_3-NP applied in the nanocomposite affected the cell viability of the lung and liver cells Fig.7-9 (b). The extract of nanocomposites containing 200 nm or 150 nm modified Al_2O_3-NP reduced the cell viability significantly (Fig.7-9, b). However, no effect was obtained for the other investigated particle sizes (175 nm, 130 nm and 120 nm) (Fig.7-9, b). Altogether, compared to the toxicity studies with the nanoparticle suspension, exposure of nanocomposite extracts leads to decrease of cell vitality. One explanation could be the content of styrene in the nanocomposites. Depending on nanoparticle solids content in the nanocomposites, the styrene content varies.

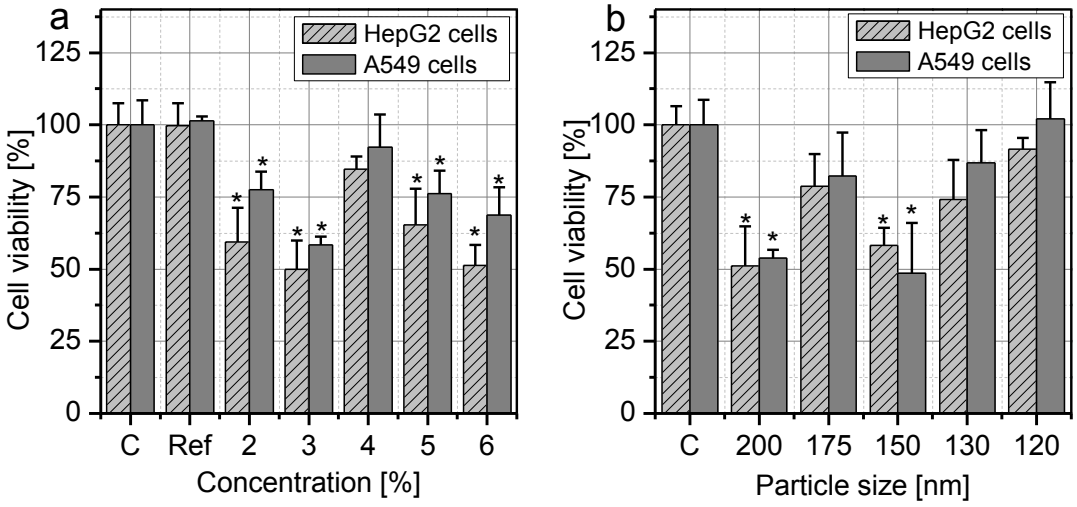

Fig. 7-9 Cell viability of A549 cells and HepG2 cells after exposure of various extracts of nanocomposite for 24 hours. The modified Al_2O_3-NP concentrations (a) and the particle size (b) were varied in the nanocomposites. The fluorescence signal of untreated cells were set as the 100% viability (C). The composite consists of gelcoat and styrene; the sample without nanoparticles is indicated as the reference (Ref). Data points are mean ± standard derivation of three independent experiments. Significant differences versus control group are indicated in the figure (* $p < 0.01$).

7.2.4.5 Correlation of Viability and Surface Roughness

The correlation of surface roughness of nanocomposites and determined cell viability of both cell lines after extract exposure of various nanocomposites were displayed in Fig. 7-10. The impact on cell viability after extract exposure was revealed in dependence of the measured surface roughness of the nanocomposite. Minor roughness of the nanocomposites lead to a decrease of cell viability (Fig.7-10 a, b). This effect was observed for A549 cells as well as for HepG2 cells.

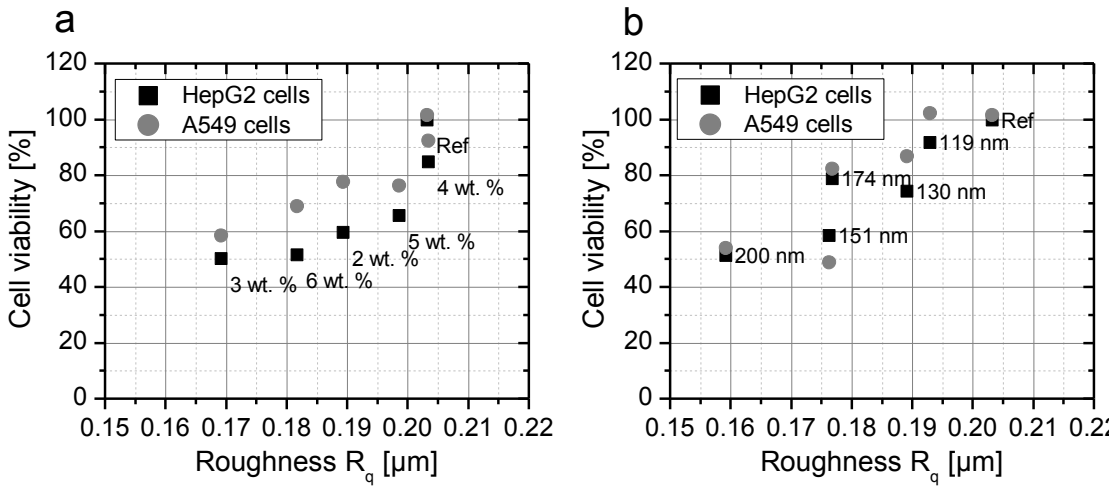

Fig. 7-10 Correlation of surface roughness of nanocomposites and determined cell viability of A549 and HepG2 cells after extract exposure. The Al_2O_3-NP concentration (a) and the particle size (b) were varied in the nanocomposites. The composite consists of gelcoat and styrene but without nanoparticles were indicated as the reference (Ref). Data points are means three independent experiments.

Presumably, the rougher the surface of the nanocomposites the higher the mechanical stability of the nanocomposite. The lowest roughness indicated the lowest viability.

7.2.4.6 Impact of Styrene Concentration in the Nanocomposite on Cell Viability

In addition, the impact of subsequent tempering of the nanocomposite on the cell viability was investigated. Therefore, the period of drying time in the oven after nanocomposite production was varied and extracts were obtained. In dependence on the drying time, the amount of styrene in the coatings varies, so that the coatings which were dried for 240 minutes have the lowest styrene content (Fig.7-11, a). The cell viability of A549 and HepG2 cells was decreased in a time-dependent manner after exposure to the extracts (Fig.7-11, b). Shorter drying times lead to cell death of both cell lines (Fig.7-11, b).

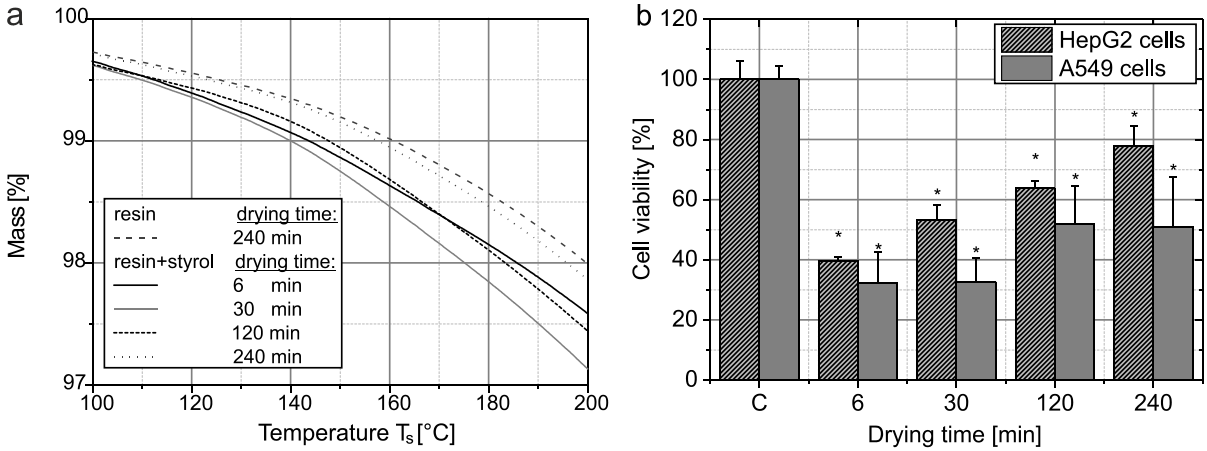

Fig. 7-11 Mass of the nanocomposites depending on the temperature (a) and cell viability of A549 cells and HepG2 cells after extract exposure of different nanocomposites. The final drying time of the nanocomposites in the oven was varied. The fluorescence signal of untreated cells were set as the 100% viability (C). Data points are mean ± standard derivation of three independent experiments. Significant differences versus control group are indicated in the figure (* $p < 0.01$).

The results clearly demonstrated a correlation of the time of subsequent tempering of the nanocomposites and the investigated cell viability. In addition, higher styrene concentrations were determined for shorter period of tempering in the nanocomposites (Fig. 7-11 a). Thus, the cell viability negatively affected by styrene leeched extracted from the nanocomposites. Several studies have investigated the toxic effects of styrene to lung and liver cells in mice [387, 388]. Styrene exposure lead the decrease of the glutathione level indicating oxidative stress [387], and tumor formations in rat and mice [389]. Moreover, in human lung epithelial cells (A549 cells) inflammatory responses and oxidative stress were investigated after styrene exposure [390]. The detailed mode of the action is still unclear, however, the metabolism of styrene to an active styrene oxide has been proposed [387-390].

7.2.5 Conclusion

In this study we have investigated the whole process chain from particle dispersion to coating characterization and could identify correlations between the formulation parameters and the coating properties. Small particle sizes and solids content of about 4-5 wt.% leads to higher contact angles. In addition, if the amount of styrene in the basic resin formulation were reduced it leads to higher hardness.

Furthermore, aluminum oxide nanoparticles (Al_2O_3-NP) in aqueous solutions did not affect the cell viability of the A549 and HepG2 cells. In addition, the toxicological characterization of the nanocomposites identify decrease in cell viability depending on the applied particle size and concentration in the nanocomposites. However, cell viability after extract exposure was not reduced in a dose-dependent manner. Moreover, the decrease in viability was affected by surface roughness. A relatively low cytotoxic effect was investigated for nanocomposites with solid contents of 4% and particle sizes of 175 nm, 130 nm, or 120 nm. The styrene concentration correlates with the period of subsequent tempering of the nanocomposites and reduced the cell viability in a dose-dependent manner.

Acknowledgement

This work was supported by the European Regional Development Fund (EFRE Project “Nanokomp”, grant number: 60421066). The authors would like to thank Uwe Stüwe, Stephanie Michel, Jan Kalina, Sebastian Melzig and Marlene Hülsebrock for the assistance in the experiments.

8 Zusammenfassung und Ausblick

In den letzten Jahren haben Nanopartikel die Eigenschaften von diversen Konsumgütern und Industrieprodukten deutlich verbessert. Doch trotz der vielen positiven Eigenschaften und Anwendungen der Nanotechnologie müssen auch etwaige Risiken der Nanoprodukte für Mensch und Umwelt hinreichend geklärt sowie Regularien für die Anwendung dieser festgelegt werden. Nanopartikel könnten sich über die Konsumgüter oder auch bei industriellen Prozessen in Gewässern und Böden anreichern. Allerdings fehlen derzeit präzise Detektionsmethoden für die Bestimmung der realen Umweltbelastung. Des Weiteren ist das Risiko schwierig abzuschätzen, da es von vielen Faktoren bestimmt wird. Äußere Faktoren wie Scherkräfte, Licht, Hitze oder auch die chemische Zusammensetzung der Lösungen können die Stabilität der Nanopartikel beeinflussen. Zudem ist die Anreicherung in der Nahrungskette, die Wirkung auf komplexe Ökosysteme und deren Diversität entscheidend. Das Gefährdungspotential bei Industriearbeitern, Wissenschaftlern, Konsumenten und Werkstoffarbeitern ist unterschiedlich. Generell können die Nanopartikel dermal, okular, respiratorisch oder gastrointestinal vom menschlichen Organismus aufgenommen werden und sich dort verteilen. Physiologische Barrieren wie Blut-Hirn-Schranke oder Blut-Plazenta-Schranke können dabei überwunden werden.

Für die nationale und internationale Gesetzgebung ist die Klassifizierung und Definition der Nanopartikel von entscheidender Bedeutung. Zukünftig ist zu klären, ob die Definitionsgrenze von 100 nm und die Oberflächengröße von 60 m^2/cm^3 standhält. Die derzeitigen Verordnungen und Richtlinien sind überwiegend nicht speziell auf die Eigenschaften der Nanomaterialien ausgerichtet. Anpassungen in den Regularien müssen zukünftig vorgenommen werden, die die Veränderung der Eigenschaften der Nanomaterialien im Laufe des Lebenszyklus berücksichtigt. Hierfür sind umfangreiche, detaillierte und vor allem standardisierte Untersuchungen der Nanomaterialien notwendig.
Durch die Vielzahl an Nanoprodukten erhöht sich das Kontaktrisiko von verschiedenen Personengruppen mit den Nanopartikeln. Da sich die Eigenschaften und Risiken der Nanoprodukte während Herstellung, Formulierung und Anwendung verändern, sind Vorstufen sowie Endprodukte zu untersuchen. Die Herausforderungen der derzeitigen Nanotoxikologie-Forschung sind Einflussfaktoren wie die Stabilität in physiologischen Medien, die Aggregat- und Agglomerat-Bildung, die Proteinhülle an der Nanopartikel-Oberfläche und die Anlagerung von Endotoxinen. Des Weiteren können Nanopartikel mit *Assay*-Komponenten oder Markermolekülen interagieren sowie eine Eigenfluoreszenz aufweisen. Im Fokus der *in-vitro*-Testung steht zudem die Übertragbarkeit der Ergebnisse auf den Menschen. Es gilt die physiologischen Bedingungen im menschlichen Organismus mit einer realistischen Nanopartikelbelastung möglichst gut zu simulieren.

In der vorliegenden Arbeit wurde ein zellbasiertes, iteratives *Screening*-System entwickelt mit dem die prozessbegleitende toxikologische Analyse von großen Nanopartikelmengen ermöglicht wird. Um dies

zu realisieren ist das *Screening*-System in *Pre-*, *Fine-*, und *Complex-Screening* gegliedert. Zum Aufbau des *Screening*-Systems und der jeweiligen Methoden wurden die beiden *Benchmark*-Nanopartikel Zinkoxid (ZnO)- und Titandioxid (TiO_2)-Nanopartikel eingesetzt und die Wirkungen an den Modellzelllinien A549- und NIH-3T3-Zellen untersucht. Diese beiden Nanopartikel haben exemplarisch das *Screening*-System durchlaufen.

Da viele Nanopartikel im Zellkulturmedium nicht stabil vorliegen, wurden alternative Testverfahren entwickelt. In dem *Screening*-System können die Wirkungen von Partikeln in Suspensionen, Beschichtungen und Kompositen auf verschiedene Zellsysteme analysiert werden. Hierbei kann das Zellwachstum auf beschichteten Oberflächen sowie die Wirkung von herausgelösten Nanopartikeln bestimmt werden. Außerdem wurden diverse Toxizitätstests zur Bestimmung der Stoffwechselaktivitäten im System integriert. Die Sensitivität der Methoden und die Komplexität der Zellsysteme erhöhen sich innerhalb des *Screening*-Systems von *Pre-*, *Fine-* bis hin zum *Complex-Screening*. Durch diese schrittweise Selektion wird die Analyse von einer Vielzahl von Vorstufen und Endprodukten möglich.

Während im *Pre-Screening* zunächst einfache Viabiliätstests und Zellmorphologie-Analysen eingesetzt werden, liefert das *Fine-Screening* Informationen über den Energiestoffwechsel, Zelltod, die Proliferation, Genexpression, DNA-Schädigungen, Zelladhäsion und die Nanopartikel-Aufnahme. Im *Pre-Screening*, das mit allen Materialien durchgeführt wird, erfolgt die erste Selektion der Nanomaterialien. Nur Materialien die im *Pre-Screening* keine signifikanten Effekte aufzeigen, werden im *Fine-* bzw. im *Complex-Screening* detaillierter untersucht. Da einige Nanopartikel mit *Assay*-Komponenten oder Markermolekülen interagieren können, kommen verschiedene Detektionsmethoden wie Mikrokopie, Absorption, Fluoreszenz, Lumineszenz und Impedanz zum Einsatz. Fehlinterpretationen bedingt durch Interferenzen können auf diese Weise minimiert werden.

Neben der Erhöhung der Sensitivität der Zytotoxizitätsmethoden wird auch die Komplexität der Zellsysteme erweitert. Hier kommen verschiedene Zelllinien zum Einsatz, wie Fibroblasten, Lungen-, Leber-, Nieren- oder Darm-Zellen, die dann im weiteren Verlauf des *Screenings* durch Primärzellen ersetzt werden. Die Zellphysiologie der Primärzellen entspricht dabei eher den Zellen im menschlichen Organismus. Des Weiteren werden im *Complex-Screening* dreidimensionale (3D) Zellkulturen anstelle von zweidimensionalen (2D) Kulturen angewendet, mit denen die Zell-Zell-Wechselwirkungen und die *in-vivo*-Zellumgebung besser simuliert werden können. Zur Simulation des Strömungsverhaltens des menschlichen Blut- und Herzkreislaufes wurden zudem dynamische Kultivierungsbedingungen im *Complex-Screening* integriert. Der auf die Zellen wirkende Scherstress sowie die Nanopartikelverteilung beeinflussten die Zellantworten. Es konnte z.B. gezeigt werden, dass die Fibroblasten (NIH-3T3-Zellen) sich bei dynamischer Kultivierung in Fließrichtung ausrichten, wohingegen dieser Effekt bei den Lungenepithelzellen (A549-Zellen) nicht beobachtet wurde. Im

Complex-Screening werden zunächst die Methoden des *Pre-Screenings* auf die 3D-Modelle bzw. die dynamische Kultivierung angewendet und anschließend die Methoden des *Fine-Screenings*.

Um 3D-Zellwachstum *in vitro* zu realisieren, wurden drei verschiedene 3D-Modelle für den Einsatz im *Complex-Screening* untersucht. Hierbei wurde das Sphäroid-Modell (Zellaggregate), das *Scaffold*-Modell (Besiedelung von Zellen auf Gerüstsubstanzen) und das Hydrogel-Modell (Einkapselung der Zellen im Hydrogel) eingesetzt und die Wirkung der Nanopartikel analysiert. Das Sphäroid- und das Hydrogel-Modell sind geeignet, um Morphologieänderungen der Zellen mikroskopisch zu verfolgen, wohingegen bei dem *Scaffold*-Modell dies nur mit aufwendigen Elektronenmikroskopen möglich ist. Die NIH-3T3-Zellen bildeten z.B. im Gegensatz zu den A549-Zellen sehr kompakte Sphäroid-Strukturen aus. Zeitraffer-Aufnahmen zeigten zudem, dass die Sphäroid-Bildung bereits nach ca. sechs Stunden abgeschlossen ist. Insgesamt sollte das im *Complex-Screening* verwendete 3D-Modell angepasst werden an den jeweiligen Anwendungsbereich des zu untersuchenden Nanomaterials, da jeweils unterschiedliche Zell-Zell-Interaktionen und Zellphysiologien im Fokus stehen. Während das Sphäroid-Modell besonders für die Analyse des Nanopartikel-gesteuerten Wirkstofftransports innerhalb eines Tumors geeignet ist, sind die anderen beiden 3D-Modelle eher für die Simulation von anderen Organstrukturen vorgesehen.

Mit den ZnO-Nanopartikeln wurden mit allen Methoden des *Screening*-Systems toxische Effekte auf die Zellen ermittelt. Die ZnO-Nanopartikel-Exposition führte zu Dosis-abhängigen Morphologieänderungen in 2D-Kulturen, in 3D-Modellen sowie unter dynamischen Bedingungen. Im *Fine-Screening* wurden mittels Genexpressionsanalyse Entzündungsreaktionen und oxidative Stressreaktionen detektiert. Das *Electric-Cell-Substrate-Impedance-Sensing* zeigte die Wirkung der Nanopartikel online auf. Direkt nach Zugabe der ZnO-Nanopartikel nahm das Impedanz-Signal ab, was auf eine verminderte Zelladhäsion zurückzuführen ist. Der Vergleich der Wirkung ZnO-Nanopartikel auf die Zellen in den verschiedenen 3D-Modellen im *Complex-Screening* zeigte unterschiedliche Sensitivitäten auf. In 2D und im Sphäroid-Modell waren die Zellen sensitiver im Vergleich zu den Zellen im Hydrogel- oder *Scaffold*-Modell. Außerdem hat der Zeitpunkt der Nanopartikel-Exposition bei dem Sphäroid-Modell einen Einfluss auf die Morphologie der Sphäroide. Werden die Nanopartikel nach abgeschlossener Sphäroid-Bildung hinzugegeben, so waren keine signifikanten Änderungen zu beobachten. Bei direkter Zugabe der Partikel während der Sphäroid-Bildung nahm mit steigender ZnO-Nanopartikel-Konzentration der Sphäroid-Durchmesser zu. Des Weiteren waren die Zellen unter dynamischen Bedingungen sensitiver gegenüber ZnO-Nanopartikeln als unter statischen.

Bei dem *Screening* der TiO_2-Nanopartikel wurde der Erfolg des *Screening*-Systems gezeigt. Während im *Pre-Screening* zunächst keine Veränderungen im Vergleich zu den Kontrollzellen beobachtet wurden, konnten im weiteren *Screening*-Verlauf Effekte festgestellt werden. So wurden im *Pre-Screening* mit 2D-Kulturen weder Morphologieänderungen noch eine Reduktion der Viabilität beobachtet. Auch im *Fine-Screening* lieferten Genexpressionsanalyse, Impedanz-Messung oder Zell-

todanalyse keine Anzeichen auf eine toxische Wirkung. Über die Granularität der Zellen konnte mittels Durchflusszytometrie demonstriert werden, dass die Partikel von den Zellen aufgenommen werden. Eine Zunahme des Seitwärtsstreulicht in Abhängigkeit von der TiO_2-Nanopartikel-konzentration konnte gezeigt werden. Dabei war für die NIH-3T3-Zellen zugleich eine zeitabhängige Aufnahme festzustellen. Mit dem im *Complex-Screening* verwendeten 3D-Hydrogel und dem 3D-*Scaffold*-Modell wurden keine signifikanten Effekte beobachtet. Hingegen konnten, wie auch bei den ZnO-Nanopartikeln, bei direkter Nanopartikel-Exposition während der Sphäroid-Bildung Unterschiede in der Zellantwort festgestellt werden. Anstelle eines einzelnen Sphäroids wurden viele kleine Sphäroide gebildet, deren Anzahl mit der TiO_2-Konzentration zunahm. Im *Complex-Screening* konnte demnach demonstriert werden, dass diese Partikel einen Einfluss auf die Zell-Zell-Wechselwirkungen aufweisen. Die TiO_2-Nanopartikel-Exposition unter dynamischen Kultivierungsbedingungen beeinflusste dabei nicht die Zellviabilität. Lediglich die Orientierung der NIH-3T3-Zellen in Fließrichtung wurde nicht festgestellt. Auch mittels sensitiveren Methoden wie der ECIS-Messung konnten keine signifikanten Effekte festgestellt werden. Insgesamt ist das Risiko von TiO_2-Nanopartikeln gering einzuschätzen, da erst im *Complex-Screening* schwache Effekte beobachtet werden konnten. Für die abschließende Risikobewertung der TiO_2-Nanopatikel wird daher die Durchführung von *in-vivo*-Studien empfohlen.

Neben ZnO und TiO_2-Nanopartikeln wurden auch Silber-Nanopartikel und Silber-Ionen mittels der Methoden im *Screening*-System untersucht. Dabei waren die Ag-Nanopartikel wesentlich toxischer als Ag^+-Ionen. Die toxische Wirkung der Ag-Nanopartikel überwiegt daher. Durch die Aufnahme der Ag-Nanopartikel in die Zelle können die Funktionen der Zellorganellen und die DNA geschädigt werden. Zudem induzieren die Ag-Nanopartikel die ROS-Bildung, die einen oxidativen Stress für die Zellen darstellt. Von den untersuchten Zelllinien waren die NIH-3T3- und die PC-12-Zellen am sensitivsten Des Weiteren wurden unterschiedliche Zelltod-Mechanismen festgestellt. Während die Partikel die Apoptose einleiteten, führten Ionen zur Nekrose. Zusätzlich wurde das *Screening*-System für die Entwicklung von Nanokompositen angewendet, die als hydrophobe Oberflächen im Sanitärbereich eingesetzt werden sollen. Die modifizierten Aluminiumoxid (Al_2O_3)-Nanopartikel könnten sich von den Oberflächen ablösen und somit mit dem Menschen in Kontakt kommen sowie über das Abwasser in die Umwelt gelangen. Die charakteristischen Eigenschaften der Nanokomposite wie Benetzbarkeit und Härte wurden durch Variation der Partikelgröße und -Konzentration optimiert und prozessbegleitend die Toxizität der Vorläuferprodukte analysiert. Die Al_2O_3-Nanopartikel in wässriger Suspension zeigten keine Wirkungen auf die Zellviabiliät. Zur Untersuchung der Stabilität der Nanokomposite wurden Extrakte gewonnen. Hierbei wurde nur eine relativ geringe zytotoxische Wirkung beobachtet, die von der im Nanokomposit verwendeten Partikelgröße und Feststoffgehalt abhing. Al_2O_3-Nanopartikel-Komposite mit einem Feststoffgehalt von 4 % und einer Partikelgröße ≤ 130 nm zeigten dabei die besten mechanischen Eigenschaften (Hydrophobizität, Härte) und geringsten Auswirkungen auf die Zellen.

Zudem wurde in der vorliegenden Dissertation demonstriert, dass das *Screening*-System nicht nur auf die Analyse von Nanomaterialien beschränkt ist. Erste Analysen über die Toxizität des Medizinproduktes 4DryField® PH der Firma PlantTec Medial wurden z.B. erfolgreich durchgeführt. Die Erkenntnisse konnten von den Kooperationspartnern mit *in-vivo*-Experimenten bestätigt werden. Außerdem konnte das System für die Biokompatibilitäts-Testung von Materialien, wie verschiedene Polyamid-Pulver, für das 3D-Drukverfahren angewendet werden. Das 3D-Druckverfahren bietet die Möglichkeit spezielle 3D-Gerüststrukturen und miniaturisierte Gefäßstrukturen zu konstruieren. Um diese für die *in-vitro*-Testung einsetzen zu können, kann die Biokompatibilität der eingesetzten Materialien mittels des *Screening*-Systems überprüft werden.

Insgesamt konnten verschiedene Nanopartikel, Nanokomposite mittels des *Screening*-Systems analysiert sowie die Biokompatibilität von Materialien überprüft werden. Vor allem anhand der TiO_2-Nanopartikel konnte der Erfolg des *Screening*-Systems und die Bedeutung von komplexen 3D-Modellen für die Risikoanalyse von Nanopartikeln demonstriert werden. Erst mit den sensitiven und komplexen Zellsystemen des *Complex-Screening* wurden signifikante Effekte der TiO_2-Nanopartikel aufgezeigt. Zukünftig sind die Methoden des *Fine-Screening* weiter zu optimieren, so dass auch komplexe Zellsysteme analysiert werden können. Derzeit kann aus den 3D-Zellsystemen sowie Fluidsystemen für die Genexpressionsanalyse keine ausreichende RNA-Menge isoliert werden. Des Weiteren sind Langzeitanalysen mit den Partikeln von besonderem Interesse. Hierfür ist die Kombination von 3D-Modellen und dynamischen Kultivierungsbedingungen im *Screening*-System vorgesehen. Auch die *Organ-on-a-Chip*-Technologie weist ein enormes Potential auf in das *Complex-Screening* integriert zu werden. Im Rahmen der Dissertation wurden bereits zwei verschiedene Bioreaktoren konzipiert, die unterschiedliche Strömungsbedingungen im menschlichen Organismus simulieren können. Bei dem einen Reaktor werden die 3D-Zellmodelle vom Medium überströmt (horizontale Fließrichtung), wohingegen beim zweiten Reaktor die Zellkonstrukte perfundiert werden (vertikale Fließrichtung). Erste Vorexperimente im Perfusionsbioreaktor zeigten eine sensitivere Zellantwort des 3D-*Scaffold*-Modell im Vergleich zu den statischen Kontrollen.

In der vorliegenden Dissertation wurden durch die Entwicklung des *Screening*-Systems wichtige Strategien für eine umfassende Risikoanalyse der Nanomaterialien geschaffen. Zukünftig können durch intelligente Kombination verschiedener Technologien wie das 3D-Zellwachstum, die Mikro- und Makrofluidik sowie das 3D-Druckverfahren die *in-vitro*-Systeme weiter optimiert werden. Die ethische Verantwortung besteht in der maßgeschneiderten Risikobewertung für Mensch und Umwelt und der Reduktion von Tierversuchen. Diese Vorgehensweise führt die Nanotechnologie zukünftig auf einen vielversprechenden Erfolgspfad.

Literaturverzeichnis

1. Sanchez-Quiles, D. and A. Tovar-Sanchez, *Sunscreens as a Source of Hydrogen Peroxide Production in Coastal Waters.* Environmental Science & Technology, 2014. **48**(16): p. 9037-9042.
2. Beer, C., et al., *Toxicity of silver nanoparticles—Nanoparticle or silver ion?* Toxicology Letters, 2012. **208**(3): p. 286-292.
3. Beddoes, C.M., C.P. Case, and W.H. Briscoe, *Understanding nanoparticle cellular entry: A physicochemical perspective.* Advances in Colloid and Interface Science, 2015. **218**(0): p. 48-68.
4. Alshatwi, A.A., et al., *Aluminium oxide nanoparticles induce mitochondrial-mediated oxidative stress and alter the expression of antioxidant enzymes in human mesenchymal stem cells.* Food Additives and Contaminants Part a-Chemistry Analysis Control Exposure & Risk Assessment, 2013. **30**(1): p. 1-10.
5. Sun, J., et al., *Cytotoxicity, permeability, and inflammation of metal oxide nanoparticles in human cardiac microvascular endothelial cells: cytotoxicity, permeability, and inflammation of metal oxide nanoparticles.* Cell Biol Toxicol, 2011. **27**(5): p. 333-42.
6. Radziun, E., et al., *Assessment of the cytotoxicity of aluminium oxide nanoparticles on selected mammalian cells.* Toxicol In Vitro, 2011. **25**(8): p. 1694-700.
7. Piccinno, F., et al., *Industrial production quantities and uses of ten engineered nanomaterials in Europe and the world.* Journal of Nanoparticle Research, 2012. **14**(9): p. 1-11.
8. Asmatulu, R., P. Nguyen, and E. Asmatulu, *Chapter 5 - Nanotechnology Safety in the Automotive Industry*, in *Nanotechnology Safety*, R. Asmatulu, Editor. 2013, Elsevier: Amsterdam. p. 57-72.
9. Kaiser, J.-P., S. Zuin, and P. Wick, *Is nanotechnology revolutionizing the paint and lacquer industry? A critical opinion.* Science of The Total Environment, 2013. **442**(0): p. 282-289.
10. Mueller, N.C. and B. Nowack, *Exposure Modeling of Engineered Nanoparticles in the Environment.* Environmental Science & Technology, 2008. **42**(12): p. 4447-4453.
11. Pietroiusti, A., *Health implications of engineered nanomaterials.* Nanoscale, 2012. **4**(4): p. 1231-47.
12. Gomes, T., et al., *Genotoxicity of copper oxide and silver nanoparticles in the mussel Mytilus galloprovincialis.* Marine Environmental Research, 2013. **84**(0): p. 51-59.
13. Fujishima, A., T.N. Rao, and D.A. Tryk, *Titanium dioxide photocatalysis.* Journal of Photochemistry and Photobiology C: Photochemistry Reviews, 2000. **1**(1): p. 1-21.
14. John, S., et al., *Enhancement of corrosion protection of mild steel by chitosan/ZnO nanoparticle composite membranes.* Progress in Organic Coatings, 2015. **84**(0): p. 28-34.
15. Holtz, R.D., et al., *Nanostructured silver vanadate as a promising antibacterial additive to water-based paints.* Nanomedicine: Nanotechnology, Biology and Medicine, 2012. **8**(6): p. 935-940.
16. Romanello, M.B. and M.M. Fidalgo de Cortalezzi, *An experimental study on the aggregation of TiO2 nanoparticles under environmentally relevant conditions.* Water Research, 2013. **47**(12): p. 3887-3898.
17. Thompson, C.S., R.A. Fleming, and M. Zou, *Transparent self-cleaning and antifogging silica nanoparticle films.* Solar Energy Materials and Solar Cells, 2013. **115**(0): p. 108-113.
18. Manoudis, P.N., et al., *Fabrication of super-hydrophobic surfaces for enhanced stone protection.* Surface and Coatings Technology, 2009. **203**(10–11): p. 1322-1328.
19. Alatraktchi, F.A.a., Y. Zhang, and I. Angelidaki, *Nanomodification of the electrodes in microbial fuel cell: Impact of nanoparticle density on electricity production and microbial community.* Applied Energy, 2014. **116**(0): p. 216-222.
20. Hong, T., F. Chen, and C. Xia, *Barium carbonate nanoparticle as high temperature oxygen reduction catalyst for solid oxide fuel cell.* Electrochemistry Communications, 2015. **51**(0): p. 93-97.
21. Liao, H., A. Fisher, and Z.J. Xu, *Surface Segregation in Bimetallic Nanoparticles: A Critical Issue in Electrocatalyst Engineering.* Small, 2015: p. n/a-n/a.

22. Figueiredo, M.C., et al., *Carbon-supported shape-controlled Pt nanoparticle electrocatalysts for direct alcohol fuel cells.* Electrochemistry Communications, 2015(0).
23. He, Q., D.C. Joy, and D.J. Keffer, *Nanoparticle adhesion in proton exchange membrane fuel cell electrodes.* Journal of Power Sources, 2013. **241**(0): p. 634-646.
24. Ahn, H.-J., et al., *Three-dimensional nanostructured carbon nanotube array/PtRu nanoparticle electrodes for micro-fuel cells.* Electrochemistry Communications, 2009. **11**(3): p. 635-638.
25. Sekine, N., et al., *ZnO nano-ridge structure and its application in inverted polymer solar cell.* Organic Electronics, 2009. **10**(8): p. 1473-1477.
26. Shao, S., et al., *Optimizing ZnO nanoparticle surface for bulk heterojunction hybrid solar cells.* Solar Energy Materials and Solar Cells, 2013. **118**(0): p. 43-47.
27. Apostoluk, A., et al., *Improvement of the solar cell efficiency by the ZnO nanoparticle layer via the down-shifting effect.* Microelectronic Engineering, 2014. **127**(0): p. 51-56.
28. Layek, A., et al., *Synthesis of ZnO composited TiO2 nanoparticle and its application in dye sensitized solar cells: A novel approach in enhancing open-circuit voltage.* Materials Letters, 2014. **126**(0): p. 214-216.
29. Lou, Y., et al., *A simple route for decorating TiO2 nanoparticle over ZnO aggregates dye-sensitized solar cell.* Chemical Engineering Journal, 2013. **229**(0): p. 190-196.
30. Shaafi, T. and R. Velraj, *Influence of alumina nanoparticles, ethanol and isopropanol blend as additive with diesel–soybean biodiesel blend fuel: Combustion, engine performance and emissions.* Renewable Energy, 2015. **80**(0): p. 655-663.
31. Mehta, R.N., M. Chakraborty, and P.A. Parikh, *Nanofuels: Combustion, engine performance and emissions.* Fuel, 2014. **120**(0): p. 91-97.
32. Snow, S.J., et al., *Inhaled diesel emissions generated with cerium oxide nanoparticle fuel additive induce adverse pulmonary and systemic effects.* Toxicol Sci, 2014. **142**(2): p. 403-17.
33. Arul Mozhi Selvan, V., R.B. Anand, and M. Udayakumar, *Effect of Cerium Oxide Nanoparticles and Carbon Nanotubes as fuel-borne additives in Diesterol blends on the performance, combustion and emission characteristics of a variable compression ratio engine.* Fuel, 2014. **130**(0): p. 160-167.
34. Xu, Y., et al., *Synthesis and tribological studies of nanoparticle additives for pyrolysis bio-oil formulated as a diesel fuel.* Energy, 2015. **83**(0): p. 80-88.
35. Vidor, F.F., G.I. Wirth, and U. Hilleringmann, *Low temperature fabrication of a ZnO nanoparticle thin-film transistor suitable for flexible electronics.* Microelectronics Reliability, 2014. **54**(12): p. 2760-2765.
36. Byeon, K.-J., et al., *Fabrication of high-brightness GaN-based light-emitting diodes via thermal nanoimprinting of ZnO-nanoparticle-dispersed resin.* Applied Surface Science, 2015(0).
37. Habuda-Stanić, M. and M. Nujić, *Arsenic removal by nanoparticles: a review.* Environmental Science and Pollution Research, 2015: p. 1-30.
38. Mahmoudi, M., et al., *Magnetic Resonance Imaging Tracking of Stem Cells in Vivo Using Iron Oxide Nanoparticles as a Tool for the Advancement of Clinical Regenerative Medicine.* Chemical Reviews, 2011. **111**(2): p. 253-280.
39. Jiang, S., et al., *Preparation, characterization, and antitumor activities of folate-decorated docetaxel-loaded human serum albumin nanoparticles.* Drug Delivery, 2015. **22**(2): p. 206-213.
40. Deng, Z.J., et al., *Nanoparticle-induced unfolding of fibrinogen promotes Mac-1 receptor activation and inflammation.* Nat Nano, 2011. **6**(1): p. 39-44.
41. Doane, T.L. and C. Burda, *The unique role of nanoparticles in nanomedicine: imaging, drug delivery and therapy.* Chemical Society Reviews, 2012. **41**(7): p. 2885-2911.
42. Dreaden, E.C., et al., *Beating cancer in multiple ways using nanogold.* Chemical Society Reviews, 2011. **40**(7): p. 3391-3404.
43. Paur, H.-R., et al., *In-vitro cell exposure studies for the assessment of nanoparticle toxicity in the lung—A dialog between aerosol science and biology.* Journal of Aerosol Science, 2011. **42**(10): p. 668-692.
44. Yameen, B., et al., *Insight into nanoparticle cellular uptake and intracellular targeting.* Journal of Controlled Release, 2014. **190**: p. 485-499.

45. Majewski, A.P., et al., *Dual-Responsive Magnetic Core–Shell Nanoparticles for Nonviral Gene Delivery and Cell Separation.* Biomacromolecules, 2012. **13**(3): p. 857-866.
46. Bhise, N.S., et al., *Organ-on-a-chip platforms for studying drug delivery systems.* Journal of Controlled Release, 2014. **190**(0): p. 82-93.
47. Yamada, Y. and H. Harashima, *Delivery of bioactive molecules to the mitochondrial genome using a membrane-fusing, liposome-based carrier, DF-MITO-Porter.* Biomaterials, 2012. **33**(5): p. 1589-1595.
48. Cui, Y., et al., *Transferrin-conjugated magnetic silica PLGA nanoparticles loaded with doxorubicin and paclitaxel for brain glioma treatment.* Biomaterials, 2013. **34**(33): p. 8511-8520.
49. Zhang, H., et al., *A strategy for ZnO nanorod mediated multi-mode cancer treatment.* Biomaterials, 2011. **32**(7): p. 1906-1914.
50. Rasmussen, J.W., et al., *Zinc Oxide Nanoparticles for Selective Destruction of Tumor Cells and Potential for Drug Delivery Applications.* Expert opinion on drug delivery, 2010. **7**(9): p. 1063-1077.
51. Dreaden, E.C. and M.A. El-Sayed, *Detecting and Destroying Cancer Cells in More than One Way with Noble Metals and Different Confinement Properties on the Nanoscale.* Accounts of Chemical Research, 2012. **45**(11): p. 1854-1865.
52. Huang, X., et al., *Cancer Cell Imaging and Photothermal Therapy in the Near-Infrared Region by Using Gold Nanorods.* Journal of the American Chemical Society, 2006. **128**(6): p. 2115-2120.
53. Gobin, A.M., et al., *Near-Infrared Resonant Nanoshells for Combined Optical Imaging and Photothermal Cancer Therapy.* Nano Letters, 2007. **7**(7): p. 1929-1934.
54. Chen, J., et al., *Gold Nanocages as Photothermal Transducers for Cancer Treatment.* Small, 2010. **6**(7): p. 811-817.
55. Topete, A., et al., *Polymeric-Gold Nanohybrids for Combined Imaging and Cancer Therapy.* Advanced Healthcare Materials, 2014. **3**(8): p. 1309-1325.
56. Ruan, J., et al., *HER2 monoclonal antibody conjugated RNase-A-associated CdTe quantum dots for targeted imaging and therapy of gastric cancer.* Biomaterials, 2012. **33**(29): p. 7093-7102.
57. Choi, Y.J., et al., *Cyto-/genotoxic effect of CdSe/ZnS quantum dots in human lung adenocarcinoma cells for potential photodynamic UV therapy applications.* J Nanosci Nanotechnol, 2012. **12**(3): p. 2160-8.
58. Chu, M., et al., *The therapeutic efficacy of CdTe and CdSe quantum dots for photothermal cancer therapy.* Biomaterials, 2012. **33**(29): p. 7071-7083.
59. Hackenberg, S., et al., *Zinc oxide nanoparticles induce photocatalytic cell death in human head and neck squamous cell carcinoma cell lines in vitro.* Int J Oncol, 2010. **37**(6): p. 1583-90.
60. Metreveli, G., A. Philippe, and G.E. Schaumann, *Disaggregation of silver nanoparticle homoaggregates in a river water matrix.* Science of The Total Environment, 2014(0).
61. Yu, W., et al., *Microarray-based bioinformatics analysis of osteoblasts on TiO2 nanotube layers.* Colloids and Surfaces B: Biointerfaces, 2012. **93**(0): p. 135-142.
62. Homan, K.A., et al., *Silver Nanoplate Contrast Agents for in Vivo Molecular Photoacoustic Imaging.* ACS Nano, 2012. **6**(1): p. 641-650.
63. Qian, X., et al., *In vivo tumor targeting and spectroscopic detection with surface-enhanced Raman nanoparticle tags.* Nat Biotech, 2008. **26**(1): p. 83-90.
64. Alvarez-Puebla, R.A., et al., *Self-assembled nanorod supercrystals for ultrasensitive SERS diagnostics.* Nano Today, 2012. **7**(1): p. 6-9.
65. Shevtsov, M.A., et al., *Superparamagnetic iron oxide nanoparticles conjugated with epidermal growth factor (SPION–EGF) for targeting brain tumors.* International Journal of Nanomedicine, 2014. **9**: p. 273-287.
66. Högemann, D., et al., *Improvement of MRI Probes To Allow Efficient Detection of Gene Expression.* Bioconjugate Chemistry, 2000. **11**(6): p. 941-946.
67. Weissleder, R., et al., *In vivo magnetic resonance imaging of transgene expression.* Nat Med, 2000. **6**(3): p. 351-354.

68. Parak, W.J., T. Pellegrino, and C. Plank, *Labelling of cells with quantum dots.* Nanotechnology, 2005. **16**(2): p. R9-R25.
69. Peng, C.-W., et al., *Quantum-dots based simultaneous detection of multiple biomarkers of tumor stromal features to predict clinical outcomes in gastric cancer.* Biomaterials, 2012. **33**(23): p. 5742-5752.
70. Meyer, K., et al., *ZnO nanoparticles induce apoptosis in human dermal fibroblasts via p53 and p38 pathways.* Toxicology in Vitro, 2011. **25**(8): p. 1721-1726.
71. Hong, H., et al., *Cancer-Targeted Optical Imaging with Fluorescent Zinc Oxide Nanowires.* Nano Letters, 2011. **11**(9): p. 3744-3750.
72. Yang, S.C., et al., *Tumor detection strategy using ZnO light-emitting nanoprobes.* Nanotechnology, 2012. **23**(5): p. 055202.
73. Nohynek, G. and E. Dufour, *Nano-sized cosmetic formulations or solid nanoparticles in sunscreens: A risk to human health?* Archives of Toxicology, 2012. **86**(7): p. 1063-1075.
74. Borowska, S. and M.M. Brzóska, *Metals in cosmetics: implications for human health.* Journal of Applied Toxicology, 2015: p. n/a-n/a.
75. Popov, A.P., et al., *Effect of size of TiO2 nanoparticles embedded into stratum corneum on ultraviolet-A and ultraviolet-B sun-blocking properties of the skin.* Journal of Biomedical Optics, 2005. **10**(6): p. 064037-064037-9.
76. Hwang, S.H., et al., *Electrospun ZnO/TiO2 composite nanofibers as a bactericidal agent.* Chemical Communications, 2011. **47**(32): p. 9164-9166.
77. McCormick, P.G. and T. Tsuzuki, *In vitro testing of zinc oxide sunscreens.* International Journal of Cosmetic Science, 2012. **34**(4): p. 291-297.
78. Osmond, M.J. and M.J. Mccall, *Zinc oxide nanoparticles in modern sunscreens: An analysis of potential exposure and hazard.* Nanotoxicology, 2010. **4**(1): p. 15-41.
79. Vemula, P.K., R.R. Anderson, and J.M. Karp, *Nanoparticles reduce nickel allergy by capturing metal ions.* Nat Nano, 2011. **6**(5): p. 291-295.
80. Mu, L. and R.L. Sprando, *Application of nanotechnology in cosmetics.* Pharm Res, 2010. **27**(8): p. 1746-9.
81. Raj, S., et al., *Nanotechnology in cosmetics: Opportunities and challenges.* Journal of Pharmacy & Bioallied Sciences, 2012. **4**(3): p. 186-193.
82. Hannon, J.C., et al., *Advances and challenges for the use of engineered nanoparticles in food contact materials.* Trends in Food Science & Technology, 2015. **43**(1): p. 43-62.
83. Periasamy, V.S., et al., *Identification of titanium dioxide nanoparticles in food products: Induce intracellular oxidative stress mediated by TNF and CYP1A genes in human lung fibroblast cells.* Environmental Toxicology and Pharmacology, 2015. **39**(1): p. 176-186.
84. Duncan, T.V., *Applications of nanotechnology in food packaging and food safety: Barrier materials, antimicrobials and sensors.* Journal of Colloid and Interface Science, 2011. **363**(1): p. 1-24.
85. Hassabo, A.G., et al., *Impregnation of silver nanoparticles into polysaccharide substrates and their properties.* Carbohydrate Polymers, 2015. **122**(0): p. 343-350.
86. Xue, C.-H., et al., *Superhydrophobic conductive textiles with antibacterial property by coating fibers with silver nanoparticles.* Applied Surface Science, 2012. **258**(7): p. 2468-2472.
87. Joshi, M. and A. Bhattacharyya, *Nanotechnology – a new route to high-performance functional textiles.* Textile Progress, 2011. **43**(3): p. 155-233.
88. Salaün, F., et al., *Polymer nanoparticles to decrease thermal conductivity of phase change materials.* Thermochimica Acta, 2008. **477**(1–2): p. 25-31.
89. Yadav, A., et al., *Functional finishing in cotton fabrics using zinc oxide nanoparticles.* Bulletin of Materials Science, 2006. **29**(6): p. 641-645.
90. Xu, S., et al., *Targeting receptor-mediated endocytotic pathways with nanoparticles: rationale and advances.* Advanced drug delivery reviews, 2013. **65**(1): p. 121-138.
91. EU, C., *Commission Recommendation of 18 October 2011 on the definition of nanomaterial.* Official Journal, 2011. **L 275,** (2011/696/EU): p. 38-40.
92. Bleeker, E.A.J., et al., *Considerations on the EU definition of a nanomaterial: Science to support policy making.* Regulatory Toxicology and Pharmacology, 2013. **65**(1): p. 119-125.
93. Weir, A., et al., *Titanium Dioxide Nanoparticles in Food and Personal Care Products.* Environmental Science & Technology, 2012. **46**(4): p. 2242-2250.

94. O'Shaughnessy, P.T., *Occupational health risk to nanoparticulate exposure.* Environ Sci Process Impacts, 2013. **15**(1): p. 49-62.
95. Wurster, U., *Nanomaterialien: Regulierungen national - international*. 2012: LUBW Landesanstalt für Umwelt, Messungen und Naturschutz Baden-Württemberg.
96. Maynard, A.D., *Chapter 1 - Challenges in Nanoparticle Risk Assessment*, in *Assessing Nanoparticle Risks to Human Health*, G. Ramachandran, Editor. 2011, William Andrew Publishing: Oxford. p. 1-19.
97. Bour, A., et al., *Environmentally relevant approaches to assess nanoparticles ecotoxicity: a review.* J Hazard Mater, 2015. **283**: p. 764-77.
98. Wigger, H., et al., *Influences of use activities and waste management on environmental releases of engineered nanomaterials.* Science of The Total Environment, 2015(0).
99. Sun, T.Y., et al., *Comprehensive probabilistic modelling of environmental emissions of engineered nanomaterials.* Environmental Pollution, 2014. **185**(0): p. 69-76.
100. Foltête, A.-S., et al., *Environmental impact of sunscreen nanomaterials: Ecotoxicity and genotoxicity of altered TiO2 nanocomposites on Vicia faba.* Environmental Pollution, 2011. **159**(10): p. 2515-2522.
101. Das, P., M. Xenopoulos, and C. Metcalfe, *Toxicity of Silver and Titanium Dioxide Nanoparticle Suspensions to the Aquatic Invertebrate, Daphnia magna.* Bulletin of Environmental Contamination and Toxicology, 2013. **91**(1): p. 76-82.
102. Kaegi, R., et al., *Synthetic TiO2 nanoparticle emission from exterior facades into the aquatic environment.* Environmental Pollution, 2008. **156**(2): p. 233-239.
103. Gottschalk, F., T. Sun, and B. Nowack, *Environmental concentrations of engineered nanomaterials: Review of modeling and analytical studies.* Environmental Pollution, 2013. **181**(0): p. 287-300.
104. Judy, J.D., J.M. Unrine, and P.M. Bertsch, *Evidence for Biomagnification of Gold Nanoparticles within a Terrestrial Food Chain.* Environmental Science & Technology, 2011. **45**(2): p. 776-781.
105. Unrine, J.M., et al., *Trophic Transfer of Au Nanoparticles from Soil along a Simulated Terrestrial Food Chain.* Environmental Science & Technology, 2012. **46**(17): p. 9753-9760.
106. Holbrook, R.D., et al., *Trophic transfer of nanoparticles in a simplified invertebrate food web.* Nat Nano, 2008. **3**(6): p. 352-355.
107. Fouqueray, M., et al., *Exposure of juvenile Danio rerio to aged TiO2 nanomaterial from sunscreen.* Environmental Science and Pollution Research, 2013. **20**(5): p. 3340-3350.
108. Kulacki, K.J., et al., *How do stream organisms respond to, and influence, the concentration of titanium dioxide nanoparticles? A mesocosm study with algae and herbivores.* Environmental Toxicology and Chemistry, 2012. **31**(10): p. 2414-2422.
109. Ferry, J.L., et al., *Transfer of gold nanoparticles from the water column to the estuarine food web.* Nat Nano, 2009. **4**(7): p. 441-444.
110. Colman, B.P., et al., *Emerging Contaminant or an Old Toxin in Disguise? Silver Nanoparticle Impacts on Ecosystems.* Environmental Science & Technology, 2014. **48**(9): p. 5229-5236.
111. Cleveland, D., et al., *Pilot estuarine mesocosm study on the environmental fate of Silver nanomaterials leached from consumer products.* Science of The Total Environment, 2012. **421–422**(0): p. 267-272.
112. Braydich-Stolle, L.K., et al., *Nanosized aluminum altered immune function.* ACS Nano, 2010. **4**(7): p. 3661-70.
113. Zarogouldis, P., et al., *Vectors for Inhaled Gene Therapy in Lung Cancer. Application for Nano Oncology and Safety of Bio Nanotechnology.* International Journal of Molecular Sciences, 2012. **13**(9): p. 10828-10862.
114. Monteiro-Riviere, N.A. and J.E. Riviere, *Interaction of nanomaterials with skin: Aspects of absorption and biodistribution.* Nanotoxicology, 2009. **3**(3): p. 188-193.
115. Taccola, L., et al., *Zinc oxide nanoparticles as selective killers of proliferating cells.* Int J Nanomedicine, 2011. **6**: p. 1129-40.
116. Mark, D., *Chapter 4 Occupational Exposure to Nanoparticles and Nanotubes*, in *Nanotechnology: Consequences for Human Health and the Environment*. 2007, The Royal Society of Chemistry. p. 50-80.

117. Ma, D., *Enhancing endosomal escape for nanoparticle mediated siRNA delivery.* Nanoscale, 2014. **6**(12): p. 6415-6425.
118. Vasir, J.K. and V. Labhasetwar, *Quantification of the Force of Nanoparticle-Cell Membrane Interactions and Its Influence on Intracellular Trafficking of Nanoparticles.* Biomaterials, 2008. **29**(31): p. 4244-4252.
119. Huang, D.M., et al., *Highly efficient cellular labeling of mesoporous nanoparticles in human mesenchymal stem cells: implication for stem cell tracking.* Faseb Journal, 2005. **19**(12): p. 2014-+.
120. Verano-Braga, T., et al., *Insights into the Cellular Response Triggered by Silver Nanoparticles Using Quantitative Proteomics.* ACS Nano, 2014. **8**(3): p. 2161-2175.
121. Chu, Z., et al., *Cellular uptake, evolution, and excretion of silica nanoparticles in human cells.* Nanoscale, 2011. **3**(8): p. 3291-3299.
122. Chithrani, B.D., A.A. Ghazani, and W.C.W. Chan, *Determining the Size and Shape Dependence of Gold Nanoparticle Uptake into Mammalian Cells.* Nano Letters, 2006. **6**(4): p. 662-668.
123. Vranic, S., et al., *Deciphering the mechanisms of cellular uptake of engineered nanoparticles by accurate evaluation of internalization using imaging flow cytometry.* Particle and Fibre Toxicology, 2013. **10**: p. 2-2.
124. Osaki, F., et al., *A Quantum Dot Conjugated Sugar Ball and Its Cellular Uptake. On the Size Effects of Endocytosis in the Subviral Region.* Journal of the American Chemical Society, 2004. **126**(21): p. 6520-6521.
125. Gratton, S.E.A., et al., *The effect of particle design on cellular internalization pathways.* Proceedings of the National Academy of Sciences, 2008. **105**(33): p. 11613-11618.
126. Black, K.C.L., et al., *Radioactive 198Au-Doped Nanostructures with Different Shapes for In Vivo Analyses of Their Biodistribution, Tumor Uptake, and Intratumoral Distribution.* ACS Nano, 2014. **8**(5): p. 4385-4394.
127. Ding, H.-m., W.-d. Tian, and Y.-q. Ma, *Designing Nanoparticle Translocation through Membranes by Computer Simulations.* ACS Nano, 2012. **6**(2): p. 1230-1238.
128. Wong-Ekkabut, J., et al., *Computer simulation study of fullerene translocation through lipid membranes.* Nat Nano, 2008. **3**(6): p. 363-368.
129. Qiao, R., et al., *Translocation of C60 and Its Derivatives Across a Lipid Bilayer.* Nano Letters, 2007. **7**(3): p. 614-619.
130. Goodman, C.M., et al., *Toxicity of Gold Nanoparticles Functionalized with Cationic and Anionic Side Chains.* Bioconjugate Chemistry, 2004. **15**(4): p. 897-900.
131. Rocha, E.L.d., G.F. Caramori, and C.R. Rambo, *Nanoparticle translocation through a lipid bilayer tuned by surface chemistry.* Physical Chemistry Chemical Physics, 2013. **15**(7): p. 2282-2290.
132. Song, W., et al., *Role of the dissolved zinc ion and reactive oxygen species in cytotoxicity of ZnO nanoparticles.* Toxicol Lett, 2010. **199**(3): p. 389-97.
133. Soenen, S.J., et al., *(Intra)Cellular Stability of Inorganic Nanoparticles: Effects on Cytotoxicity, Particle Functionality, and Biomedical Applications.* Chemical Reviews, 2015. **115**(5): p. 2109-2135.
134. Nel, A., et al., *Toxic Potential of Materials at the Nanolevel.* Science, 2006. **311**(5761): p. 622-627.
135. Park, E.-J., et al., *Oxidative stress and apoptosis induced by titanium dioxide nanoparticles in cultured BEAS-2B cells.* Toxicology Letters, 2008. **180**(3): p. 222-229.
136. Hackenberg, S., et al., *Intracellular distribution, geno- and cytotoxic effects of nanosized titanium dioxide particles in the anatase crystal phase on human nasal mucosa cells.* Toxicology Letters, 2010. **195**(1): p. 9-14.
137. Demir, E., et al., *Genotoxic and cell-transforming effects of titanium dioxide nanoparticles.* Environmental Research, 2015. **136**(0): p. 300-308.
138. Wan, R., et al., *DNA Damage Caused by Metal Nanoparticles: Involvement of Oxidative Stress and Activation of ATM.* Chemical Research in Toxicology, 2012. **25**(7): p. 1402-1411.
139. Hamzeh, M. and G.I. Sunahara, *In vitro cytotoxicity and genotoxicity studies of titanium dioxide (TiO2) nanoparticles in Chinese hamster lung fibroblast cells.* Toxicology in Vitro, 2013. **27**(2): p. 864-873.

140. Liu, S., et al., *Oxidative stress and apoptosis induced by nanosized titanium dioxide in PC12 cells.* Toxicology, 2010. **267**(1–3): p. 172-177.
141. Jiang, J., et al., *Does nanoparticle activity depend upon size and crystal phase?* Nanotoxicology, 2008. **2**(1): p. 33-42.
142. Sayes, C.M., et al., *Correlating Nanoscale Titania Structure with Toxicity: A Cytotoxicity and Inflammatory Response Study with Human Dermal Fibroblasts and Human Lung Epithelial Cells.* Toxicological Sciences, 2006. **92**(1): p. 174-185.
143. Pandurangan, M., M. Veerappan, and D. Kim, *Cytotoxicity of Zinc Oxide Nanoparticles on Antioxidant Enzyme Activities and mRNA Expression in the Cocultured C2C12 and 3T3-L1 Cells.* Applied Biochemistry and Biotechnology, 2015. **175**(3): p. 1270-1280.
144. Knuckles, T.L., et al., *Nanoparticle inhalation alters systemic arteriolar vasoreactivity through sympathetic and cyclooxygenase-mediated pathways.* Nanotoxicology, 2012. **6**(7): p. 724-735.
145. Kang, G.S., et al., *Long-Term Inhalation Exposure to Nickel Nanoparticles Exacerbated Atherosclerosis in a Susceptible Mouse Model.* Environmental Health Perspectives, 2011. **119**(2): p. 176-181.
146. Fukui, H., et al., *Association of zinc ion release and oxidative stress induced by intratracheal instillation of ZnO nanoparticles to rat lung.* Chemico-Biological Interactions, 2012. **198**(1–3): p. 29-37.
147. Hamilton, R., et al., *Particle length-dependent titanium dioxide nanomaterials toxicity and bioactivity.* Particle and Fibre Toxicology, 2009. **6**(1): p. 35.
148. Mortensen, L.J., et al., *In vivo skin penetration of quantum dot nanoparticles in the murine model: the effect of UVR.* Nano Lett, 2008. **8**(9): p. 2779-87.
149. Murray, A.R., et al., *Oxidative stress and inflammatory response in dermal toxicity of single-walled carbon nanotubes.* Toxicology, 2009. **257**(3): p. 161-171.
150. Nelson, M.A., et al., *Effects of acute and subchronic exposure of topically applied fullerene extracts on the mouse skin.* Toxicol Ind Health, 1993. **9**(4): p. 623-30.
151. Yokoyama, A., et al., *Biological Behavior of Hat-Stacked Carbon Nanofibers in the Subcutaneous Tissue in Rats.* Nano Letters, 2005. **5**(1): p. 157-161.
152. Radomski, A., et al., *Nanoparticle-induced platelet aggregation and vascular thrombosis.* British Journal of Pharmacology, 2005. **146**(6): p. 882-893.
153. McGuinnes, C., et al., *Surface derivatization state of polystyrene latex nanoparticles determines both their potency and their mechanism of causing human platelet aggregation in vitro.* Toxicol Sci, 2011. **119**(2): p. 359-68.
154. Zhu, M.-T., et al., *Endothelial dysfunction and inflammation induced by iron oxide nanoparticle exposure: Risk factors for early atherosclerosis.* Toxicology Letters, 2011. **203**(2): p. 162-171.
155. Trickler, W.J., et al., *Silver nanoparticle induced blood-brain barrier inflammation and increased permeability in primary rat brain microvessel endothelial cells.* Toxicol Sci, 2010. **118**(1): p. 160-70.
156. Chen, L., et al., *Manufactured Aluminum Oxide Nanoparticles Decrease Expression of Tight Junction Proteins in Brain Vasculature.* Journal of neuroimmune pharmacology : the official journal of the Society on NeuroImmune Pharmacology, 2008. **3**(4): p. 286-295.
157. Sharma, H.S., *Nanoneuroscience: emerging concepts on nanoneurotoxicity and nanoneuroprotection.* Nanomedicine, 2007. **2**(6): p. 753-758.
158. Takeda, K., et al., *Nanoparticles Transferred from Pregnant Mice to Their Offspring Can Damage the Genital and Cranial Nerve Systems.* Journal of Health Science, 2009. **55**(1): p. 95-102.
159. Tsuchiya, T., et al., *Novel harmful effects of [60]fullerene on mouse embryos in vitro and in vivo.* FEBS Letters, 1996. **393**(1): p. 139-145.
160. Wick, P., et al., *Barrier capacity of human placenta for nanosized materials.* Environ Health Perspect, 2010. **118**(3): p. 432-6.
161. Yamashita, K., et al., *Silica and titanium dioxide nanoparticles cause pregnancy complications in mice.* Nat Nano, 2011. **6**(5): p. 321-328.

162. Tran, L., et al., *Chapter 6 Human Effects of Nanoparticle Exposure*, in *Nanotechnology: Consequences for Human Health and the Environment*. 2007, The Royal Society of Chemistry. p. 102-117.
163. BMEL, *Anzahl der für Versuche und andere wissenschaftliche Zwecke verwendete Wirbeltiere*, B.f.E.u. Landwirtschaft, Editor 2014.
164. Lesniak, A., et al., *Effects of the Presence or Absence of a Protein Corona on Silica Nanoparticle Uptake and Impact on Cells.* Acs Nano, 2012. **6**(7): p. 5845-5857.
165. Kroll, A., et al., *Current in vitro methods in nanoparticle risk assessment: limitations and challenges.* Eur J Pharm Biopharm, 2009. **72**(2): p. 370-7.
166. Chiu, C.-c., et al., *Size-dependent hydrophobic to hydrophilic transition for nanoparticles: A molecular dynamics study.* The Journal of Chemical Physics, 2009. **131**(24): p. 244706.
167. Simon-Deckers, A., et al., *In vitro investigation of oxide nanoparticle and carbon nanotube toxicity and intracellular accumulation in A549 human pneumocytes.* Toxicology, 2008. **253**(1-3): p. 137-146.
168. Jeng, H.A. and J. Swanson, *Toxicity of metal oxide nanoparticles in mammalian cells.* J Environ Sci Health A Tox Hazard Subst Environ Eng, 2006. **41**(12): p. 2699-711.
169. Deng, X., et al., *Nanosized zinc oxide particles induce neural stem cell apoptosis.* Nanotechnology, 2009. **20**(11): p. 115101.
170. Lin, J., et al., *Penetration of Lipid Membranes by Gold Nanoparticles: Insights into Cellular Uptake, Cytotoxicity, and Their Relationship.* ACS Nano, 2010. **4**(9): p. 5421-5429.
171. Tan, J., et al., *The influence of size, shape and vessel geometry on nanoparticle distribution.* Microfluidics and nanofluidics, 2013. **14**(1-2): p. 77-87.
172. Livadaru, L. and A. Kovalenko, *Fundamental Mechanism of Translocation across Liquidlike Membranes: Toward Control over Nanoparticle Behavior.* Nano Letters, 2006. **6**(1): p. 78-83.
173. Shah, S., et al., *Modeling Particle Shape-Dependent Dynamics in Nanomedicine.* Journal of nanoscience and nanotechnology, 2011. **11**(2): p. 919-928.
174. Guzman, E., et al., *Influence of silica nanoparticles on dilational rheology of DPPC-palmitic acid Langmuir monolayers.* Soft Matter, 2012. **8**(14): p. 3938-3948.
175. Guzmán, E., et al., *Mixed DPPC–cholesterol Langmuir monolayers in presence of hydrophilic silica nanoparticles.* Colloids and Surfaces B: Biointerfaces, 2013. **105**(0): p. 284-293.
176. Liu, J., et al., *Soft fibrin gels promote selection and growth of tumorigenic cells.* Nat Mater, 2012. **11**(8): p. 734-741.
177. Gao, D., et al., *Recent developments in microfluidic devices for in vitro cell culture for cell-biology research.* Trac-Trends in Analytical Chemistry, 2012. **35**: p. 150-164.
178. Tsui, J.H., et al., *Microfluidics-assisted in vitro drug screening and carrier production.* Adv Drug Deliv Rev, 2013. **65**(11-12): p. 1575-88.
179. Valencia, P.M., et al., *Microfluidic technologies for accelerating the clinical translation of nanoparticles.* Nat Nanotechnol, 2012. **7**(10): p. 623-9.
180. Kim, J. and R.C. Hayward, *Mimicking dynamic in vivo environments with stimuli-responsive materials for cell culture.* Trends Biotechnol, 2012. **30**(8): p. 426-39.
181. Kusunose, J., et al., *Microfluidic system for facilitated quantification of nanoparticle accumulation to cells under laminar flow.* Ann Biomed Eng, 2013. **41**(1): p. 89-99.
182. Thomas, A., J. Tan, and Y. Liu, *Characterization of nanoparticle delivery in microcirculation using a microfluidic device.* Microvasc Res, 2014. **94**: p. 17-27.
183. Gao, D., et al., *Evaluation of the Absorption of Methotrexate on Cells and Its Cytotoxicity Assay by Using an Integrated Microfluidic Device Coupled to a Mass Spectrometer.* Analytical Chemistry, 2012. **84**(21): p. 9230-9237.
184. Gamboa, J.M. and K.W. Leong, *In vitro and in vivo models for the study of oral delivery of nanoparticles.* Advanced Drug Delivery Reviews, 2013. **65**(6): p. 800-810.
185. Steinke, M., et al., *An engineered 3D human airway mucosa model based on an SIS scaffold.* Biomaterials, 2014. **35**(26): p. 7355-62.
186. Huang, S., et al., *In vitro organ culture models of asthma.* Drug Discovery Today: Disease Models, 2009. **6**(4): p. 137-144.
187. Khetani, S.R. and S.N. Bhatia, *Microscale culture of human liver cells for drug development.* Nat Biotech, 2008. **26**(1): p. 120-126.

188. Ballabh, P., A. Braun, and M. Nedergaard, *The blood–brain barrier: an overview: Structure, regulation, and clinical implications.* Neurobiology of Disease, 2004. **16**(1): p. 1-13.
189. Weksler, B., I.A. Romero, and P.-O. Couraud, *The hCMEC/D3 cell line as a model of the human blood brain barrier.* Fluids and Barriers of the CNS, 2013. **10**: p. 16-16.
190. Clevers, *Chapter 13 - Human Stem Cells for Organs-on-Chips: Clinical Trials Without Patients?1*, in *Stem Cells (Second Edition)*, C.M.v.d.S.A.J.R. Clevers, Editor. 2014, Academic Press: Boston. p. 343-361.
191. Valencia, P.M., et al., *Microfluidic technologies for accelerating the clinical translation of nanoparticles.* Nat Nano, 2012. **7**(10): p. 623-629.
192. Huh, D., et al., *Reconstituting Organ-Level Lung Functions on a Chip.* Science, 2010. **328**(5986): p. 1662-1668.
193. Huh, D., et al., *A human disease model of drug toxicity-induced pulmonary edema in a lung-on-a-chip microdevice.* Sci Transl Med, 2012. **4**(159): p. 159ra147.
194. Kniazeva, T., et al., *A microfluidic respiratory assist device with high gas permeance for artificial lung applications.* Biomedical Microdevices, 2011. **13**(2): p. 315-323.
195. Kim, H.J., et al., *Human gut-on-a-chip inhabited by microbial flora that experiences intestinal peristalsis-like motions and flow.* Lab on a Chip, 2012. **12**(12): p. 2165-2174.
196. Huh, D., G.A. Hamilton, and D.E. Ingber, *From 3D cell culture to organs-on-chips.* Trends in Cell Biology, 2011. **21**(12): p. 745-754.
197. Sung, J.H., et al., *Microscale 3-D hydrogel scaffold for biomimetic gastrointestinal (GI) tract model.* Lab on a Chip, 2011. **11**(3): p. 389-392.
198. Dragoni, S., et al., *Gold Nanoparticles Uptake and Cytotoxicity Assessed on Rat Liver Precision-Cut Slices.* Toxicological Sciences, 2012. **128**(1): p. 186-197.
199. Nakao, Y., et al., *Bile canaliculi formation by aligning rat primary hepatocytes in a microfluidic device.* Biomicrofluidics, 2011. **5**(2): p. 022212.
200. Jang, K.-J., et al., *Human kidney proximal tubule-on-a-chip for drug transport and nephrotoxicity assessment.* Integrative Biology, 2013. **5**(9): p. 1119-1129.
201. Hasan, A., et al., *Microfluidic techniques for development of 3D vascularized tissue.* Biomaterials, 2014. **35**(26): p. 7308-7325.
202. Wlodkowic, D. and J.M. Cooper, *Tumors on chips: oncology meets microfluidics.* Current Opinion in Chemical Biology, 2010. **14**(5): p. 556-567.
203. Kim, D., et al., *On-chip evaluation of platelet adhesion and aggregation upon exposure to mesoporous silica nanoparticles.* Analyst, 2014. **139**(5): p. 906-913.
204. Annabi, N., et al., *Hydrogel-coated microfluidic channels for cardiomyocyte culture.* Lab on a chip, 2013. **13**(18): p. 3569-3577.
205. Giridharan, G.A., et al., *Microfluidic Cardiac Cell Culture Model (μCCCM).* Analytical Chemistry, 2010. **82**(18): p. 7581-7587.
206. Grosberg, A., et al., *Ensembles of engineered cardiac tissues for physiological and pharmacological study: Heart on a chip().* Lab on a chip, 2011. **11**(24): p. 4165-4173.
207. Shimizu, T., et al., *Fabrication of pulsatile cardiac tissue grafts using a novel 3-dimensional cell sheet manipulation technique and temperature-responsive cell culture surfaces.* Circ Res, 2002. **90**(3): p. e40.
208. Wagner, I., et al., *A dynamic multi-organ-chip for long-term cultivation and substance testing proven by 3D human liver and skin tissue co-culture.* Lab on a Chip, 2013. **13**(18): p. 3538-3547.
209. Materne, E.-M., et al., *A multi-organ chip co-culture of neurospheres and liver equivalents for long-term substance testing.* Journal of Biotechnology, 2015(0).
210. Zhang, C., et al., *Towards a human-on-chip: Culturing multiple cell types on a chip with compartmentalized microenvironments.* Lab on a Chip, 2009. **9**(22): p. 3185-3192.
211. Arora, S., J.M. Rajwade, and K.M. Paknikar, *Nanotoxicology and in vitro studies: the need of the hour.* Toxicol Appl Pharmacol, 2012. **258**(2): p. 151-65.
212. Soenen, S.J., et al., *(Intra)Cellular stability of inorganic nanoparticles: effects on cytotoxicity, particle functionality, and biomedical applications.* Chem Rev, 2015. **115**(5): p. 2109-35.
213. Quent, V.M.C., et al., *Discrepancies between metabolic activity and DNA content as tool to assess cell proliferation in cancer research.* Journal of Cellular and Molecular Medicine, 2010. **14**(4): p. 1003-1013.

214. Wang, S.G., H.T. Yu, and J.K. Wickliffe, *Limitation of the MTT and XTT assays for measuring cell viability due to superoxide formation induced by nano-scale TiO2.* Toxicology in Vitro, 2011. **25**(8): p. 2147-2151.
215. Jones, C.F. and D.W. Grainger, *In vitro assessments of nanomaterial toxicity.* Advanced Drug Delivery Reviews, 2009. **61**(6): p. 438-456.
216. Fujita, K., et al., *Effects of ultrafine TiO2 particles on gene expression profile in human keratinocytes without illumination: Involvement of extracellular matrix and cell adhesion.* Toxicology Letters, 2009. **191**(2-3): p. 109-117.
217. Han, X., et al., *Assessing the relevance of in vitro studies in nanotoxicology by examining correlations between in vitro and in vivo data.* Toxicology, 2012. **297**(1-3): p. 1-9.
218. Kim, H., et al., *Nanoparticulate-induced toxicity and related mechanism in vitro and in vivo.* Journal of Nanoparticle Research, 2009. **11**(1): p. 55-65.
219. Hsiao, I.L. and Y.J. Huang, *Titanium oxide shell coatings decrease the cytotoxicity of ZnO nanoparticles.* Chem Res Toxicol, 2011. **24**(3): p. 303-13.
220. Fukui, H., et al., *Association of zinc ion release and oxidative stress induced by intratracheal instillation of ZnO nanoparticles to rat lung.* Chem Biol Interact, 2012. **198**(1-3): p. 29-37.
221. Li, S., W. Song, and M. Gao, *Single and Combined Cytotoxicity Research of Propiconazole and Nano-zinc Oxide on the NIH/3T3 Cell*, in *2013 International Symposium on Environmental Science and Technology (2013 ISEST)*2013. p. 100-105.
222. Wagner, S., et al., *Cytotoxicity of titanium and silicon dioxide nanoparticles.* Journal of Physics: Conference Series, 2008. **170**(1).
223. Demir, E., et al., *Genotoxic and cell-transforming effects of titanium dioxide nanoparticles.* Environ Res, 2014. **136C**: p. 300-308.
224. Shi, H., et al., *Titanium dioxide nanoparticles: a review of current toxicological data.* Particle and Fibre Toxicology, 2013. **10**(1): p. 15.
225. Aueviriyavit, S., et al., *Titanium Dioxide Nanoparticles-Mediated In Vitro Cytotoxicity Does Not Induce Hsp70 and Grp78 Expression in Human Bronchial Epithelial A549 Cells.* Biological Trace Element Research, 2012. **149**(1): p. 123-132.
226. Bloh, J.Z., R. Dillert, and D.W. Bahnemann, *Ruthenium-modified zinc oxide, a highly active vis-photocatalyst: the nature and reactivity of photoactive centres.* Physical Chemistry Chemical Physics, 2014. **16**(12): p. 5833-5845.
227. Bloh, J.Z., R. Dillert, and D.W. Bahnemann, *Transition metal-modified zinc oxides for UV and visible light photocatalysis.* Environ Sci Pollut Res Int, 2012. **19**(9): p. 3688-95.
228. Sambale F, L.A., Stahl F, Blume C, Stiesch M, Kasper C, Bahnemann D, Scheper T, *Three Dimensional Spheroid Cell Culture for Nanoparticle Safety Testing.* Journal of Biotechnology, 2015(http://dx.doi.org/10.1016/j.jbiotec.2015.01.001).
229. (NSAI), N.S.A.o.I., *Biological evaluation of medical devices—part 12: Sample preparation and reference materials (ISO 10993–12:2012).* 2012.
230. Denizot, F. and R. Lang, *Rapid colorimetric assay for cell growth and survival. Modifications to the tetrazolium dye procedure giving improved sensitivity and reliability.* J Immunol Methods, 1986. **89**(2): p. 271-7.
231. Bruns, S., et al., *Fast and efficient screening system for new biomaterials in tissue engineering: A model for peripheral nerve regeneration.* Journal of Biomedical Materials Research Part A, 2007. **81A**(3): p. 736-747.
232. Kroll, A., et al., *Cytotoxicity screening of 23 engineered nanomaterials using a test matrix of ten cell lines and three different assays.* Part Fibre Toxicol, 2011. **8**: p. 9.
233. Mueller, D., et al., *3D organotypic HepaRG cultures as in vitro model for acute and repeated dose toxicity studies.* Toxicol In Vitro, 2014. **28**(1): p. 104-12.
234. da Rocha, E.L., L.M. Porto, and C.R. Rambo, *Nanotechnology meets 3D in vitro models: tissue engineered tumors and cancer therapies.* Mater Sci Eng C Mater Biol Appl, 2014. **34**: p. 270-9.
235. Sauer, U.G., et al., *In vivo-in vitro comparison of acute respiratory tract toxicity using human 3D airway epithelial models and human A549 and murine 3T3 monolayer cell systems.* Toxicol In Vitro, 2013. **27**(1): p. 174-90.
236. Zink, C., et al., *Orthogonal nanometer-micrometer roughness gradients probe morphological influences on cell behavior.* Biomaterials, 2012. **33**(32): p. 8055-61.

237. Deligianni, D.D., et al., *Effect of surface roughness of hydroxyapatite on human bone marrow cell adhesion, proliferation, differentiation and detachment strength.* Biomaterials, 2001. **22**(1): p. 87-96.
238. Ventrelli, L., et al., *Influence of nanoparticle-embedded polymeric surfaces on cellular adhesion, proliferation, and differentiation.* J Biomed Mater Res A, 2014. **102**(8): p. 2652-61.
239. Paddle-Ledinek, J.E., Z. Nasa, and H.J. Cleland, *Effect of different wound dressings on cell viability and proliferation.* Plastic and Reconstructive Surgery, 2006. **117**(7): p. 110s-118s.
240. Seiffert, J.M., et al., *Dynamic monitoring of metal oxide nanoparticle toxicity by label free impedance sensing.* Chem Res Toxicol, 2012. **25**(1): p. 140-52.
241. Yan, Z., et al., *Transcriptional and posttranscriptional regulation and endocytosis were involved in zinc oxide nanoparticle-induced interleukin-8 overexpression in human bronchial epithelial cells.* Cell Biol Toxicol, 2014. **30**(2): p. 79-88.
242. Singh, S., et al., *Endocytosis, oxidative stress and IL-8 expression in human lung epithelial cells upon treatment with fine and ultrafine TiO2: role of the specific surface area and of surface methylation of the particles.* Toxicol Appl Pharmacol, 2007. **222**(2): p. 141-51.
243. Silver, J.T. and E.G. Noble, *Regulation of survival gene hsp70.* Cell Stress Chaperones, 2012. **17**(1): p. 1-9.
244. Okuda-Shimazaki, J., et al., *Effects of titanium dioxide nanoparticle aggregate size on gene expression.* Int J Mol Sci, 2010. **11**(6): p. 2383-92.
245. Chen, J.K., et al., *Particulate nature of inhaled zinc oxide nanoparticles determines systemic effects and mechanisms of pulmonary inflammation in mice.* Nanotoxicology, 2014.
246. Frohlich, E., et al., *Use of whole genome expression analysis in the toxicity screening of nanoparticles.* Toxicol Appl Pharmacol, 2014. **280**(2): p. 272-84.
247. Sun, Q., et al., *Pulmotoxicological effects caused by long-term titanium dioxide nanoparticles exposure in mice.* J Hazard Mater, 2012. **235-236**: p. 47-53.
248. Gui, S., et al., *Molecular mechanism of kidney injury of mice caused by exposure to titanium dioxide nanoparticles.* J Hazard Mater, 2011. **195**: p. 365-70.
249. Ahamed, M., et al., *Silver nanoparticles induced heat shock protein 70, oxidative stress and apoptosis in Drosophila melanogaster.* Toxicol Appl Pharmacol, 2010. **242**(3): p. 263-9.
250. Ahamed, M., et al., *Genotoxic potential of copper oxide nanoparticles in human lung epithelial cells.* Biochem Biophys Res Commun, 2010. **396**(2): p. 578-83.
251. Chen, P., et al., *Detection of cellular response to titanium dioxide nanoparticle agglomerates by sensor cells using heat shock protein promoter.* Biotechnol Bioeng, 2012. **109**(12): p. 3112-8.
252. Chae, Y.J., et al., *Evaluation of the toxic impact of silver nanoparticles on Japanese medaka (Oryzias latipes).* Aquat Toxicol, 2009. **94**(4): p. 320-7.
253. Pham, C.H., J. Yi, and M.B. Gu, *Biomarker gene response in male Medaka (Oryzias latipes) chronically exposed to silver nanoparticle.* Ecotoxicol Environ Saf, 2012. **78**: p. 239-45.
254. Foucaud, L., et al., *Oxidative stress induction by nanoparticles in THP-1 cells with 4-HNE production: stress biomarker or oxidative stress signalling molecule?* Toxicol In Vitro, 2010. **24**(6): p. 1512-20.
255. Posgai, R., et al., *Inhalation method for delivery of nanoparticles to the Drosophila respiratory system for toxicity testing.* Sci Total Environ, 2009. **408**(2): p. 439-43.
256. Male, K.B., et al., *Monitoring of potential cytotoxic and inhibitory effects of titanium dioxide using on-line and non-invasive cell-based impedance spectroscopy.* Anal Chim Acta, 2013. **777**: p. 78-85.
257. Zhu, X., et al., *Biosensing approaches for rapid genotoxicity and cytotoxicity assays upon nanomaterial exposure.* Small, 2013. **9**(9-10): p. 1821-30.
258. Moe, B., S. Gabos, and X.F. Li, *Real-time cell-microelectronic sensing of nanoparticle-induced cytotoxic effects.* Anal Chim Acta, 2013. **789**: p. 83-90.
259. Li, Z. and Z. Cui, *Three-dimensional perfused cell culture.* Biotechnol Adv, 2014. **32**(2): p. 243-54.
260. Ruedinger, F., et al., *Hydrogels for 3D mammalian cell culture: a starting guide for laboratory practice.* Appl Microbiol Biotechnol, 2014.
261. Drewitz, M., et al., *Towards automated production and drug sensitivity testing using scaffold-free spherical tumor microtissues.* Biotechnol J, 2011. **6**(12): p. 1488-96.

262. Lee, J., et al., *In vitro toxicity testing of nanoparticles in 3D cell culture.* Small, 2009. **5**(10): p. 1213-21.
263. Astashkina, A.I., et al., *Nanoparticle toxicity assessment using an in vitro 3-D kidney organoid culture model.* Biomaterials, 2014. **35**(24): p. 6323-31.
264. Xu, X., et al., *A hydrogel-based tumor model for the evaluation of nanoparticle-based cancer therapeutics.* Biomaterials, 2014. **35**(10): p. 3319-30.
265. Wagner, S., et al., *Toxicological issues of nanoparticles employed in photocatalysis.* Green, 2011. **1**(2): p. 171-188.
266. Jeon, H.J., S.C. Yi, and S.G. Oh, *Preparation and antibacterial effects of Ag-SiO2 thin films by sol-gel method.* Biomaterials, 2003. **24**(27): p. 4921-8.
267. Rigo, C., et al., *Active Silver Nanoparticles for Wound Healing.* International Journal of Molecular Sciences, 2013. **14**(3): p. 4817-4840.
268. Quang, D.V., et al., *Effective water disinfection using silver nanoparticle containing silica beads.* Applied Surface Science, 2013. **266**: p. 280-287.
269. Klasen, H.J., *A historical review of the use of silver in the treatment of burns. II. Renewed interest for silver.* Burns, 2000. **26**(2): p. 131-138.
270. Lewis, L.N., *Chemical Catalysis by Colloids and Clusters.* Chemical Reviews, 1993. **93**(8): p. 2693-2730.
271. Luo, J., et al., *A Silver Nanoparticle-Modified Evanescent Field Optical Fiber Sensor for Methylene Blue Detection.* Sensors, 2013. **13**(3): p. 3986-3997.
272. Murphy, C.J., et al., *Anisotropic metal nanoparticles: Synthesis, assembly, and optical applications.* Journal of Physical Chemistry B, 2005. **109**(29): p. 13857-13870.
273. Li, Y.N., Y.L. Wu, and B.S. Ong, *Facile synthesis of silver nanoparticles useful for fabrication of high-conductivity elements for printed electronics.* Journal of the American Chemical Society, 2005. **127**(10): p. 3266-3267.
274. Prabhu, S. and E. Poulose, *Silver nanoparticles: mechanism of antimicrobial action, synthesis, medical applications, and toxicity effects.* International Nano Letters 2012. **32**(2): p. 1-10.
275. Buzea, C., I.I. Pacheco, and K. Robbie, *Nanomaterials and nanoparticles: Sources and toxicity.* Biointerphases, 2007. **2**(4): p. Mr17-Mr71.
276. Lee, H.J., S.Y. Yeo, and S.H. Jeong, *Antibacterial effect of nanosized silver colloidal solution on textile fabrics.* Journal of Materials Science, 2003. **38**(10): p. 2199-2204.
277. Lee, H.J. and S.H. Jeong, *Bacteriostasis and skin innoxiousness of nanosize silver colloids on textile fabrics.* Textile Research Journal, 2005. **75**(7): p. 551-556.
278. Chen, C.Y. and C.L. Chiang, *Preparation of cotton fibers with antibacterial silver nanoparticles.* Materials Letters, 2008. **62**(21-22): p. 3607-3609.
279. Vasilev, K., J. Cook, and H.J. Griesser, *Antibacterial surfaces for biomedical devices.* Expert Review of Medical Devices, 2009. **6**(5): p. 553-567.
280. Sotiriou, G.A. and S.E. Pratsinis, *Antibacterial Activity of Nanosilver Ions and Particles.* Environmental Science & Technology, 2010. **44**(14): p. 5649-5654.
281. Fabrega, J., et al., *Silver Nanoparticle Impact on Bacterial Growth: Effect of pH, Concentration, and Organic Matter.* Environmental Science & Technology, 2009. **43**(19): p. 7285-7290.
282. Navarro, E., et al., *Toxicity of Silver Nanoparticles to Chlamydomonas reinhardtii.* Environmental Science & Technology, 2008. **42**(23): p. 8959-8964.
283. Zhao, C.M. and W.X. Wang, *Biokinetic Uptake and Efflux of Silver Nanoparticles in Daphnia magna.* Environmental Science & Technology, 2010. **44**(19): p. 7699-7704.
284. Chen, X. and H.J. Schluesener, *Nanosilver: A nanoproduct in medical application.* Toxicology Letters, 2008. **176**(1): p. 1-12.
285. Hussain, N., V. Jaitley, and A.T. Florence, *Recent advances in the understanding of uptake of microparticulates across the gastrointestinal lymphatics.* Advanced Drug Delivery Reviews, 2001. **50**(1-2): p. 107-142.
286. Kim, J.S., et al., *Toxicity and tissue distribution of magnetic nanoparticles in mice.* Toxicological Sciences, 2006. **89**(1): p. 338-347.
287. Foley, S., et al., *Cellular localisation of a water-soluble fullerene derivative.* Biochemical and Biophysical Research Communications, 2002. **294**(1): p. 116-119.

288. Kashiwada, S., *Distribution of nanoparticles in the see-through medaka (Oryzias latipes).* Environmental Health Perspectives, 2006. **114**(11): p. 1697-1702.
289. Chairuangkitti, P., et al., *Silver nanoparticles induce toxicity in A549 cells via ROS-dependent and ROS-independent pathways.* Toxicology in Vitro, 2013. **27**(1): p. 330-338.
290. Soto, K.F., et al., *Comparative in vitro cytotoxicity assessment of some manufactured nanoparticulate materials characterized by transmission electron microscopy.* Journal of Nanoparticle Research, 2005. **7**(2-3): p. 145-169.
291. Braydich-Stolle, L., et al., *In vitro cytotoxicity of nanoparticles in mammalian germline stem cells.* Toxicological Sciences, 2005. **88**(2): p. 412-419.
292. Hussain, S.M., et al., *In vitro toxicity of nanoparticles in BRL 3A rat liver cells.* Toxicology in Vitro, 2005. **19**(7): p. 975-983.
293. Grodzik, M. and E. Sawosz, *The influence of silver nanoparticles on chicken embryo development and bursa of Fabricius morphology.* Journal of Animal and Feed Sciences, 2006. **15**: p. 111-114.
294. Wen, H.C., et al., *Observation of Growth of Human Fibroblasts on Silver Nanoparticles.* Proceedings of the International Conference on Nanoscience and Technology, 2007. **61**: p. 445-449.
295. Hussain, S.M., et al., *The interaction of manganese nanoparticles with PC-12 cells induces dopamine depletion.* Toxicological Sciences, 2006. **92**(2): p. 456-463.
296. Kawata, K., M. Osawa, and S. Okabe, *In Vitro Toxicity of Silver Nanoparticles at Noncytotoxic Doses to HepG2 Human Hepatoma Cells.* Environmental Science & Technology, 2009. **43**(15): p. 6046-6051.
297. AshaRani, P.V., et al., *Cytotoxicity and Genotoxicity of Silver Nanoparticles in Human Cells.* Acs Nano, 2009. **3**(2): p. 279-290.
298. Khaydaroy, R.A., et al., *Water disinfection using electrolytically generated silver, copper and gold ions.* Journal of Water Supply Research and Technology-Aqua, 2004. **53**(8): p. 567-572.
299. Khaydarov, R.A., et al., *Electrochemical method for the synthesis of silver nanoparticles.* Journal of Nanoparticle Research, 2009. **11**(5): p. 1193-1200.
300. De Soete, D., R. Gijbels, and J. Hoste, *Neutron Activation Analysis* 1972. 393-444.
301. Mosmann, T., *Rapid Colorimetric Assay for Cellular Growth and Survival - Application to Proliferation and Cyto-Toxicity Assays.* Journal of Immunological Methods, 1983. **65**(1-2): p. 55-63.
302. Haase, A., et al., *A novel type of silver nanoparticles and their advantages in toxicity testing in cell culture systems.* Archives of Toxicology, 2012. **86**(7): p. 1089-1098.
303. Meißner, T., A. Potthoff, and V. Richter, *Suspension characterization as imporant key for toxicological investigations.*, in *J Phys (Conf Ser) Nanosafe 2008*2009.
304. Deguchi, S., et al., *Stabilization of C-60 nanoparticles by protein adsorption and its implications for toxicity studies.* Chemical Research in Toxicology, 2007. **20**(6): p. 854-858.
305. Siller, L., et al., *Silver nanoparticle toxicity in sea urchin Paracentrotus lividus.* Environmental Pollution, 2013. **178**: p. 498-502.
306. da Rocha, E.L., L.M. Porto, and C.R. Rambo, *Nanotechnology meets 3D in vitro models: tissue engineered tumors and cancer therapies.* Mater Sci Eng C Mater Biol Appl, 2013. **34**: p. 270-9.
307. Fennema, E., et al., *Spheroid culture as a tool for creating 3D complex tissues.* Trends in Biotechnology, 2013. **31**(2): p. 108-115.
308. Li, Z. and Z. Cui, *Three-dimensional perfused cell culture.* Biotechnol Adv, 2013. **32**(2): p. 243-54.
309. Astashkina, A., B. Mann, and D.W. Grainger, *A critical evaluation of in vitro cell culture models for high-throughput drug screening and toxicity.* Pharmacol Ther, 2012. **134**(1): p. 82-106.
310. Luca, A.C., et al., *Impact of the 3D Microenvironment on Phenotype, Gene Expression, and EGFR Inhibition of Colorectal Cancer Cell Lines.* Plos One, 2013. **8**(3).
311. Kim, J.A., et al., *High-throughput generation of spheroids using magnetic nanoparticles for three-dimensional cell culture.* Biomaterials, 2013. **34**(34): p. 8555-63.
312. Haycock, J.W., *3D cell culture: a review of current approaches and techniques.* Methods Mol Biol, 2011. **695**: p. 1-15.

313. Asthana, A. and W.S. Kisaalita, *Microtissue size and hypoxia in HTS with 3D cultures.* Drug Discov Today, 2012. **17**(15-16): p. 810-7.
314. Griffith, L.G. and M.A. Swartz, *Capturing complex 3D tissue physiology in vitro.* Nat Rev Mol Cell Biol, 2006. **7**(3): p. 211-24.
315. Friedrich, J., R. Ebner, and L.A. Kunz-Schughart, *Experimental anti-tumor therapy in 3-D: spheroids--old hat or new challenge?* Int J Radiat Biol, 2007. **83**(11-12): p. 849-71.
316. Gao, Y., et al., *Predictive models of diffusive nanoparticle transport in 3-dimensional tumor cell spheroids.* AAPS J, 2013. **15**(3): p. 816-31.
317. Goodman, T.T., P.L. Olive, and S.H. Pun, *Increased nanoparticle penetration in collagenase-treated multicellular spheroids.* Int J Nanomedicine, 2007. **2**(2): p. 265-74.
318. Sahu, D., et al., *Nanosized zinc oxide induces toxicity in human lung cells.* ISRN Toxicol, 2013. **2013**: p. 316075.
319. Taccola, L., et al., *Zinc oxide nanoparticles as selective killers of proliferating cells.* International Journal of Nanomedicine, 2011. **6**.
320. Zhao, J.X., et al., *Involvement of reactive oxygen species and high-voltage-activated calcium currents in nanoparticle zinc oxide-induced cytotoxicity in vitro.* Journal of Nanoparticle Research, 2012. **14**(11).
321. Heng, B.C., et al., *Toxicity of zinc oxide (ZnO) nanoparticles on human bronchial epithelial cells (BEAS-2B) is accentuated by oxidative stress.* Food Chem Toxicol, 2010. **48**(6): p. 1762-6.
322. Ng, K.W., et al., *The role of the tumor suppressor p53 pathway in the cellular DNA damage response to zinc oxide nanoparticles.* Biomaterials, 2011. **32**(32): p. 8218-8225.
323. Meyer, K., et al., *ZnO nanoparticles induce apoptosis in human dermal fibroblasts via p53 and p38 pathways.* Toxicology in Vitro, 2011. **25**(8): p. 1721-1726.
324. Liu, S., et al., *Oxidative stress and apoptosis induced by nanosized titanium dioxide in PC12 cells.* Toxicology, 2010. **267**(1-3): p. 172-7.
325. Srivastava, R.K., et al., *Nano-titanium dioxide induces genotoxicity and apoptosis in human lung cancer cell line, A549.* Human & Experimental Toxicology, 2013. **32**(2): p. 153-166.
326. Hou, Y., et al., *Effects of titanium nanoparticles on adhesion, migration, proliferation, and differentiation of mesenchymal stem cells.* Int J Nanomedicine, 2013. **8**: p. 3619-30.
327. Aueviriyavit, S., et al., *Titanium dioxide nanoparticles-mediated in vitro cytotoxicity does not induce Hsp70 and Grp78 expression in human bronchial epithelial A549 cells.* Biol Trace Elem Res, 2012. **149**(1): p. 123-32.
328. Marquez-Ramirez, S.G., et al., *Titanium dioxide nanoparticles inhibit proliferation and induce morphological changes and apoptosis in glial cells.* Toxicology, 2012. **302**(2-3): p. 146-56.
329. Fisichella, M., et al., *Intestinal toxicity evaluation of TiO2 degraded surface-treated nanoparticles: a combined physico-chemical and toxicogenomics approach in caco-2 cells.* Part Fibre Toxicol, 2012. **9**: p. 18.
330. Kim, E., et al., *Decrease of reactive oxygen species-related biomarkers in the tissue-mimic 3D spheroid culture of human lung cells exposed to zinc oxide nanoparticles.* J Nanosci Nanotechnol, 2014. **14**(5): p. 3356-65.
331. Yamaguchi, S., et al., *Novel photodynamic therapy using water-dispersed TiO2-polyethylene glycol compound: evaluation of antitumor effect on glioma cells and spheroids in vitro.* Photochem Photobiol, 2010. **86**(4): p. 964-71.
332. Friedrich, *A reliable tool to determine cell viability in complex 3-D culture: The acid phosphatase assay (Vol 12, pg 925, 2007).* Journal of Biomolecular Screening, 2007. **12**(8): p. 1115-1119.
333. Shinto, H., et al., *Adhesion of melanoma cells to the surfaces of microspheres studied by atomic force microscopy.* Colloids Surf B Biointerfaces, 2012. **91**: p. 114-21.
334. Fujita, K., et al., *Effects of ultrafine TiO2 particles on gene expression profile in human keratinocytes without illumination: involvement of extracellular matrix and cell adhesion.* Toxicol Lett, 2009. **191**(2-3): p. 109-17.
335. Freese, C., et al., *In vitro investigation of silica nanoparticle uptake into human endothelial cells under physiological cyclic stretch.* Part Fibre Toxicol, 2014. **11**(1): p. 1.

336. Steinritz, D., et al., *Use of the Cultex(R) Radial Flow System as an in vitro exposure method to assess acute pulmonary toxicity of fine dusts and nanoparticles with special focus on the intra- and inter-laboratory reproducibility.* Chem Biol Interact, 2013. **206**(3): p. 479-90.
337. Mahto, S.K., T.H. Yoon, and S.W. Rhee, *A new perspective on in vitro assessment method for evaluating quantum dot toxicity by using microfluidics technology.* Biomicrofluidics, 2010. **4**(3).
338. Ucciferri, N., et al., *In vitro toxicological screening of nanoparticles on primary human endothelial cells and the role of flow in modulating cell response.* Nanotoxicology, 2014. **8**(6): p. 697-708.
339. Ditto, A.J., et al., *The Interactions between L-tyrosine based nanoparticles decorated with folic acid and cervical cancer cells under physiological flow.* Mol Pharm, 2012. **9**(11): p. 3089-98.
340. Xia, L., et al., *Laminar-flow immediate-overlay hepatocyte sandwich perfusion system for drug hepatotoxicity testing.* Biomaterials, 2009. **30**(30): p. 5927-36.
341. Fede, C., et al., *Evaluation of gold nanoparticles toxicity towards human endothelial cells under static and flow conditions.* Microvasc Res, 2015. **97**: p. 147-55.
342. Park, J., Z. Fan, and C.X. Deng, *Effects of shear stress cultivation on cell membrane disruption and intracellular calcium concentration in sonoporation of endothelial cells.* J Biomech, 2011. **44**(1): p. 164-9.
343. Ying, B., et al., *Mechanical strain-induced c-fos expression in pulmonary epithelial cell line A549.* Biochem Biophys Res Commun, 2006. **347**(1): p. 369-72.
344. Conant, C., Nevill JT, Ionescu-Zanetti Cristian, *Live Cell Analysis Under Shear Flow.* Micofluidic Cell Culture Systems, 2013.
345. Sambale, F., et al., *Three dimensional spheroid cell culture for nanoparticle safety testing.* J Biotechnol, 2015.
346. Sambale F., et al., *Advanced Cellular Screening System for Nanoparticle Safety Testing.* Submitted to Environmental Science: Nano, 2015.
347. Dechsakulthorn, F., et al., *In vitro cytotoxicity assessment of selected nanoparticles using human skin fiborblasts.* AATEX, 2007. **14**(Special Issue): p. 397-400.
348. Fernández, D., C. García-Gómez, and M. Babín, *In vitro evaluation of cellular responses induced by ZnO nanoparticles, zinc ions and bulk ZnO in fish cells.* Science of The Total Environment, 2013. **452–453**(0): p. 262-274.
349. Lin, W., et al., *Toxicity of nano- and micro-sized ZnO particles in human lung epithelial cells.* Journal of Nanoparticle Research, 2009. **11**(1): p. 25-39.
350. Kao, Y.Y., et al., *Zinc Oxide Nanoparticles Interfere With Zinc Ion Homeostasis to Cause Cytotoxicity.* Toxicological Sciences, 2012. **125**(2): p. 462-472.
351. Li, J., et al., *The Photodynamic Effect of Different Size ZnO Nanoparticles on Cancer Cell Proliferation In Vitro.* Nanoscale Research Letters, 2010. **5**(6): p. 1063-1071.
352. Hanley, C., et al., *The Influences of Cell Type and ZnO Nanoparticle Size on Immune Cell Cytotoxicity and Cytokine Induction.* Nanoscale Research Letters, 2009. **4**(12): p. 1409 - 1420.
353. Heng, B., et al., *Evaluation of the cytotoxic and inflammatory potential of differentially shaped zinc oxide nanoparticles.* Archives of Toxicology, 2011. **85**(12): p. 1517-1528.
354. Zhang, H., et al., *Use of Metal Oxide Nanoparticle Band Gap To Develop a Predictive Paradigm for Oxidative Stress and Acute Pulmonary Inflammation.* ACS Nano, 2012. **6**(5): p. 4349-4368.
355. Tang, Z., et al., *Shear stress-dependent cell detachment from temperature-responsive cell culture surfaces in a microfluidic device.* Biomaterials, 2012. **33**(30): p. 7405-11.
356. Gamerdinger, K., et al., *Mechanical load and mechanical integrity of lung cells - Experimental mechanostimulation of epithelial cell- and fibroblast-monolayers.* Journal of the Mechanical Behavior of Biomedical Materials, 2014. **40**: p. 201-209.
357. Chivukula, V.K., et al., *Alterations in cancer cell mechanical properties after fluid shear stress exposure: a micropipette aspiration study.* Cell health and cytoskeleton, 2015. **7**: p. 25-35.
358. Hattori, K., et al., *Microfluidic perfusion culture chip providing different strengths of shear stress for analysis of vascular endothelial function.* Journal of Bioscience and Bioengineering, 2014. **118**(3): p. 327-332.

359. Fulda, S., et al., *Cellular stress responses: cell survival and cell death.* Int J Cell Biol, 2010. **2010**: p. 214074.
360. Di Virgilio, A.L., et al., *Comparative study of the cytotoxic and genotoxic effects of titanium oxide and aluminium oxide nanoparticles in Chinese hamster ovary (CHO-K1) cells.* J Hazard Mater, 2010. **177**(1-3): p. 711-8.
361. Weber, D., et al., *Functionalized ZnO nanoparticles for thin-film transistors: support of ligand removal by non-thermal methods.* Journal of Materials Chemistry C, 2013. **1**(18): p. 3098-3103.
362. Baghery, P., et al., *Ni–TiO2 nanocomposite coating with high resistance to corrosion and wear.* Surface and Coatings Technology, 2010. **204**(23): p. 3804-3810.
363. Lakshmi, R.V., T. Bharathidasan, and B.J. Basu, *Superhydrophobic sol–gel nanocomposite coatings with enhanced hardness.* Applied Surface Science, 2011. **257**(24): p. 10421-10426.
364. Yaghoubi, H., N. Taghavinia, and E.K. Alamdari, *Self cleaning TiO2 coating on polycarbonate: Surface treatment, photocatalytic and nanomechanical properties.* Surface and Coatings Technology, 2010. **204**(9–10): p. 1562-1568.
365. Metreveli, G., A. Philippe, and G.E. Schaumann, *Disaggregation of silver nanoparticle homoaggregates in a river water matrix.* Sci Total Environ, 2014.
366. Yao, D., et al., *Limitation and Challenge Faced to the Researches on Environmental Risk of Nanotechnology.* Procedia Environmental Sciences, 2013. **18**(0): p. 149-156.
367. Haufe, H. and G. Risse, *Hydrophile Schicht und Verfahren zur Herstellung der Schicht*, 2011, Google Patents.
368. Morrison, C., et al., *In vitro biocompatibility testing of polymers for orthopaedic implants using cultured fibroblasts and osteoblasts.* Biomaterials, 1995. **16**(13): p. 987-92.
369. Paddle-Ledinek, J.E., Z. Nasa, and H.J. Cleland, *Effect of different wound dressings on cell viability and proliferation.* Plast Reconstr Surg, 2006. **117**(7 Suppl): p. 110S-118S; discussion 119S-120S.
370. Kejlova, K., et al., *Hydrophilic polymers--biocompatibility testing in vitro.* Toxicol In Vitro, 2005. **19**(7): p. 957-62.
371. Dahl, J.E., M.J. Frangou-Polyzois, and G.L. Polyzois, *In vitro biocompatibility of denture relining materials.* Gerodontology, 2006. **23**(1): p. 17-22.
372. Mitzner, E., et al., *Material Properties and In Vitro Biocompatibility of a Newly Developed Bone Cement.* Materials Research-Ibero-American Journal of Materials, 2009. **12**(4): p. 447-454.
373. Barth, N., C. Schilde, and A. Kwade, *Influence of Particle Size Distribution on Micromechanical Properties of thin Nanoparticulate Coatings.* Physics Procedia, 2013. **40**: p. 9-18.
374. Ramachandran, K.M. and C.P. Tsokos, *Chapter 10 - Analysis of Variance*, in *Mathematical Statistics with Applications in R (Second Edition)*, K.M.R.P. Tsokos, Editor. 2015, Academic Press: Boston. p. 495-547.
375. Schilde, C., I. Kampen, and A. Kwade, *Dispersion kinetics of nano-sized particles for different dispersing machines.* Chemical Engineering Science, 2010. **65**(11): p. 3518-3527.
376. Schilde, C., et al., *Grinding kinetics of nano-sized particles for different electrostatic stabilizing acids in a stirred media mill.* Powder Technology, 2013. **235**(3): p. 1008-1016.
377. Becker, M., A. Kwade, and J. Schwedes, *Stress intensity in stirred media mills and its effect on specific energy requirement.* Int. J. Miner. Process., 2001. **61**(3): p. 189-208.
378. Kwade, A. and J. Schwedes, *Breaking charakteristics of different materials and their effect on stress intensity and stress number in stirred media mills.* Powder Technology, 2002. **122**: p. 109-121.
379. Kwade, A. and J. Schwedes, *Wet grinding in stirred media mills.* Handbook of Powder Technology : Particle Breakage, 2007. **12**(chapter 6): p. 251-382.
380. Schilde, C., et al., *Efficiency of different dispersing devices for dispersing nanosized silica and alumina.* Powder Technology, 2011. **207**(1–3): p. 353-361.
381. Schilde, C., C. Arlt, and A. Kwade, *Einfluss des Dispergierprozesses bei der Herstellung nanopartikelverstärkter Verbundwerkstoffe.* Chemie Ingenieur Technik, 2009. **81**(6): p. 775-783.

382. Knieke, C., et al., *Nanoparticle Production with Stirred-Media Mills: Opportunities and Limits.* Chemical Engineering & Technology, 2010. **33**(9): p. 1401-1411.
383. Schönstedt, B., *Dispergierung pyrogener Nanopartikel und deren Anwendung in dünnen Sol-Gel-Schichten*, ed. A. Kwade. 2012.
384. Zhou, X.B. and J.T.M. De Hosson, *Influence of surface roughness on the wetting angle.* Journal of Materials Research, 1995. **10**(08): p. 1984-1992.
385. Miller, J.D., et al., *Effect of roughness as determined by atomic force microscopy on the wetting properties of PTFE thin films.* Polymer Engineering & Science, 1996. **36**(14): p. 1849-1855.
386. Cho, J., M.S. Joshi, and C.T. Sun, *Effect of inclusion size on mechanical properties of polymeric composites with micro and nano particles.* Composites Science and Technology, 2006. **66**(13): p. 1941-1952.
387. Carlson, G.P., M. Turner, and N.A. Mantick, *Effects of styrene and styrene oxide on glutathione-related antioxidant enzymes.* Toxicology, 2006. **227**(3): p. 217-226.
388. Carlson, G.P., *Modification of the metabolism and toxicity of styrene and styrene oxide in hepatic cytochrome P450 reductase deficient mice and CYP2F2 deficient mice.* Toxicology, 2012. **294**(2-3): p. 104-108.
389. Cruzan, G., et al., *Studies of styrene, styrene oxide and 4-hydroxystyrene toxicity in CYP2F2 knockout and CYP2F1 humanized mice support lack of human relevance for mouse lung tumors.* Regulatory Toxicology and Pharmacology, 2013. **66**(1): p. 24-29.
390. Roder-Stolinski, C., et al., *Styrene induces an inflammatory response in human lung epithelial cells via oxidative stress and NF-kappa B activation.* Toxicology and Applied Pharmacology, 2008. **231**(2): p. 241-247.
391. Pampaloni, F., E.G. Reynaud, and E.H.K. Stelzer, *The third dimension bridges the gap between cell culture and live tissue.* Nature Reviews Molecular Cell Biology, 2007. **8**(10): p. 839-845.
392. Stevens, M.M., *Testing in the third dimension.* Nature Nanotechnology, 2009. **4**(6): p. 342-343.
393. da Rocha, E.L., L.M. Porto, and C.R. Rambo, *Nanotechnology meets 3D in vitro models: Tissue engineered tumors and cancer therapies.* Materials Science & Engineering C-Materials for Biological Applications, 2014. **34**: p. 270-279.
394. Griffith, L.G. and M.A. Swartz, *Capturing complex 3D tissue physiology in vitro.* Nature Reviews Molecular Cell Biology, 2006. **7**(3): p. 211-224.
395. Kim, E., et al., *Decrease of Reactive Oxygen Species-Related Biomarkers in the Tissue-Mimic 3D Spheroid Culture of Human Lung Cells Exposed to Zinc Oxide Nanoparticles.* Journal of Nanoscience and Nanotechnology, 2014. **14**(5): p. 3356-3365.
396. Elliott, N.T. and F. Yuan, *A Review of Three-Dimensional In Vitro Tissue Models for Drug Discovery and Transport Studies.* Journal of Pharmaceutical Sciences, 2011. **100**(1): p. 59-74.
397. Ivascu, A. and M. Kubbies, *Rapid generation of single-tumor spheroids for high-throughput cell function and toxicity analysis.* Journal of Biomolecular Screening, 2006. **11**(8): p. 922-932.
398. Zhang, X.L., et al., *Development of an in vitro multicellular tumor spheroid model using microencapsulation and its application in anticancer drug screening and testing.* Biotechnology Progress, 2005. **21**(4): p. 1289-1296.
399. Goodman, T.T., C.P. Ng, and S.H. Pun, *3-D Tissue Culture Systems for the Evaluation and Optimization of Nanoparticle-Based Drug Carriers.* Bioconjugate Chemistry, 2008. **19**(10): p. 1951-1959.
400. Li, Z.H. and Z.F. Cui, *Three-dimensional perfused cell culture.* Biotechnology Advances, 2014. **32**(2): p. 243-254.
401. Akin, M., et al., *PAMAM-functionalized water soluble quantum dots for cancer cell targeting.* Journal of Materials Chemistry, 2012. **22**(23): p. 11529-11536.
402. Tang, R., et al., *Tunable Ultrasmall Visible-to-Extended Near-Infrared Emitting Silver Sulfide Quantum Dots for Integrin-Targeted Cancer Imaging.* ACS Nano, 2015. **9**(1): p. 220-30.
403. Probst, C.E., et al., *Quantum dots as a platform for nanoparticle drug delivery vehicle design.* Adv Drug Deliv Rev, 2013. **65**(5): p. 703-18.

404. Ulusoy, M., et al., *One-pot aqueous synthesis of highly strained CdTe/CdS/ZnS nanocrystals and their interactions with cells.* RSC Advances, 2015. **5**: p. 7485-7494.
405. Rogach, A.L. and M. Ogris, *Near-infrared-emitting semiconductor quantum dots for tumor imaging and targeting.* Curr Opin Mol Ther, 2010. **12**(3): p. 331-9.
406. Chang, P., et al., *Multi-therapeutic effects of human adipose-derived mesenchymal stem cells on radiation-induced intestinal injury.* Cell Death & Disease, 2013. **4**.
407. Ivanov, D.P., et al., *Multiplexing Spheroid Volume, Resazurin and Acid Phosphatase Viability Assays for High-Throughput Screening of Tumour Spheroids and Stem Cell Neurospheres.* Plos One, 2014. **9**(8).
408. Asthana, A. and W.S. Kisaalita, *Microtissue size and hypoxia in HTS with 3D cultures.* Drug Discovery Today, 2012. **17**(15-16): p. 810-817.
409. Gao, Y., et al., *Predictive Models of Diffusive Nanoparticle Transport in 3-Dimensional Tumor Cell Spheroids.* Aaps Journal, 2013. **15**(3): p. 816-831.
410. Lee, J., et al., *In vitro Toxicity Testing of Nanoparticles in 3D Cell Culture.* Small, 2009. **5**(10): p. 1213-1221.
411. Lieleg, O., et al., *Specific Integrin Labeling in Living Cells Using Functionalized Nanocrystals.* Small, 2007. **3**(9): p. 1560-1565.
412. Docheva, D., et al., *Human mesenchymal stem cells in contact with their environment: surface characteristics and the integrin system.* Journal of Cellular and Molecular Medicine, 2007. **11**(1): p. 21-38.
413. Shinto, H., et al., *Adhesion of melanoma cells to the surfaces of microspheres studied by atomic force microscopy.* Colloids and Surfaces B-Biointerfaces, 2012. **91**: p. 114-121.
414. Lesniak, A., et al., *Nanoparticle Adhesion to the Cell Membrane and Its Effect on Nanoparticle Uptake Efficiency.* Journal of the American Chemical Society, 2013. **135**(4): p. 1438-1444.
415. Brakebusch, C., et al., *Integrins in invasive growth.* Journal of Clinical Investigation, 2002. **109**(8): p. 999-1006.
416. Heckmann, L., et al., *Mesenchymal progenitor cells communicate via alpha and beta integrins with a three-dimensional collagen type I matrix.* Cells Tissues Organs, 2006. **182**(3-4): p. 143-154.
417. Liu, Z.X., et al., *Effects of Internalized Gold Nanoparticles with Respect to Cytotoxicity and Invasion Activity in Lung Cancer Cells.* Plos One, 2014. **9**(6).
418. Worle-Knirsch, J.M., K. Pulskamp, and H.F. Krug, *Oops they did it again! Carbon nanotubes hoax scientists in viability assays.* Nano Letters, 2006. **6**(6): p. 1261-1268.
419. Tsoi, K.M., et al., *Are Quantum Dots Toxic? Exploring the Discrepancy Between Cell Culture and Animal Studies.* Accounts of Chemical Research, 2013. **46**(3): p. 662-671.
420. Friedrich, J., et al., *A reliable tool to determine cell viability in complex 3-D culture: The acid phosphatase assay.* Journal of Biomolecular Screening, 2007. **12**(7): p. 925-937.
421. Monteiro-Riviere, N.A., A.O. Inman, and L.W. Zhang, *Limitations and relative utility of screening assays to assess engineered nanoparticle toxicity in a human cell line.* Toxicology and Applied Pharmacology, 2009. **234**(2): p. 222-235.
422. Nascarella, M.A. and E.J. Calabrese, *A Method to Evaluate Hormesis in Nanoparticle Dose-Responses.* Dose-Response, 2012. **10**(3): p. 344-354.
423. Guo, Y.Y., et al., *Cytotoxic and genotoxic effects of multi-wall carbon nanotubes on human umbilical vein endothelial cells in vitro.* Mutation Research-Genetic Toxicology and Environmental Mutagenesis, 2011. **721**(2): p. 184-191.
424. Jan, E., et al., *High-content screening as a universal tool for fingerprinting of cytotoxicity of nanoparticles.* Acs Nano, 2008. **2**(5): p. 928-938.
425. Iavicoli, I., E.J. Calabrese, and M.A. Nascarella, *Exposure to Nanoparticles and Hormesis.* Dose-Response, 2010. **8**(4): p. 501-517.
426. O'Brien, J., et al., *Investigation of the Alamar Blue (resazurin) fluorescent dye for the assessment of mammalian cell cytotoxicity.* European Journal of Biochemistry, 2000. **267**(17): p. 5421-5426.
427. Romoser, A., et al., *Mitigation of Quantum Dot Cytotoxicity by Microencapsulation.* Plos One, 2011. **6**(7).

428. Breznan, D., et al., *Non-specific interaction of carbon nanotubes with the resazurin assay reagent: Impact on in vitro assessment of nanoparticle cytotoxicity.* Toxicology in Vitro, 2015. **29**(1): p. 142-147.
429. Gloeckner, H., T. Jonuleit, and H.D. Lemke, *Monitoring of cell viability and cell growth in a hollow-fiber bioreactor by use of the dye Alamar Blue (TM).* Journal of Immunological Methods, 2001. **252**(1-2): p. 131-138.
430. Albrecht, D.R., et al., *Probing the role of multicellular organization in three-dimensional microenvironments.* Nature Methods, 2006. **3**(5): p. 369-375.
431. Bokhari, M., et al., *Culture of HepG2 liver cells on three dimensional polystyrene scaffolds enhances cell structure and function during toxicological challenge.* Journal of Anatomy, 2007. **211**(4): p. 567-576.
432. Oishi, M., et al., *Enhanced growth inhibition of hepatic multicellular tumor spheroids by lactosylated poly(ethylene glycol)-siRNA conjugate formulated in PEGylated polyplexes.* Chemmedchem, 2007. **2**(9): p. 1290-1297.
433. Mueller, D., et al., *3D organotypic HepaRG cultures as in vitro model for acute and repeated dose toxicity studies.* Toxicology in Vitro, 2014. **28**(1): p. 104-112.
434. Hauck, T.S., et al., *In vivo Quantum-Dot Toxicity Assessment.* Small, 2010. **6**(1): p. 138-144.
435. Chou, L.Y.T. and W.C.W. Chan, *NANOTOXICOLOGY No signs of illness.* Nature Nanotechnology, 2012. **7**(7): p. 416-417.
436. Nurunnabi, M., et al., *In Vivo Biodistribution and Toxicology of Carboxylated Graphene Quantum Dots.* Acs Nano, 2013. **7**(8): p. 6858-6867.
437. Charwat, V., et al., *Potential and limitations of microscopy and Raman spectroscopy for live-cell analysis of 3D cell cultures.* J Biotechnol, 2015. **205**: p. 70-81.
438. Seyednejad, H., et al., *Topical haemostatic agents.* Br J Surg, 2008. **95**(10): p. 1197-225.
439. Robinson, K., *Controlling bleeding in the field: hemostatic powders and dressings debut in the prehospital setting.* J Emerg Nurs, 2004. **30**(2): p. 160-1.
440. Hanke, A.A., et al., *Effects of a New Microporous Polysaccharide Powder on Viscoelastic Characteristics of Clot Formation*, in *Anesthesiology 2011, American Society of Anesthesiologists Annual Meeting*2011: Chicago.
441. Bjorses, K. and J. Holst, *Various local hemostatic agents with different modes of action; an in vivo comparative randomized vascular surgical experimental study.* European Journal of Vascular and Endovascular Surgery, 2007. **33**(3): p. 363-370.
442. Hirschelmann, A., et al., *A review of the problematic adhesion prophylaxis in gynaecological surgery.* Arch Gynecol Obstet, 2012. **285**(4): p. 1089-97.
443. Menzies, D. and H. Ellis, *Intestinal obstruction from adhesions - how big is the problem?* Ann R Coll Surg Engl, 1990. **72**(1): p. 60-63.
444. Ray, N.F., et al., *Abdominal adhesiolysis: inpatient care and expenditures in the United States in 1994.* J Am Coll Surg, 1998. **186**(1): p. 1–9.
445. Kamel, R.M., *Prevention of postoperative peritoneal adhesions.* Eur J Obstet Gynecol Reprod Biol, 2010. **150**(2): p. 111-118.
446. Korell, M., *Combined Hemostasis and Adhesion Prevention with the Novel Agent 4DryField® PH—Initial Observations.* Surgical Science, 2014. **05**(12): p. 533-539.
447. Pöhnert, D., et al., *Marked reduction of peritoneal adhesion formation in rat model of cecal abrasion by a novel anti-adhesive agent, 4DryField® PH*, in *131st Congress of the German Society for Surgery*, J. Jähne, Editor 2014, Langenbecks Arch Surg: Berlin (Germany). p. 371-413.
448. Pöhnert, D., et al., *High reproducibility of adhesion formation in rat with meso-stich approximation of injured cecum and abdominal wall.* Int J Med Sci, 2015. **12**(1): p. 1-6.
449. Gao, H.W., et al., *Oxidized cellulose (Surgicel (TM)) granuloma mimicking a primary ovarian tumor.* International Journal of Gynecological Pathology, 2002. **21**(4): p. 422-423.
450. Henry, M.C.W., et al., *Postoperative paraplegia secondary to the use of oxidized cellulose (Surgicel).* Journal of Pediatric Surgery, 2005. **40**(4): p. E9-E13.
451. Ibrahim, M.F., C. Aps, and C.P. Young, *A foreign body reaction to Surgicel® mimicking an abscess following cardiac surgery.* European Journal of Cardio-Thoracic Surgery, 2002. **22**(3): p. 489-490.

452. Iwabuchi, S., et al., *Iatrogenic paraplegia caused by Surgicel used for hemostasis during a thoracotomy: Report of a case.* Surgery Today-the Japanese Journal of Surgery, 1997. **27**(10): p. 969-970.
453. Sandhu, G.S., J.A. ElexpuruCamiruaga, and S. Buckley, *Oxidized cellulose (Surgicel®) granulomata mimicking tumour recurrence.* British Journal of Neurosurgery, 1996. **10**(6): p. 617-619.
454. Ereth, M.H., et al., *Comparative Safety and Efficacy of Topical Hemostatic Agents in a Rat Neurosurgical Model.* Neurosurgery, 2008. **63**(4): p. 369-372.
455. Schonauer, C., et al., *The use of local agents: bone wax, gelatin, collagen, oxidized cellulose.* European Spine Journal, 2004. **13**: p. S89-S96.
456. Zwischenberger, J.B., et al., *Comparison of two topical collagen-based hemostatic sponges during cardiothoracic procedures.* Journal of Investigative Surgery, 1999. **12**(2): p. 101-106.
457. Rothwell, S.W., et al., *Wound healing and the immune response in swine treated with a hemostatic bandage composed of salmon thrombin and fibrinogen.* Journal of Materials Science-Materials in Medicine, 2009. **20**(10): p. 2155-2166.
458. Barbolt, T.A., et al., *Pre-clinical subdural tissue reaction and absorption study of absorbable hemostatic devices.* Neurological Research, 2001. **23**(5): p. 537-542.
459. Yuen, T. and A.H. Kaye, *Persistence of Bioglue® in spinal dural repair.* Journal of Clinical Neuroscience, 2005. **12**(1): p. 100-101.
460. diZerega, G.S. and J.D. Campeau, *Peritoneal repair and post-surgical adhesion formation.* Hum Reprod Update, 2001. **7**(6): p. 547–555.
461. Funke, M., et al., *The baffled microtiter plate: increased oxygen transfer and improved online monitoring in small scale fermentations.* Biotechnol Bioeng, 2009. **103**(6): p. 1118-28.
462. Grote, K.-H. and E.K. Antonsson, *Springer Handbook of Mechanical Engineering* 2009, New York: Springer 1580.
463. (NSAI), N.S.A.o.I., *Biological evaluation of medical devices—part 5: Tests for in vitro cytotoxicity (ISO 10993–5:2009).* 2009.
464. Lücking, T.H., et al., *3D-printed individual labware in biosciences by rapid prototyping: A proof of principle.* Engineering in Life Sciences, 2015. **15**(1): p. 51-56.
465. Upcraft, S. and R. Fletcher, *The rapid prototyping technologies.* Assem. Autom, 2003. **23**: p. 318-330.
466. Cheah, C.M., et al., *Rapid prototyping and tooling techniques: A review of applications for rapid investment casting.* Int. J. Adv.Manuf. Technol, 2004. **25**: p. 308-320.
467. Rawlings, B. and H. Pora, *Environmental impact of single-use and reusable bioprocess systems.* BioProcess Int., 2009. **2**: p. 18-25.
468. Jacobs, G., *A review of the effects of gamma radiation on pharmaceutical materials.* J. Biomater. Appl, 1995. **10**: p. 59-96.
469. Halliwell, B., *Oxidative stress in cell culture: An underappreciated problem?* FEBS Lett, 2003. **540**: p. 3-6.
470. Gutteridge, J.M.C. and B. Halliwell, *Free radicals andantioxidants in the year 2000: A historical look to the future.* Ann. N Y Acad. Sci., 2006. **899**: p. 136-147.
471. Halliwell, B., *Biochemistry of oxidative stress.* Biochem. Soc. Trans., 2007. **35**: p. 1147-1150.
472. Deckard, C., *Apparatus for producing parts by selective sintering*, in *US Patent 56390701*997.
473. Allison, J., C. Childers, and C. Hull, *Method of making a threedimensional object by stereolithography*, in *US Patent 56098121*993.
474. Lewis, M., F. Little, and R. Pitlak, *Rapid and accurate production of stereolithographic parts*, in *US Patent 56108241*997.
475. Comb, J. and S. Crump, *Process of support removal for fused deposition modeling*, in *US Patent 55037851*996.
476. Hull, C., P. Jacobs, and K. Schmidt, *Method of building three dimensional objects with sheets*, in *US Patent 56371691*997.
477. Deckard, C., *Method for producing parts by selective sintering*, in *US Patent 56390701*997.
478. Anderson, R., D. Barnes, and E. Sitzmann, *Increasing the useful range of cationic photoinitiators in stereolithography*, in *US Patent 54946181*996.
479. Almquist, T., A. Cohen, and C. Hull, *Recoating of stereolithographic layers*, in *US Patent 56519341*997.

480. Brown, R., C. Kirschman, and H. Menhennett, *Apparatus and method for thermal normalization in three-dimensional article manufacturing*, in *US Patent 55724311*996.
481. Khoshevis, B., *Additive fabrication apparatus and method*, in *US Patent 55294711*996.
482. Forderhase, P. and M. Ganninger, *Selective laser sinteringwith composite plastic material,*, in *US Patent 57334971*998.
483. Hull, C., *Method for production of three-dimensional objects by stereolithography*, in *US Patent 57628561*990.
484. Berman, B., *3-D printing: The new industrial revolution.* Bus. Horiz., 2012. **55**: p. 155–162.
485. Eibl, R. and D. Eibl, *Single-use Technology in Biopharmaceutical Manufacture.* JohnWiley & Sons, Hoboken, 2010: p. 1-5.
486. Eibl, R., S. Werner, and D. Eibl, *Disposable bioreactors for plant liquid cultures at Litre-scale.* Eng. Life Sci., 2009. **9**: p. 156-553.
487. Bluma, A., et al., *Process analytical sensors and image-based techniques for singleuse bioreactors.* Eng. Life Sci., 2011. **11**: p. 550–553.
488. Fang, J.-J., et al., *Complex facial deformity reconstruction with a surgical guide incorporating a built-in occlusal stent as the positioning reference.* J. Craniofac. Surg Obes Relat Dis, 2013. **24**: p. e260–e265.
489. Webb, P.A., *A review of rapid prototyping (RP) techniques in the medical and biomedical sector.* J. Med. Eng. Technol., 2000. **24**: p. 149–153.
490. Azari, A. and S. Nikzad, *The evolution of rapid prototyping in dentistry: A review.* Rapid Prototyp. J., 2009. **15**: p. 216–225.
491. Peltola, S.M., et al., *Areview of rapid prototyping techniques for tissue engineering purposes.* Ann. Med., 2008. **40**: p. 268–280.
492. Landers, R., et al., *Fabrication of soft tissue engineering scaffolds by means of rapid prototyping techniques.* J. Mater. Sci., 2002. **37**: p. 3107–3116.
493. Tan, K.H., et al., *Selective laser sintering of biocompatible polymers for applications in tissue engineering,.* Biomed. Mater. Eng., 2005. **15**: p. 113–124.
494. Murphy, S.V., A. Skardal, and A. Atala, *Evaluation of hydrogels for bio-printing applications.* J. Biomed. Mater. Res. A, 2013. **101**: p. 272–284.
495. Wang, X., Y. Yan, and R. Zhang, *Rapid prototyping as a tool for manufacturing bioartificial livers.* Trends Biotechnol, 2007. **25**: p. 505–513.
496. Tsang, V.L. and S.N. Bhatia, *Three-dimensional tissue fabrication.* Adv. Drug Deliv. Rev., 2004. **56**: p. 1635–1647.
497. Lee, J.-Y., et al., *Customized biomimetic scaffolds created by indirect three-dimensional printing for tissue engineering.* Biofabrication 2013, 2013. **5**: p. 045003. doi: 10.1088/1758-5082/5/4/045003.
498. Derby, B., *Printing and prototyping of tissues and scaffolds.* Science, 2012. **338**: p. 921–926.
499. Luo, Y., A.R. Akkineni, and M. Gelinsky, *Three-dimensional plotting is a versatile rapid prototyping method for the customized manufacturing of complex scaffolds and tissue engineering constructs.* Zhongguo Xiu Fu Chong Jian Wai Ke Za Zhi, 2014. **28**: p. 279-285.
500. El-Sherbiny, I. and M. Yacoub, *Hydrogel scaffolds for tissue engineering: Progress and challenges.* Glob. Cardiol. Sci. Pract. 2013, 2013: p. 316–342.
501. Billiet, T., et al., *A review of trends and limitations in hydrogelrapid prototyping for tissue engineering.* Biomaterials, 2012. **33**: p. 6020–6041.
502. McDonald, J.C., et al., *Prototyping of microfluidic devices in poly(dimethylsiloxane) using solid-object printing.* Anal. Chem., 2002. **74**: p. 1537–1545.
503. Moore, J.L., et al., *Behavior of capillary valves in centrifugal microfluidic devices prepared by three-dimensional printing.* Microfluid. Nanofluidics, 2010. **10**: p. 877–888.
504. Symes, M.D., et al., *Integrated 3D-printed reactionware for chemical synthesis and analysis.* Nat. Chem., 2012. **4**: p. 349–354.
505. Sachs, E., M. Cima, and J. Cornie, *Three-dimensional printing: Rapid tooling and prototypes directly from a CAD model.* CIRP Ann. Manuf. Technol., 1990. **39**: p. 201–204.
506. Pham, D. and R. Gault, *A comparison of rapid prototyping technologies.* Int. J. Mach. Tools Manuf., 1998. **38**: p. 1257–1287.
507. Chen, Y.H., C. Ng, and Y. Wang, *Data reduction in integrated reverse engineering and rapid prototyping.* Int. J. Comput. Integr. Manuf., 1999. **12**: p. 97–103.

508. Chua, C.K., et al., *Rapid prototyping: Principles and applications.* World Scientific,Hackensack, 2010: p. 301-357.
509. Gibson, I. and D. Shi, *Material properties and fabrication parameters in selective LASER sintering process.* Rapid Prototyp. J., 1997. **3**: p. 129–136.
510. Lücking, T.H., et al., *3D-printed individual labware in biosciences by rapid prototyping: In vitro biocompatibility and applications for eukaryotic cell cultures.* Eng. Life Sci., 2015. **15**: p. 57–64.
511. Storhas, W., *Bioreaktoren und periphere Einrichtungen*. 1994, Braunschweig: Viewe. 167.

A Anhang

A.1 Evaluation of CdTe/CdS/ZnS core/shell/shell Quantum dot Toxicity on Three-dimensional Spheroids

Mehriban Ulusoy,[a] Antonina Lavrentieva,*[a] Johanna-Gabriela Walter,[a] Franziska Sambale,[a] Frank Stahl,[a] Mark Green[b] and Thomas Scheper[a]

[a] Gottfried Wilhelm Leibniz University of Hannover, Institute of Technical Chemistry, 30167 Hanover, Germany.
[b] King's College London, Department of Physics, The Strand, WC2R 2LS London, UK. Phone: +44 02078482121.

Reprinted from Toxicology Research, 2015, Advance Article (DOI: 10.1039/C5TX00236B) with kind permission from Royal Chemistry Society.

A.1.1 Abstract

In this work, three-dimensional (3D) spheroid cultures of human adipose-derived mesenchymal stem cells (hAD-MSCs), with tissue-mimetic morphology through well developed cell–cell and cell–matrix interactions and distinct diffusion/transport characteristics, were assessed for dose-dependent toxic effects of red-emitting CdTe/CdS/ZnS quantum dots (Qdots). Morphological investigations and time resolved microscopy analysis in addition to cell metabolic activity studies revealed that 3D spheroid cultures are more resistant to Qdot-induced cytotoxicity in comparison to conventional 2D cultures. The obtained results suggest the presence of two distinct cell populations in 2D cultures with different sensitivity to Qdots, however that effect wasn't observed in 3D spheroids. Our investigations were aimed to improve the prediction of nanotoxicity of Qdot on tissue-level and provide the essential screening steps prior to any in vivo application. Moreover, penetration ability of highly fluorescent Qdots to densely packed spheroids will fortify the biological application of developed Qdots in tissue-like structures.

A.1.2 Introduction

Conventional two-dimensional (2D) cell culture where a cell monolayer grows on flat plastic or glass surfaces lacks reflecting essential physiology of real tissues. Since cells in the body grow in three-dimensional (3D) environment, a 3D approach as an alternative to 2D culture can reduce the gap between cell culture and living tissue. Therefore, it exhibits a significant potential to improve the physiological relevance of cell-based assays [391-394]. In many studies, 3D cell cultures were proven to display the induced extracellular matrix (ECM)-related biological functions such intercellular signalling and interactions, cellular function and maintenance, molecular transport, and tissue morphology.[307, 310, 395] Cellular spheroids, being a simplified reductionist model of 3D cell cultures, take advantages of natural tendency of cells to aggregate as a principle.[396] The cells produce ECM which in turn enhances intercellular adhesion. Thus, they don't require an external scaffold for the aggregation of the cells. For that reason, it is the most widely used model for high-

throughput screens for straightforward cell function and toxicity analysis for biomedical applications.[307, 397, 398] For nanoparticle (NP)-based cytotoxicity, labeling and delivery studies, 3D spheroid models hold advantages over monolayer cell cultures.[393] Monolayer cell cultures produce less dense ECM material on apical side whereas cells grown in 3D extend ECM matrix production to all dimensions. Therefore, 2D models present a less significant barrier for transport and reduced cell binding compared to cells in 3D environment.[399] For that reason, results obtained from NP-based research on 2D cell cultures do not reflect similar results as obtained from 3D cultures.

3D models, however, posses some limitations in terms of translation of so far available 2D-based analysis methods to 3D. Yet, cell-based high-throughput screening methods for rapid analysis of drug or NP-based cellular responses such as dose-dependent cell viability, cell migration and cell-cell/cell-matrix interaction haven't been optimized for 3D culture models. Remaining limitations to overcome are scalability, reproducibility, sensitivity and compatibility of analytical methods with available screening systems. Despite the increasing number of publications for 3D-based cell culture studies, optimization of available analytical methods in order to address the nanoparticle and drug interactions remains to be challenging.[400]

Nanocrystals, so-called quantum dot (Qdot) nanoparticles composed of different metal ions, represent one of the most diverse NP class owing to spectacular optical and structural properties which allow for a very wide application area from molecular imaging to targeted drug delivery.[401-403] Very recently, we described one-pot aqueous synthesis of near-infrared emitting CdTe/CdS/ZnS $core_{(small)}/shell_{(thick)}/shell_{(small)}$ CSS Qdots with high quantum yields (~ 64%) as well as great stability against photobleaching.[404] The developed CSS Qdots hold a great potential for cellular imaging studies to owing near-infrared emission, which will allow them to be monitored in thick and highly scattering 3D tissue samples.[405] Regarding heavy metal containing composition of Qdots, it is mandatory to investigate their cytotoxicity prior to any bioapplication. Until now, for almost all studies on Qdot toxicity, 2D cell cultures were assessed for determination of dose-dependent cell viability and therefore it will be an essential step to explore Qdot effects on 3D spheroid models.

In this report, a study was conducted for the first time for evaluation of dose-dependent adverse effects of CdTe/CdS/ZnS $core_{(small)}/shell_{(thick)}/shell_{(small)}$ (CSS) Qdots ($\lambda_{emission}$= 676 nm) on 3D spheroid cultures. As a model system, we utilized human primary adipose-derived human mesenchymal stem cells (hAD-MSCs) spheroid cultures as they are considered to be a promising candidate for cell therapy.[406] Besides, stem cells were found to be more susceptible to Qdot toxicity (IC_{50} 40 µg/ml) in comparison to A549 lung adenocarcinoma cell lines (IC_{50} 150 µg/ml) regarding to our previous study.[404] For that reason, hAD-MSCs were chosen as a suitable candidate to determine Qdot toxicity. The adverse effects of Qdots were examined using two different approaches, including morphology and metabolic activity. Dose-dependent cell viability was determined with two different cell viability assays; CellTiter-Blue (CTB) and adenosine triphosphate (ATP) assay, and results were compared with monolayer 2D cultures. Morphological observations as well as metabolic activity

studies were discussed in details. Our results marked interesting as well as significant findings for that they project physiologically relevant data for Qdot-induced toxicity. We believe that outcomes of this study can contribute to the establishment of analytical methods for nanoparticle based cytotoxicity studies in tissue-like *in vitro* systems. Also, they provide important data to increase our understanding of Qdots toxicity on tissue levels.

A.1.3 Experimental Procedures

A.1.3.1 Materials

$CdCl_2.2^{1/2}$ H_2O (cadmium chloride hemi(pentahydrate), 98%>), Na_2TeO_3 (sodium tellurite, 99.5%), $ZnCl_2$ (zinc chloride, anhydrous, 99.99%), 3-mercaptopropionic acid (MPA, 99%), $NaBH_4$ (sodium borohydride, > 98.0%) and trisodium citrate dehydrate were purchased from Sigma-Aldrich GmbH, Munich. CellTiter-Blue® and CellTiter-Glo® cell viability assay kits were purchased from Promega Corp., USA. For cell culture experiments, Minumum Essential Medium Alpha (MEM-α, Gibco Invitrogen, USA) supplemented with 10% human serum (HS, c.c.pro GmbH, Germany) and 0.5% gentamicin (Biochrom GmbH, Germany) was used as cell culture medium. For 2D cell cultures, 96-well flat bottom standard plates (Sarstedt AG&Co. Germany) and for 3D spheroid cultures, 96-well round bottom plates coated with ultra-low attachment surface (Corning Inc., USA) were used.

A.1.3.2 Synthesis of CdTe/CdS/ZnS Quantum Dots

CdTe/CdS/ZnS Qdot were synthesized as described previously.[404] First, CdTe/CdS Qdot having a $core_{(small)}/shell_{(thick)}$ structure was synthesized as follows: 21 ml ddH_2O, $CdCl_2$ (125 mM, 1 ml), 18.5 µl 3-mercaptopropionic acid (MPA), trisodium citrate dehydrate (42.5 mM, 1 ml), sodium tellurite (5 mM, 1 ml) and sodium borohydride (125 mM, 1 ml) were added sequentially into a three-neck round bottom flask. The molar ratio of Cd/Te/MPA was set to be 1/0.04/1.7. Under mixing, the solution pH was adjusted to 11.4 with 1 M NaOH. The reaction solution was then refluxed with an air condenser (Findenser, Radleys, UK) at 90 °C. When the emission wavelength of CdTe/CdS Qdot reached to 655 ± 5 nm, the nanoparticle growth was stopped by simply cooling the reaction temperature to 4 °C. The as-prepared CdTe/CdS solution was directly used for the external synthesis of ZnS shell. 12 ml of the CdTe/CdS crude solution, 12 ml ddH_2O and 1 ml $ZnCl_2$ solution (25 mM) was added together giving a final volume of 25 ml. The final pH of the reaction solution was adjusted to 11.5 with 1 M NaOH. Then, the solution was heated slowly to 65 °C and the ZnS shell growth was proceeded for 3 h, yielding in CdTe/CdS/ZnS $core_{(small)}/shell_{(thick)}/shell_{(small)}$ Qdot ($\lambda_{emission}$= 676 ± 2 nm, QY_{max} ~ 64%). Later, samples were precipitated with 2-propanol and collected via centrifugation. The colloidal precipitate was weighed after drying under vacuum and re-dissolved in water. For storage, it was washed with ddH_2O using 30 kDa MWCO PES membrane filters (Vivaspin, Sartorius Stedim Biotech GmbH, Germany) and kept at 4 °C. For cell culture applications, Qdots solutions after dilution with culture medium were filtrated with 0.2 µm pore-sized membrane filters for sterilization.

A.1.3.3 Cell Culture and Qdot Treatment

Human adipose-derived mesenchymal stem cells (hAD-MSCs) were isolated from subcutaneous adipose tissues of 3 different patients scheduled for abdominoplasty after obtaining informed written consent, as approved by the Institutional Review Board, project #2251-2014 on 15th May, 2014. The isolated populations have been extensively characterized as mesenchymal stem cells by surface marker analysis and functional properties (differentiation capacity). Cells were cultured with MEM-α medium supplemented with 10 % HS and 0.5 % gentamicin in standard T-175 culture flasks (Sarstedt AG&Co, Germany) until they reached desired sub-confluency (37 ^{o}C, 5% CO_2). After washing with warm PBS, they were detached from the culture flask using Accutase solution (Sigma-Aldrich). Following centrifugation at 300 g for 5 min, cell suspension was collected and the number of viable cells was determined by trypan blue exclusion. For 2D culture, 8000 cells in 100 µl of culture medium were seeded to 96-well flat bottom standard plates. After 24 h of adhesion at 37 ^{o}C, 5% CO_2, medium was replaced with 100 µl of Qdot solutions diluted with culture medium. A control group was treated with fresh culture medium without Qdots. For 3D culture, two different treatment models were applied according to the Qdot exposure time. In the first model, Qdots were introduced to cells after 24 h when they completed spheroid formation (t_{QDOT}= 24 h). The procedure was performed as follows: 3000 cells in 75 µl of culture medium were seeded to 96-well round bottom spheroid plates and incubated for 24 h for spheroid formation. Afterwards, 75 µl of Qdot solutions in culture medium were added to each well and incubated further for another 24 h. In the second model, cells were exposed to Qdots solution at the beginning of spheroid formation (t_{QDOT}= 0 h). The procedure was performed as follows: 3000 cells in 75 µl of culture medium and 75 µl of Qdot solutions in culture medium were seeded together to spheroid well-plates and incubated for 24 h (37 ^{o}C, 5% CO_2).

A.1.3.4 Adenosine Triphosphate (ATP) Assay

ATP assay was performed by using CellTiter-Glo assay kit (Promega Corp., USA) according to manufacturer instructions. Intracellular ATP amount was measured via enzymatic reaction of luciferase in presence of ATP, Mg^{2+} and molecular oxygen. The luminescent signals produced from the reaction are proportional to the amount of ATP present in metabolically active cells. Assay kit enables cell lysis for the release of intracellular ATP for the production of luminescence signal. For 2D cell culture, after removing culture medium, 50 µl CellTiter-Glo stock solution and 50 µl supplement-free MEM-α medium was added to the wells and incubated for 10 minutes (37 ^{o}C, 5% CO_2). For 3D spheroid cultures**,** 75 µl of culture medium was replaced carefully with 75 µl of CellTiter-Glo stock solution and incubated for 2 h under continuous shaking at 250 rpm (37 ^{o}C, 5% CO_2) in order to allow spheroid lysis. The resulting luminescence signals were measured with Perkin-Elmer Wallac Victor 2v HTS Counter 1420.

A.1.3.5 CellTiter-Blue (CTB) Assay

The metabolic activity of viable cells in terms of their reduction capacity of resazurin was measured via CTB assay kit (Promega Corp., USA). For 2D cell culture, culture medium was removed gently and 100 µl of CTB reagent (diluted 1:6 with supplement-free MEM-α medium) was added to each well and incubated for 2 h (37 °C, 5% CO_2). For 3D spheroid cultures, 100 µl of medium was replaced with CTB reagent (diluted 1:4 with supplement-free MEM-α medium, giving a final dilution of 1:6). Spheroids incubated for 48 hours under continuous shaking at 250 rpm (37 °C, 5% CO_2) for the release of fluorescence resorufin dye. The resulting fluorescence intensities ($544_{Ex}/590_{Em}$) were recorded with fluorometer (Fluoroskan Ascent, Thermo Fischer Scientific Inc. USA).

A.1.3.6 Statistical Analysis

Concentration-dependent normalized cell viability data obtained from ATP and CTB assays were fitted from 0 to 100 by using non-linear curve fitting/growth/sigmoidal/dose-response fitting functions (OriginPro 8.6.0 b70, OriginLab Corp. USA). Half-maximal inhibitory concentrations (IC_{50}) were calculated from the fitted dose-response curves. The shown data are from at least two independent experiments, and all individual experiments were conducted with four replicates (n=4). Levene's test was performed first to assess the homogeneity of variance of replicates at the level of 0.01 (α=0.01). Then, one-way analysis of variance (ANOVA) and Tukey tests for the comparisons of mean values of independent groups were performed at the level of 0.01 (OriginPro 8.6.0 b70). A significant effect was reported at * $p < \alpha$ (0.01).

A.1.3.7 Microscopy Studies

Bright field images of spheroids were taken prior to viability assays with inverse microscope (Olympus IX50, Olympus Corp., Japan) using cellSens software (cellSens standard 1.7.1, Olympus). The mean diameter of spheroids was measured using areas of spheroids, assuming they are all spherical, with ImageJ 1.49b software. Time-lapse bright field microscope images of spheroids were captured using 4x objective with LumaScope 600 microscope (Etaluma Inc.,USA).

A.1.4 Results and Discussion

Morphological investigations

Initially, single spheroids in the middle of each well were produced as liquid overlay spheroid cultures in commercially available low-attachment 96 well-plates. Spheroid growth, size and morphology were monitored by means of bright-field and time-lapse microscopy. Spheroid sizes between 100-500 µm have been commonly accepted to form healthy spheroid structure owing to sufficient oxygen and nutrition transport. [407-409] Alternatively, small spheroids (<100 µm) might fail to display complexity of real tissue with little growth rates, whereas large spheroids (>500 µm) might have pronounced necrotic core due to diffusion limitations for oxygen and nutrition.[407] For that reason, we produced intermediate sized spheroids with a mean diameter of 312 µm ± 20 (CV = 6%, n=30) to ensure optimum growth and diffusion rates. The low variation in spheroid size proves the

reproducibility of spheroid formation by using low-attachment 96 well-plates which is one of the most important criteria to obtain reproducible data.

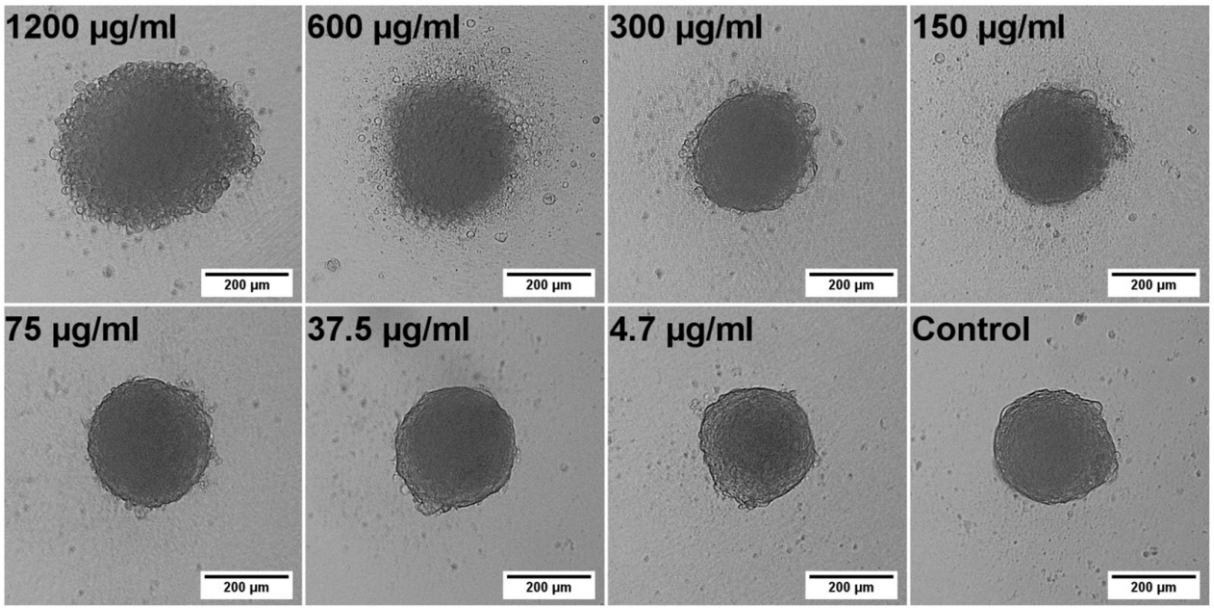

Fig. A.1-1 Bright-field microscope images of hAD-MSCs spheroids treated with different Qdot concentrations for 24 h. The Qdot solutions were introduced to the spheroids after cells were incubated for 24 h for spheroid formation (tQDOT= 24 h). Scale bar is 200 µm.

Following this, we investigated the morphological changes of hAD-MSCs spheroids when they were treated with different Qdot doses, thereby providing initial data on any adverse effects. For that, two different treatment models were performed according to Qdot exposure time. In the first model, cells were exposed to Qdots after 24 h when they formed spheroid (t_{QDOT}= 24 h) in order to investigate the effect of Qdots to spheroids. In the second model, cells were treated with Qdots at the beginning of spheroid formation (t_{QDOT}= 0 h) to observe the Qdots effect on the spheroid formation. Firstly, different Qdots concentrations administrated to hAD-MSCs spheroids after they were incubated for 24 h for spheroid formation (t_{QDOT}= 24 h). Microscope images of spheroids revealed that Qdots induced significant effects to the morphology of hAD-MSCs spheroids with a concentration-dependent manner (Fig. A.1-1). Low Qdot concentrations (<300 µg/ml) didn't illustrate any observable alterations to spheroids whereas higher Qdot doses caused a rough surface formation due to protruding of granular shaped cells. As the Qdot concentration was increased to 1200 µg/ml, increase in surface roughness was pronounced and formation of round cells became obvious, corresponding to a significant increase in cell death. The round cells, however, did not detach from the spheroid, preserving the overall spherical structure, but they increased the diameter of the spheroid by 48%. hAD-MSCs form very tightly packed spheroids. Therefore, tight cell junctions prevent cells to lose their interactions and allow them to remain in the spheroid.[410] Time-lapse microscope images of hAD-MSCs spheroid treated with 1200 µg/ml Qdots are given in Fig. A.1-5 (see also ESI†, Video S1). After 3h of Qdot exposure, cells started to slowly morph to granular shape and to swell outward the spheroid forming a rugged surface, resulting in a concomitant increase in spheroid diameter.

Interestingly, the increase in spheroid diameter showed a linear relationship for exposure times in the range of 2 h- 8 h (Adj. R^2= 0.977). After 8 h of exposure, the increase in diameter slowed down and reached a plateau until 20 h (see ESI†, Fig. A.1-6).

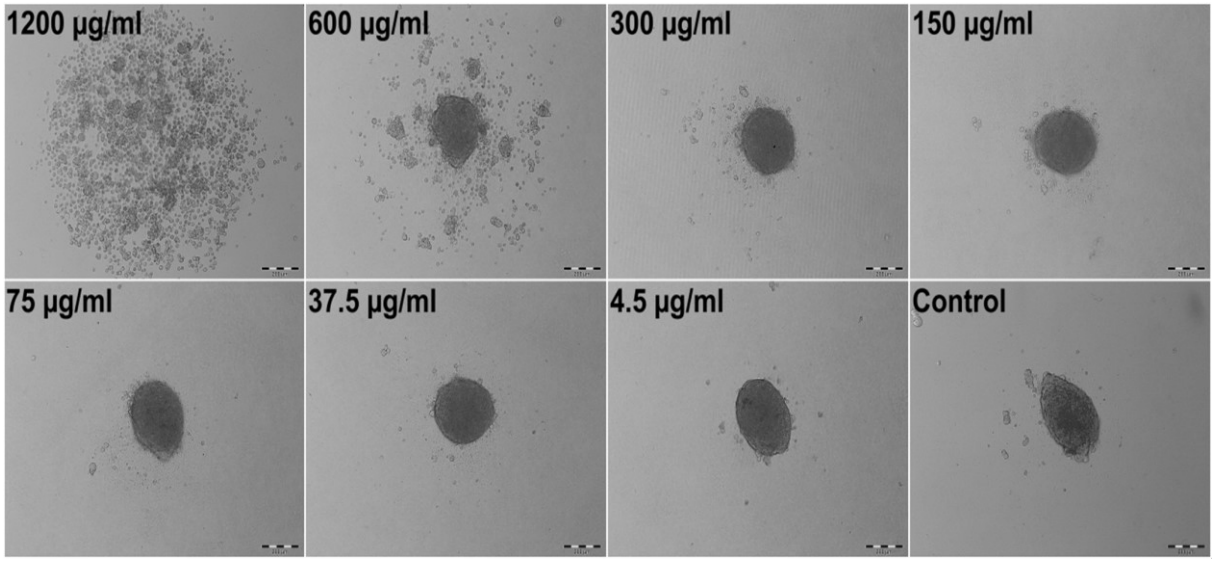

Fig. A.1-2 Effect of Qdot nanoparticles to the formation of hAD-MSCs spheroids. hAD-MSCs were exposed to different Qdot concentrations at the beginning of spheroid formation (tQDOT= 0 h). Bright-field microscope images were taken after 24 h of Qdot treatment. Scale bar is 200 µm.

Stem cell spheroids with compact structures might create stronger diffusion barrier for nanoparticle transport, thus mitigate nanoparticle interactions. Despite the fact that NP *in vivo* face very similar even more severe diffusion limitations, we also aimed to explore the effect of Qdots on spheroid formation by seeding the hAD-MSCs directly with Qdots (t_{QDOT}= 0 h). That means, the diffusion related issues could be eliminated, and it can be ensured that all cells make contact with Qdots. Following that, morphologies of spheroids were imaged after 24 h of incubation (Fig. A.1-2). Herein, Qdots induced cells to undergo more significant morphological alterations in comparison to previous model (Fig. A.1-1). 300 µg/ml and lower Qdot concentrations didn't result in any observable effect, whereas higher amounts elicited distinct changes on cellular aggregation behavior of hAD-MSCs. Cell-cell/ cell-ECM interactions are weakened significantly resulting in formation of several smaller spheroids instead of one large spheroid. When cells were exposed to 1200 µg/ml of Qdot, the effect became more significant and cells lost their ability to form aggregates completely. Furthermore, in respect to their granular structure, it can be assumed that they lost their viability, as well. Consequently, we can confirm that high Qdot doses impair cell-cell/cell-ECM interactions; thus preventing cells to form spheroids as they habituated. This drastic phenomenon wasn't observed in the previous 3D model (t_{QDOT}= 24 h). We suggest that, in the later 3D model (t_{QDOT}= 0 h), cells were not protected by well-developed ECM when they were subjected to toxic Qdot doses. Due to the absence of ECM, their contact with neighboring cells was reduced to a minimum level. Time-lapse microscope images of hAD-MSCs, which were treated with 600 µg/ml Qdots before spheroid formation (t_{QDOT}= 0 h) are presented in Fig. A.1-3 (see also ESI†, Video S2). After 6 h of incubation in the

presence of high Qdots concentration, hAD-MSCs started to feature distinct cell aggregation behavior. Afterwards uneven sized spheroids formation was observed.

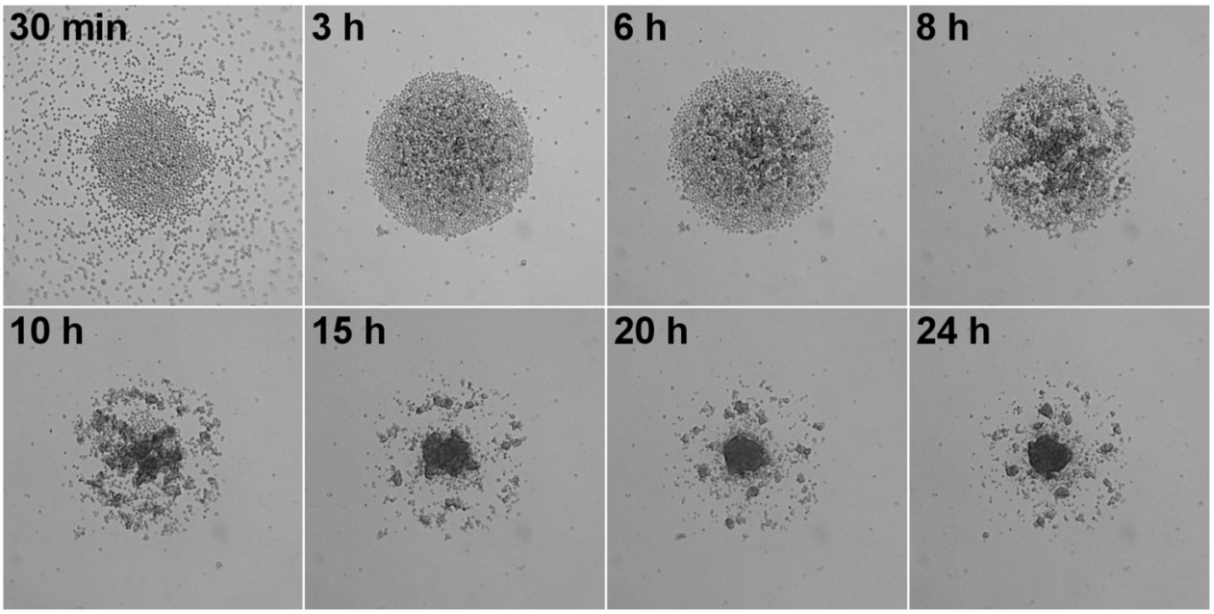

Fig. A.1-3 Time-lapse bright-field images of hAD-MSCs exposed to 600 µg/ml Qdots solution at the beginning of spheroid formation (t_{QDOT} = 0 h). The effect of Qdots to the spheroid formation was monitored for 24 h.

One explanation may be the nonspecific interaction of Qdots with transmembrane integrin proteins which may in result impair the receptor-ligand interactions for cell adhesion. Integrins regulate cell-cell/ cell-ECM interactions; therefore play critical roles in cell proliferation, migration, differentiation, adhesion and apoptosis.[411] They were also identified on MSCs cell surfaces and various studies showed their importance for the attachment and survival of MSCs.[412] Shinto *et al.* proposed a nonspecific carboxyl (COOH)-integrin interaction mechanism which may cause blocking of actual integrin-ligand interactions.[413] Since Qdots used in this study consist of surface COOH groups for their aqueous stabilization, such nonspecific COOH/integrin interactions might have occurred. Additionally, unmodified Qdots, having high surface energy, tend to bind nonspecifically to cell membranes in order to reduce their energy.[414] These two phenomena both separately or in combination can result in nonspecific binding of Qdots to cell surface integrin receptors, and in turn might impair cell-cell/ cell-ECM interactions. Furthermore, it was found that when the integrin-ligand binding was blocked, the cells rounded up and elevated expression of matrix metalloproteinases (MMPs) which are responsible for partial degradation of surrounding ECM in order to facilitate cell motility.[415, 416] Some studies supported these findings by discovering NP-induced overexpression of MMPs.[216], [417] Thereby, we can presume that high Qdot doses might exhibit similar inflammatory effects which can be later associated with diminishing cell-cell/cell-ECM interactions in hAD-MSCs. These hypotheses, however, need further investigation.

Cell viability studies

Following the morphological investigations, cell viability assays were performed in order to give more detailed insight into Qdots-based cellular toxicity with respect to hAD-MSCs metabolic activities. Nanoparticles featuring broad absorption spectra such as quantum dots, carbon nanotubes and silver nanoparticles might restrict the application of various conventional viability assays based on colorimetric measurements, such as acid phosphatase (APH) and methyl tetrazolium (MTT) assays,[297, 418, 419] although they were successfully utilized for determination of cell viability in untreated 3D cell cultures.[410, 419, 420] Moreover, high Qdot concentrations can interfere with the signals, thus causing significant false positive results as well as distorted data in viability results.[421] For that reason, we performed adenosine triphosphate (ATP) luminescence cell viability assay and CellTiter-Blue (CTB) fluorescence viability assay as an alternative. ATP assay is based on the enzymatic activity of luciferase enzyme to produce luminescent oxyluciferin in the presence of ATP, molecular oxygen and Mg^{2+}. The amount of luminescence signal produced from the enzymatic reaction is proportional to the ATP content present in viable cells. ATP assay also requires cell lysis for the release of ATP via disrupting the cell membrane (CellTiter-Glo assay kit, Promega). On the other hand, CTB viability assay is based on intracellular reduction of resazurin by metabolically active cells which yielding a highly fluorescent resorufin compound. The disruption of cells is not particularly necessary due to the diffusion of reduced resazurin outside of the cells.

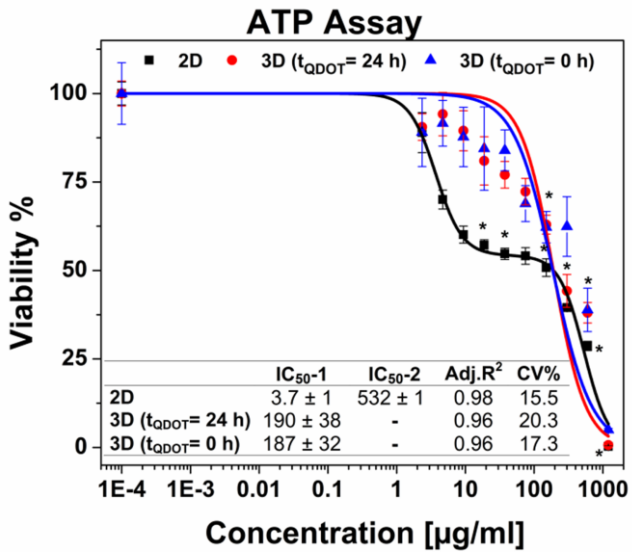

Fig. A.1-4 Cell viability data obtained from ATP assay. The luminescence signals were normalized to the signal of untreated control samples. Data points are means ± standard error of 3±1 independent experiments which each were conducted in 4 replicates. * indicates significant difference at 0.01 level. $p < \alpha$=0.01 (one-way ANOVA). Inset table shows half-maximal inhibitory concentrations (IC_{50}) in µg/ml. 2D cell culture having a biphasic dose-response curve possesses two IC_{50} values (IC_{50}-1 and IC_{50}-2) whereas each 3D spheroid cultures have one IC_{50} value owing to monotonic dose-response pattern. Acceptance criteria is CV (coefficient of variance) < 20%.

Therefore, cells maintain their activity during the assay for given incubation periods. Both assays were tested for their cross-reactivity with highest Qdots dose (1200 µg/ml) in cell culture medium in absence of cells and there wasn't any signals detected higher than the background signals.

Concentration-dependent cell viability results including dose-response fit curves obtained from ATP assay are shown in Fig. A.1-4. Monolayer 2D cell culture exhibited distinct dose-response pattern featuring biphasic dose-response (non-monotonic) unlike 3D spheroid cultures which exhibited monophasic (monotonic) dose-response pattern. Biphasic behavior of hAD-MSCs in 2D culture might be explained by presence of two distinct cell populations with different sensitivity to Qdots. Initially, there occurred a sharp decrease in viability to ~50% at concentrations approaching to 20 µg/ml. Beyond this concentration point, viability of cells was decreased slightly when the dose was increased to 150 µg/ml. This was followed by a moderate decrease at the highest Qdot concentration (1200 µg/ml) at which all cells were dead. Meanwhile, 3D spheroid cultures demonstrated higher resistance to Qdot induced cellular toxicity than 2D culture with a mean IC_{50} value of 190 µg/ml for 3D (t_{QDOT}= 24 h) and 187 µg/ml for 3D (t_{QDOT}= 0 h). Accordingly, Qdots didn't result in pronounced adverse alterations of viability to 3D (t_{QDOT}= 0 h) model although cells were exposed to Qdots at the beginning of spheroid formation. Consequently, cells sustained their viability at the similar levels in both 3D models.

The dose-dependent viability responses acquired from CTB assay for 3D cultures demonstrated an increase in viability at low Qdot doses in comparison to control samples (see ESI† Fig. A.1-7). One may attribute this result to hormesis, which is a low-dose stimulatory or inhibitory effect in dose-responses above or below the toxicological thresholds.[422] NP-induced hormesis was attributed to increasing ROS levels with low-doses, giving rise to cell activities to suppress the imbalance, thus causing increase in metabolic activities.[423] So far, various studies reported for several nanoparticles (CdTe, TiO_2, aluminum NPs, single-walled carbon nanotubes) inducing hormesis.[424, 425] Though, CTB assay for 2D culture and ATP assay for 3D cultures didn't demonstrate similar pattern. Hence, we can neglect the possibility of hormesis. Meanwhile, O'Brien *et al*. described that cell lines with high metabolism rates can reduce resazurin further to colorless and nonfluorescent hydroresorufin.[426] In such a case, untreated cells with high metabolic activity can further reduce resazurin to nonfluorescent hydroresorufin resulting in low fluorescent signals at the end-point in comparison to treated cells.[426-428] This can lead to unsubstantial results causing misinterpretation of data and underestimation of cell activity. Moreover, in this study, the resazurin incubation time was prolonged to 48 h because of the slow diffusion of reduced resazurin from highly compact structured HAD-MSCs spheroids. Only after 48 h, fluorescence signals reached to rational and detectable levels. For that reason, we can presume that the prolonged incubation time for resazurin (48 h) may have enabled over-reduction of resazurin by untreated cells followed by a decrease in their fluorescence signals. In the meantime, cells treated with Qdots sustained their reduction capacity and respectively

produced higher signals than control samples. We should also note that, resazurin dye, also known as Alamar Blue, was proved to be toxic to the cells for long incubation periods (>24 h).[426, 429]

Last of all, signal qualities of ATP and CTB assays were compared by determining signal-to-noise (S/N) ratios for all culture types. For 2D culture, S/N ratios were calculated to be 172 ± 19 for ATP assay and 11 ± 4 for CTB assay. For 3D culture, S/N ratios were estimated to be 27 ± 4 for ATP assay and 4 ± 1 for CTB assay. Consequently, ATP assay signal qualities were found to be 16-fold greater in 2D culture and 7-fold in 3D culture than CTB assay. In summary, we concluded that CTB assay is not a reliable assay for determination of Qdot toxicity in the case of highly active and densely-packed hAD-MSCs spheroids. However, other cell lines particularly those forming loose cell aggregates and have relatively low metabolic activities, such as A549 lung carcinoma, HepG2 hepatocellular carcinoma and medulloblastoma tumour cells, can be suitable for CTB assay.[345, 407]

Similar to our findings, conventional monolayer cell cultures being more sensitive against NPs or drug molecules in comparison to various 3D cell culture systems have been also reported by other groups.[395, 430-433] So far, only Lee and co-workers assessed single-dose toxicity of CdTe Qdots on HepG2 spheroid cultures. They showed that 10 µg/ml of CdTe reduced the cell viability to 56% in 2D culture and 31% in 3D culture after 12 h of NP exposure.[410] The results of the study cannot be directly compared to our findings since different cell types as well as different Qdot compositions were tested. Nevertheless, we can state that the same dose (10µg/ml) for core/shell/shell CdTe/CdS/ZnS Qdots didn't create any damage to hAD-MSCs spheroids. This may be attributed to the presence of protective outer shell layers of CdS/ZnS acting as a strong barrier against Cd^{2+} leakage.

Regarding *in vivo* Qdot-induced toxicity analysis; Hauck *et al.* reported that CdSe/ZnS core/shell Qdot didn't cause any significant toxicity in healthy Sprague–Dawley rats.[434] Later, Chou *et al.* confirmed that Cd, Se and Zn containing Qdot didn't demonstrate toxicity to rats in 90 days.[435] Another study reported by Nurunnabi *et al.* pointing out that carboxylated graphene Qdots didn't induce apparent toxicity in rats after 22 days of exposure.[436] The discrepancy in results in the context of Qdot toxicity between monolayer cell culture and animal models was attributed to the presence of complex physiological processes in the body that NPs inevitable undergo after their uptake. Their circulation in blood stream, accumulation by specific organs and renal excretion play a deterministic role for their fate in the body.[419] Yet, structural diversities in Qdot properties, such as size, shape, charge, material composition, and surface chemistry etc., necessitate the investigation of every Qdot structure-based effects individually. Not to mention that petri-dish cultures lack all of these physiological processes being isolated on plastic substrates and therefore all cells facilitate NP interactions easily without facing any transport limitations. On the other hand, complex and diverse *in vivo* uptake mechanisms reduce the interaction of Qdots with the target organ and therefore they cooperatively act to minimize adverse effects of Qdots. Nevertheless, arising developments for *in vitro*

3D cultures fortify their application potential to fill the gap between petri-dish cultures and animal models with hope that they will also decrease the use of laboratory animals.[391]

Labeling spheroids with Qdots

Carboxyl-functionalized Qdot were tested for their applicability in 3D spheroid imaging. For that, hAD-MSC spheroids treated with Qdots were monitored with fluorescence and confocal microscopes, and the obtained images are presented in Fig. A.1-5. Fluorescence microscope images with a standard (x, y) view illustrated surface fluorescence of labelled spheroid (Fig. A.1-5 a). On the other hand, z-stacked confocal images provided a better insight to the penetration and the uptake of Qdots in spheroids [437]. According to the fluorescence confocal images, after 4 h Qdots appeared to be uptaken mostly by peripheral cells in the spheroid structure.

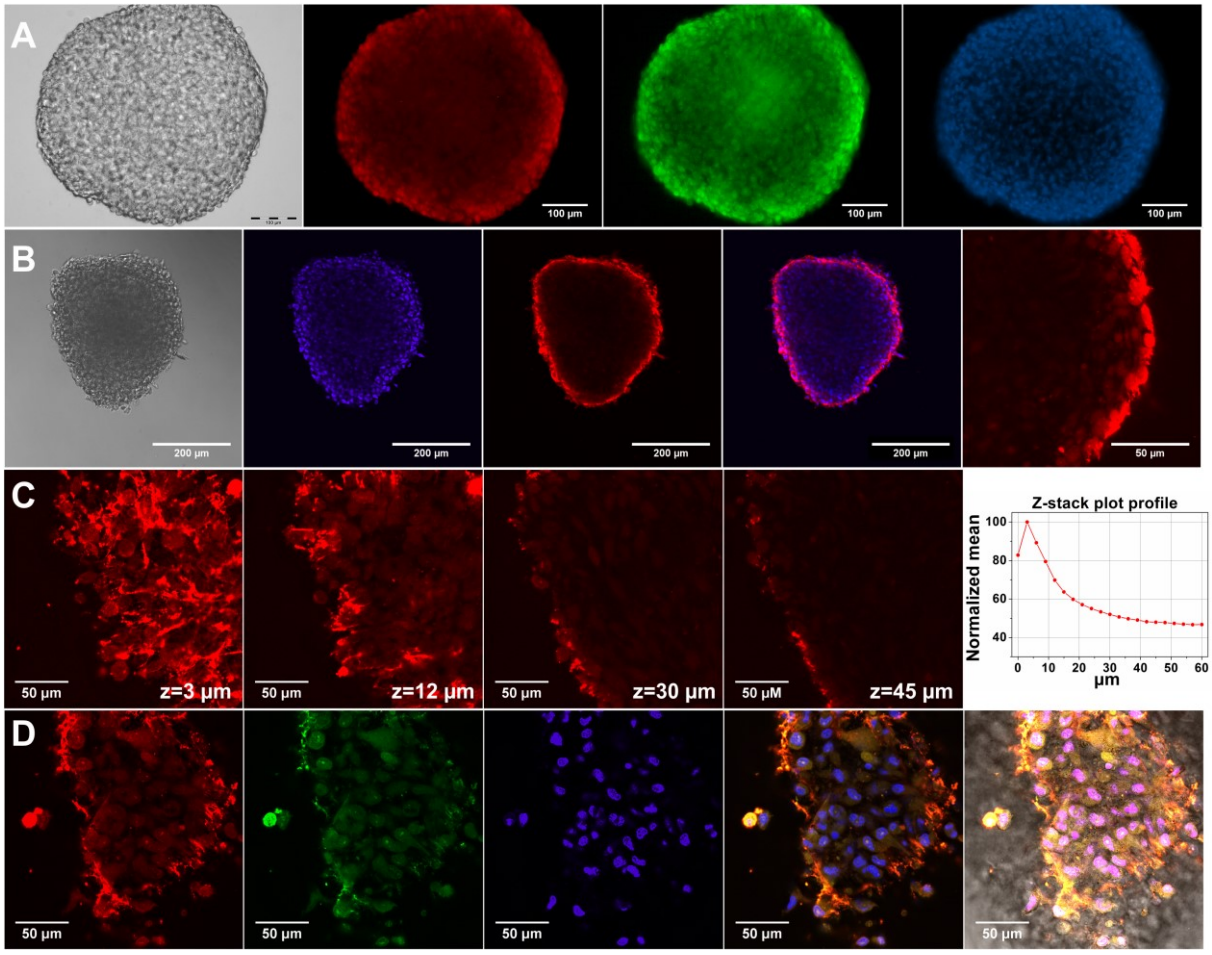

Fig. A.1-5 Fluorescence imaging of hAD-MSCs spheroids treated with CdTe/CdS/ZnS Qdots for 4 h. (A) Fluorescence images captured from fluorescence microscopy from left-to-right: bright-field, Qdot (red), Calcein-AM (green) and DAPI (blue). (B) Single plane confocal images collected with 10× objective, from left-to-right: bright-field, DAPI (blue), Qdot (red), merge image of Qdot + DAPI and magnified spheroid. (C) Z-stacked confocal images of spheroid at individual z-planes. Z-stacks were acquired with 3 µm step size. The inserted graphic shows z-stack plot profile for normalized Qdot fluorescence mean intensity versus z-stack height (µm). (D) Single-plane confocal fluorescence images of spheroid at the bottom surface, from left-to-right: Qdot (red), Calcein-AM (green), DAPI (blue), merged image of Qdot + Calcein-AM + DAPI, and merge image of bright-field +Qdot + Calcein-AM + DAPI.

As it can be seen from Fig. A.1-5 b, strong red fluorescence signals appeared only at the outer region, while signals decreased towards the inner region of the spheroid. In Fig. A.1-5 c, z-stacked images taken at individual zplanes at 3 μm step size from bottom surface towards centre of spheroid showed that highest Qdot labelling occurred at peripheral regions. Z-stack mean intensity plot (Fig. A.1-5 d-right) reveals that fluorescence intensity of Qdots decreases by 50% within 36 μm focal distance. These observations might suggest presence of diffusion limitations for the transport of Qdots into spheroid inner region [263]. Fluorescence images taken from the bottom edge of the spheroid (Fig. A.1-5 d) show that Qdots were internalized by the cells rather than being non-specifically captured by extracellular matrix material. Live cell staining with Calcein-AM (Fig. A.1-5 d) shows that cells at the bottom surface of the spheroid retained their viability during Qdot treatment; thus, uptake of Qdots did not induce cell death. As a result, within the given incubation time (4 h) Qdots enabled staining into intact stem cell spheroids due to their inherent small size and surface structure. We can conclude that penetration of Qdots into tissue-like intact spheroid structures can make them a suitable tool for targeted imaging and drug delivery studies.

A.1.5 Conclusions

In summary, we described for the first time the dose dependent adverse effects of CdTe/CdS/ZnS $core_{(small)}/shell_{(thick)}/shell_{(small)}$ Qdots on the 3D spheroid culture of primary human mesenchymal stem cells. Morphological alterations in spheroid models (t_{QDOT} = 0 h, t_{QDOT} = 24 h) caused by toxic levels of Qdots revealed distinct characteristics. Either end-point microscope images or time-lapse studies demonstrated that Qdots expressed more drastic effect on spheroid formation, where cells were incubated in presence of Qdots during cell aggregation. Additionally, we detected a correlation in the spheroid diameters with increasing Qdot concentrations when hAD-MSCs were exposed to Qdots after spheroid formation (tQDOT = 24 h). Further, ATP and CTB cell viability tests were assayed to address the impact of dose dependent Qdot toxicity to cell metabolic activities. According to ATP assays, significant differences were observed between 2D and 3D cell cultures. Interestingly, dose–response curves for 2D culture featured a reproducible biphasic curve model in contrast to spheroid cultures with monotonic dose–response patterns. As a result, monolayer cell cultures, on one side attaching to plastic substrate and on the other side being exposed to medium and having only periphery cell contacts, were found to be more susceptible to Qdot toxicity. Alternatively, in 3D spheroids, fully formed cell–cell and cell–ECM interactions in all three dimensions played a protective role and resulted in greater resistance to Qdot-induced toxicity. Meanwhile, CTB assays were proved to be an unreliable viability assay for densely packed stem cell spheroids due to diffusion limitations for resazurin/resorufin and therefore produced aberrant results. Overall, well-defined 3D spheroid cultures with the presence of microtissue-like cell clusters and ECM layer as well as mass transport characteristics constitute an initial testing platform to address physiologically relevant toxicity issues of nanoparticles for automated cell based high throughput screening methods. Lastly, penetration ability of highly-fluorescent CdTe/CdS/ZnS Qdots demonstrates versatility of Qdots in 3D spheroid

imaging. Their optical and structural features can be utilized in the future for targeted imaging and delivery studies using solid tumor spheroids.

Notes and References

† Electronic supplementary information (ESI) available: Details of experimental procedures and supporting figures and tables. See DOI: 10.1039/C5TX00236B.

A.1.6 Supplementary Figures

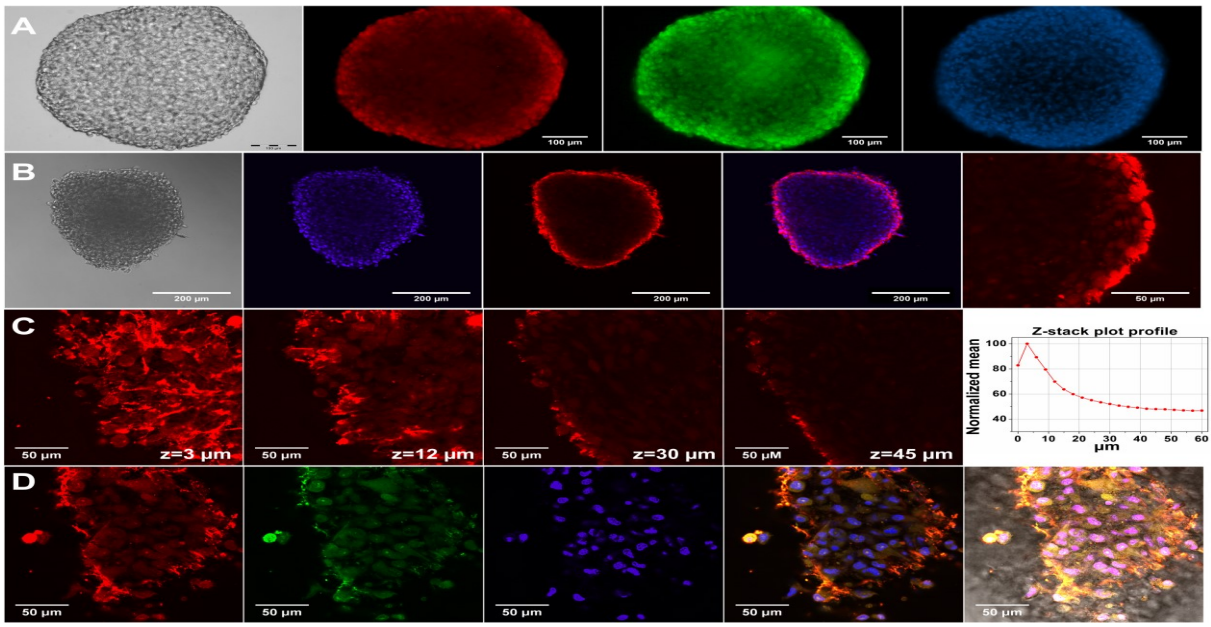

Fig. A.1-6 Time-lapse microscope images of hAD-MSCs spheroids treated with 1200 µg/ml Qdot solution. Qdots were introduced to the spheroid after cells were incubated for 24 for spheroid formation (t_{QDOT}= 24 h). Effect of Qdots to spheroid morphology was monitored for 24 h.

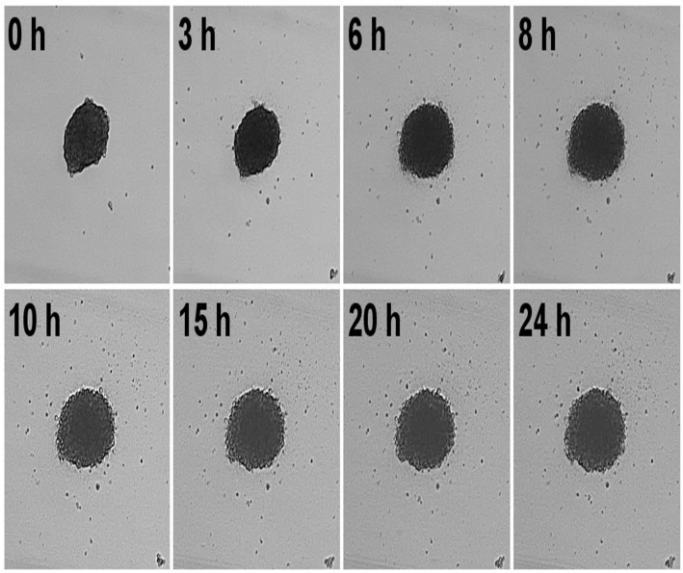

Fig. A.1-7 Increase in hAD-MSCs spheroid diameters during Qdot exposure (1200 µg/ml) until 24 h. Spheroid diameters were normalized to the diameter of spheroid at the time= 0 h. Inset graph shows the linear relationship between the Qdot exposure time and the increase in spheroid diameter until 8 h (Adj. R^2=0.977).

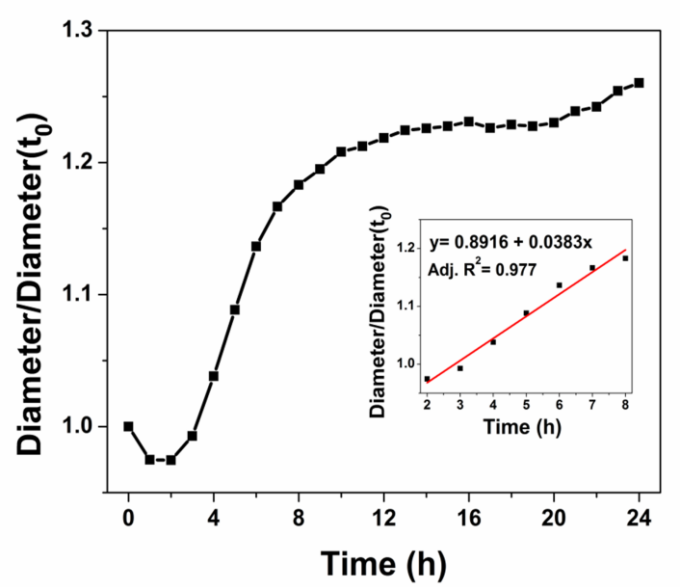

Fig. A.1-8 Cell viability data obtained from CTB assay. The fluorescence signals were normalized to untreated control samples. Data points are means ± standard error of 3±1 independent experiments which were conducted with 4 replicates. * indicates significant difference at 0.01 level. $p < \alpha$=0.01 (one way ANOVA).

A.2 Evaluation of the biological tolerability of the starch-based medical device 4DryField® PH *in vitro* and *in vivo* a rat model

Daniel Poehnert[1*], Mahmoud Abbas[2], Lavinia Maegel[2], Franziska Sambale[3], Antonina Lavrentieva[3], Hans-Heinrich Kreipe[2], Jürgen Klempnauer[1], Markus Winny[1]

[1]Department of General, Abdominal and Transplant Surgery, Hannover Medical School, Germany

[2]Department of Pathology, Hannover Medical School, Germany

[3]Institute of Technical Chemistry, Leibniz University Hannover, Germany

*Corresponding author: Daniel Poehnert, Department of General, Abdominal and Transplant Surgery, Hannover Medical School, Carl-Neuberg-Straße 1, D-30625 Hannover, Germany. Email: poehnert.daniel@mh-hannover.de

Published in *Journal of Biomaterials Applications* 0(0) 1–9, 2015 (DOI: 10.1177/0885328215592257). Reprinted with kind permission from SAGE.

A.2.1 Abstract

Purpose: To evaluate in vitro cytotoxicity/biocompatibility as well as in vivo tolerability of the novel polysaccharide 4DryField® PH, certified for haemostasis and adhesion prevention.

Methods: In vitro cytotoxicity/viability testing according to ISO EN 10,993 using murine and human tumour cell lines incubated with 4DryField® PH (PlantTec Medical GmbH). Using a rat model the impact of 4DryField® PH on animals viability and in vivo effects were macro- and micropathologically assessed.

Results: *In vitro* testing revealed no cytotoxic effect of 4DryField® PH nor enhancement of viability to tumour cell lines. In vivo viability of rats was unimpaired by 4DryField® PH. Bodyweight loss in animals with abdominal injury plus treatment with 4DryField® PH was in the range of controls and less than in injured rats without treatment. At day 7 after surgery no formation of adhesions, neither macroscopic nor histological remnants nor signs of foreign body reaction were present in animals without injury. In animals with peritoneal injury and 4DryField® PH application, histopathological observation revealed minor residuals of polysaccharide in the depth of wound cavity embedded in a thickened subperitoneal layer; however, with a suggested intact neoperitoneum. The presence of mononuclear cells surrounding polysaccharide particles in varying states of degradation was observable as well. Conclusion: 4DryField® PH is not cytotoxic and does not enhance viability of tumour cell lines. High dose of 4DryField® PH of 1.09 g/kg bodyweight is well tolerated and reduces weight loss in animals with peritoneal injury. The biocompatibility of 4DryField® PH can be rated as being excellent.

Keywords: 4DryField® PH, polysaccharide, haemostatic agent, adhesion prevention agent, biocompatibility, *in vitro* cytotoxicity testing, *in vivo* rat model

A.2.2 Introduction

If conventional measures for haemostasis like compression, cautery, and suturing are not applicable or successful, other techniques such as the use of topical haemostats have to be taken into consideration [438]. Most of these are cellulose-based or derived from mammalian and/or human components. They exert their effect in various ways like primary improvement of haemostasis, stimulation of fibrin formation or providing pro-coagulant substances on vehicles such as collagen [438]. The use of modified starch particles for haemostasis is a relatively recent addition to the haemostatic arsenal. Applied as powder to bleeding areas, polysaccharide particles absorb water from the wound blood resulting in concentration of plasmatic fibrinogen and accelerating the natural blood clotting process [439-441]. In a situation of diffuse bleeding, a larger quantity of haemostatic agent might be of necessity, raising the question of biocompatibility of those agents.

Adhesions can be a result of previous surgery. They might lead to considerable patient morbidity and are a mounting burden for surgeons, patients, and the health care system [442-444]. Prophylaxis of adhesions including the use of biodegradable agents gains more and more awareness [444, 445]. Extensive abdominal and pelvic surgery including operations for symptomatic adhesions can result in large peritoneal defects necessitating large quantities of adhesion prevention agents. Again the question of biocompatibility arises.

The novel agent 4DryField® PH (PlantTec Medical GmbH, Bad Bevensen, Germany) is certified for haemostasis and adhesion prevention, both actions base on its excellent capability to absorb water. In context with haemostasis, it could be shown that coagula induced by 4DryField® PH have physical properties comparable to those of genuine clots even if there is 50% haemo dilution [440]. With respect to adhesion prevention it was shown that a gel formed from 4DryField® PH is highly effective as a barrier against adhesion formation [446, 447].

This study investigates the biocompatibility of 4DryField® PH. With *in vitro* testing on murine and human cells a potential cytotoxic effect of 4DryField® PH is analysed. For the *in vivo* testing a previously described rat model is used [447, 448]. Biocompatibility is assessed with viability scoring, course of bodyweight, and macroscopic and histopathological investigations.

A.2.3 Materials and Methods

A.2.3.1 In Vitro Cytotoxicity Tests

To evaluate the impact of 4DryField® PH on cell growth and viability, two assays were performed. The MTS assay is a standard procedure to estimate the viability of mammalian cell cultures. In the conducted assay a CellTiter 96 Aqueous One Solution Cell Proliferation Assay kit (Promega, USA) was used. For viability testing murine fibrosarcoma L929 cells were cultivated in 96-well plates in Roswell Park Memorial Institute (RPMI) 1640 cell culture medium with 10% fetal calf serum. The metabolic rate was standardized to background signals of culture medium without cells (blank). As control, negative (aged cell culture medium), not cytotoxic (reference material in accordance with ISO

10993-12) and cytotoxic (reference material in accordance with ISO 10993-12) controls were conducted. The mean viability score of the negative control was defined as 100% viability. Eight replicates were performed for each sample. In the assay, 4DryField® PH was applied to the culture medium as an extract prepared as followed:

In accordance with ISO EN 10,993-12-2009, a material to extraction ratio of 0.2 g/mL was used plus additional 15mL absorption volume per 1 g 4DryField® PH. Therefore, 1 g 4DryField® PH per 20mL RPMI 1640 cell culture medium with 10% fetal calf serum (0.05 g/mL) was used and the solution was incubated for 24 h at 37°C, 5% CO_2 and 92% humidity. After this procedure, the saturated 4DryField® PH solution was centrifuged and the resulting supernatant was termed '100% extract'. Dilutions of the extract were prepared with RPMI medium and incubated for 24 h at 37°C. According to ISO EN 10,993-5, cytotoxicity should be considered where the viability value falls below 70% of the negative control. Viabilty results obtained with 4DryField® PH referred to negative controls.

To evaluate the impact of 4DryField® PH powder on the viability of human cells using a standard Cell Titer 96™ Non-Radioactive Cell Proliferation Assay (Promega, Germany), 4DryField® PH was applied as a powder directly on the surface of A549 cells. A standardized MTT assay was performed. Human A549 cells were grown in 24-well or 96-well plates in concentrations of 40,000–15,000 cells per plate in RPMI cell culture medium. Before 4DryField® PH application, a 24–72 h cell adhesion and recovery phase was carried out, followed by the evaluation of cell viability after 24 h of 4DryField® PH exposition. 4DryField® PH was added as a powder directly to adherent A549 cells in concentrations varying from 0.001–15 mg/mL 4DryField® PH per total culture medium. Each concentration was tested as triplicate. Viability scores refer to controls without 4DryField® PH powder in culture medium as 100% viability.

A.2.3.2 In Vivo Testing for 4DryField® PH Tolerability

Preoperative Preparation.

To assess the tolerability of 4DryField® PH *in vivo*, male Lewis rats were used in this study. All protocols were conducted in accordance with animal protection laws. Animal experiments were performed at Zentrales Tierlabor of Hannover Medical School (MHH, Hanover, Germany), providing the knowledge (housing, caretaking, etc.) to assure life quality of laboratory animals. The Lower Saxony State Office for Consumer Protection and Food Safety (LAVES) approved this study. Rats had continuous access to fresh water and were fed ad libitum. Animals' welfare was assessed by monitoring of bodyweight and behavioural changes with the use of a standard observation chart (body condition scoring, GV-SOLAS, Charité - Universitätsmedizin Berlin) (Tab. A.2-1).

Tab. A.2-1. Viability scheme covering day 1‒7 after surgery according to GV-SOLAS.

Grade	Quality	Criteria
1	Agile, active	Typical fast movement, curiosity, feed and water intake
2	Active	Typical movement, rarely persistent, normal feed and water
3	Limited active	Reaction to environmental stimulus, frequent persistence, limited
4	Retarded	Sleepiness, retarded movement and reaction, excessive limited
5	Lethargical	No activity, no reaction, no feed and water intake

Surgical procedure.

General anaesthesia was achieved by intraperitoneal injection of 80 mg/kg bodyweight Ketamine and 5 mg/kg Xylazine. The required level of narcosis for surgery was reached if flexor reflexes failed to appear. The abdomen was shaved and disinfected. A 3 cm median laparotomy was performed to gain access to the abdominal cavity. After treatment according to grouping (see Test groups), the abdomen was closed using a two-layer closure technique and a consecutive suture. All animals were sacrificed at trial day 7 by carbon dioxide narcosis followed by cervical dislocation. The peritoneal cavity was re-entered via an incision remote to the former laparotomy scar. The abdominal cavity was thoroughly explored and healing of provoked abdominal injuries were evaluated. Sample material of the cecum and abdominal wall for histological assessment was taken according to a standard protocol.

Postoperative Management.

After surgery, animals were monitored until complete awakening and kept warm with an infrared lamp. Concerning expectable postoperative pain in the postoperative period, animals received Novalminsulfon (non-recurring subcutaneously after surgery with 200 mg/kg bodyweight and continuously by mixing 1g in 500 ml drinking water).

Test Groups.

Prior to the surgical intervention, rats were separated into four groups: 10 animals received only laparotomy and closing of the abdomen (group 1). These animals were used as controls to assess the impact of surgical procedure on animal behaviour and weight course. Additional eight rats received 300 mg of 4DryField® PH in the lower right abdomen in addition to the laparotomy (group 2). Group 2 was used to evaluate the impact and safety of 4DryField® PH given into the unimpaired abdomen. In addition, the effect of 4DryField® PH on animals with a severe abdominal lesion and its subsequent healing process was analysed. In both lesion groups (groups 3 and 4), abrasion of the cecum and a wound in the opposite abdominal wall were created to simulate bleeding and to form trauma areas. Therefore, the cecum was treated with a gauze swab to remove visceral peritoneum and provoke capillary bleeding in an area of 1 x 2 cm. Additionally, an about 1 x 2 cm sized patch of parietal peritoneum with its underlying inner muscular layer was resected off the right abdominal wall lateral to the midline laparotomy. Of those treated 15 rats served as control to evaluate regular wound healing and bodyweight courses (group 3). Another 14 rats were treated in the same manner followed by application of 300 mg of 4DryField® PH (group 4). 4DryField® PH powder was given in the area of

injury (group 4) or rather in the right lower abdominal quadrant (group 2). All animals received 1.5 ml saline solution 0.9% in the peritoneal cavity at the end of surgery. If 4DryField® PH was applied, this procedure was used to transform the starch powder into a gel.

Evaluation Parameters.

Animals' constitution was subjected to daily routine observations and was scored according to GV-SOLAS (Tab. A.2-1). Bodyweight was determined at trial day 0 (before surgical procedure) and at least on trial day 7. Upon autopsy at postoperative day 7, the abdominal cavity in general, as well as the areas of cecum and the abdominal sidewall in particular, were macroscopically evaluated and searched for polysaccharide remnants.

Histology.

Specimen for histological examinations were collected from all animals to evaluate whether 4DryField® PH had an impact on unimpaired tissue and wound healing and to investigate 4DryField® PH degradation characteristics. Samples were excised *en bloc* and fixed in 10% formaldehyde solution. After processing, specimens were embedded in paraffin blocks. Serial sections were stained with haematoxylin and eosin or Alcian blue and PAS stain kit (Sigma-Aldrich, St. Louis, USA), respectively, and visualised by light microscopy. 4DryField® PH polysaccharide remnants were detected by PAS staining (blue/purple colour of polysaccharides). Both, the macroscopic and the histopathological observers were blinded to the study.

Statistical Analysis.

Statistical analyses of bodyweight courses were performed using GraphPad PRISM software for a two-way multi-comparison ANOVA corrected for multiple comparison with Turkeys post-hoc test. Significance levels were set as $p < 0.05$.

A.2.4 Results

A.2.4.1 In Vitro Cytotoxicity Assays

Two different *in vitro* cytotoxicity assays were conducted to reveal 4DryField® PH impact on cell viability. On L929 cells the 100% 4DryField® PH extract resulted in a mean viability score of 86.5 ± 4.8% in the used MTS assay. Extract dilutions of 50, 25 and 12.5% revealed viability scores of 103.7 ± 5.4, 100 ± 6.9 and 99.1 ± 6.7%, respectively. These results indicated no cytotoxicity of 4DryField® PH extract (Tab. A.2-2).

Tab. A.2-2 Median, mean and standard deviation of murine tumour cell line L929 viability after incubation for 24h with 4DryField® PH-RPMI extract in different concentrations

Concentration of extract (%)	Median	Mean value ± standard deviation	Result
100	86.6	86.5 ± 4.8	Not cytotoxic
50	104.1	103.7 ± 5.4	Not cytotoxic
25	99.5	100.0 ± 6.9	Not cytotoxic
12.5	99.2	99.1 ± 6.7	Not cytotoxic

Vaying amounts of 4DryField® PH powder were applied directly on the surface of adherent A549 cells to analyse cell viability of human cells in direct contact with 4DryField® PH powder. Fig. A.2-1 shows testing of different amounts of 4DryField® PH powder in culture medium and its subsequent influence on cell viability referring to a control without 4DryField® PH. 4DryField® PH amounts ranging from 0.001 to 15 mg/ml 4DryField® PH were applied, resulting in viability scores between 111–72% with a mean cell viability of 87.8 ± 15.5%.

Thus, *in vitro* testing of 4DryField® PH when administered to tumour cell lines in an extract form or a powder showed neither cytotoxic nor beneficial effects on tumour cell viability.

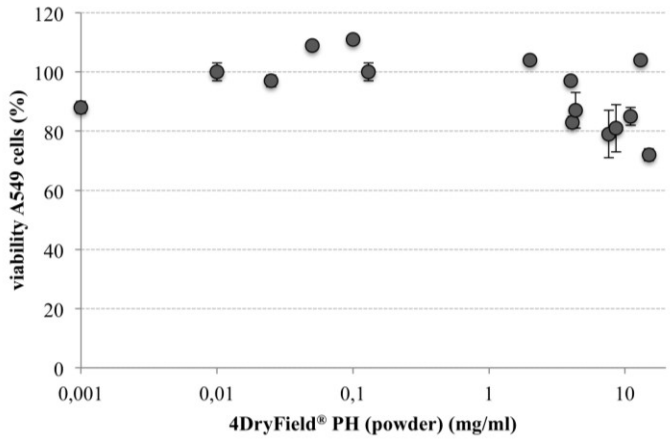

Fig. A.2-1. Influence of varying amounts of 4DryField® PH powder on cell viability of human tumour cell line A549 in a standardised MTT assay after incubation for 24 h.

A.2.4.2 In Vivo 4DryField® PH Tolerability

On the first day after surgery, all rats were graded with a GV-SOLAS viability score of 1 and/or 2 (Tab. A.2-1). Throughout the remaining study all animals were graded with a viability score of 1 (Tab. A.2-3), meaning that neither the surgical procedure nor the 4DryField® PH application did sustainably influence animals' viability.

Tab. A.2-3 Postoperative viability scoring of animals.

Group	Mean viability grade		n
	Day 1	Day 7	
(1) Control	1.1	1.0	10
(2) 4DryField® PH	1.1	1.0	8
(3) Control lesion	1.0	1.0	15
(4) 4DryField® PH lesion	1.2	1.0	14

Surgery was performed without complications, and due to a plain postoperative course no animal had to be sacrificed or died during the course of investigations. Tab. A.2-4 summarises the animal grouping and preoperative bodyweight. All rats of groups 2 and 4 received the same amount of 4DryField® PH (300 mg). Preoperative bodyweight of these animals was in a range of 276-431 g. Hence, the amount of 4DryField® PH given varied from 0.7-1.09 g 4DryField® PH /kg bodyweight.

Tab. A.2-4. Preoperative bodyweight data of complete cohort of rats. [1] Mean amount of 4DryField® PH (4DF) in gram per kilogram bodyweight (BW)

Group	Weight (g)	Mean weight (g)	4DF / BW[1]
(1) control	327–361	343 ± 11	
(2) 4DryField® PH	393–431	409 ± 13	0.73 ± 0.02
(3) control lesion	270–358	321 ± 29	
(4) 4DryField® PH lesion	276–423	358 ± 59	0.86 ± 0.15

The average bodyweight loss of all rats was 4.6 ± 3.8% one week after surgery (Tab. A.2-5). Weight loss was most pronounced in animals with cecal abrasion and abdominal wall defect but without 4DryField® PH treatment (group 3, mean weight loss 23 g; 7.2%) (Fig. A.2-2). In contrast, in group 1 mean weight loss was 10 g (2.9%), 14 g (3.4%) in group 2, and 14 g (3.7%) in group 4. Interestingly, the animals with surgical lesions and 4DryField® PH treatment (group 4) revealed a course of bodyweight similar to groups 1 and 2 without lesions (Fig. A.2-2). Statistical analyses showed a significant difference between animals of group 1 and group 3 with increased weight loss in group 3 ($p = 0.04$). Additionally, group 3 showed a significantly increased weight loss compared to animals of group 4 ($p = 0.04$).

Tab. A.2-5 Comparison of pre- and postoperative bodyweight.

Group	Mean bodyweight (g)			(%)
	Day 0	Day 7	Δ	Weight loss
(1) Control	343 ± 11	333 ± 11	10 ± 7	2.9 ± 2.1
(2) 4DryField® PH	409 ± 13	395 ± 17	14 ± 6	3.4 ± 1.4
(3) Control lesion	321 ± 29	297 ± 30	23 ± 17	7.2 ± 5.6
(4) 4DryField® PH lesion	358 ± 59	344 ± 54	14 ± 7	3.7 ± 1.6
All rats	351 ± 47	335 ± 48	16 ± 12	4.6 ± 3.8

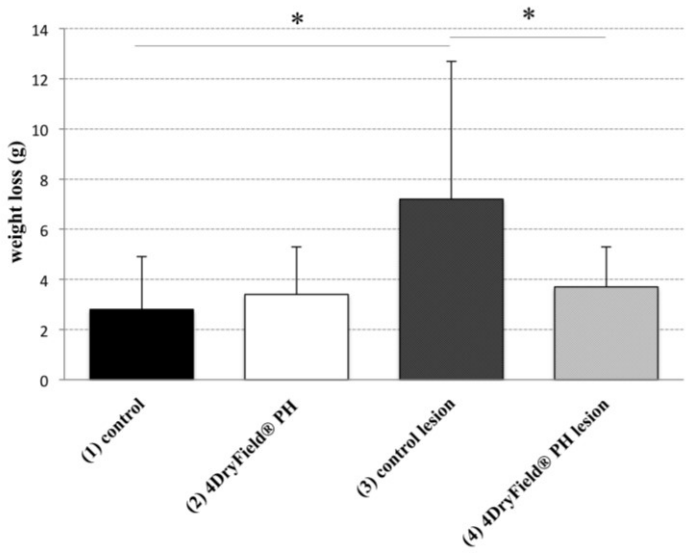

Fig. A.2-2. Relative bodyweight loss and standard deviation of animals with sole laparotomy without (group 1, control) and with 4DryField® PH treatment (group 2, 4DryField® PH) and weight loss of animals with cecal abrasion and abdominal wall defect (group 3, control lesion) and with 4DryField® PH treatment (group 4, 4DryField® PH lesion).

By defining bodyweight depending cohorts (Tab. A.2-6) mean values of 0.72-1.06 g 4DryField® PH / kg bodyweight were applied. The amount of 4DryField® PH administered seemed to have no adverse effect on the course of viability and bodyweight, even when applied in a concentration of 1.09 g/kg. Furthermore, 4DryField® PH exhibited a beneficial effect on course of bodyweight in animals with severe surgical injury (group 4).

Tab. A.2-6. Influence of 300 mg 4DryField® PH given intraperitoneally on animal viability and weight loss in different weight cohorts. [a] Mean amount of 4DryField® PH (4DF) in gram per kilogram bodyweight (BW)

Weight cohorts	n	Mean weight (g) d0	Weight loss (%) d0 – d7	4DF / BW[a]
250–300	4	284.5 ± 9.5	-2.9 ± 1.8	1.06 ± 0.04
301–350	3	330.6 ± 13.7	-2.8 ± 0.5	0.91 ± 0.04
351–400	4	392.8 ± 6	-4 ± 1.7	0.76 ± 0.01
401–450	11	415.8 ± 7.4	-3.9 ± 1.5	0.72 ± 0.02

Macroscopic inspection of the abdominal cavity of animals with sole laparotomy (group 1) appeared inconspicuous. In particular, 4DryField® PH treated animals (group 2) showed no distinctive features, e.g. polysaccharide remnants, signs of dehydration or foreign body reactions. Rats with cecal abrasion and an abdominal wall defect (group 3) showed massive adhesions as a result of injured peritoneal tissue. In contrast, animals with additional 4DryField® PH treatment of group 4 had a normal abdominal cavity and apparently no adhesions, revealing an anti-adhesive effect of 4DryField® PH in injured peritoneal areas. Here the zones of surgical injury had regained a shiny surface, appearing like healthy mesothelium. In the area of the abdominal wall defect, some zones appeared whitish (so called Winny-effect, named after its discoverer).

Histopathological assessment of 4DryField® PH impact on tissue structure is visualised in a representative animal of group 2 in Fig. A.2-3 (a and b). The overall impression of cecum and abdominal wall tissue structure and layering appeared normal. Besides few accumulations of mononuclear cells in some regions of submesothelial layer of the abdominal wall the administration of 4DryField® PH in the healthy abdominal cavity revealed no abnormalities (Fig. A.2-3 (b)).

In rats of group 3, the abdominal and cecal wall tissue layers were agglutinated with fibrous tissue sections and, thus, did not show normal tissue layering or functionality (data not shown). 4DryField® PH treated animals of group 4 revealed a normal tissue layering (despite of the surgical muscular defect) with separated abdominal wall and intestine. The former lesion areas showed a thickening of submesothelial layers (Fig. A.2-3 (c) and (d)) as an indicator of active healing processes. Interestingly, the visceral and parietal peritoneum were reconstituted.

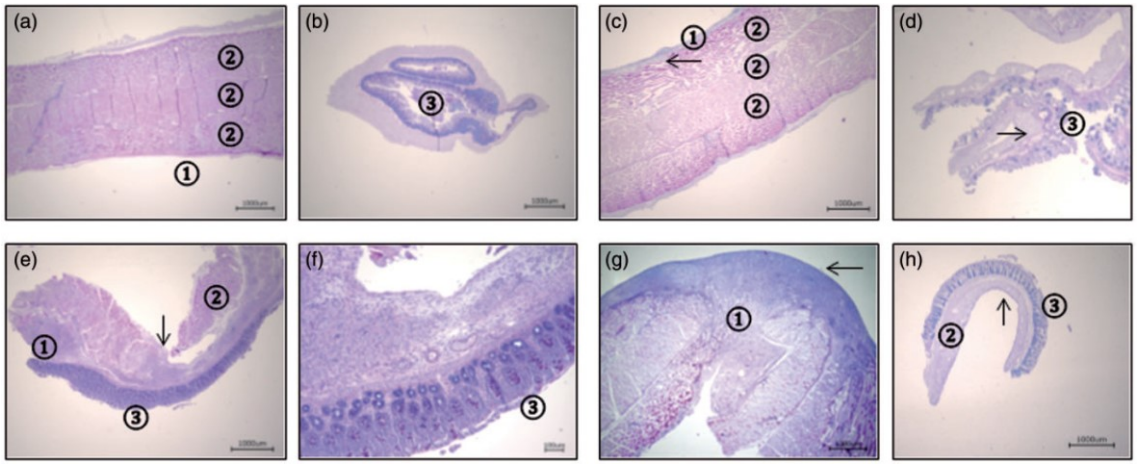

Fig. A.2-3 Representative Alcian blue stained histologies of cecal and abdominal wall biopsies seven days after 4DryField® PH application in rat abdomen of a representative animal of group 1 (a, b), group 2 (c, d), group 3 (e, f) or group 4 (g, h), respectively. Pictures (a) and (b) demonstrate normal abdominal wall (①: peritoneum, ②: intact muscle layers) and cecal anatomy (C: cecal mucosa). (c and d) Abdominal wall and cecum after laparotomy and application of 4DryField® PH showed normal peritoneum ①, muscle layers ② and cecal mucosa ③. After application of 4DryField® PH abdominal wall and cecum showed an accumulation of mononuclear cells in the subperitoneal space (arrow), otherwise no pathological features were seen. (e, f) demonstrate a high level adhesion after creation of an abdominal wall defect (①: mononuclear cells as a sign of inlammation due to healing processes, ②: defect in abdominal wall muscle layers, ③: cecal mucosa). (g) Abdominal wall after creating an abdominal wall defect (① defect in muscle layer) and treatment with 4DryField® PH seemed to have an intact neoperitoneum (arrow) with slightly enlarged subperitoneal granulating tissue. (h) Cecal wall after peritoneal abrasion and treatment with 4DryField® PH showed normal cecal mucosa and submucosa ③. The intact neoperitoneum (arrow) had an enlarged subperitoneal fibrous tissue with infiltrating mononuclear cell ②.

In higher magnification of healed abdominal wall lesion areas of group 4, a few isolated polysaccharide particles could be found in varying levels of degradation (Fig.A.2-4). Fig.A.2-4 (a) and (b) show a single remnant particle, surrounded and invaded by mononuclear cells and polynuclear giant cells. After complete absorption of 4DryField® PH particles, normal granulating tissue was seen (Fig.A.2-4 (c)).

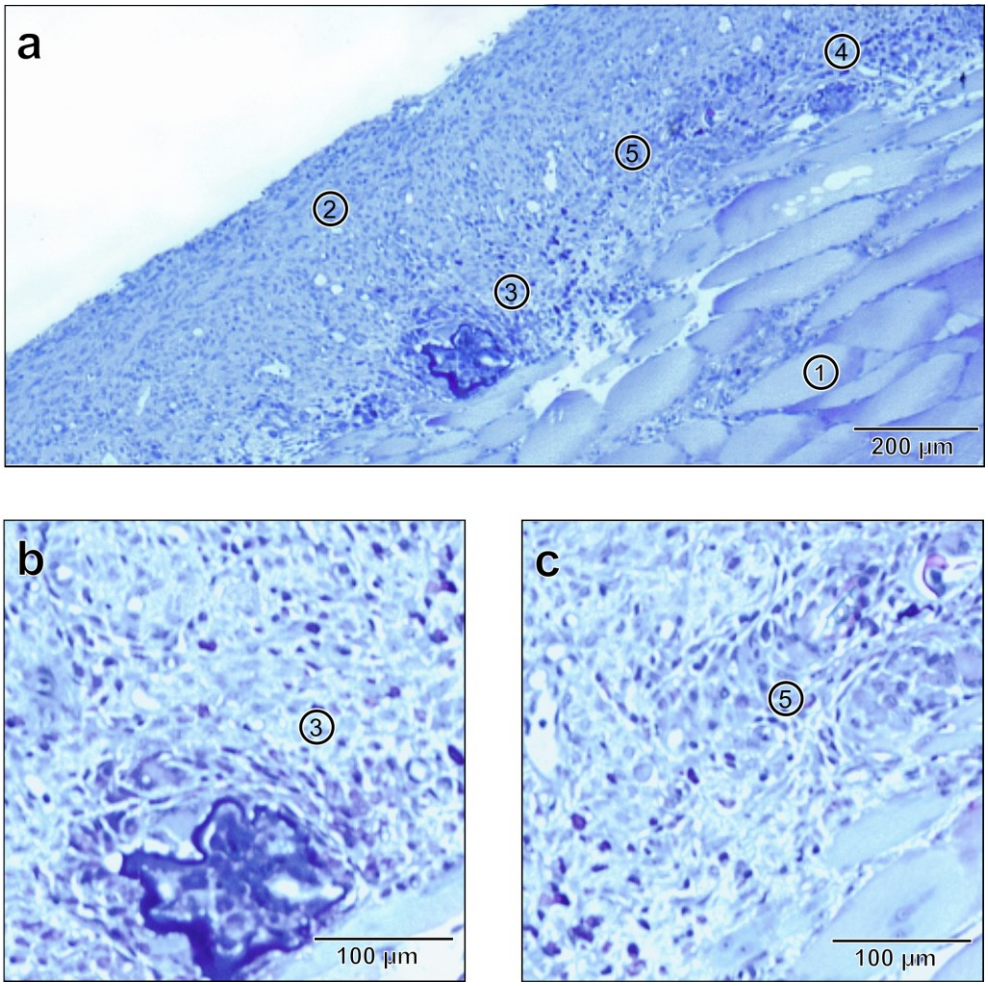

Fig. A.2-4. Histology of mesothelial site of abdominal wall at day 7 after creation of a multilayer abdominal wall defect and 4DryField® PH application in a representative animal of group 4 (Alcian blue and PAS staining). The peritoneal wall was already healed with a continuous neoperitoneum. (a) Overview with ① skeletal muscle of abdominal wall, ② inner surface of the abdominal wall with intact neoperitoneum and an enlarged submesothelial layer; ③, ④, and ⑤ show different stages of degradation of polysaccharide particles. (b) Higher magnification of residual polysaccharide particle ③, which is surrounded by mononuclear cells. (c) Higher magnification of resolving groups of mononuclear cells after degradation of polysaccharide particles ⑤.

A.2.5 Discussion

Several topical haemostatic agents are currently available exerting their effect in improving primary haemostasis, stimulating fibrin formation or inhibiting fibrinolysis [438]. Oxidised cellulose or oxidised regenerated cellulose have been used as haemostats for decades and are still substantially present on the market [438]. As plant-based agents, they are quite well biocompatible baring a low risk of allergic reactions or transferal of diseases caused by foreign proteins and/or blood born pathogens. However, they have a degradation time of about 3-4 weeks [438]. If left in the body in significant amounts, they can be the focus of severe adverse events including adhesion formation [438, 449-453]. Their appearance as granulomata leads to the suggestion that degradation time might even be longer than weeks [454].

Since 1970, mammalian derived products mostly based on bovine, porcine, or other domestic animal albumin, collagen, or gelatin have been used [438, 455, 456]. These agents are often combined with

human agents like thrombin, fibrinogen, or other coagulation factors. Despite improved technologies of screening, transferal of diseases can still not be ruled out completely [438].

Mammalian-based products can be the basis of allergy and immunologic reaction [457] and transient granulomatous inflammation of variable intensity [454, 458]. Degradation times of 3-4 weeks and longer for collagen and gelatin based haemostats implies the patients' metabolism being faced with foreign proteins for a substantial period of time. The property of cellulose- and mammalian-based agents to induce granuloma formation has been shown in an experimental comparative study [454]. If haemostats include components like glutaraldehyde, degradation time can be massively prolonged; in spinal surgery this type of haemostat has been reported to persist for two years [459].

Current polysaccharide based haemostatic agents act by their capability to absorb water leading to a relative enrichment of coagulation factors. They have a short retention time in the body [438, 454] and thus exhibit a low risk to cause a granulomatous reaction [454]. A non-pharmacological approach to prevent adhesions is the use of temporary or permanent barriers to separate the injured tissue from the surrounding organs throughout the critical time for adhesion formation during peritoneal healing [442]. Since post-surgical regeneration of the peritoneum occurs within days [460], a timely degradation or excretion of devices is desirable to decrease the risk of an immunological response or foreign body reaction.

4DryField® PH is a new device being certified for both, haemostasis and adhesion prevention [440, 446, 447]. In case of diffuse bleeding or extensive peritoneal defects, higher amounts of 4DryField® PH might be indicated and the question of biocompatibility arises. Cytotoxicity tests of 4DryField® PH indicate that even in the pure extract there is only a slight decrease of cell viability far from the level of cytotoxicity (defined as 70% baseline level) according to the European and US American regulatory administrations. On the other hand and importantly, viability was not elevated in direct contact and/or extract dilutions which indicates that tumour derived cell lines from sarcoma and adenocarcinoma do not profit from the presence of 4DryField® PH. By this 4DryField® PH as powder or gel can be considered in tumour surgery.

Application of 4DryField® PH to peritoneal cavity of rats revealed that the polysaccharide powder did not induce adverse events, including adhesion formation. Since no remnants of 4DryField® PH could be found micro- and macroscopically, it can be assumed that 4DryField® PH gel disperses on the intact peritoneum; some accumulation of mononuclear cells subperitoneal indicate that degradation processes might occur there.

Interestingly, animals with abdominal injury by cecal abrasion combined with a multi-layer abdominal wall defect and 4DryField® PH treatment had a course of bodyweight comparable to animals with only laparotomy. In contrast, injured rats without 4DryField® PH revealed a significant increased loss of bodyweight, suggesting that 4DryField® PH gel given on the injured area might enhance recovery.

The few 4DryField® PH remnants in the area of the former peritoneal wall defect are the result of a combined effect: 4DryField® PH was given there into a deep wound and trapped additionally by the suture fixed cecum, resulting in a local enrichment. Overall, the amount of 4DryField® PH found seven days after surgery can be judged minor with only few single particles left surrounded by mononuclear cells. This indicates that 4DryField® PH is degraded within days even if large quantities are locally present. Overall, the data show that 4DryField® PH in amounts of 0.7-1.09 g/kg bodyweight is well tolerated and contributes to favourable peritoneal healing.

A.2.6 Conclusions

In vitro cytotoxicity testing indicates that 4DryField® PH is not cytotoxic and that on the other hand human and murine tumour cell lines do not profit from the presence of 4DryField® PH. The *in vivo* studies in rats with unimpaired abdomen show that doses of up to 1.09 g/kg bodyweight of 4DryField® PH are well tolerated and are mainly degraded within days. 4DryField® PH has no negative impact on animals' general wellbeing nor on normal peritoneal tissue. Animals with abdominal injury do gain a benefit from the application of 4DryField® PH by showing reduced adhesion formation and a favourable course of bodyweight. The biocompatibility of 4DryField® PH can be rated excellent.

Acknowledgements

The authors thank Anneke Loos and Eveline Sowa-Söhle, Biocompatibility Laboratory, BioMedimplant, Hanover Medical School for technical assistance and their critical review of this work.

Declaration of conflicting interests

None declared.

Funding

This research received no specific grant from any funding agency in the public, commercial, or not-for-profit sectors.

A.3 3D-printed individual labware in biosciences by rapid prototyping: *In vitro* biocompatibility and applications for eukaryotic cell cultures

Tim H. Lücking[1], Franziska Sambale[1], Birte Schnaars[1], David Bulnes-Abundis[1], Sascha Beutel[1] and Thomas Scheper[1]

[1] Gottfried Wilhelm Leibniz University of Hannover, Institute of Technical Chemistry, 30167 Hanover, Germany.

Correspondence: Dr. Sascha Beutel (Beutel@iftc.uni-hannover.de), Institute of Technical Chemistry, Gottfried Wilhelm Leibniz Universitat Hannover, Callinstraße 5, D-30167 Hannover

Published in Engineering in Life Sciences, 2015. 15(1): p. 57-64, DOI: 10.1002/elsc.201400094.
Reprinted with kind permission from Enginering in Life Science

A.3.1 Abstract

Three-dimensional (3D) printing techniques are continuously evolving, thus their application fields are also growing very fast. The applications discussed here highlight the use of rapid prototyping in a dedicated biotechnology laboratory environment. The combination of improving prototypes using fused deposition modeling printers and producing useable parts with selective laser sintering printers enables a cost and time-efficient use of such techniques. Biocompatible materials for 3D printing are already available and the printed parts can directly be used in the laboratory. To demonstrate this, we tested 3D printing materials for their *in vitro* biocompatibility. To exemplify the versatility of the 3D printing process applied to a biotechnology laboratory, a normal well plate design was modified *in silico* to include different baffle geometries. This plate was subsequently 3D printed and used for cultivation. In the near future, this design and print possibility will revolutionize the industry. Advanced printers will be available for laboratories and can be used for creating individual labware or standard disposables on demand. These applications have the potential to change the way research is done and change the management of stock-keeping, leading to more flexibility and promoting creativity of the scientists.

Keywords: 3D printing / Biotechnology / Cell culture / Labware / Rapid prototyping

A.3.2 Introduction

Nowadays, the development of new components for the use in biotechnology laboratories, such as simple disposable labware, is very time consuming and requires adequate manufacturing installations and methods. The design and manufacturing of new labware and their new applications is relegated basically to the big companies. One recent example is the introduction of a 5-mL Eppendorf tube. Development and manufacturing of prototypes are complex processes comprising multiple steps to obtain a fully functional end product. The fabrication difficulties are explained using the design and construction of a modified baffled well plate, compared to the normal designs, for increasing the oxygen intake. For the high-quality fabrication of well plates, an appropriate casting mold has to be created and used as a tool for a further deep-drawing process. Funke et al. used laser cutting to cut the well geometries out of acrylic glass plates [461]. This step has multiple drawbacks in terms of

usability of the prototypes. For instance, only material up to certain thicknesses can be processed with laser cutting machines and furthermore just few materials allow focusing of the laser beam [462]. After this step, a bottom plate had to be glued under this geometry plate to seal it completely. Here, it was done via gluing, which itself leads to multiple problems. The glue should completely seal the geometries without creating trapped areas or hard-to-clean gaps. The glue used must withstand sterilization, which can include irradiation or steam sterilization, and should be biocompatible.

All these problems and the multistep building process can be simplified and accelerated with the use of three-dimensional (3D) printing. The same scenario of the well plate construction is not only simplified, but design possibilities are extended. Modifying the wells individually, e.g. defining rounded corners on the bottom or even geometry differences within the height of a single well. The plate is still created from one solid piece. This is not possible using 2D laser cutting techniques. To create this 3D-printed well plate, it should be digitalized into a 3D model using computer-aided design (CAD) software. The obtained 3D model must be prepared for printing, which is done by digitally slicing the model into different 2D layers. This is done via specific software, usually proprietary, depending on the printer to be used. The printer used for printing the laboratory labware is based on the selective laser sintering (SLS) method, in which a polymer powder is spread across the printer's building platform forming a flat surface, where one slice of the model will be printed by melting (sintering) the polymer with a focused laser. After the slice is printed the process is repeated adding layer over layer until the complete model is finished. To be able to benefit from 3D printing in the area of biotechnology, it is fundamental that the used material meets several requirements. These requirements include chemical stability and biocompatibility, as well as resistance to temperature and radiation for sterilization purposes. In this article, we focus on biocompatibility and sterilization resistance, as compliance with these two will yield a usable device for the general biotechnological use.

To assess the biocompatibility of our 3D-printed prototypes, several tests were conducted. The first experiments were to test the raw material itself, the norm ISO 10993–12:2012 was followed to obtain an extraction medium that was tested on several adherent and suspension cell lines [229, 463]. On another experiment, adherent cell lines were directly cultivated in the printed well plates.

Having shown general biocompatibility, we proceeded to demonstrate the potential of 3D-printed individual labware with the example of a completely printed baffled well plate. This well plate contains wells of different geometries and design. These modifications are meant to modify and increase the oxygen intake in the culture media compared to a normal round-shaped well. Such a well plate can be used to study organism's behavior in different oxygen concentration conditions in parallel due to the individual differences in k_La obtained by the baffle design. Another use could be the evaluation of mixing performance due to the modification of the wells. To demonstrate the usability of this well plate and the effect of these geometries, we cultivated *Saccharomyces cerevisiae* as a

eukaryotic model organism. This was selected due to its higher oxygen consumption and faster growth in comparison to mammalian cells. By using a high oxygen demanding microorganism, growth rate can be used as an indication of oxygen limitation and correlated to the oxygen transfer created by the different well geometries.

This well plate is just one example used to highlight the possibilities of 3D printing in a biotechnological laboratory. Scientists face only their imagination as a limit and can now create new labware designed especially for their needs. A proof of principle with different practical examples is also available [464].

A.3.3 Materials and Methods

A.3.3.1 Modeling and Printer Technology

All models for 3D printing were created with the CAD software Autodesk Inventor Professional 2014 (Autodesk, Inc., San Rafael, CA, USA).

For the construction of the new prototypes, two different 3D printing techniques were used—FDM (fused deposition modeling, the term FDM is trademarked by Stratasys, Inc.) and SLS.

Printing with the FDM technique was done with a desktop oriented, low-priced CubeX Trio printer (3D Systems, RockHill, SC, USA) [465]. This printer enabled us to get the first physical models and optimize geometries that suited our needs. The materials available for this printer are polylactic acid and acrylonitrile butadiene styrene. Unfortunately these materials are not suitable for laboratory use. Printing with the SLS technique was done by Blue Production (Paderborn, Germany). With this printer system, the material used was polyamide (PA) 12 powder (herein after referred to as PA12) [465]. Models created with this technique are potentially suitable to use in the laboratory environment when it comes to chemical stability, biocompatibility, and withstanding sterilization conditions.

A.3.3.2 Three-Dimensional Printing Raw Materials and Preparation of Extraction Media

The SLS 3D-printed well plates and the unprocessed PA powder were obtained from Blue Production. Two different types of PA were used — PA12 and the PA12 combined with an undisclosed UV stabilizer (in the following referred to as PA12 UV). For the biocompatibility experiments, an extraction medium was created according to ISO 10993–12:2012 (Biological evaluation of medical devices—Part 12: Sample preparation and reference materials) [229]. Therefore, the powder was sterilized by autoclaving (121°C, 2 bar, 30 min).

The culture medium appropriate for each cell line (see below) was mixed with the PA powder (0.2 g/mL). These media mixtures were placed in an incubator at 37°C for 72 h at a shaking speed of 160 rpm. To remove the powder, the media was centrifuged at 3,000 × *g* for 1 h (Centrifuge 5702, Eppendorf AG, Hamburg, Germany). The supernatants were filtered using a 0.22 μm sterile filter (Filtropur S, Sarstedt, Nuembrecht, Germany). The obtained extraction medium was used for the cultivation experiments.

A.3.3.3 Three-Dimensional Printed Well Plates

For the direct cultivation experiments, two different designs of well plates were modeled—type A and B—and were 3D printed with an SLS machine out of the PA12- and PA12 UV material. Type A is an exact replica of a commercially available 24-well plate (Culture Plate Flat Bottom, Sarstedt, Newton, NC, USA), it was used for the biocompatibility experiments using adherent mammalian cells.

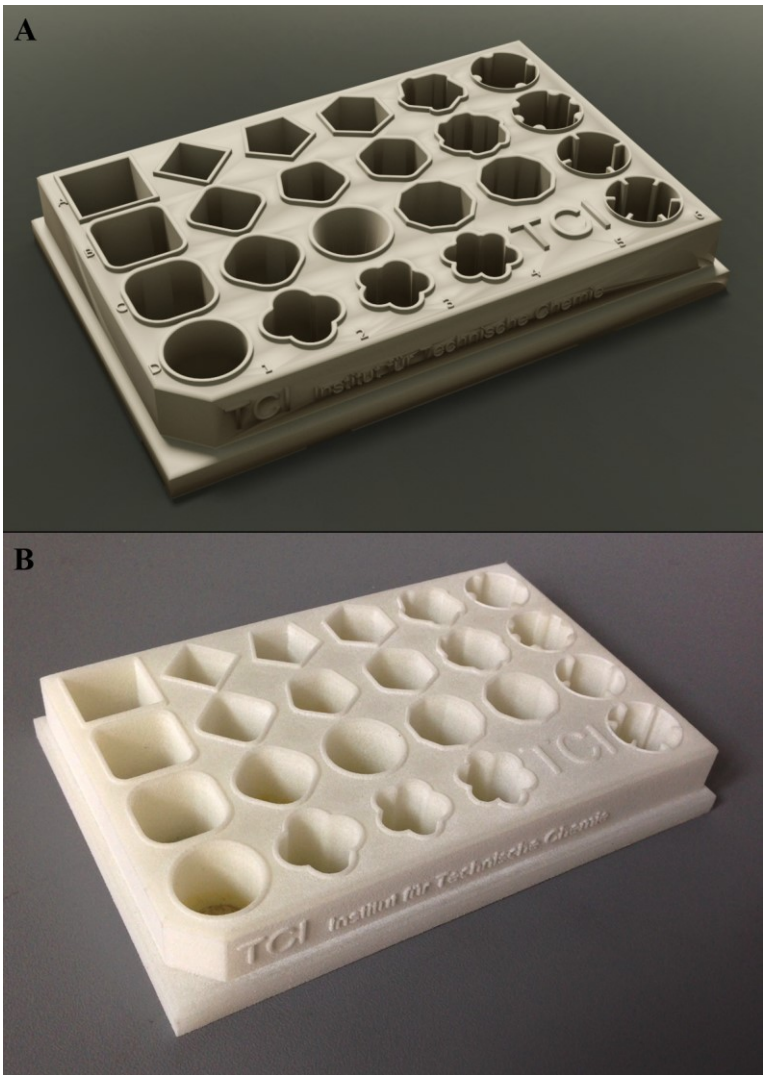

Fig.A.3-1 (A) Rendered CAD image and (B) photo of the printed baffled well plate type B. The printed plate was used for cultivation experiments with S. cerevisiae. A 3D view of the well plate type B is available in the online Supporting information.

Type B is a custom-designed well plate with 23 different well geometries. The type B design was used for the culture of yeast cells.[461] A rendered CAD image (A) and the printed model (B) of the well plate type B are shown in Fig. A.3-1.

A.3.3.4 Cell Culture and Cell treatment—Adherent Cells

The raw material biocompatibility tests were carried out in standard 24-well plates, 1.82 cm^2 growth area, approximately 1 mL maximum working volume (Culture Plate Flat Bottom, Sarstedt, Newton, NC, USA). Two different adherent cell lines were used, a human epithelial lung cell line A549 (DSMZ no.: ACC 107), and mouse fibroblasts NIH-3T3 (DSMZno.:ACC59). Both were maintained in

DMEM(Sigma Aldrich, St. Louis, MO, USA) supplemented with 10% FCS (Biochrom GmbH, Berlin, Germany) and 1% v/v Penicilin/Streptomycin (PAA Laboratories GmbH, Pasching, Austria). A549 and NIH-3T3 cells were seeded at a density of 1.5 × 104 cells/cm^2 with a final volume of 300 μL and maintained at 37°C with 5% v/v CO_2.

The normal culture media was removed from the 24-well plate after 24 h and extraction media was added for another cultivation period of 24 h. To test the actual 3D-printed well plates, cells were cultured in the printed well plate type A for 48 h. A standard 24-well plate cultivation was run in parallel for reference.

In both cases after the cultivation period was over, the cell count was measured and the CellTiter-Blue ® (CTB) cell viability assay and the CytoTox-ONE™ homogeneous membrane integrity assay (lactate dehydrogenase (LDH)) were performed.

A.3.3.5 Cell Culture and Cell Treatment—Suspension Cells

Suspension adapted Chinese hamster ovary cells CHO-K1-HP (provided by AG Cell Culture Technology, University of Bielefeld, Germany) were maintained in shaking flasks using CHOMACS CD media (Miltenyi Biotec, Bergisch Gladbach, Germany) supplemented with l-glutamine (8 mM, Biochrom, Berlin, Germany).

Raw material biocompatibility test was done using CHO-K1-HP cells cultured in extraction media and untreated media (as reference) in 250 mL shaking flasks (Corning, Tewksbury, MA, USA) maintained at 37°C, 5% CO_2 v/v, and 160 rpm for 5 days starting with a cell density of 4.5 × 105 cells/mL.

A.3.3.6 CTB Cell Viability Assay

To determine the cell viability of A549 and NIH-3T3 cells, the CTB cell viability assay (Promega, Mannheim, Germany) was used. Living cells are able to convert resazurin into resorufin, which fluoresces. Necrotic cells, however, are not able to reduce resazurin and therefore are not generating the fluorescent product.

After the incubation period, the CTB assay was performed as instructed by the manufacturer, including background and control groups. At first the medium was removed from each well and 250 μL of fresh medium containing 10% v/v of the CTB stock solution were added to each well and incubated for 2 h. The fluorescence of resorufin reduced by viable cells is measured at 544/590 nm with a fluorescence plate reader (Fluoroskan Acent, Thermo Fisher Scientific, Inc., Waltham, MA, USA).

A.3.3.7 CytoTox-ONE™ Homogeneous Membrane Integrity Assay (LDH)

The CytoTox-ONE™ homogeneous membrane integrity assay (Promega) was used to determine the membrane integrity of cultured cells. Through the loss of membrane integrity the enzyme LDH is released from the cells into the surrounding culture medium. The amount of leaked LDH is measured by the conversion of added resazurin into resorufin using fluorescence measurement at 544/590 nm. The amount of leaked LDH is proportional to the number of nonviable cells and can be used to

calculate the percentage of a cytotoxic effect. The assay can also be used in combination with a lysis solution, to get an estimation about the total cell count. The LDH assay was performed with A549 and NIH-3T3 cells. Cells were seeded as described above. For the determination of cell death, 100 μL medium from each well were transferred into a new 96-well plate. For calculation of cell count after exposure, cell lysis was induced before collecting the culture media. Both variants of the protocol, with and without cell lysis, were used for the experiments. Afterwards, the LDH assay was used as instructed by the manufacturer.

A.3.3.8 Measuring Cell Proliferation (Cell Counting)

For the adherent cells, the cell proliferation was measured by determination of the cell count using an improved Neubauer chamber. Cells were cultured as described before. After the cultivation media was removed, cells were detached from the well plates using 0.2% trypsin/0.02% EDTA solution (approximately 5 min, 37°C, 5% v/v CO_2). For the suspension cells, CHO-K1-HP proliferation and viability was measured using the cell counter Cedex (Roche Innovatis AG, Penzberg, Germany). During the 5-day incubation period (see above), the measurement was performed twice a day.

A.3.3.9 Cultivation of S. Cerevisiae

Yeast media containing 3 g/L yeast extract, 3 g/L maltose, and 5 g/L soy broth dissolved in deionized water were used. The pH value of the medium was adjusted to approximately pH5.5. After autoclaving, 10 g/L glucose (separately sterilized) was added. For the *S. cerevisiae* pre culture, a colony was taken from an agar plate and suspended in a 250-mL shaking flask containing 100 mL yeast medium. The culture was incubated at 30°C on a shaker at 220 rpm for 24 h. For the experiment, the OD of the culture was measured at 600 nm. The OD was adjusted to $OD_{600\ nm} = 0.5$ by mixing with fresh culture medium in a new flask. For the cultivation in the 3D-printed well plates type B 1000 μL of prepared yeast culture was seeded into each individual well. The well plates were incubated for 24 h at 30°C and shaken at 175 rpm. After the incubation time, the OD of each well was measured at 600 nm using a spectrometer (Multiskan™ GO, Thermo Scientific).

A.3.4 Results and Discussion

Every rapid prototyping (RP) technology has its own advantages and disadvantages. Especially the demanding requirements for the use with mammalian cell culture narrow the choice of the possible printing methods. The most promising method is SLS printing, because it has the broadest range of usable materials. However, one of the main issues with the SLS printing technology is that sintered materials tend to have a rather porous structure [466]. The chosen manufacturer optimized the sintering method together with the material composition to achieve minimal porosity. During experiments, we observed that a complete leak-proofness depends on the sterilization method. Although the material is able to withstand standard steam sterilization methods (121°C, 2 bar, 30 min) without observable changes, the 3D-printed parts become more porous. Furthermore, if the material gets in contact with alcohol, e.g. 70% isopropanol or ethanol for cleaning purposes, the volatile

solutions swell the structure, leading to leaking of the liquids. When it comes to the use of RP for generation of scaffolds for tissue engineering, this porosity can be a desired trait; but for creating culture vessels this is a drawback. Different approaches to sterilize the well plates were used. For the experiments with yeast, it was sufficient to irradiate the plates with UV light (HERAsafe KS, Thermo Electron, Langenselbold, Germany, 10 cm distance, 60 min) and achieve thereby a germ-poor environment. For the use with mammalian cells, sterilization with gamma irradiation was chosen as the standard technique that is already widely used for labware and especially single-use equipment and bioprocess systems [467, 468]. With the use of irradiation sterilization, the created parts are not physically altered and can be used directly for cultivation purposes.

The leak-tightness is still a problem that can be faced in further optimization steps. This problem can be removed by improving fabrication parameters, e.g. the sintering time by the laser beam or by adding a post processing of the printed parts. This could be an infiltration with a suitable and also biocompatible material, e.g. a resin that would be vacuum-impregnated into the part using a desiccator and subsequently completed in a curing oven.

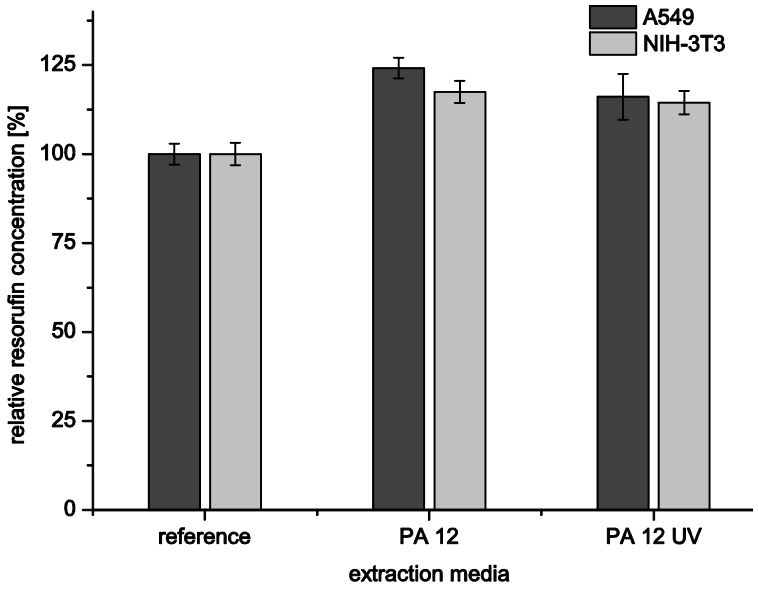

Fig. A.3-2. The relative resorufin concentration compared to the reference. Resorufin is reduced by viable cells and thus provides information about the culture viability. The experiments were replicated thrice with four replicas within each experiment (error bars indicate the SD of the experiments).

A.3.4.1 Adherent cell cultivation in extraction media

As model organisms for the biocompatibility testing, epithelial cells (A549) and fibroblasts (NIH-3T3) were cultivated. To detect the possible toxic effects, the cells and the supernatant were tested with different assays for adherent cell cultivations. The used methods were CTB assay and LDH assay. The first method provides evidence about the vitality measured by the metabolic activity of the cells and the second gives a statement about the amount of necrotic cells. An additional manual cell counting was carried out. Results from the CTB assay are summarized in Fig A.3-2.

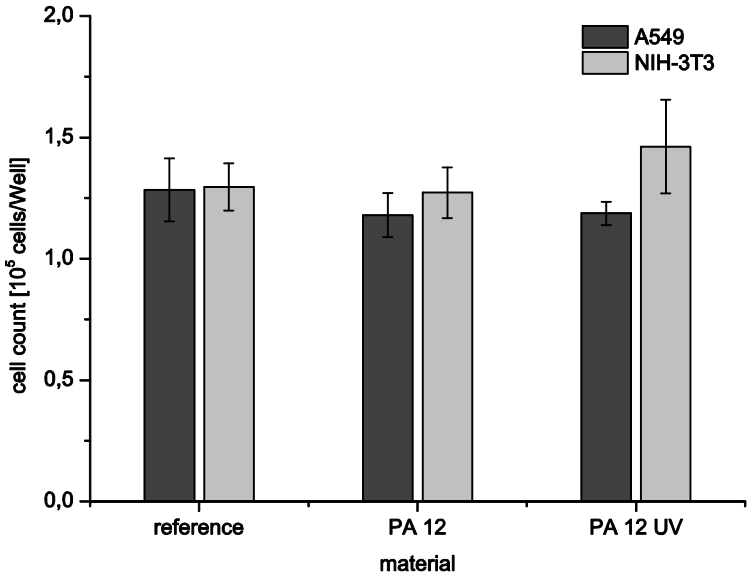

Fig. A.3-3 Absolute cell count per well (average of four wells, error bars indicate the SD of the experiments). Cells were cultivated for 48 h and detached using trypsin. Counting was performed manually with a Neubauer chamber.

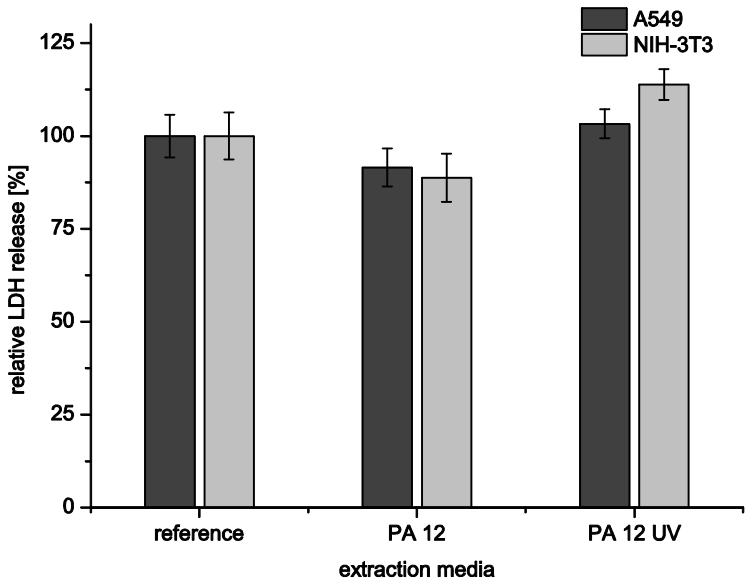

Fig. A.3-4 Relative LDH concentration after lysis of the cells. Because of the cell lysis, these results provide information about the absolute cell concentration in each well. The shown data are an average of four parallel experiments (error bars indicate the SD of the experiments).

The CTB test indirectly measures the metabolic activity of the cells and thus gives an indication of the cell vitality. Both cell lines show the same behavior after being in contact with the extraction media for one day. Compared to the reference cultures, both experiments with extraction media show a slightly improved metabolic activity. The comparison of the PA12- and PA12 UV extraction media cultivations shows no large variations among them. Cell count of the same experiment is shown in Fig. A.3-3. All cultures reach a relative similar concentration. Both cultivations with extraction media present the same behavior. They show a small deviation in cell count. The LDH concentration set free by cell lysis is shown in Fig. A.3-4. The results show a slightly lower LDH release and thus lower cell count with the PA12 extraction media and a slightly higher cell count with the PA12 UV extraction

media. This effect is more visible in the experiments with NIH-3T3 cells. In our experience, NIH-3T3 cells are always more sensitive to toxic effects compared to A549 cells [232].

A.3.4.2 Adherent cultivation in printed 24-well plates

In addition to the extraction media experiments, cultivation directly in a printed 24-well plate (well plate type A) was carried out. These experiments will test a more prolonged and intense contact of the cells and material. It will also reflect any discrepancy between raw material and processed 3D-printed material properties regarding biocompatibility. This well plate was modeled as an exact replica of the used standard well plates, which at the same time was used as a reference. Because of the initial results and the already known biocompatibility of the PA12 material, this experiment was carried out only with the well plate made of PA12 UV material. The surface of the printed well plate is rougher in comparison to a commercial well plate, this made detaching the cells from the surface very difficult. For that reason, only the LDH assay for determination of cell death, without cell lysis, was performed. The results for the LDH release are shown in Fig. A.3-5. It shows that the reference and the well plate type A made of PA12 UV have the same amount of active cells after the cultivation period. This is the case for the A549 cells, as well as for the NIH-3T3 cells.

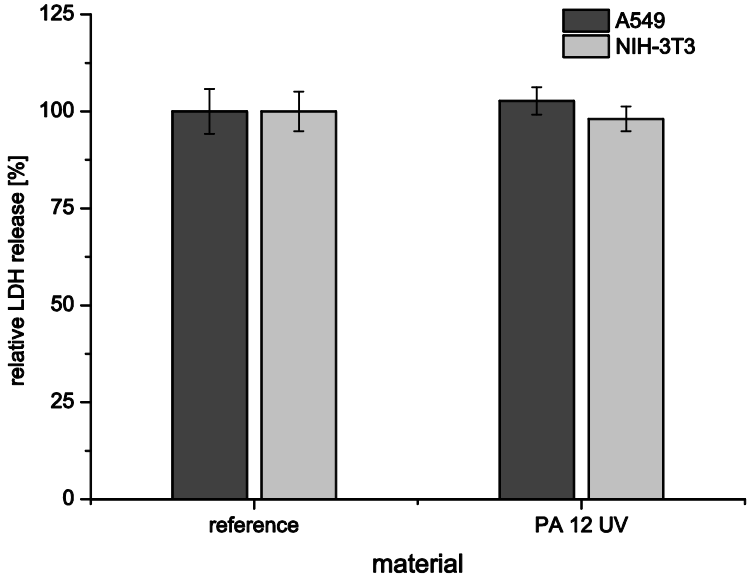

Fig. A.3-5. Relative LDH release in the supernatant without cell lysis. These measurements are used for determination of cell death. The LDH release in the supernatant is caused by the loss of membrane integrity of the cells and indicates necrotic cells. Both cell strains were cultivated in 3D-printed replicas of a 24-well plate, as well as in the standard well plate as a reference. The shown data are an average of four parallel experiments (error bars indicate the SD of the experiments).

A.3.4.3 CHO-K1-HP suspension cultivation

For the biocompatibility testing with suspension cells, CHO-K1-HP were cultured in shaking flasks with the prepared PA12- and PA12 UV extraction media. The growth curves were compared to cells cultivated in untreated media to see the effect of possible extractables or leachables out of the material. Since the cells grew in suspension and a higher volume of cell suspension was available, the culture condition could be measured using an automated cell counter. Therefore, it was not necessary to use the above mentioned assays.

The results of the cultivations are shown in Fig. A.3-6. The results show two different growth behaviors. All flasks started with cell concentration of 4.5×10^5 cells/ml. The extraction medium, which was created with the PA12 UV powder, resulted in the best growth behavior. Compared to the cultivation with PA12 extraction medium and the reference, the cell concentration after 92 h was almost two times higher (1.96 times higher). The reference cultivation started with a slightly lower cell growth, but caught up after 3 days. Taking this into account, the cultures with reference media and the PA12 extracted media have similar growth behavior and thus endorse the biocompatibility of this material. Therefore these results confirm the U.S. Pharmacopeia (USP) biocompatibility certification of the PA12 material. The experiments with the extracted PA12 UV media also support the biocompatibility of the material. Furthermore it shows unexpected promises in other aspects, such as the observed increasing cell number.

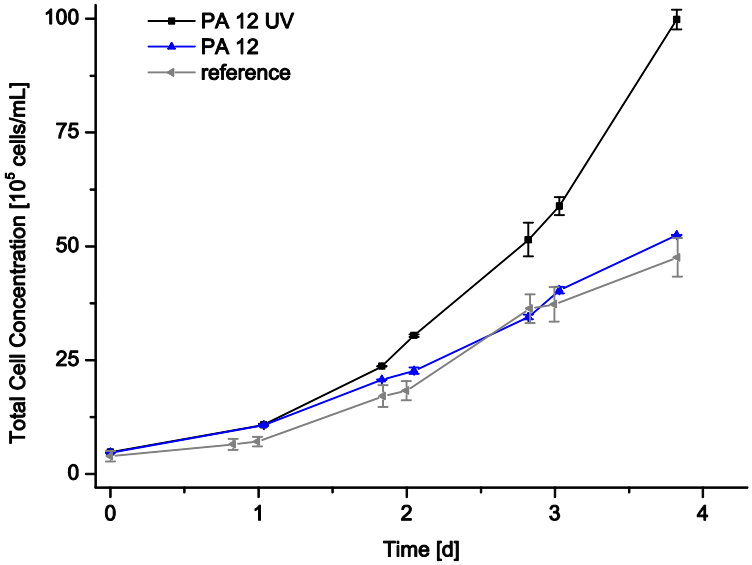

Fig. A.3-6 CHO-K1-HP growth curve, showing the viable cell concentration. The cells were cultured in CHOMACS CD media at 37°C and 5% v/v CO2 at 160 rpm orbital shaking. The shown data are the average of two parallel experiments, error bars indicate the SD.

To achieve the UV stability of the improved PA12 material, an undisclosed amount of an antioxidant was added to the powder. Antioxidants have in general a stabilizing effect on cells. This supports the assumption that oxidative stress is a major problem in cell cultures and that medium is often not sufficiently supplemented with antioxidants [469-471]. This could explain why the cultures treated with this antioxidant enriched medium have a higher proliferation than the others. The proprietary composition of the used media, CHOMACSCD, seems to be insufficiently provided with proper antioxidants.

The comparison between the adherent cells cultivated in well plates and the suspension cells cultivated in shaking flasks (Fig. A.3-6) shows that there was no strong positive or negative effect within the adherent cell experiments. We assume that the reason is the reduced oxygen diffusion in the stationary well plates compared to the orbital shaken flasks. The bigger oxygen transfer in the flasks could have resulted in larger amounts of radical oxygen species being formed in the culture media. Therefore the

positive effect of the added antioxidant could be more easily observed. The absence of radical oxygen species in the stationary well plates could explain why those results show no great difference between the PA12- and PA12 UV material. Nevertheless the PA12 UV material shows equal and in some cases even better results, than the USP-certified PA12 material. This backs up the use of the novel UV-stable material for certain applications, and supports the biocompatibility of the standard material.

A.3.4.4 Yeast cultivation in baffled well plates

After showing that the material is biocompatible and suitable for cultivation purposes, an application example was tested. A baffled well plate with 23 different well geometries within one well plate was designed and 3D printed (well plate type B). In contrast to previous publications of other work groups, we simplified the fabrication drastically and created the well plate as one solid piece all in one step [461]. For this experiment we chose *S. cerevisiae* as a eukaryotic model organism with quick growth and higher oxygen consumption. Fig. A.3-7 shows the results of four different well geometries, starting from the square-shaped well and increasing the roundness of the corners until a completely round well is achieved. We observed the highest growth after 24 h in the square shaped well. Optical densities decreased with increasing corner radius of the well geometry (Fig. A.3-7).

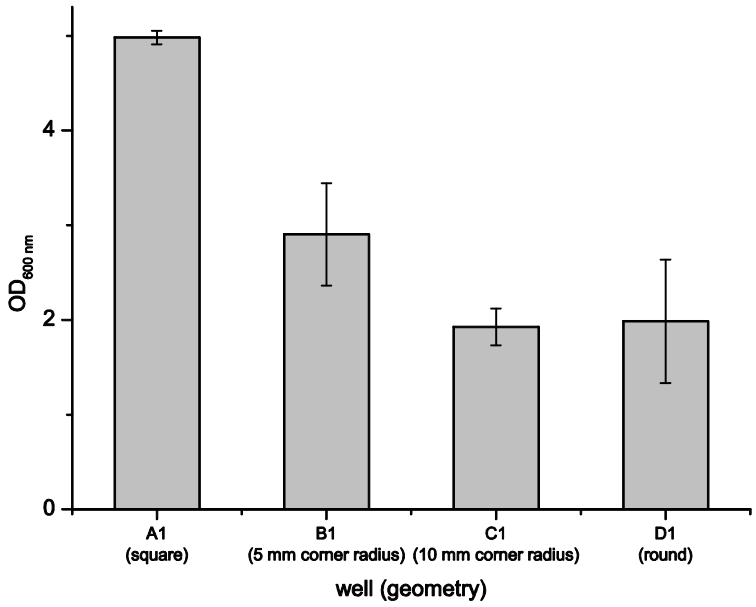

Fig. A.3-7 Results of *S. cerevisiae* cultivation in 3D-printed well plate type B. Columns show theOD600 nm measurements after 24 h of cultivation at 30°C and 175 rpm. The influence of increasing the corner radius from square until a completely round well is shown. This experiment was repeated three times (error bars indicate the SD of the experiments).

The results illustrate the effect of including edges in the well geometry. Their inclusion increases the turbulent mixing and thus leads to a higher oxygen intake. This corresponds with the observations of Funke et al. and therefore shows the feasibility of optimizing commonly used labware with 3D printing techniques and their comparison to conventional fabricated labware [461]. Going further from the specific results of this experiment, this study demonstrates the applicability of the novel manufactured printed labware. This enables the possibility to adapt the labware to the specific needs of the organism being used, regardless of their wide differences.

A.3.5 Concluding Remarks

Our results demonstrate the possibility to integrate 3D-printed devices or culture vessels in a dedicated laboratory environment. It enables more time-efficient development of new prototypes and will help scientists around the world to create almost any construction without needing dedicated knowledge and skills of complex manufacturing processes. Precision engineering workshops are often not available for all laboratories or are not able to create complex working prototypes within a short time. Furthermore RP is very cost-effective, if small quantities are needed which is often the case for prototypes or individual solutions. With this new technology, it is basically sufficient to use CAD software to create the desired geometries and subsequently transfer those to a 3D printer.

Labware being used now was designed long ago and with only a few organisms in mind, which had at that time not so complex requirements. More sensitive and demanding organisms, such as mammalian cells, require more sophisticated conditions. Biocompatibility of this new labware must be certified and should be able to withstand the relatively long duration of mammalian cell cultivations. The experiments using extraction media and the two adherent cell strains A549 and NIH-3T3, as well as the suspension cell strain CHO-K1-HP, confirm the biocompatibility of the already certified PA12 material, as well as the so far uncertified PA12 UV material. Furthermore the improvement of the UV-stable material by adding antioxidants benefits the proliferation conditions for the cell culture. This is reflected in better cell growth in UV-stable material compared to the USP-certified PA12 material.

The yeast cultivations in baffled well plates exemplify the usability and possibilities of design-driven 3D printing in a biotechnological laboratory. It was possible to reach a sufficient oxygen intake by adding different baffle geometries. More important than the results itself is that this experiment shows how easily a new design, e.g. a well plate or any other cultivation vessel, can be materialized with RP technology. One of the present problems with 3D printing and especially with SLS technology concerning labware is the leak-tightness of the printed object. SLS is the most suitable 3D printing method, because of the wide range of applicable materials, but the sintering process itself has to be further optimized. The results, exposed here, show that it is possible to create complex labware that is biocompatible and can be used in real-life biotechnology applications. Also we could observe that the process of SLS fabrication does not change the properties of the material with regard to the biocompatibility.

The future RP technology will support new approaches in developing novel products for biotechnology purposes such as probes, reactors, or basic consumables. As a result, it will also have an effect on the logistics. A laboratory of the future may not need to rely any more on elaborate stock keeping of all necessary labware, it will be able to maintain its own inventory and produce new consumables over night or just in time on demand. Therefore even the direct integration of future generation 3D printers in laboratory benches is imaginable.

The laying of the foundation stone for this future vision was the expiration of one major patent for SLS on January 28, 2014 [472]. Many other key patents connected with 3D printing are expiring from now until the middle of 2015 [473-483]. As patents expire novel printers become more affordable and the development and improvement of the techniques advance rapidly. Similar to the 3D printing revolution that accompanied the expiration of major FDM patents, a new movement is expected to appear. This second revolution will shake up the industry and make the yet high priced devices more affordable for small companies and especially laboratories. With the future advancements in premises to the printer technology, it will be possible to use the RP directly in a dedicated biotechnological laboratory for creating the needed labware or even complete bioreactors. This would lead to new approaches of developing and producing consumables and is, as a consequence, an important topic for today's manufactures to deal with.

Practical application

Individual labware created with 3D printers directly in a laboratory will advance science and research in the near future. As an example, a specifically designed well plate is used to illustrate this approach. Using 3D printing technologies, it will be possible to adapt the labware design to fulfill specific requirements of an experiment or an organism that is being cultured, instead of fitting a broad range of needs to standard labware design. Furthermore, the 3D printing material was examined for their applicability within a biotechnological laboratory. The expiration of patents protecting specific 3D printing technologies and the fast-paced advancements will make this technology available for many laboratories around the world within a couple of years.

A.4 3D-printed individual labware in biosciences by rapid prototyping: A proof of principle, Engineering in Life Sciences

Tim H. Lücking[1], Franziska Sambale[1], Sascha Beutel[1*] and Thomas Scheper[1]

[1] Gottfried Wilhelm Leibniz University of Hannover, Institute of Technical Chemistry, 30167 Hanover, Germany.

Correspondence: Dr. Sascha Beutel (Beutel@iftc.uni-hannover.de), Institute of Technical Chemistry, Gottfried Wilhelm Leibniz Universitat Hannover, Callinstraße 5, D-30167 Hannover

Published in Engineering in Life Sciences, 2015. 15(1): p. 51-56, DOI: 10.1002/elsc.201400093.
Reprinted with kind permission from Enginering in Life Science

A.4.1 Abstract

The fabrication of individual labware is a sophisticated task that requires dedicated machines and skills. Three-dimensional (3D) printing has the great potential to simplify this procedure drastically. In the near future, scientists will design labware digitally and then print them three dimensionally directly in the laboratory. With the available rapid prototyping printer systems, it is possible to achieve this. The materials accessible meet the needs of biotechnological laboratories that include biocompatibility and withstanding sterilization conditions. This will lead to a completely new approach of adapting the labware to the experiment or even tailor-made it to the organism it is being used for, not adapting the experiment to a certain standard labware. Thus, it will encourage the creativity of scientists and enrich the future laboratory work. We present different examples illustrating the potential and possibilities of using 3D printing for individualizing labware. This includes a well plate with different baffle geometries, shake flask cap with built-in luer connections, and filter holder for an in-house developed membrane reactor system.

Keywords: 3D printing / Biotechnology / Cell culture / Labware / Rapid prototyping

A.4.2 Introduction

The recent developments in the area of rapid prototyping (RP) are leading to a consumer-oriented availability of desktop or bench-top printing devices. This progress, often described as revolution of the manufacturing industry, enables the cost-effective use of self-developed and thus individually designed labware ranging from single-use (SU) flasks up to reusable bioreactor components or even easily accessible replacement equipment [484]. The continuously expanding sector of SU systems in the biopharmaceutical production has emphasized the demand of inexpensive disposable consumables [485-487]. This SU system can be as simple as a vessel or as complex as a whole system designed to perform more elaborated tasks. The possibilities described in this report contain the individual customization of standard lab useables, e.g. a well plate with special baffles to increase the oxygen transfer or custom shake flask lids for connection of other devices or correction fluids during cultivation.

A.4.2.1 Fields of Applications in Biosciences, Medicine, and Chemistry

So far, most RP applications in the area of bioscience are situated in the fields of medical engineering and tissue engineering. Before performing a surgery, models of bones, limbs, or even organs of a patient help the physicians to have an in-depth look into the anatomy of a patient. The construction and fitting of an implant is much easier with a physical model [488]. A descriptive example is the reconstruction of a massive skull fraction. When parts of the cranial vault are missing, e.g. after an accident, it is possible to reconstruct the missing parts with computer assistance. The three-dimensional (3D) data can be obtained via a computed tomography (CT) scan, and the missing parts can be reconstructed using computer-aided design (CAD) software. These virtual models can be built afterwards with an RP method and fitted precisely before the critical surgery. Not only implantable prostheses are being created, even precisely fitted prosthetic limbs are possible [489]. RP in prosthetic dentistry is nowadays a standard technology [490]. Many of the recent dental prostheses are built with a technique that uses biocompatible metal powder as base material. This technology has ousted the classical cast modeling due to higher efficiency.

In the area of tissue engineering, RP is likewise expanding its application field. Reaching from normal cell culture vessels all the way to creating 3D scaffolds for cell growth, which can be tailored to support the proliferation, migration, and differentiation of the cells [491-493]. Research is underway to enable printing human tissue to heal burn injuries [494] as well as using RP techniques to manufacture bioartificial livers [495]. Furthermore, various scaffold fabrication methods use RP techniques for directly obtaining the desired geometries or creating molds for casting the scaffolds [496-501].

Other fields of research are aiming in the direction of microfluidics, where specific multilevel channel structures can be built without complex manufacturing methods. For example, it is possible to construct a cooling coil around a central channel in which a reaction takes place much easier [502, 503]. A relatively new approach is situated in the area of synthetic chemistry, where Symes et al. used a 3D printing system to build reaction ware. These specific small-scale vessels contained all needed solutions that could be mixed together in a reaction chamber. It is even possible to pause the printing process to manually insert a glass observation window. All materials for the vessel, as well as the solutions, were dosed with the printer system [504].
This technical report will demonstrate the practical capabilities of integrating 3D printer technology directly in a biotechnological laboratory environment and exemplify the benefits with some applications. Unlike the application of Symes et al., the material used in the biotechnology field has to fulfill more sophisticated requirements due to the direct cell contact.

A.4.2.2 2 Basic Principles of the Appropriate RP Methods for Biotechnological Applications

The basic principles of the main RP technologies are adequately known and explained through prior published reviews and papers, especially in the field of tissue engineering and medical engineering [465, 466, 489, 491, 505, 506]. The used methods for the prototypes shown in this report are explained

briefly hereafter. The basis of every RP model is a 3D dataset. This can be obtained by direct 3D scan or CAD modeling. The actual physical models are built by printing in 2½ dimensions; this means that one 2D cross-section layer of the object is printed on the print bed and then connected with the next following layer in *z*-direction. This process is repeated subsequently for every layer until the complete model is printed. Therefore, the printing procedure requires translation of the 3D dataset into *n* different layer datasets that can be interpreted and processed by the printer. An international standard file type, called STL, has been established for this purpose [507, 508]. RP procedures differ mainly in the method each layer is created and connected to the others.

In the last year, a big step to achieve a consumer accessible printer was made through the introduction of low-priced printers that use the fused deposition modeling (FDM) method. FDM is an invention from Stratasys (Eden Prairie, USA) [465]. The polymer material used is often in the form of a filament that is wound up onto a coil. This filament is transported to a heated nozzle extruder that is able to melt the polymer at its specific melting point. The extruder is computer-driven and moves in a plane defined by the *x*- and *y*-axis across the building platform that itself is movable in *z*-axis. The nozzle is driven close to the surface of the platform, where it releases the fused material according to the current layer dataset. During extrusion, the material solidifies directly on the print bed. After finishing the layer, the platform is lowered one step and the next layer is printed onto it, the heat of the extruded material directly melts and connects it to the previous layer.
Low-cost FDM printers currently reach a resolution as low as 100 μm [508], which is sufficient for most applications and especially the evaluation of new prototypes. The biggest disadvantage so far is the limited availability of adequate material for the laboratory purpose. The most affordable printers process either acrylonitrile butadiene styrene or polylactic acid. But it is only a matter of time until more versatile materials such as polyamide (PA) become available for these bench-top printers. Recent optimizations are aiming to directly use Nylon (PA 6.6) as a new construction material.

A more sophisticated RP technology is selective laser sintering (SLS). Unlike FDM, where the material in the form of a filament is melted and deposited, SLS uses the material in powder form. The powder is spread as a thin layer across the building platform. Then a laser is used to generate enough thermal energy to melt the powder particles together punctually and accurately while moving along the plot of the cross-section dataset. After finishing one layer, the building platform is lowered and new powder is spread across the surface. During the sintering of the subsequent layer, the previous one is also connected [465, 466]. The biggest advantage of this method is the wider range of materials that can be used. Besides standard polymers it is also possible to use metal powder, glass-filled polymers, or after certain adaptations theoretically any material that can be manufactured in powder form and melted with an appropriate laser [509]. Concerning the later applications in a laboratory, this opens new possibilities for creating SU as well as reuseable equipment.

The biggest obstacle of the SLS prototypes is the still relatively high acquisition costs of the sinter station itself. Also, the high degree of know-how needed to optimize the printing procedure presents an obstacle, e.g. the importance of correct placement of the model in the installation space to minimize warping of the prototype or compensating the normal shrinking process during cooling down.

The optimization of machine parameters is likewise very important, e.g. the normally relatively porous SLS models can reach a gas- and watertight state through modifications of diverse parameters, e.g. the vertical movement speed and intensity of the laser beam. Thus, the current optimal approach of building new prototypes is to combine different methods and use capable contractors with the needed equipment and expert knowledge.

The presented models were built following this approach. All models were first built with the cost-efficient FDM method to examine the general applicability. Thus, it was possible to optimize the model in detail before starting the external production with the desired material. After the final model was generated, the dataset was submitted to a contractor where the models were printed with the above-mentioned PA materials.

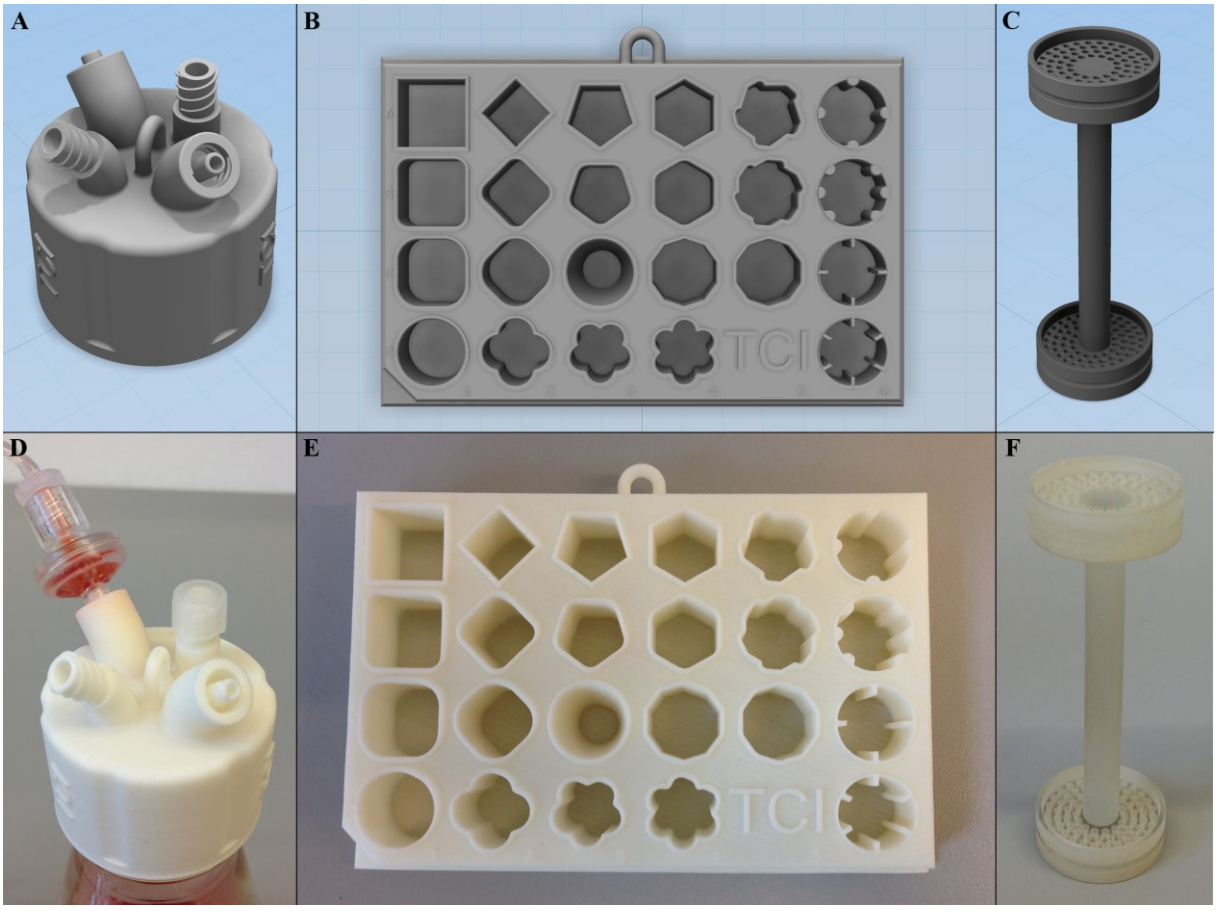

Fig. A.4-1 The example components as (A–C) CAD models and (D–F) printed parts are shown here. (A, D) The installed shaking flask cap, (B, E) a proof-of-principle well plate with different well geometries and (C, F) a holder for ceramic membranes. A 3D view of the models is available in the online Supporting information.

A.4.3 Practical Examples

A.4.3.1 Example 1: Individual Shaking Flask Cap

An applied example represents the construction of an individually configurable shaking flask cap (Fig.A.4-1A and D). The standard shaking flasks are used for cultivation of all different kinds of organisms. If the purpose of such flask cultivations is not only to harvest biomass or a product at end point, but to monitor the growth frequently or even adding a feed or correction fluid, the standard lid has to be either altered or removed under a clean bench. The frequent handling and moving of the flask from an incubator to a clean bench, and the removing of the lid, increases the risk of contamination. Therefore a cap with special, universally compatible connections directly integrated is needed. The concept was to include luer lock connections on the cap, both male and female luers, to obtain a flexible and easy to reconfigure cap.

For this task, the first step was to reconstruct the basic cap with CAD software (Autodesk Inventor Professional 2014, Autodesk, Inc., San Rafael, California, USA). For the digitalization of the existing cap, it was essential to reconstruct the dimensions of the shape itself and especially the threads and their pitch. After the cap model was designed, the designs of the luer connections were made and attached to it. The first resulting models were printed with the above-explained FDM method, to quickly verify the thread fitting on the original flasks. This approach highlighted fast some false design decisions, e.g. a too thin wall thickness at the female luer adapters. After correcting these details, the optimized cap design was converted to the STL format and printed by a contractor. The resulting models were useable immediately after the printing and cooling process.

A.4.3.2 Example 2: Well Plate with Baffles

The second example is the realization of an individual well plate design (Fig. A.4-1B and E). In recent publications, it was shown that a change in well geometry of a microtiter plate can provide sufficient oxygen supply to aerobic cultivations [461]. Such geometries can be easily designed with CAD software. With the usage of RP, it is likewise easy to build those complex geometries as a physical model. For proof of principle, a well plate with 23 different baffle shapes was printed and used for *Saccharomyces cerevisiae* cultivation [510]. This example illustrates the biggest advantage of the RP technologies for the direct use in laboratories: The possibility to create almost every conceivable and required geometry within an extremely short period of time and without complex manufacturing processes.

A.4.3.3 Example 3: Ceramic Membrane Module

The third and last example is an in-house developed capillary module (Fig. A.4-1C and F). This module contains a retaining cylinder in which capillaries are mounted. It is used to separate cells from the culture media during cultivations. Until now this cylinder was made of stainless steel. Due to this, the individual parts had to be machined with turning and milling, the holes for the holding functionality manually drilled, and afterwards all parts had to be welded together. If another setup was

desired, e.g. with larger capillaries, this expensive, complex, and time-consuming process had to be repeated. Furthermore, the weld seams are problematic with regard to sterile constructions. The risk of contaminations caused by biofilms increases due to a rough and uneven surface in those areas that are very difficult to clean and sterilize [511].With the advantages of the RP technologies shown here, it is possible to construct the holding cylinder once and change the number, size, or design of the brackets within minutes. Afterwards the model can be directly printed and used right away. This opens the possibility to achieve different modes of operation of the same device through different designs, e.g. to close several brackets on one side to achieve a dead-end flow. The comparison of both fabrication methods highlights the advantages of the RP usage. The building of the stainless steel membrane holder takes approximately 6 h. The costs are estimated in the range of 100 EUR. 3D printing takes around 4 h and the total costs for building it with the SLS method are around 40 EUR. In this example the time consumption is relatively even, but it has to be taken into account that the stainless steel holder has to be created manually and the printer runs by its own.

A.4.4 Material Compatibility Experiments

The material of choice for these intended applications needs to fulfill certain physical properties, especially when it comes to the usage associated with mammalian cell cultures. For such applications the properties have to include a general biocompatibility, an acceptable chemical resistance and to withstand steam sterilization (121°C for 20 min, 2 bar). Steam sterilization instead of radiation sterilization is the preferred method, because it is a present standard in most laboratories. All these properties are fulfilled by a PA material that is already one of the standard materials used for SU consumables [485, 493]. This material is commercially available, e.g. under the name of DuraForm PA from 3D Systems, Inc. (Rock Hill, USA). For the shown prototypes, a newly developed material from the company Blue Production (Paderborn, Germany) was also used. It possesses a higher UV-stability attributable to additives. The commercially available DuraForm PA material is already USP Class VI certified for its biocompatibility. The newly developed UV-stable material, as well as the standard material as reference, was tested in our laboratories according to ISO 10993-5:2009 for their *in vitro* cytotoxicity [463]. For the first experiments, a cocultivation of the material directly floating in a suspension culture—CHOK1- HP (provided by AG Cell Culture Technology, University of Bielefeld, Germany) in CHOMACS CD medium (Miltenyi Biotec, Bergisch Gladbach, Germany) with additional 8 mM l-glutamine (Biochrom, Berlin, Germany)—was studied. Suspension cultivations were carried out for 7 days with negative controls; all experiments were made in duplicates (Fig. A.4-2). These first tests confirmed the compatibility of the previously certified reference PA material and also revealed no negative influence of the UV-stable material. Further experiments with different cell lines are published in a separate research article [510]. All the models mentioned above were fabricated out of both the standard DuraForm PA material and new UV-stable PA material. The surface finish of the fabricated parts is also important to be considered. If cell adhesion is desired, the slightly rough surface has a positive influence and provides a larger surface area. If the used cells are

growing in suspension, this roughness could present drawbacks. Therefore, the material can be processed afterwards or the smoothness of the surface can be modified via optimization of the fabrication parameters if desired.

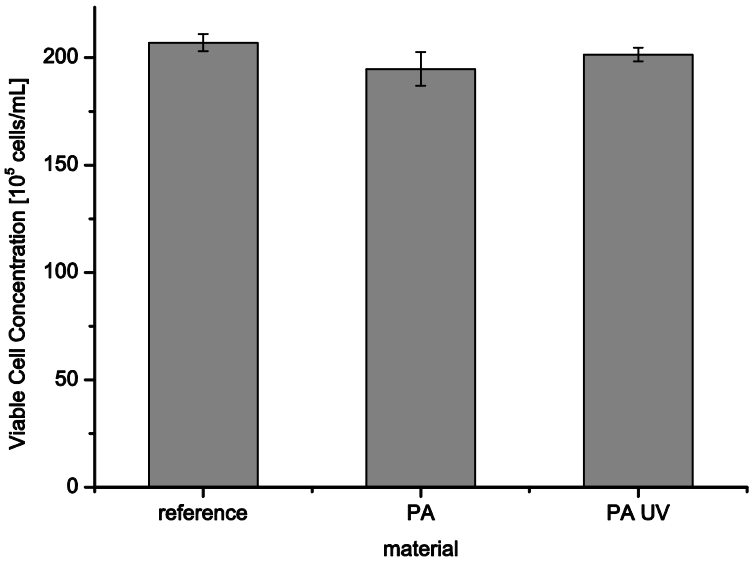

Fig. A.4-2. Viable cell concentration of CHO-K1-HP cultivation after 123 h. Cultivation was carried out in 250 mL shaking flasks with a working volume of 75 mL at 37 °C, 5% v/v CO_2, and 160 rpm. During the whole cultivation, pieces of the sample material were kept in the medium with direct cell contact. PA is the well-established biocompatible material; PA UV is the improved UV-stable material. The references shown are shaking flask cultivations without a material piece in the media. Mean values resulted from two parallel experiments (error bars indicate the SD of the experiments).

A.4.5 Concluding Remarks

All these examples and compatibility tests demonstrate the great capability of integrating RP technology within a sophisticated biotechnological laboratory environment. Compared to the metal prototyping generally used nowadays, RP enables a cost- and time-effective realization of new concepts. It enables to create individual parts just as they are needed for a specific experiment or device. As shown here, these components can be as simple as a retainer for capillaries or more complex as the microtiter plate or the flexible and versatile shaking flask cap shown above. Another application example could be the development of individual bioreactor stirrer designs. This would make it possible to use specific impellers for particular cell lines, e.g. to minimize shear stress or to support the detachment of cell aggregates. Likewise this would be a great approach for scale up purposes to equally adjust the impeller size and design to the specific reactor volume and shape.

With the rapid advancements of new printers and technologies, it is only a matter of time until the more complex printers, such as the SLS systems, become more conveniently priced and easier in use. This step started in the beginning of 2014, when the patents for the SLS technology began to expire. From then on, it will be more practical for a wider range of laboratories around the world to create their own individual labware and devices in house without a long time requirement. And there might come a time, when laboratory infrastructure will evolve where all disposable labware will be produced on demand overnight directly in the laboratory.

Practical application

3D printing revolutionizes the way of working as it is in biotechnological laboratories today. It will enable scientists around the world to create new individual labware with ease and print them three dimensionally for direct use in the laboratory. This approach will lead to a very time- and cost-efficient way of optimizing already available labware or create completely new designs. This technical report presents practical examples that highlight the possibilities and reveal the great potential of using 3D printing in a dedicated biotechnology laboratory. Due to the fast progression of 3D printer technologies and their wider availability for laboratories, the labware consumable industry will start facing competition from self-developed labware. Nevertheless, this industry can also benefit from new, innovative designs that will emerge from the science community.

Lebenslauf

Persönliche Daten

Name	Franziska Sambale
Geburtsdatum	26.05.1987, Hannover
Nationalität	Deutsch

Akademische und schulische Ausbildung

11/2012 – 08/2015	**Promotionsstudium Chemie und wissenschaftliche Mitarbeiterin** Institut für Technische Chemie, Leibniz Universität Hannover Thema: Nanopartikel-Biotestung mittels *in-vitro*-Kulturen von Säugerzellen
10/2010 – 10/2012	**Masterstudium Life Science (M.Sc.)** Leibniz Universität Hannover
10/2007 – 09/2010	**Bachelorstudium Life Science (B.Sc.)** Leibniz Universität Hannover
08/2000 – 07/2007	**Gymnasium (Abitur)** Elsa-Brändström Schule, Hannover

Auslandserfahrungen

09/2011 – 03/2012	**Forschungspraktikum: Biosynthese von Aminoglykosiden** University of Cambridge, Cambridge, Großbritannien
09/2011 – 03/2012	**Auslandsstudium Biochemie** (Natural Sciences Tripos Part III Biochemistry) University of Cambridge, Department of Biochemistry Cambridge, Großbritannien
03/2011 – 04/2011	**Forschungspraktikum: Charakterisierung von Acetylxylanesterasen** Technion, Israel Institute of Technology, Haifa, Israel
08/2010 – 09/2010	**Forschungspraktikum: Detektion von gentechnisch veränderten Organismen** Al-Faraby Kazakh National University, Almaty, Kasachstan